Deciphering the molecular mechanisms of ocular developmental defects through the analysis of coding and non-coding genome

Clémentine Angée

Université Paris Cité

École doctorale 562 - Bio Sorbonne Paris Cité

IHU Imagine – Institut des Maladies Génétiques (UMR-S1163)

Deciphering the molecular mechanisms of ocular developmental defects through the analysis of coding and non-coding genome

Par Clémentine ANGÉE

Thèse de doctorat de **Génétique**

Dirigée par **Lucas FARES TAIE**

Présentée et soutenue publiquement

le 12/12/2023

Devant un jury composé de :

Elfride DEBAERE, Full Professor, Ghent University	Rapportrice
Guy LENAERS, DR2, Université d'Angers	Rapporteur
Hélène DOLLFUS, PU-PH, Université de Strasbourg	Examinatrice
Didier SURDEZ, Professor, Balgrist University Hospital	Examinateur
Glenda COMAI, CR, Université Paris Cité	Examinatrice
Jean-Michel ROZET, DR2, Université Paris Cité	*Membre invité*

Acknowledgments

Je tiens tout d'abord à remercier mon jury pour leur participation à ma soutenance. Je remercie le **Dr. Elfride DeBaere** ainsi que le **Dr. Guy Lenaers** d'avoir accepté d'être les rapporteurs de cette thèse, j'attends avec impatience vos retours sur ce travail. Merci également aux **Drs. Hélène Dollfus**, **Didier Surfez** et **Glenda Comai**. Vos champs d'expertise variés sauront apporter un regard neuf sur cette thèse.

Toute ma gratitude va pour mon directeur de thèse, **Lucas**. Je ne saurais jamais te remercier assez pour tout ce que tu as fait pour moi, merci de m'avoir intégrée à ce projet qui me tient tant à cœur, merci de la confiance que tu m'as accordée et merci de ton soutien indéfectible. Un grand merci à **Jean-Michel**, mon premier directeur de thèse. Merci encore pour ton humanité, ta disponibilité et tes précieux conseils. Je pense que vous ne serez jamais d'accord tous les deux, mais vos divergences m'ont permis d'élargir ma vision des choses, merci à tous les deux. J'ai tant grandi et appris à vos côtés pendant ces 5 années et vous avez su me rendre une confiance en moi longtemps perdue.

Je remercie évidemment tout le laboratoire de génétique ophtalmologique. Merci **Isabelle** pour ta gentillesse et ta présence si solide à nos côtés. C'est certainement grâce à toi que le LGO est un laboratoire aussi agréable à vivre. Je tiens également à remercier **Brigitte**, qui m'a formée à mes débuts et m'a grandement aidé à la paillasse. Ce travail ne serait pas ce qu'il est aujourd'hui sans toi. Merci aussi à **Josseline**, pilier du laboratoire, et **Sylvie** pour ton aide.

J'ai commencé ma thèse en 2019 avec les deux meilleures doctorantes : Iris, Sabrina, je ne pouvais pas rêver de mieux comme étudiantes à prendre en exemple. Si différentes, vous m'avez toutes deux fascinée par votre détermination et votre dévouement à votre travail. Merci **Sabrina** pour ta bonne humeur qui égayait notre petit bureau, et ton humour à toute épreuve. J'ai tant de respect pour toi, merci d'avoir été là pour moi. Merci **Iris** pour tout ce que tu m'as appris. Je n'ai pas les mots pour te dire à quel point je suis reconnaissante de toutes les fois où tu es venue à mon secours. Merci à vous deux, vous êtes comme des sœurs pour moi, et j'ai toujours tous vos petits mots d'encouragement avec moi. Je remercie également toutes les filles de cette belle époque : **Camille**, merci d'être un soutien sans faille et toujours à l'écoute (et pour la sangria aussi), merci à **Sarah** également pour ton grand cœur ; **Nancy** et **Valeria**, vous m'avez sauvé la vie plus d'une fois, j'aimerais pouvoir vous rendre la pareille un jour.

Comment ne pas remercier **Elisa** ? Sans toi, je ne serai jamais allée aussi loin, mille fois merci. Tu es une travailleuse acharnée, et je sais que tu arriveras à mener à bien ce beau projet qu'on partage. Je crois en toi, alors ne perds jamais ton courage et ta bonne humeur ! **Andrea**, merci pour tout, tu es une personne rayonnante et également si talentueuse. Restez comme vous êtes les filles, vous y êtes presque ! Merci aussi à **Joseph**, tes petites siestes me feront toujours rire. Merci à tous les trois d'avoir fait perdurer la gaieté du bureau 409, tout comme **Zoéline** et **Carole**, j'aurais aimé vous rencontrer plus tôt, mais j'ai encore le temps de me rattraper un peu avec toi Zoéline. Tu es brillante, et je suis sûre que ta thèse qui commence se déroulera au mieux. Je remercie également tous les stagiaires que j'ai pu côtoyer, **Ryme** avec qui j'ai démarré, **Nelson**, **Lucie** (ma vie pour tes gâteaux de semoule), **Pénélope**, **Yaelle** (merci encore pour toutes ces myrtilles ma belle), **Julie**, **Jules** et **Noémie** (petite stagiaire pour longtemps dans mon cœur).

J'ai quitté ce chouette bureau pour finir ma thèse, et je ne peux évidemment pas manquer de remercier tous les membres de l'équipe d'**Agnès Rotig**. Merci à **Nolan**, **Manon, Mathieu**, **Agathe**, **Sylvia** et **Mohammed** pour m'avoir intégrée à vos soirées jeux. Gros merci à toi **Juliette**, nouvelle arrivée mais devenue une amie si vite. Je te remercie d'avoir pris le temps de me parler et de m'écouter, d'avoir eu les mots pour me rassurer et m'encourager. Je te souhaite le meilleur pour la suite. Et évidemment, un énorme merci à **Clovis**. Merci d'être là et de toujours me remonter le moral. Je t'adore et j'espère que notre amitié durera longtemps.

Je remercie tous mes proches qui m'ont soutenu de près ou de loin. Merci à **Marie-Ombeline** de toujours garder de mes nouvelles malgré mes absences. Tu as été un tel soutien dans ma vie, merci pour tout, tu es vraiment incroyable. Merci aussi à **Nolwenn**, **Valentine**, **Mélanie** et **Aurélie** d'avoir continué de me donner la force de croire en moi. Et enfin, **Camille**, mon roc, ma queen, la plus incroyablement incroyable. Toujours là depuis tout ce temps, nous avons tellement grandi ensemble et je suis si fière de la femme si exceptionnelle que tu es devenue. Je ne serai jamais allée si loin sans toi, je t'en remercie sincèrement, reste comme tu es.

Je remercie toute ma famille : **mes parents** qui m'ont toujours soutenu dans mes choix, et que j'espère rendre fiers par ce travail. **Lucile**, la meilleure sœur au monde, toujours là quand j'en ai besoin, ma première alliée qui a mis au monde mes deux magnifiques nièces. **Rose, Lilas**, vous êtes mes petites fiertés, et ce travail je le fais pour vous. Merci du fond cœur à **Hugo**, je ne pensais pas rencontrer quelqu'un d'aussi avenant que toi ; tu as été mon pilier pendant cette période difficile et je ne pense pas que j'aurais accompli autant de choses sans toi à mes côtés. Merci.

Table of contents

List of figures

List of abbreviations

AH: **A**queous **h**umor

ASD: **A**nterior **s**egment **d**ysgenesis

ATOH: **Ato**nal b**H**LH TF

bHLH: **B**asic **h**elix-**l**oop-**h**elix

BMP: **B**one **m**orphogenetic **p**rotein

Bp: **B**ase **p**air

CB: **C**iliary **b**ody

CRE: **C**is-**r**egulatory **e**lement

CRX: **C**one-**r**od homeobo**x**

CTCF:**C**CC**TC** binding **f**actor

DCT: **D**opa**c**hrome **t**automerase

DM: Iris **d**ilator **m**uscle

DNA: **D**eoxyribo**n**ucleic **a**cid

EF: **E**ye **f**ield

FGF: **F**ibroblast **g**rowth **f**actor

FOX: **Fo**rkhead homeobo**x**

GLC: **Gl**au**c**oma

HES: **H**airy and **e**nhancer of **s**plit

hGD: **H**uman **g**estation **d**ay

hGW: **H**uman **g**estation **w**eek

HMG: **H**igh **m**obility **g**roup

IAE: **I**ris **a**nterior **e**pithelium

IPE: **I**ris **p**osterior **e**pithelium

IOP: **I**ntra**o**cular **p**ressure

IRD: **I**nherited **r**etinal **d**ystrophy

LHX: **L**IM **h**omeobo**x**

MAC: **M**icrophthalmia-**a**nophthalmia-**c**oloboma

MCOR: Congenital **m**icro**cor**ia

mE: **M**ouse **e**mbryonic day

MITF: **Mi**crophthalmia-associated **t**ranscription **f**actor

mRNA: **m**essenger **RNA**

MSX: **Ms**h homeobo**x**

NEUROG: **Neurog**enin

NPE: **N**on **p**igmented **e**pithelium

OC: **O**ptic **c**up

ODD: **O**cular **d**evelopmental **d**efect

ON: **O**ptic **n**erve

OTX: **Ot**hodenticle homeobo**x**

PAX: **Pa**ired-bo**x**

PE: **P**igmented **e**pithelium

PIC: **P**re**i**nitiation **c**omplex

PITX: **Pit**uitary homeobo**x**

POAG: **P**rimary **o**pen-**a**ngle **g**laucoma

POM: **P**eri**o**cular **m**esenchyme

RA: **R**etinoic **a**cid

RAX: **R**etina and **a**nterior neural fold homeobo**x**

RGC: **R**etinal **g**anglion **c**ell

RNA: **R**ibo**n**ucleic **a**cid

RPC: **R**etinal **p**rogenitor **c**ell

RPE: **R**etinal **p**igment **e**pithelium

SHH: **S**onic **h**edge**h**og

SIX: **Si**ne oculis homeobo**x**

SM: Iris **s**phincter **m**uscle

SNV: **S**ingle **n**ucleotide **v**ariant

SOX: ***S****RY*-related HMG-b**ox**

SRY: **S**ex-determining **r**egion **Y**

SV: **S**tructural **v**ariant

TAD: **T**opologically **a**ssociated **d**omain

TBX: **T**-**B**o**x** transcription factor

TF: **T**ranscription **f**actor

TGFb: **T**ransforming **g**rowth **f**actor **beta**

TM: **T**rabecular **m**eshwork

TYR: **Ty**r**r**osinase

TYRP: **Ty**rosinase **r**elated **p**rotein

VAX: **V**entral **a**nterior homeobo**x**

VSX: **V**isual **s**ystem homeobo**x**

WNT: **W**i**n**gless i**nt**egration site

Introduction

1.1. Structure and function of the eye

The eye is a complex organ that allows the apprehension of our environment through high-resolution vision. The human eye is a globe composed of three main layers: the outer sclera-cornea, the intermediary uvea (which comprises the iris, ciliary body, and choroid), and the retina as the most inner layer (Figure 1). Typically, the eye can be simplified into the anterior and posterior segments, each separated by the lens. Here is a brief depiction of each structure present in each segment (Forrester et al., 2016a; Kaplan, 2007).

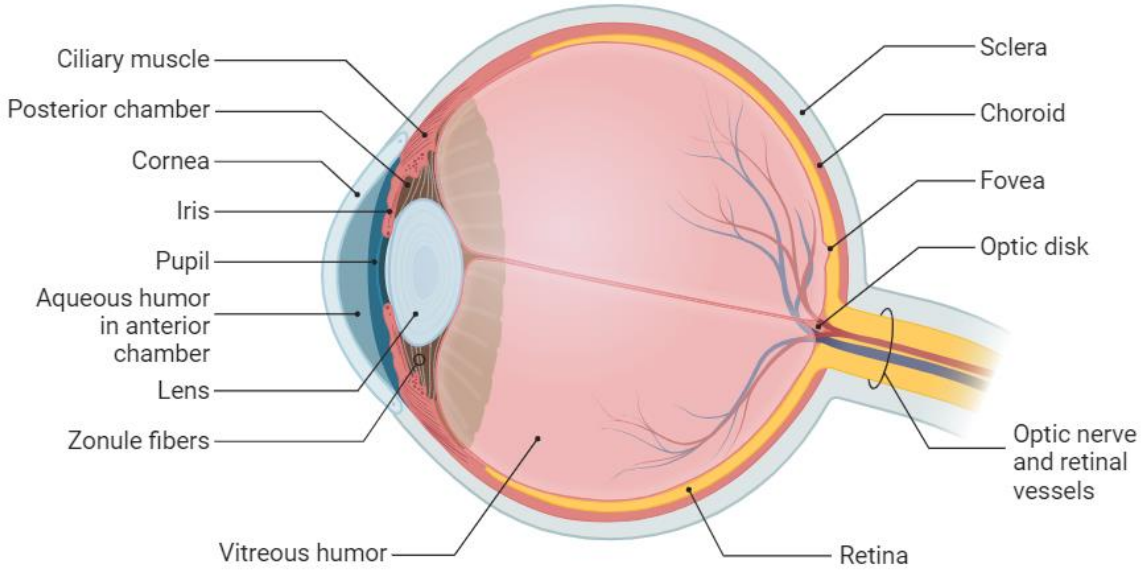

Figure 1. Schematic representation of the human eye globe in sagittal view
Reprinted from "Human Eye Anatomy", by BioRender.com (2023) and created by Sally Kim.

1.1.1. Anterior segment

The anterior segment contains the elements that allow light to enter the eye. From an antero-posterior axis, lie the cornea, the anterior chamber, filled with the aqueous humor (AH), the iris and ciliary body (CB), and the lens (Figure 2).

The sclera is a white tunic protecting the visible surface of the eye, which lies in continuity with the cornea. The latter is a transparent tissue consisting of three layers: an outer epithelium, which is the most external cell layer of the eye; a stroma, containing collagen fibers and keratocytes; and an endothelium, in direct contact with

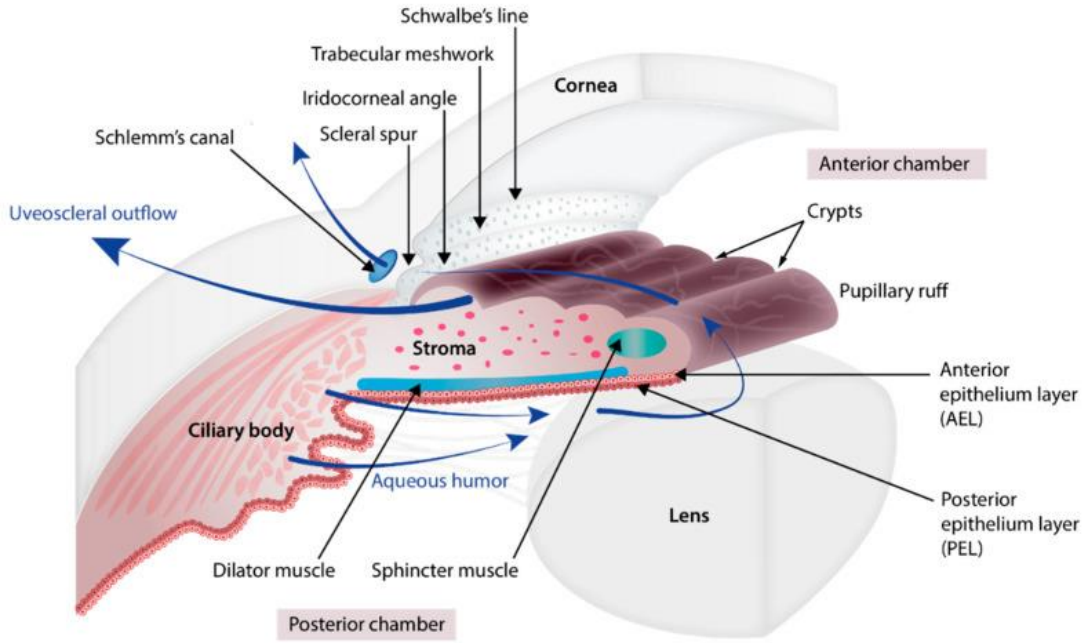

Figure 2. Anatomy of the anterior segment and aqueous humor outflow pathway
This picture details all the elements intervening in the production, circulation and drainage of the aqueous humor, whose trajectory is represented in dark blue arrows. (Reprinted from Angée *et al.* in *Genes*, 2021)

the AH (Espana and Birk, 2020). The intersection of the cornea with the iris creates an angle known as the iridocorneal angle, and located at the junction point of the cornea (Schwalbe's line) and scleral spur lies the trabecular meshwork (TM).

Visible through the cornea, the iris is composed of three main layers: the stroma, the most anterior part of the iris, containing melanocytes, blood vessels, and nerves; the anterior layer, from which the dilator muscle develop; and the pigmented posterior layer. The iris muscles (or pupil muscles), which lie within the stroma, are antagonistic smooth muscles controlling the aperture of the pupil. The dilator muscle (DM) lies longitudinally from the root of the iris to its margin, and its contraction in dim light opens the pupil, causing a mydriasis, while the sphincter muscle (SM) is located at the margin of the iris only, creating a bulge around the pupil (Ducasse, 2004). In bright light conditions, the sphincter contracts to close the pupil; this phenomenon is known as myosis. Though usually round in small mammals and primates, the pupil shape varies in several species.

The iris root is attached to the CB, at the periphery of the retina, and along the *ora serrata*. The CB is composed of ciliary muscles, an anterior pigmented epithelium, and a posterior epithelium, organized in processes. The ciliary processes are linked to the lens through zonular fibers, and the contraction of the ciliary muscles is responsible for the change in shape of the lens.

The lens is a small, translucent ball whose shape and proportion to the globe's size vary between species. Typically, the human lens is small and has an ellipsoidal shape, while mice possess a huge, round lens. Composed of fibers organized on the antero-posterior axe and surrounded by a thin capsule consisting of a single layer of epithelium in the anterior part, the lens can accommodate, changing the direction of light and aiming it to the focal point of the retina.

All these structures are maintained and nourished by the AH, a transparent fluid derived from plasma with less proteins (Skalicky, 2016). It is continuously produced by the posterior epithelium of the CB (Figure 3, Toris, 2010) and flows along the iris to fill the anterior chamber. AH is then drained through Schlemm's canal after passing through a sieve-like structure, the TM (Figure 2). This meshwork is composed of collaged beams and extracellular matrix, creating a robust filter (Buffault et al., 2020). The aqueous fluid is also drained out through the uveoscleral pathway, driven by pressure gradients through the uvea. The AH outflow is a key component of the maintenance of intraocular pressure, whose elevation severely impact the entire eye functioning (Paulavičiūtė-Baikštienė et al., 2013).

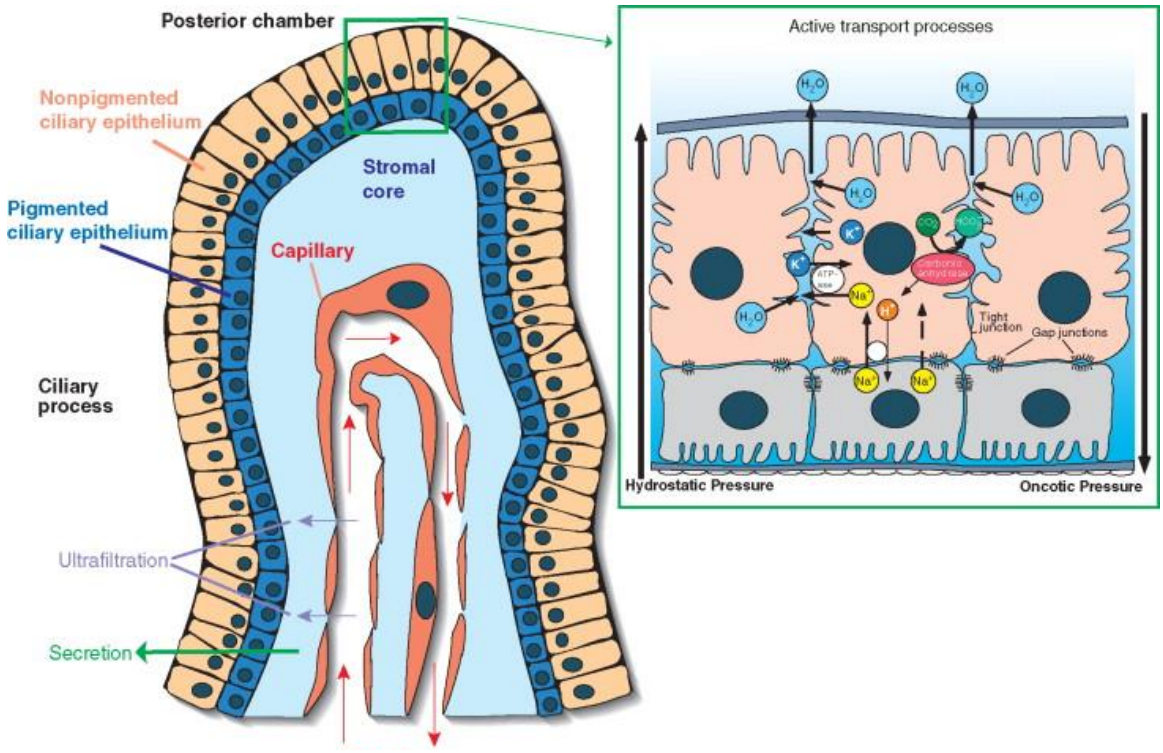

Figure 3. Aqueous humor production
Representation of a ciliary process (left). The stroma, rich in capillaries, contains plasma filtrate formed by diffusion and ultrafiltration. Aqueous humor is actively secreted from this filtrate (right). (Reprinted from Toris, *Encyclopedia of the Eye*, 2010)

1.1.2. Posterior segment

The posterior segment corresponds to the choroid, and the vitreous and retina, which convey the light directed by the lens and process the photons into an electric signal. The vitreous is the gelatinous mass between the lens and the retina. Mainly composed of water, it is surrounded by collagen, which makes it more viscous than water. Its gel-like texture is substantial enough to maintain the spherical shape of the eye globe.

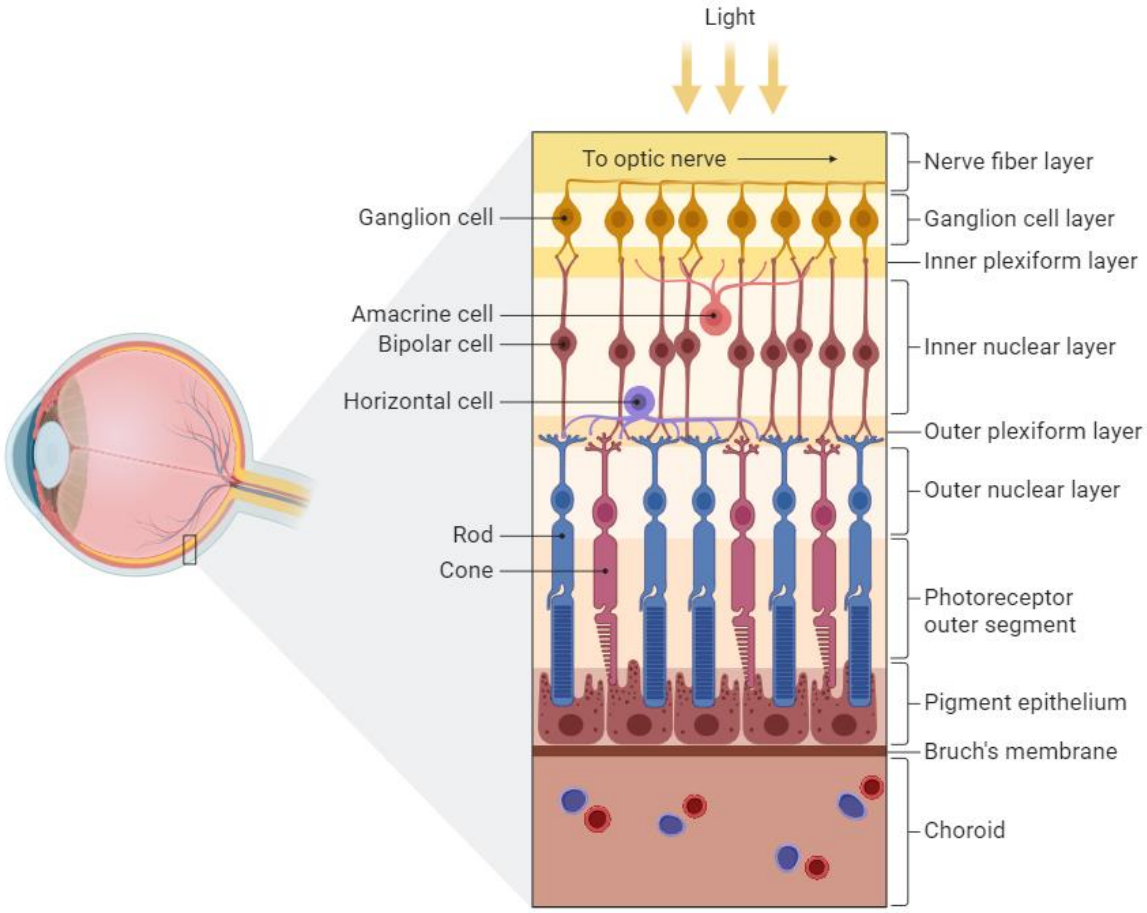

Figure 4. Schematic view of the different layers of the retina
The various cell types composing the retina are named on the left, and the layers they compose are shown on the right. The Bruch's membrane belongs to the choroid, as seen at the bottom. Reprinted from "Structure of the Retina" by Biorender.com (2023) and created by Sally Kim.

The retina (Figure 4) is composed of multiple cell types (Masland, 2001). The light crosses all layers of the retina to its outermost layer, the retinal pigment epithelium (RPE). This thin layer of dark pigmented cells, along with the choroid, acts as a blocking screen to keep photons inside the eye globe and avoid UV damage. Light can thus be captured by the cilia of the photoreceptors, whose nuclei compose the outer nuclear layer of the retina. Photoreceptors transduce the quantity of light into an electric signal and convey it to the thalamus through the bipolar and retinal ganglion cells (RGC). These cells form the inner layer of the retina, and their axons are part of the optic nerve (ON), which constitutes the link between the eye and the brain. The region where all RGCs axons converge is deprived of photoreceptors, therefore creating a blind spot at the head of the ON.

There are two different types of photoreceptors: cones and rods. For most animals, rods are prominent, as their capacity to absorb a high quantity of photons allows for detailed vision with a weak signal. The cones, however, vary a lot among species, both in type, proportion and localization. These cells capture the photons at specific wavelength ranges, depending on their types, making them less efficient at capturing all the light but capable of color vision. Some primates, including humans, possess three types of cones that encompass the colors of what we know as visible light, *i.e.,* the colors of the rainbow, ranging from 400nm to 800nm. The repartition of rods and cones in the retina depends on the lifestyle of the animal; as diurnal animals, humans possess a high number of cones (6M, 6% of all receptors) concentrated in the central region of the retina, called the macula (Purves et al., 2001). The point that offers the most accurate vision is the fovea, located at the very center of the macula (Behar-Cohen et al., 2020). On the other hand, nocturnal animals, such as mice, possess a vast majority of rods (97% of all receptors), distributed throughout the retina (Jeon et al., 1998).

1.2. Ocular development

If the eye constitutes a complex organ, its development is no less so. Deciphering the morphogenetic steps and molecular mechanisms of this process required years of study from different animal models. Although each species has its own characteristics, the earliest stages remain conserved in most vertebrates (Chow and Lang, 2001). This part describes the chronological events leading to a mature eye, focusing on human, and mouse in the early stages. Figure 5 recapitulates the main steps of this process in a mammalian eye with major timepoints and their equivalent in human eye development, given in human gestation day (hGD) or week (hGW) and mouse embryonic days (mE).

1.2.1. Eye field

During the third hGW (mE6.5), the embryonic cells move to form a third layer, namely the inter-embryonic mesoderm; this is the gastrulation, going from a didermic to a tridermic state. In the late gastrula stage, the embryo is composed of three layers: the ectoblast, mesoblast, and endoblast. The latter is the only layer that will not intervene in the eye's organogenesis (Forrester et al., 2016b; Graw, 2010).

In the course of neurulation, the dorsal ectoblast thickens to create the neural plate. Once sufficiently differentiated, its borders elevate and merge, forming the neural tube, while the neighboring cells detach from the border and become the neural crest. The rest of the ectoblast, the epiblast, will mainly give rise to the skin. At the end of hGW 3 (mE7.5), the neural tube is already organized in the different encephalon. On the anterior side, the forebrain specifies the telencephalon and diencephalon, and in between lies the eye field (EF).

1.2.2. Optic vesicles

Around hGD 22 (mE8.5), the EF is separated in its middle, creating two fields on both sides of the neural tube. Each EF migrates distally, forming two optic pits. Across the fourth hGW, both pits grow to the surface ectoderm on the temporal sides as optic vesicles (Hosseini and Tabber, 2018; Martinez-Morales et al., 2017). At 28 hGD (mE9.5), the cells reach the lens placodes, two specified regions of the epiblast that thicken at the contact of the vesicles. This close contact triggers the whole process of eye formation, starting with the invagination of both the vesicle and the placode at

32 hGD (mE10.5). The optic stalk, which corresponds to the ventral-proximal part of the optic vesicle, constitutes the future optic nerve, while the distal bulb forms the presumptive retina and epithelia of both the iris and CB (Forrester et al., 2016b; Miesfeld and Brown, 2019).

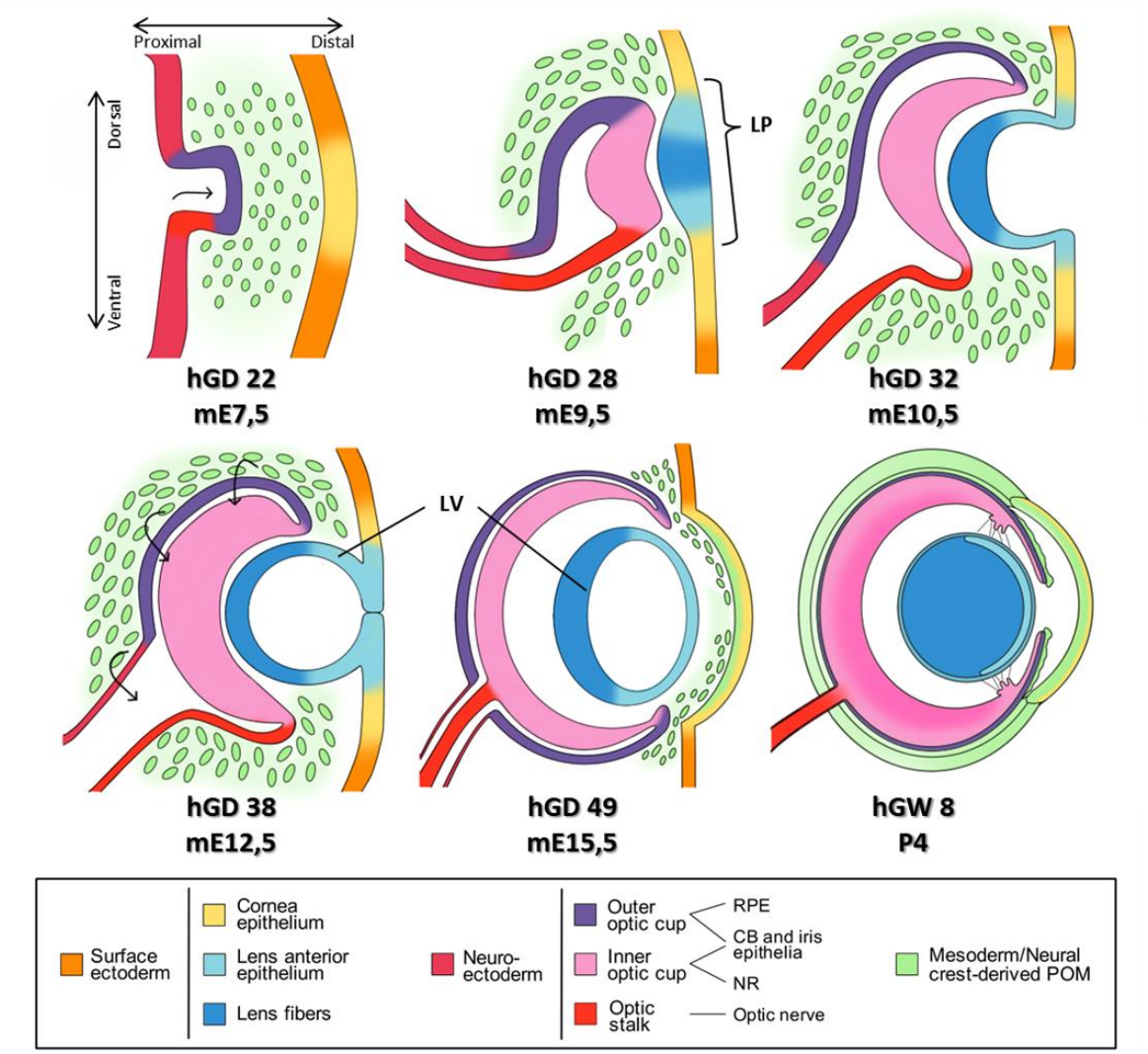

Figure 5. Main steps of mammalian eye development
This figure illustrates the morphological steps of eye development, from the formation of the optic pit to the mature eye. The neuroectoderm and surface ectoderm initially differentiate into the eye field and preplacode, to finally give rise to many distinct layers of the eyes. The fate of each embryonic layer is defined at the bottom of the picture; the POM differentiates in all remaining structures: corneal stroma and endothelium, iris and CB stroma, choroid and sclera. Arrows represent the main movements of cells migration: first, the optic vesicle moves distally toward the surface ectoderm; later, the optic cup moves toward the ventral side, along the lens vesicle, and closes ventrally, forming the choroid fissure. **LP**: Lens placode; **LV**: Lens vesicle; **NR**: neuroretina; **P**: Postnatal day (mouse); **POM**: Periocular mesenchyme; **RPE**: Retinal pigment epithelium.

1.2.3. Optic cups

The lens placode separates from the surface ectoderm, forming the lens vesicle; surrounding ectoderm will seal and give rise to the cornea. The invagination of the optic vesicle creates a two-layered cup surrounding the lens. This neuroectodermic optic cup (OC) grows in a centripetal manner between the presumptive cornea and lens. The outer layer of the OC is mostly composed of the presumptive RPE; the most distal cells will form the CB pigmented epithelium (PE) and iris anterior epithelium (IAE). The inner layer of the OC is composed of multipotent cells that start specifying into the different layers of the neuroretina (NR) at 33 hGD (mE11.5). The unspecified margin of the NR sets underneath the CB PE and IAE (Davis-Silberman and Ashery-Padan, 2008). During this period of the time, the dorsal OC proliferates and expands ventrally, enveloping the ventral optic stalk and creating the choroid fissure. The closure of the fissure, in the middle of hGW 5, allows blood vessels to access the eye, with the hyaloid vein enveloped in the optic stalk (Chow and Lang, 2001; Lutty and McLeod, 2018).

1.2.4. Differentiation of ocular structures

1.2.4.1. Anterior segment

The mesoderm surrounding the primitive eye is invaded early on by the migrating cells of the neural crest, forming the periocular mesenchyme (POM). Therefore, the origin of this mesenchyme is still unsure (Gage et al., 2005). While the remaining surface ectoderm that covers the OC forms the corneal epithelium, the POM migrates toward the pupil in three waves, constituting respectively the corneal endothelium (hGD 33), the corneal stroma (hGD 49) and finally the iris and CB stroma (hGW 7-8). It is usually accepted that these tissue originate from neuroectoderm rather than mesoderm (Ducasse, 2004; Forrester et al., 2016b; Graw, 2010). The rest of the POM embedding the OC form the choroid (hGW 8) and the sclera (hGW 12).

The ciliary body develops from the two layers of the OC margin, around the 11th hGW. The two epithelia, initially flat, starts forming processes as the vascular mesenchyme grows and pushes the epithelia inward. Ciliary muscles are formed during the 15th hGW from the nearby mesenchyme. The CB produces the AH early on, as the elements of the iridocorneal angle starts developing, from the 20th hGW. The TM and Schlemm's canal also derive from the POM lying at the chamber angle (Figure 6)(Cvekl and Tamm, 2004; Gould et al., 2004).

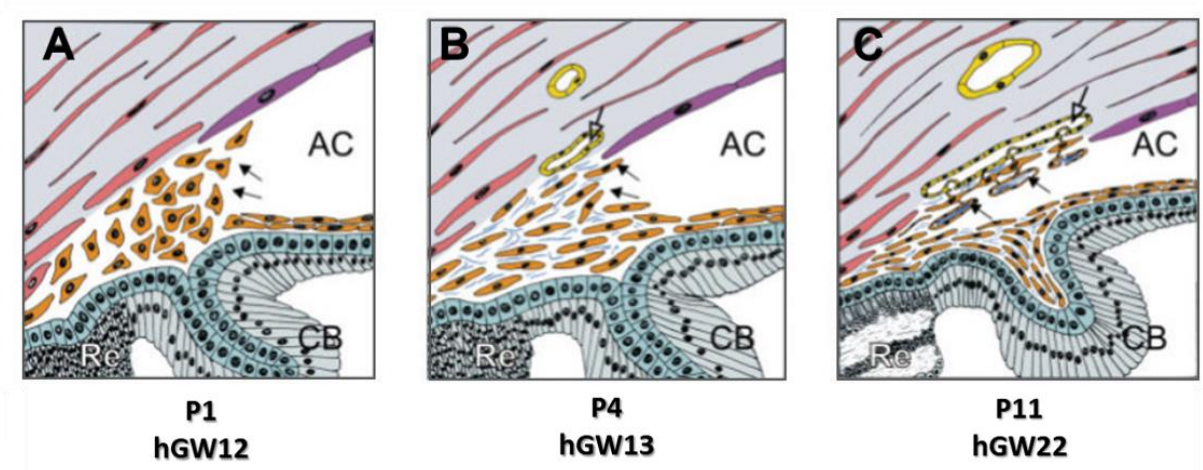

Figure 6. Development of the trabecular meshwork in the mouse eye
(**A**) At hGW12, the chamber angle is occupied by a dense mass of mesenchymal cells (arrows). (**B**) During hGW13 chamber angle cells (solid arrows) separate, leaving open spaces partially filled with extracellular fibers, and nearby vessels appear in the sclera (open arrows). At this stage, the chamber angle aligns with the future trabecular meshwork's anterior border. (**C**) From weeks 14 to 22, extracellular fibers in the chamber angle form trabecular beams are covered by trabecular meshwork cells. Simultaneously, scleral vessels near the chamber angle merge into Schlemm's canal. The peripheral anterior chamber margin shifts posteriorly, exposing the inner trabecular meshwork surface to the anterior chamber. (Adapted from Cvelk and Tamm in *Bioessays*, 2004) **AC**: Anterior chamber, **CB**: Ciliary body, **P**: Post-natal day (mouse), **Re**: Retina.

The iris differentiates shortly after the CB. Iris smooth muscles develop within the stroma as myofibrils differentiated from the iris epithelia, hence iris muscles are derived from neuroectoderm. The SM appears first, around the 14th hGW, from the peripheral cells of the IAE (Ducasse, 2004; Forrester et al., 2016b), although its precise origin is debated (Thumann, 2001). This muscle, innervated by parasympathetic fibers of the oculomotor nerve, lies in the stroma and remains independent of the iris epithelium. Later, the DM develops as basal extensions of the whole IAE during around the 28th hGW and keeps maturing after birth. This second

muscle therefore consists of myoepithelial cells, which are stimulated by the sympathetic nervous system (Figure 7). The iris stroma initially recovers the epithelia and the lens, creating a thin and transparent membrane above the pupil. This pupil coat, which contains the blood vessels, regresses from the middle of the pupil to the periphery at the 7th month of gestation. Its resorption stops in the middle of the iris, leaving a circular mark called the collarette (Davis-Silberman and Ashery-Padan, 2008; Ducasse, 2004).

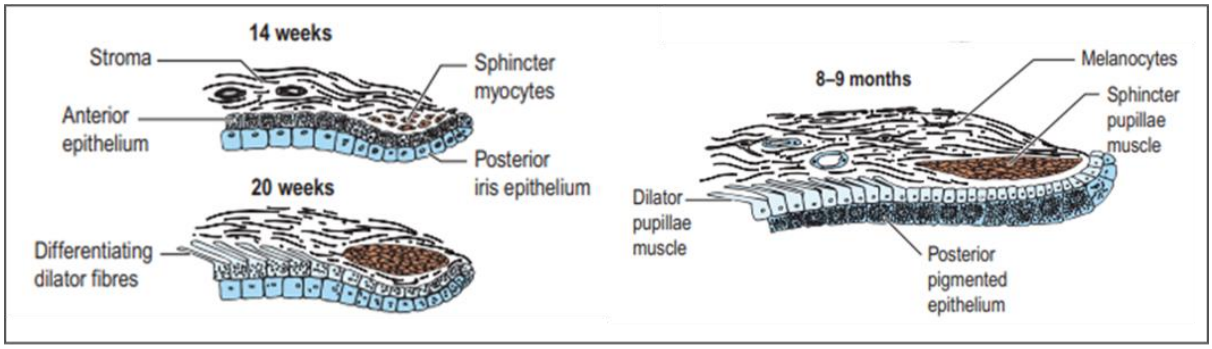

Figure 7. Development of the iris in the human eye
The iris sphincter muscle develops early within the stroma, while the first fibers of the dilator muscle appear weeks later. This figure also shows the evolution in the pigmentation of the two epithelia through embryogenesis. The anterior epithelium is initially highly pigmented and progressively loses its melanin as the dilator muscle develops, while the posterior epithelium starts gaining pigments. (Adapted from Forrester, *The Eye (Fourth Edition*), 2016)

Development of the lens is vital to the global eye morphogenesis, as its surface interacts with the rest of the anterior segment. The lens vesicle is divided by the lens equator into two parts: the posterior cells become longer and thinner, arranged longitudinally to form the primary lens fibers (Figure 8). The peripheral cells, located at the equator, provide the secondary fibers surrounding the core of the lens. These fibers lose their nuclei and mitochondria as they differentiate. The anterior side proliferates and constitutes the anterior epithelium layer, which provides a capsule protecting the fibers (Cvekl and Ashery Padan, 2014; Jean et al., 1998).

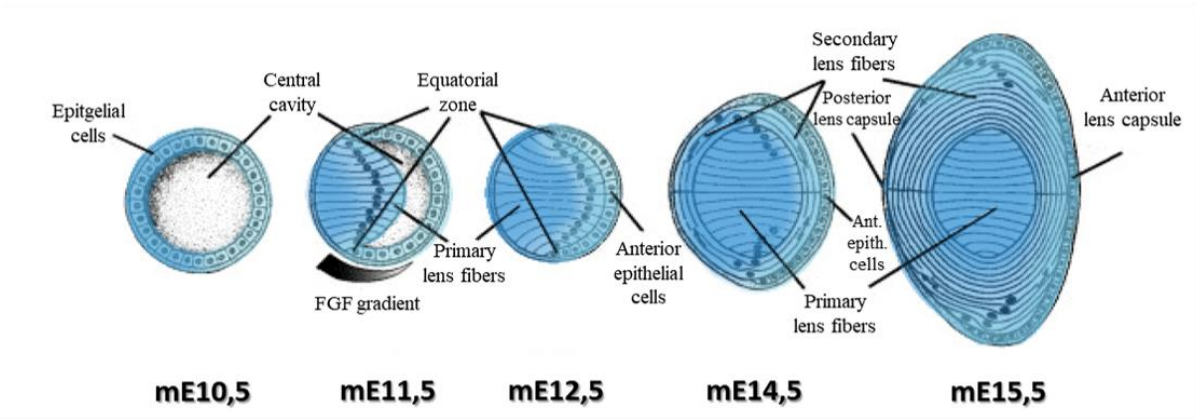

Figure 8. Development of the mouse lens
The central cavity of the lens vesicle gets filled with the primary lens fibers that form the lens core. Cells at the equatorial zone produce the second layer of lens fibers. Identity of the cells at the anterior and posterior sides of the lens is driven by a FGF gradient, promoting the fibers differentiation. In human, this process occurs from hGD39 to hGD56. (Adapted from Jean *et al.* in *Mechanisms in Development*, 1998)

1.2.4.2. Retina

The development of the human retina is a highly orchestrated process that begins in the earliest stages of the OC and the specification of progenitor cells of the NR follows a strict temporal pattern. The RGC are the first cells to differentiate during the 8th hGW; first developing at the dorsal OC, they expand to the ventral side. In the next weeks, cones and horizontal cells differentiate (hGW 9), followed by amacrine cells (hGW12), rods (hGW15), bipolar cells (hGW18) and finally Müller cells (hGW19), which constitute the only glial cells among these neuronal cells. The outer layer forms the RPE, which lies in close proximity to the POM, and its pigmentation begins at hGD 28 (Forrester et al., 2016b; Graw, 2010; Zagozewski et al., 2014).

As the cells differentiate and migrate to their appropriate positions within the retina, they form synaptic connections between them. The retina continues to mature and refine its connections throughout fetal development and into early childhood. By the time of birth, the basic structure of the retina is in place, although further refinement and fine-tuning continue to occur throughout the first years of life. In the months following birth, retinal ganglion cells have their axons myelinated (Fuhrmann, 2010; Heavner and Pevny, 2012).

1.2.5. Molecular basis of eye development

Though vertebrate eye morphogenesis has long been known thanks to embryo histology and high-resolution microscopy, understanding the molecular mechanisms of this organogenesis has been a greater challenge. Many transcription factors (TF) and signaling pathways play an important role in the formation of the eye, and a few intervene from the earliest stages of development to the specification of the different ocular tissues (Miesfeld and Brown, 2019). What follows is a non-exhaustive overview of the main genes intervening in vertebrate eye development. The complete name of all genes mentioned herein can be found in the list of abbreviations (pages 6-7).

1.2.5.1. Definition of the precursor regions

Some graded signaling pathways are required to establish the different polarities of the eye (Figure 9). The WNT gradient defines the anterior-posterior axis (A-P) of the forebrain during the earliest stages, leading to its specification in the telencephalon and EF. The association of OTX2 and SOX2 in the EF enhances *RAX* expression, which is necessary to induce the optic vesicle evagination (Bailey et al., 2004). The Sonic Hedgehog pathway (SHH) is also implicated in setting the polarity of the embryo: *SHH* is necessary to establish the midline that separates the bilateral EFs by promoting *PAX2* expression under the control of SIX3, and its gradient is also crucial in developing both the dorsal-ventral (D-V) and proximal-distal (P-D) axes of the optic vesicle, with PAX2 and PAX6 inhibiting one another to define the proximal and distal regions, respectively (Macdonald et al., 1995; Patel and Sowden, 2019).

Initially, the POM sends inhibition signals against *PAX6* expression in the surface ectoderm, and when the vesicle reaches it, LHX2 promotes BMP4, which in turn can activate *PAX6* in the ectoderm, thus defining the lens placode region (Sjödal et al., 2007). *SHH* expression also promotes *VAX1* and *VAX2*, which both define the ventral identity of the optic stalk. On the other side, the TGFb signaling is acting in the dorsal RPE, with BMP4 enhancing the expression of *TBX5*, which acts as a repressor of the *VAX* genes (Mui et al., 2005). This signaling pathway is also implicated in maintaining the RPE/NR boundary, along with the WNT pathway, through the activation in the RPE of *MITF* and *OTX2* respectively, while FGF signals from the surface ectoderm keeps the NR identity by enhancing *VSX2* expression (Nguyen and Arnheiter, 2000).

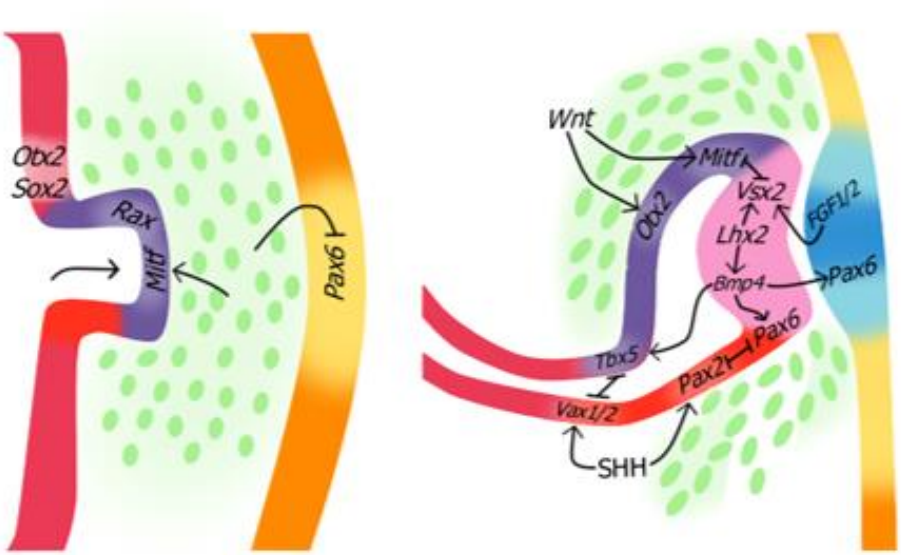

Figure 9. Genetic interactions of the optic vesicle
Initially, signals from the POM either promote the RPE identity by *Mitf* expression, or inhibit *Pax6* expression that define the lens placode identity. The contact of optic vesicle with the surface ectoderm disables the POM signaling while enabling new interactions between the two layers, allowing the expression of genes defining the both the presumptive neural retina and the lens placode. The SHH and *Wnt* pathways balance the ventral and dorsal identity of the vesicle.

1.2.5.2. Identity of the different structures

The EF TF required during the early eye development are expressed in most eye tissue during their specification. Through interactions between each region, different pathways and TF will be activated, allowing the differentiation of each structure leading to the mature, functioning eye.

In the surface ectoderm, *PAX6* expression defines the identity of the corneal endothelium and activates the production of cytokeratin in the cornea. PITX2 and FOXC1 are both specific to the POM, however only the third wave, giving rise to the iris and CB stroma, expresses *PITX2* induced by the retinoic acid (RA) pathway. The nonneural identity of cells at the margin of the OC is maintained by OTX2 and MSX1, both essential to the iris and CB development (Davis-Silberman and Ashery-Padan, 2008). PITX3 controls expression of *FOXE3*, restricted to the lens placode, and later in the lens anterior epithelium. The production of the lens fibers is induced by the FGF pathway (β- and γ-crystallin), and the association of PAX6, SIX3 and SOX2 (δ-crystallin) (Blixt et al., 2007; Cvekl and Ashery Padan, 2014).

The RPE identity is maintained by interaction with the choroid, and the production of pigment protein (TYR, TYRP1 and DCT) is driven by MITF and PAX6 (Cavodeassi and Bovolenta, 2014). While the Notch and SHH pathways allows the proliferation of the NR, each cell type differentiate under the control of PAX6 (Figure 10). RGCs express many EFTF early on, but their neuronal differentiation is due to the activation of two proneural bHLH TFs by PAX6: *NEUROG2* and *ATOH7*. These two factors then activate other RGC-specific TFs, including *POU4F2* and *ISL1*, both essential in the identity of RGCs. Photoreceptors and bipolar cells are the only *OTX2*-positive cells in the NR, and their identity will be defined by the expression of *VSX2* (bipolar cells), *PRDM1* (rods), *CRX*, and *NRL* (rods and cones). FOXEN4 and PFT1a are necessary and sufficient to induce the specification of amacrine and horizontal cells. Finally, Mugler glial cells are defined by the expression of the EFTF *HES1*, *HES5* and *RAX*. They develop last, hence their identity is the closest to that of the precursor retinal cells (Heavner and Pevny, 2012).

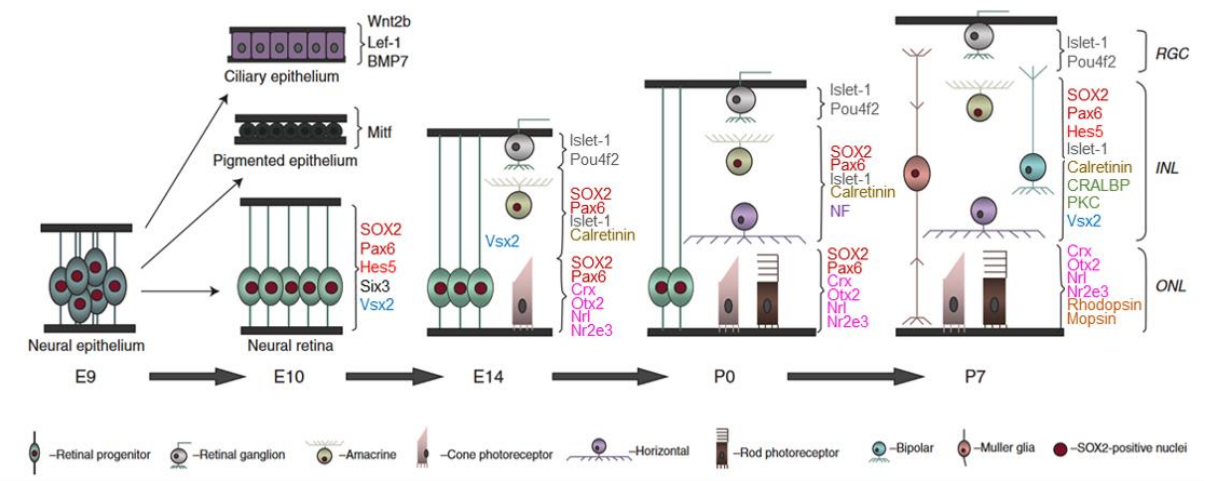

Figure 10. Differentiation of the retinal cell progenitors
During optic cup development in mice, the neural epithelium of the optic vesicle produces the pigmented epithelia of the iris, CB, and retina, along with neural progenitor cells. The embryonic phase of retinogenesis is marked by the emergence of the first retinal ganglion cells, followed. The main genes represented here are essential in both the development and the maintain of the different retinal layers. (Adapted from Heavner and Pevny in *Cold Spring Harbor Perspectives in Biology*, 2012) **INL**: Inner nuclear layer, **ONL**: Outer nuclear layer, **RGC**: retinal ganglion cells.

1.3. Ocular development defects

Ocular malformations comprise a wide spectrum of congenital anomalies of variable severity. In developed countries, these disorders are among the most common causes of serious visual impairment in newborns. This includes defaults of global development, such as anophthalmia and microphthalmia, and anomalies of the anterior segment. Although the causes of these pathologies can be multiple, genetics, and particularly development genes, are often involved.

1.3.1. Default of global eye development

These rare defects comprise microphthalmia, anophthalmia and coloboma, and are therefore often referred to as MAC. They can affect both eyes (bilateral) or only one (unilateral); in the latter case, the other can be sane or present another ocular malformation (Taha Najim et al., 2020). Anophthalmia is characterized by the complete absence of ocular tissue (Figure 11A), and microphthalmia by the reduced size of the globe (Figure 11B). It can be simple, or complex if the affected eye presents internal defects (Verma and Fitzpatrick, 2007).

Figure 11. Clinical aspects of ocular malformations
Picture of patients affected with bilateral anophthalmia (**A**) and bilateral microphthalmia (**B**). (Adapted from Harding and Moosajee in *Journal of Developmental Biology*, 2019)

Microphthalmia is diagnosed from the measurement of the axial length of the eye (from the corneal surface to the retina) and the corneal diameter. Due to the elongation of the eye during infanthood, the definition of microphthalmia varies through time: newborns are diagnosed with an axial length inferior to 14mm, while the maximal length is 21mm for adults. A severe microphthalmia is defined with a corneal diameter inferior to 4mm and an axial length inferior to 12mm after one year old, and it can be challenging to distinct a very severe microphthalmia from anophthalmia. It can also be associated with a coloboma, therefore MAC represents a spectrum, and giving a precise diagnostic can be hard (Skalicky et al., 2013).

Coloboma is due to an incomplete closure of the choroid fissure and can affect one or many parts of the eye, including the iris (Figure 12), the uvea, the retina, or the optic nerve. Although anterior coloboma are easily recognized, it is not immediately apparent when the posterior segment is affected, hence the necessity to look at the eye fundus (Shah et al., 2012). Its prevalence is 1.4 per 10.000 live births (Hornby et al., 2000), while microphthalmia and anophthalmia are estimated to affect 3/10.000 newborns (Chambers et al., 2018; Verma and Fitzpatrick, 2007).

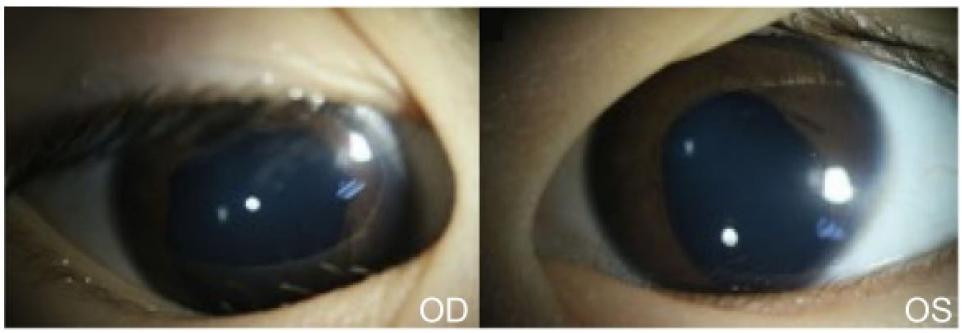

Figure 12. Clinical aspect of iris coloboma
Anterior segment picture of a patient affected with partial coloboma of the iris, characterized by keyhole-shaped pupils. (Adapted from Li *et al.* in *BMC Ophthalmology*, 2023) **OD**: Oculus dexter, **OS**: Oculus sinister.

About half of MAC are syndromic, often associated with comorbidities and neurological defects (Fahnehjelm et al., 2022; Slavotinek, 2011). In most severe cases, the ocular cavity can be enlarged using prosthetics, providing mostly a cosmetic aspect (Quaranta-Leoni, 2011). Though vision and quality of life of the young patients is negatively impacted, prosthetics have been reported to offer satisfying results (Fahnehjelm et al., 2022; Taha Najim et al., 2020).

Most MAC are related to genes involved in early development, but their exact origin can be genetics, or derive from external factors during pregnancy, such as infections or the use of drugs that might interfere with the developmental pathways (Ragge et al., 2007). Mutations in *SOX2* are often associated with MA defect (Bakrania et al., 2007; Zhou et al., 2008), but other development genes can be involved, such as *PAX6*, *RAX*, *OTX2*, or *FOXE3* (Bardakjian and Schneider, 2011; Chassaing et al., 2014; Plaisancié et al., 2019; Verma and Fitzpatrick, 2007). Overall, there are more than 90 genes reported for MA, however, only a third of MA patients receive a genetic diagnosis, hence the importance to perform genome sequencing to identify new coding and non-coding variants related to MAC (Basharat et al., 2023). MA can present different mode of inheritance, yet most cases are sporadic and monoallelic, while coloboma are usually of autosomal dominant transmission.

1.3.2. Anterior segment dysgenesis

A default of development occurring in the lens placode or at the margins of the OC might result in a rare anomaly comprised in the wide spectrum of anterior segment dysgenesis (ASD). Considering the importance of the anterior segment in the drainage of AH and maintain of intraocular pressure (IOP, *cf* part 1.1.1), it comes to no surprise that ASD is often related to an increased risk of glaucoma (GLC) (Ahmed et al., 2022; Kaushik et al., 2022). As for MAC, the genetic diagnosis is still lacking for many ASD patients, despite the recurrent role *PAX6*, *PITX2* and *FOXC1* (Ahmed et al., 2022; Reis and Semina, 2011), all three encoding TF implicated in iris and CB development (*cf* part 1.2.5). Aniridia, Axenfeld Rieger Syndrome and Peters anomaly are the most common ASD found in association with MAC.

1.3.2.1. Aniridia

Congenital aniridia is characterized by a default of iris development, either with a total absence of any iris tissue, or a slighter defect showing with a strong iris transillumination (Figure 13). Visual acuity might not be directly impacted by the iris default, yet aniridia is often associated with cataract, corneal defect or fovea hypoplasia (Landsend et al., 2021) that result in visual impairment (Edén et al., 2008; Nelson et al., 1984). In this view, aniridia can be considered as a panocular disorder. Its prevalence is estimated to 1.8 per 100.000 live births (Tripathy and Salini, 2023). Interestingly, dominant mutations *PAX6* are known to be related to aniridia (Hingorani

et al., 2012), and considering the non-coding regions of this gene recently revealed that *PAX6* actually accounts for 90% of aniridia cases (Plaisancié et al., 2018). Preventive therapy is needed to hinder the associated ocular defects (Bremond-Gignac, 2019; Landsend et al., 2021), and advances in gene therapy research might give new insights for future treatments of the disease (Gregory-Evans et al., 2014).

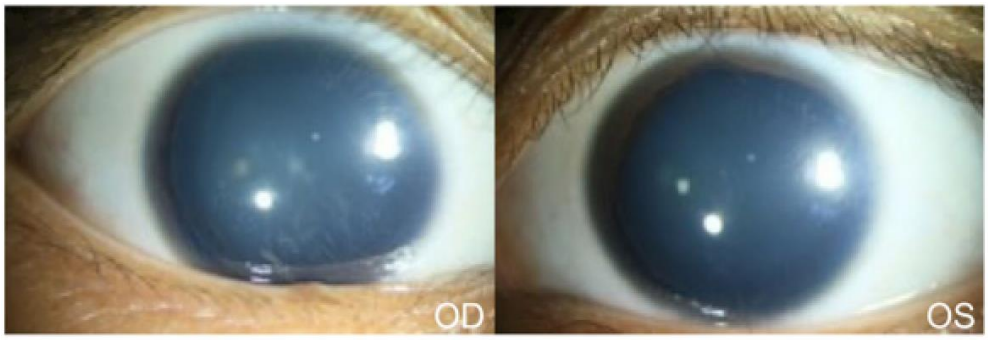

Figure 13. Clinical aspect of aniridia
Photos of a patient affected with bilateral aniridia and displaying peripheral remnants of the iris in both eyes. (Adapted from Li *et al.* in *BMC Ophthalmology*, 2023)

1.3.2.2. Peters' anomaly

Peters' anomaly is another rare dysgenesis characterized by a corneal opacity (Figure 14) and irido-corneal adhesions (Jat and Tripathy, 2023), with an autosomal, dominant and recessive transmission. Affecting 1.5/100.000 newborns (Kurilec and Zaidman, 2014), it is likely due to the late and incomplete detachment of the lens vesicle from the surface ectoderm. It is also often associated with lack of corneal endothelium and cataract. As mentioned above, mutations in *PAX6*, *PITX2* and *FOXC1* are correlated with this anomaly (Arikawa et al., 2010; Doward et al., 1999; Hanson et al., 1994; Honkanen et al., 2003), however there is a high genetic heterogeneity for the disease and only one third of cases have been diagnosed (Chesneau et al., 2022). To cite a few, *CYP1B1*, which encodes the cytochrome P450 1B1 (Vincent et al., 2006), *FOXE3* (Khan et al., 2016), and SOX2 (Chesneau et al., 2022) were also found to be responsible for Peters' anomaly. In its syndromic form caused by mutations in the coding region of *B3GALTL*, Peters plus syndrome, the ocular anomaly is combined with other developmental defects, such as brachydactyly, facial dysmorphisms and short stature (Weh et al., 2014).

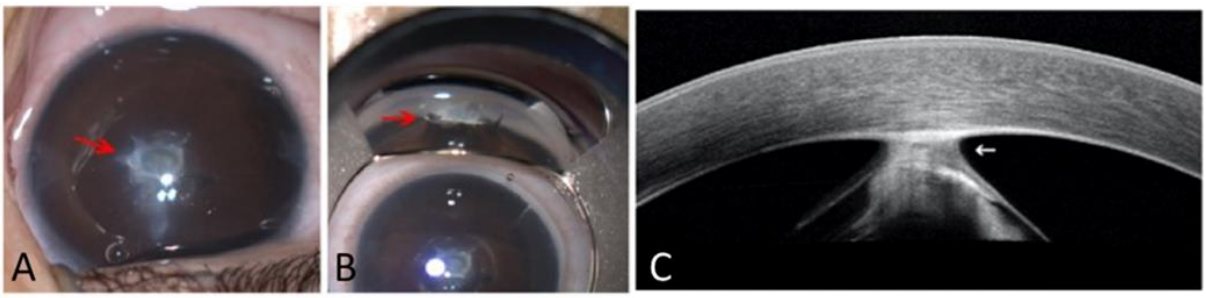

Figure 14. Clinical aspect of Peters anomaly
Picture of the anterior segment (**A**) and view of the gonioscope (**B)** of a patient affected with Peters anomaly with corneal adhesions (red arrows). (**C**) Anterior segment OCT showing typical failure in separation of the lens from the cornea, as shown in white arrow. (Adapted from Li *et al.* in *Eye Vis (Lond)*, 2020 (A,B) and Ramappa *et al.* in *Cornea*, 2022 (C))

1.3.2.3. Axenfeld Rieger syndrome

Axenfeld Rieger syndrome constitutes a spectrum of dysgenesis characterized by abnormalities in the iris (manifested by hypoplasia or polycoria), cornea, and anterior chamber (Figure 15). The Schwalbe line might be abnormal, affecting the AH outflow, and therefore glaucoma is often associated with the disease (Alward, 2000). Estimated prevalence is 1/200.000 (Zamora and Salini, 2023) and some extra-ocular defects have been described: subtle cranio-facial dysmorphism, umbilical, and dental anomalies (Michels and Bohnsack, 2023). Transmission of the disease is autosomal, dominant, and with a strong penetrance. Mutations in *FOXC1* and *PITX2* together account for more than 50% of this syndrome (Reis et al., 2023; Tümer and Bach-Holm, 2009). Interestingly, there is strong correlation between the genotype and the phenotype, as *FOXC1* mutations are often associated with in heart defect and hearing loss (Chrystal et al., 2021; R. Wang et al., 2021; Zhang et al., 2020), while cases carrying *PITX2* mutation usually display umbilical and craniofacial abnormalities (Alward, 2000; Strungaru et al., 2011).

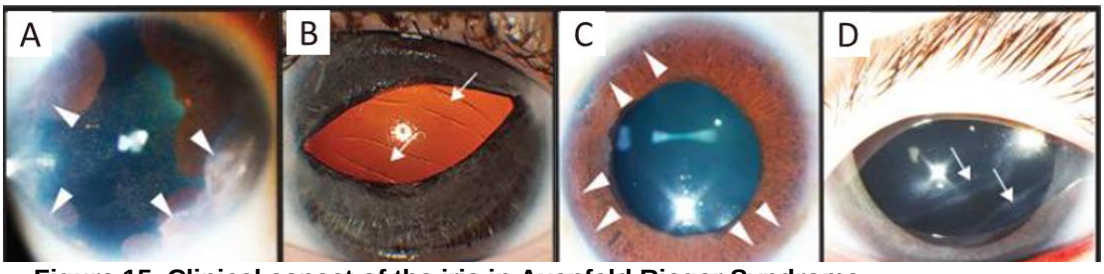

Figure 15. Clinical aspect of the iris in Axenfeld Rieger Syndrome
Anterior segment findings in four patients with Axenfeld Rieger syndrome. The eyes display typical characteristics including displaced pupil (correctopia, **A**, **B**) and anormal Schwalbe line (arrowheads, **A**, **C**). Signs of glaucoma can be seen as Haab's striae in the cornea (arrows, **B**, **D**). (Adapted from Michels and Bohnsack in *Clin Ophthalmol*, 2023)

1.3.2.4. Rare iris defects

Among the diversity of ASD, there exists some extremely rare congenital iris anomalies whose prevalences are estimated to be inferior to 1/1.000.000 live births. Gillespie syndrome is the best example: first described in 1965 by Dr. FD Gillespie (Gillespie, 1965), less than 30 patients have been reported to this day (Nabih et al., 2022). This syndrome is characterized by a partial bilateral aniridia (Figure 16A), cerebellar ataxia, and intellectual disability (De Silva et al., 2018). Mutations in the *ITPR1* gene, coding the inositol 1,4,5-triphosphate receptor type 1, were first described in 2016 (Gerber et al., 2016; McEntagart et al., 2016), and new coding and intronic mutations of the gene have been found in affected patients since (De Silva et al., 2018; Dentici et al., 2017; Keehan et al., 2021). Depending on the localization of the mutation, the transmission is either recessive or dominant (Gerber et al., 2016).

The absence of iris sphincter muscle is the main symptom of congenital mydriasis, a very rare disorder of autosomal dominant inheritance that affects mostly females (Richardson and Schulenburg, 1992). The pupil appear enlarged in both eyes from birth (Figure 16B), which often leads to a misdiagnosis of aniridia (Roulez et al., 2014), yet the pathology might remain undetected (Atik et al., 2014). Most case reports associate congenital mydriasis with extra-ocular features, including brain lesions (Gräf and Jungherr, 2002; Kurtul et al., 2016), hence the importance of recognizing this rare condition. It has been suggested to be part of a smooth muscle dysfunction syndrome, due to mutations in the *ACTA2* (Actin alpha 2) gene (Roulez et al., 2014).

In contrast, congenital miosis, or congenital microcoria (MCOR), is recognized as the complete or partial absence of dilator muscle (Figure 16C), resulting in iris hypoplasia and a small pupil (Holth and Berner, 1923). This extremely rare condition was first described in 1862 (Wilde et al., 1862), and is frequently associated with high myopia (80%) and glaucoma (30%), however no extra-ocular abnormality has ever been noted (Angée et al., 2021; Toulemont et al., 1995). As for mydriasis, microcoria can remain unnoticed by ophthalmologists, yet MCOR should be carefully taken into consideration, due to the increased risk of developing an early-onset GLC. The condition is genetically transmitted with a complete penetrance and an autosomal dominant inheritance, and it is related to submicroscopic deletions in the 13q32.1 chromosomal region (Fares-Taie et al., 2015; Rouillac et al., 1998; Sergouniotis et al., 2017), although one case carrying a deletion in the same region has been described (Pozza et al., 2020), yet the exact etiology of MCOR remains a mystery.

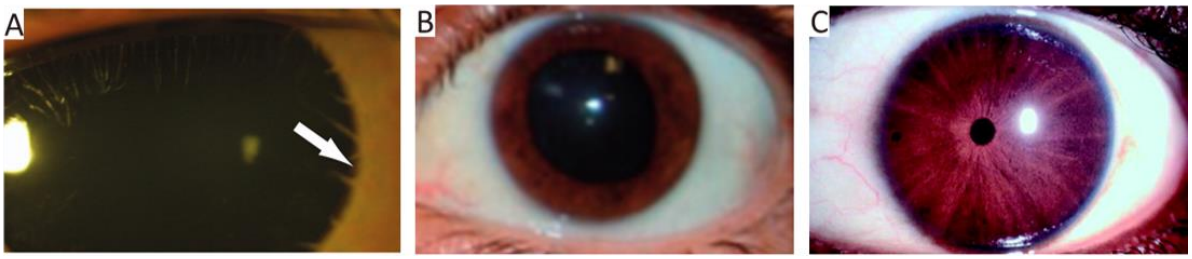

Figure 16. Clinical aspect of different iris defects
(**A**) Iris of a Gillespie syndrome patient displaying scalloped edge of the iris remnant (arrow) and aplasia of the iris central to the collarette. (**B**) Iris of a patient affected with congenital mydriasis, showing a fixed, dilated pupil. (**C**) Iris of a patient with congenital microcoria displaying a pinhole pupil with no dilation upon the use of mydriatics. (Adapted from Hall *et al.* in *Hum Genet*, 2018 (A), Atik *et al.* in *Neuro-Ophthalmology*, 2014 (B) and Bremner *et al.* in *Br J Ophthalmol*, 2004)

1.3.2.5. Congenital glaucoma

Congenital glaucoma (Figure 17) is a serious eye condition that occurs in infants and young children with an incidence of about 1 in 10.000 live birth. It is characterized by increased IOP due to a malformation in the eye's drainage system, which prevents the normal outflow of aqueous humor (AH). It's important to note that congenital GLC is a distinct condition from primary open-angle glaucoma (POAG), which typically occurs in adults are not malformative, and developmental GLC that are secondary to most forms of ASD. Symptoms of congenital GLC can include excessive tearing, photophobia, cloudy or enlarged cornea, and in more severe cases, the enlargement of the eyeball (Karaconji et al., 2022; Kaur and Gurnani, 2023).

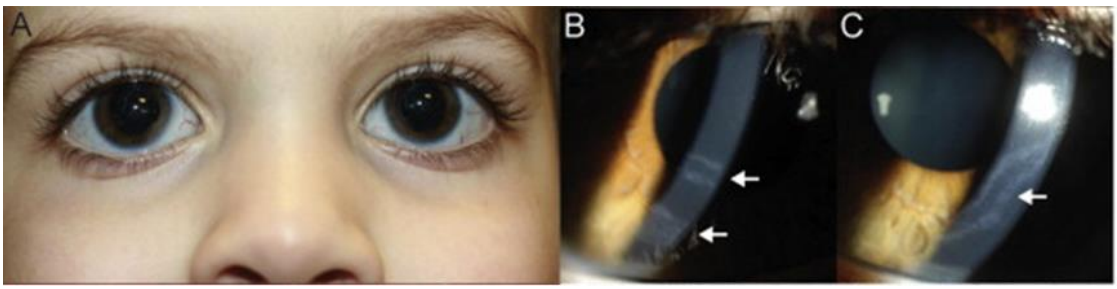

Figure 17. Clinical aspect of primary congenital glaucoma
(**A**) Picture of a young patient displaying prominence of both eyes due to an increase IOP. Slit-lamp examination of right (**B**) and left (**C**) eyes shows Haab's striae (arrows), characteristic of glaucomatous damages in the corneal endothelium. (Adapted from Yonekawa *et al.* in *The Journal of Pediatrics* ,2013)

Early diagnosis and treatment are crucial for managing congenital GLC. If left untreated, the increased IOP can lead to optic nerve (ON) damage and irreversible vision loss. With prompt intervention, many children with congenital GLC can maintain good vision. Treatment of congenital GLC aims to reduce IOP and prevent further damage to the ON. This is typically achieved through surgical procedures, such as

trabeculotomy or goniotomy, which create a new drainage pathway for AH (Mocan et al., 2019). However, even after successful treatment, individuals with congenital glaucoma often require lifelong monitoring and periodic follow-up appointments with an ophthalmologist to ensure that their condition is well-managed.

Congenital glaucoma is typically present at birth or becomes noticeable during the first few years of life. The exact age of onset can vary. The primary cause of congenital glaucoma is a developmental abnormality in the eye's drainage structures, specifically the trabecular meshwork (TM). This can be due to genetic factors or it may occur spontaneously. Mutations in *CYP1B1* and *LTBP2* (latent TFG beta binding protein 2), both involved in the development of the TM, are frequently reported (Haddad et al., 2021; Mocan et al., 2019). Most cases are sporadic, but when inherited, transmission is usually autosomal dominant (Wang and Wiggs, 2014).

1.3.3. A word on retinal dystrophies

Inherited retinal dystrophies (IRDs) affect approximately 1 in 3000 patients and are major causes of severe visual deficiency in children. They encompass a wide range of clinically and genetically heterogeneous disorders in which rod and/or cone photoreceptors degenerate in a diffuse or regional manner, resulting in varying degrees of visual impairment.

The functions involved in these disorders are highly variable and include photoreceptor cell development as demonstrated by the involvement in pediatric forms of these diseases of *CRX*, *NRL*, *NR2E3*, *OTX2*, *VSX2* (Biswas et al., 2021; Littink et al., 2018) and even *CEP290* that plays a crucial role in development of the photoreceptors outer segment (Gerard et al., 2012). Whether the degeneration is secondary to a developmental defect or a role of the genes in the homeostasis of photoreceptor cells is open to debate.

1.4. Importance of non-coding DNA in gene regulation

As mentioned above, many ocular defects are caused by mutations in genes involved in the eye development, but most patients remain without any genetic diagnosis after analysis of gene panels. Despite the possibility to discover new gene performing whole-exome sequencing (Holt et al., 2019), it is more than likely that many undiagnosed cases carry mutations in the non-coding sequence of genes already included in existing panels (Haug et al., 2021; Patel et al., 2018). In this view, it seems particularly important to focus the research on this huge part of DNA.

1.4.1. Definition

Non-coding DNA, formerly called *junk DNA*, corresponds to the 99% of all DNA that isn't coding a protein. Therefore, this definition comprises many different types of DNA that can be classified in four categories, listed below.

Firstly, all the regions that will be excluded from messenger RNA (mRNA) after maturation are part of the non-coding genome. Indeed, precursor mRNAs (pre-mRNA) are transcribed from a protein-coding gene, and undergo many steps of maturation before reaching the state of a mRNA ready to be translated into a protein. This maturation process consists of a capping of the 5' region, poly-adenylation at the 3' end of the RNA, and most importantly, splicing of the intronic region. The importance of splicing in protein production is now common knowledge, and intronic mutations are very well-documented (Love et al., 2023; Rogalska et al., 2023).

DNA transcribed into a special kind of RNA is also considered non-coding as the RNA is not meant to undergo the translation process. This category comprises transfer and ribosomal RNAs (tRNA, rRNA) that are required in protein production to transfer amino acids to the ribosome; and micro-RNAs (miRNA) and long non coding RNAs (lncRNA), which regulates protein production by blocking the recruitment of the ribosome. Well known for their role in cancer (Ratti et al., 2020), some of these miRNAs have been linked to retinal defects (Conte et al., 2015; Xu, 2015).

Repeated DNA sequences, constituting satellite DNA, is part of the structural elements of the chromosomes. These non-coding sequences are abundant in the telomeres, centromeres, and heterochromatin (Thakur et al., 2021), but can also be found throughout the euchromatin (Ugarković et al., 2022).

Finally, non-coding DNA comprises all the sequence elements involved in the gene regulation. These transcriptional regulatory elements are highly heterogenous in size, function and location, and alteration of these regions can be severely deleterious. Here, I will focus on this vast kind on non-coding DNA, after a brief description of the global transcription regulation process in eukaryotes.

1.4.2. Transcription and gene regulation

Control of gene expression is driven by regulation of transcription through various mechanisms determining when, where, and to how the gene is transcribed. The first factor to take into account is the chromatin accessibility, as determined by its level of compaction and histone marks (Figure 18). If a gene is accessible, transcription can be initiated (Cramer, 2019; Lenstra et al., 2016).

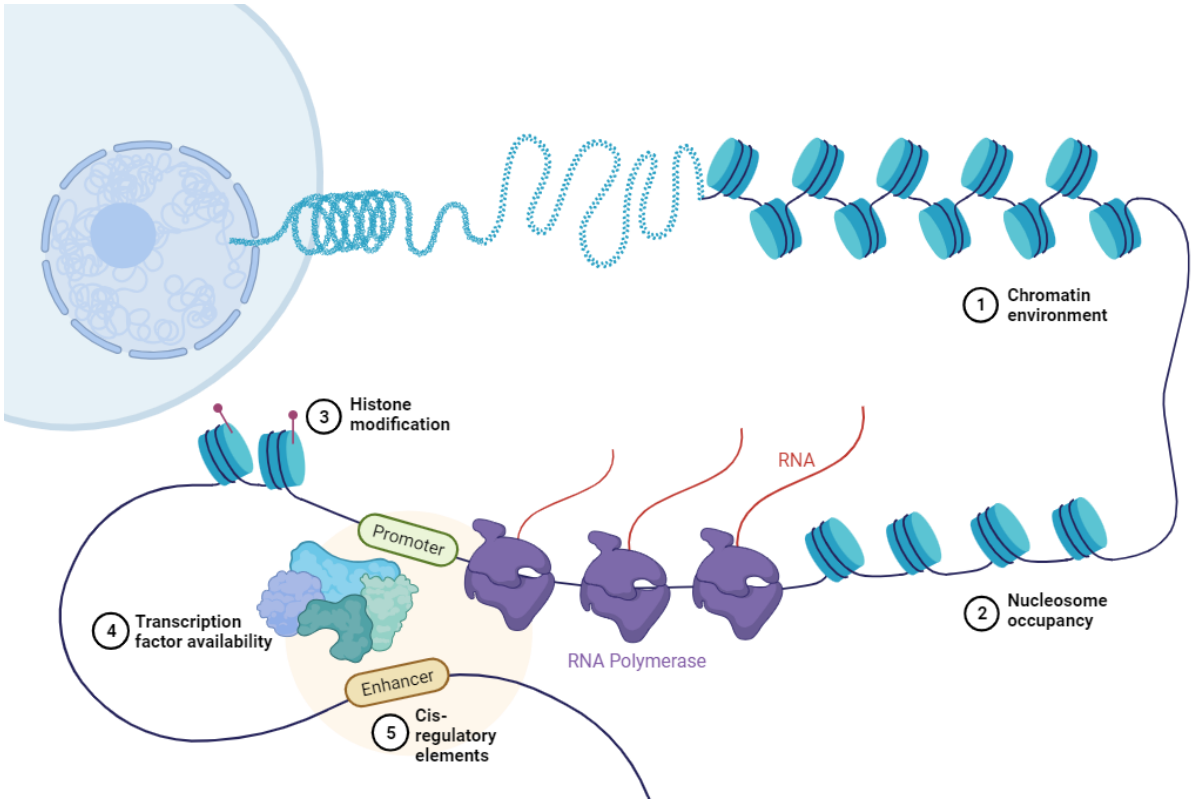

Figure 18. Regulation of transcription in eukaryotic cells
Cell identity and function is determined by precise regulation of gene transcription. This process is regulated at different levels in the nucleus of eukaryotic cells. Transcription is carried out by RNA polymerase enzymes and regulated by chromatin environment, nucleosome occupancy, histone modifications, transcription factor availability, and regulatory elements. Reprinted from “Regulation of Transcription in Eukaryotic Cells”, by BioRender.com (2023) and created by Biljana Atanasovka.

In eukaryotes, the mRNA production starts with the binding of the RNA polymerase II to a specific DNA region, namely the promoter sequence. The RNA polymerase, along with accessory proteins, forms a transcription preinitiation complex (PIC) at the promoter (Farnung and Vos, 2022). Promoters are typically found upstream of the gene being transcribed, usually found within a few hundred base pair (bp) of the transcription start site, *ie* the first transcribed codon. The most common promoter element is the TATA box (TATAAA sequence), although other kinds of sequence can be found.

Transcription regulation involves different kinds of cis-regulatory elements (CREs), such as TF, proteins that bind to promoter and enhancer regions. TFs can be activators or repressors, depending on their effects on gene expression. Transcription activators enhance gene expression by promoting the assembly of the PIC and RNA polymerase binding to the promoter. They often interact with enhancer elements. On the contrary, repressors inhibit gene expression by preventing RNA polymerase from binding the promoter or by blocking the activity of activators, and they may interact with silencer elements.

Enhancers and silencers are DNA sequences that can be located upstream, downstream, or even within the gene they regulate (Dean et al., 2021; Panigrahi and O'Malley, 2021; Plank and Dean, 2014). They can be located quite far from the gene they modulate, sometimes up to hundreds of thousands of bp away. Once the enhancer-bound TFs interact with the gene's promoter, they recruit coactivator proteins which facilitate the assembly of the PIC at the promoter. Enhancers often regulate gene expression in a cell type-specific or context-dependent manner. Activation of an enhancer, also described as enhancer priming, can is determined by histone modifications (Wang et al., 2016). Multiple enhancers can regulate the same gene, and a single enhancer can regulate multiple genes. The same applies for silencers, which can also compete with enhancers, creating a balance that determines the level of a gene's expression. This, along with the presence or absence of particular TFs, contributes to the unique gene expression profiles of different cell types and the dynamic regulation of genes during development.

1.4.3. Topologically associated domains

When in its euchromatin state, DNA can physically interact with itself within the cell's nucleus. These interactions play a crucial role in shaping the 3D structure of the genome and regulating gene expression. Topologically-associated domains (TADs, Figure 19A) are large-scale chromatin structures that define the 3D organization of the genome. They represent self-interacting genomic regions with a higher frequency of internal DNA-DNA interactions compared to interactions with regions outside the TAD, as determined by cutting-edge techniques such as chromosome conformation capture (3C) sequencing (Tanizawa and Noma, 2012). TADs serve as structural and functional units within the genome and play a critical role in gene regulation and are relatively conserved across cell types and species (McArthur and Capra, 2021). TAD boundaries act as insulators, preventing interactions between neighboring domains. This insulation helps maintain the independence of regulatory interactions within each TAD and ensures that enhancers primarily interact with genes located within the same TAD (Acemel and Lupiáñez, 2023; Zheng and Xie, 2019).

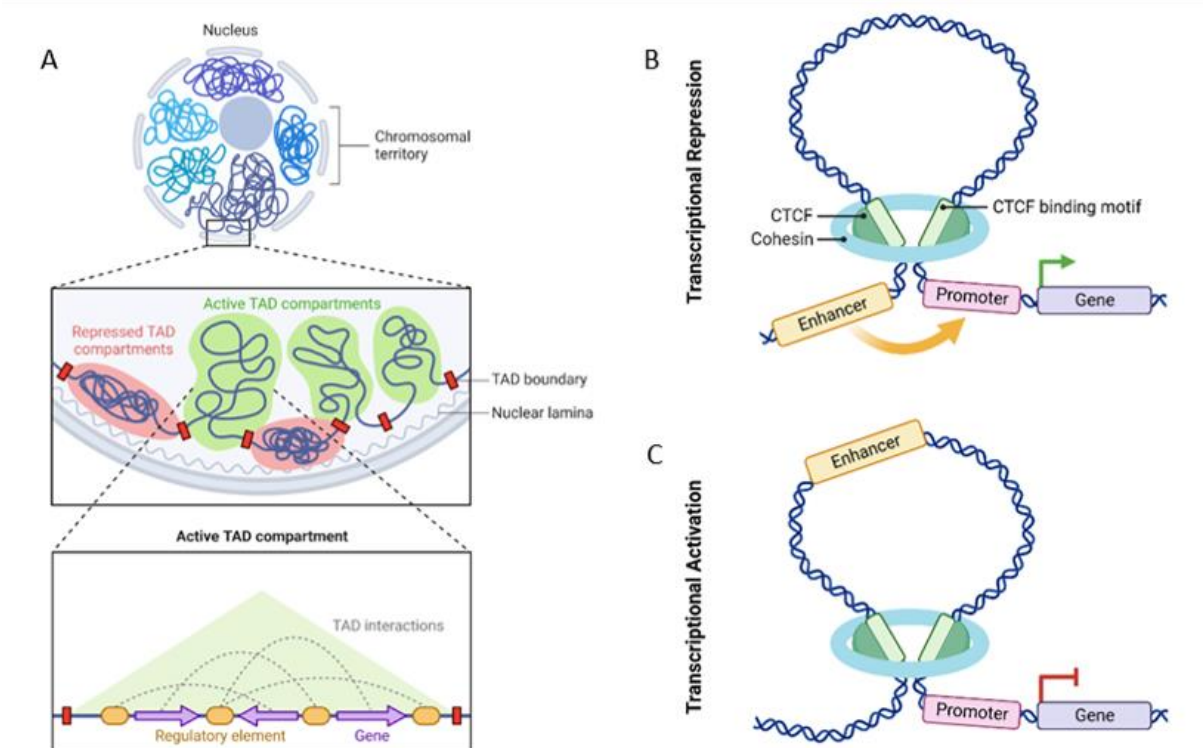

Figure 19. 3D organization of the chromatin.
(**A**) Euchromatin in the nucleus is spatially organized in compartments called TAD, in which DNA interacts with itself to regulate gene expression. These TADs are delimitated by boundaries containing CTCF elements. (**B**) and (**C**) represents the function of CTCF sites and cohesin in DNA loop. (Adapted from templates available at Biorender.com (2023): "Chromosome Organization in Nucleus – TAD" created by Eunice Huang (A) and "Transcriptional Regulation by CTCF and Cohesin" (B,C))

These boundaries contain an insulator element that often corresponds to a CTCF (CCCTC-binding factor) binding motif sequence. This protein acts in tandem to recruit a cohesin ring, thus creating a chromatin loop (Cuylen and Haering, 2010; Kim et al., 2015; Matharu and Ahituv, 2015). This phenomenon brings distant genomic regions into close spatial proximity. Looping interactions can facilitate gene regulation by allowing enhancers, silencers, and other regulatory elements to come into contact with their target genes (Figure 19B), and they can also repress transcription by preventing an enhancer to reach its target promoter (Figure 19C).

1.4.4. Non coding variant and associated pathologies

Gene regulation is an intricate process that requires the action of many elements. As a consequence, a single nucleotide variant (SNV) in one of these many elements can totally modify the expression pattern of one gene, and potentially to severe developmental defects. The most striking example is the *PAX6* gene, whose regulating elements are well-described. Mutations in one of these has been ascribed to aniridia (Bhatia et al., 2013). In some cases of Axenfeld-Rieger syndrome, a deletion of a CRE nearby the *PITX2* gene has been identified (Volkmann et al., 2011).

Recent studies further revealed new variants in cCREs that negatively affect their activity. The emergence of these variants led to the new definition of enhanceropathies. Among them, the rare North Carolina macular dystrophy, has been linked to SNVs in the enhancer region of the *PRDM13* (Green et al., 2021; Van de Sompele et al., 2022). Structural variants (SVs) are also often reported in these enhanceropathies (Figure 20A): deletions located in the distal enhancer of *ATOH7* results in defaults of the retinal development (Ghiasvand et al., 2011).

In pigs, the loss of a MITF isoform due to an ectopic silencer has been reported (Chen et al., 2016), showing that non-coding variants are able to open new regulation pathways. Mutations or structural variations that affect TAD boundaries can lead to aberrant gene regulation (Figure 20B), resulting in malformation syndromes (Lupiáñez et al., 2015; Tiukacheva et al., 2023). For instance, cases of Retinitis Pigmentosa have been ascribed to several SVs creating a new TAD, and ectopic genetic interactions within it, thus causing the overexpression of *GDP1* (Guanosine Diphosphatase 1) in the retina (de Bruijn et al., 2020).

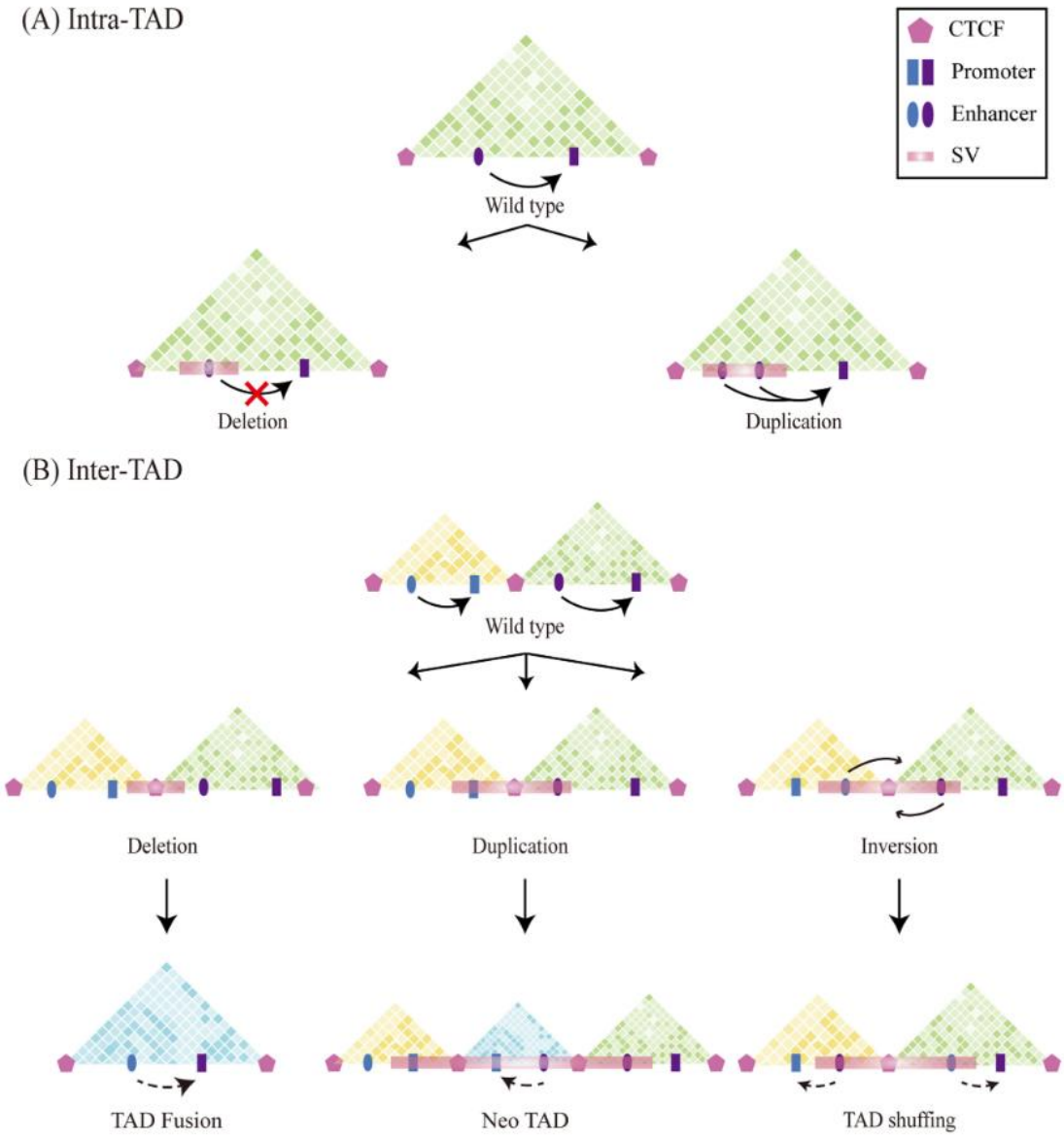

Figure 20. Different mechanisms of TAD disruption and their effect on gene expression
(**A**) Deletions or duplications of sequences within Topologically Associated Domains (TADs) primarily disrupt regulatory processes by changing the count of enhancers, resulting in aberrant expression of target genes. (**B**) Sequence deletions at the boundaries merge adjacent TADs into a new TAD, known as "TAD fusion." DNA sequence duplications at these boundaries can create a "neo-TAD" between the original TADs, where enhancers and promoters from different TADs interact independently, called "neo-TAD formation." Chromosomal inversions between adjacent TADs reposition genes and regulatory elements, leading to pathological effects referred to as "TAD shuffling.". (Reprinted from Liu *et al.* in *MedComm*, 2023)

1.5. Models of study

Again, the eye is a complex organ and ophthalmology research field require the use of a good model to reproduce its intricacy. To date, there is no perfect model to properly study ocular disease and their genetics, but in general, the use of one or more of the existing models is sufficient to characterize a pathology. This part describes the main animal and cellular models frequently used in ocular research.

1.5.1. Animals as *in vivo* models

As Metazoa evolved into plenty of complex organisms, different types of visual organs appeared. Most animals possess photoreceptor cells, with the only exception of sponges and placozoans, but high-resolution vision is specific to vertebrates, cephalopods, and arthropods, which possess either compound or camera eyes (Figure 21). These complexified organs appeared around 540 Million years ago and contain the main elements allowing focused vision through the presence of a lens, though they are much smaller in compound eyes (Nilsson, 2013).

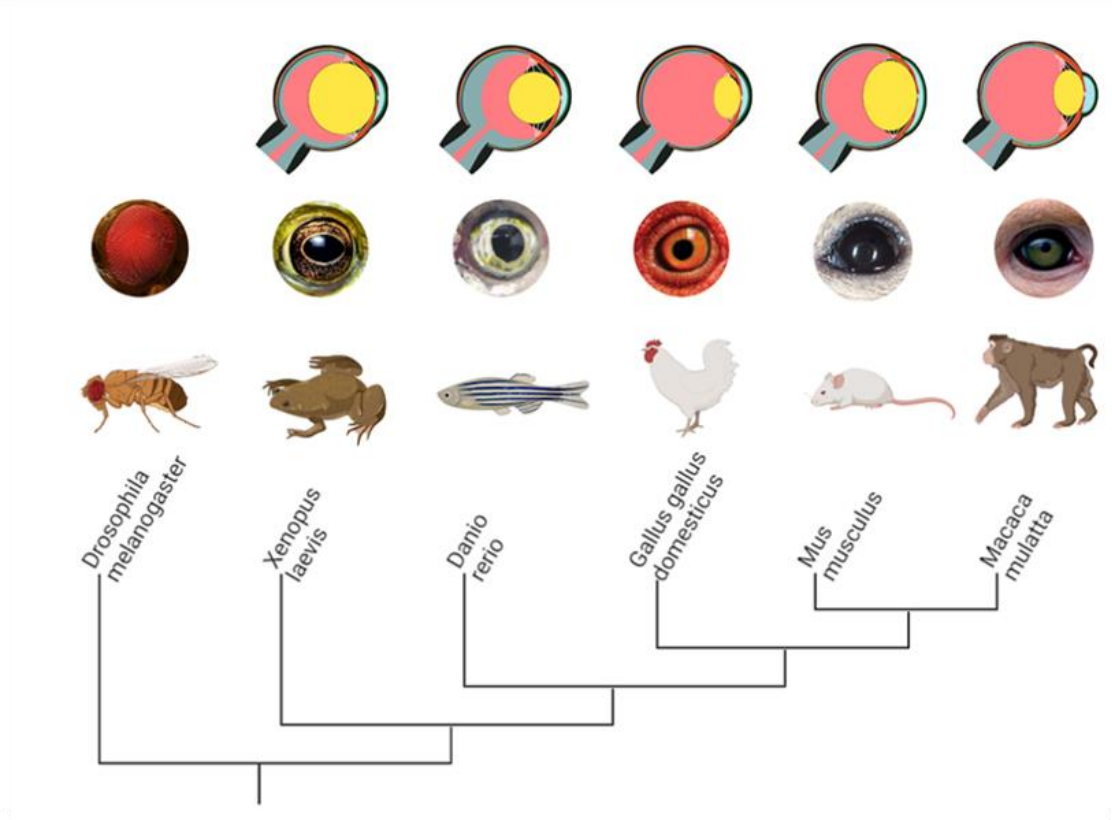

Figure 21. Phylogenetic tree of listed animals and comparison of their eyes
This tree represents the global evolution of the vertebrate eye, with visualization of each model frequently used in the field of ocular research. (Created with Biorender and adapted from Harding *et al.*, in *Ther Adv Rare Dis*, 2021)

1.5.1.1. Insects

Fruit flies (*Drosophila melanogaster*) have been invaluable in studying various aspects of genetics, development, and diseases, including ocular research. Due to their well-characterized genome, easily manipulatable genes, and short life cycle, Drosophila are particularly easy to study for researchers. Many of the genes and signaling pathways involved in development are evolutionarily conserved.

Drosophila eyes are compound, which is typical of most arthropods and specifically insects. Compound eyes are made up of thousands of individual units, each containing a cluster of photoreceptor, support and pigment cells. Though relatively simple compared to human eyes, Drosophila eyes share fundamental principles of eye development, yet they constitute a simplified model for studying eye development and function, such as photoreceptors differentiation, eye patterning and visual signal processing (Baker et al., 2014; Weasner et al., 2004).

1.5.1.2. Amphibians and fish

African clawed frog (*Xenopus laevis*) and zebrafish (*Danio rerio*) are two other commonly used animal models in ocular research. Their eyes are of the camera type, therefore they present much more structural similarities with the human eye. Both species present unique advantages in studying the eye development and can be easily genetically modified (Richardson et al., 2017).

Xenopus embryos are large, easily accessible, and develop rapidly, making them ideal for studying early eye development. Like zebrafish, they have transparent embryos, enabling to observe the development of the eye in real-time. The two organisms also have the ability to regenerate tissues, including the eye and damaged retinal tissue, which is of great interest in studying tissue repair mechanisms and retinal regeneration (Kha et al., 2019; Tseng, 2017). Zebrafish also exhibit visual behaviors that can be analyzed to assess visual function and responses to visual stimuli (Fadool and Dowling, 2008; Glass and Dahm, 2004).

1.5.1.3. Birds

The domestic chicken (*Gallus gallus domesticus*) is another valuable model organism used in various fields of biological research, including eye research (Wisely et al., 2017). Chick eyes share many structural and functional similarities with human eyes; for example, the chick retina contains rods and cones, and a fovea-like area,

similar to the human macula, and their iris possesses the two antagonist muscles found in human iris (Trejo-Reveles et al., 2018). Chicks have relatively large eyes compared to other commonly used model organisms. This large eye size makes it advantageous for studying various aspects of anatomy and physiology, and allows for *ex vivo* experimental setup (Shirazi Fard et al., 2015).

Chick embryos develop externally in eggs, which allows easy access and manipulation of developing eyes at specific stages of embryogenesis. Lens development in chick embryos has been deeply studied and characterized, making them suitable for cataract research (Li et al., 2021). Chick models have also been used to explore retinal development, degeneration and regeneration (Adler, 2000).

1.5.1.4. Mammals

Finally, rodents' mammalian eyes are highly similar to ours. Mice models are commonly used in the field of eye research, as they are easy to manage and manipulate. Therefore, their global development is very well documented (Wong et al., 2015). The main differences are the size of the lens, which takes up almost all vitreous space in rodents (Figure 22), and the photoreceptors: as nocturnal animals, mice have a reduced number of cones, and no fovea. They also possess only two types of cones, making them red-blind (Chang, 2013).

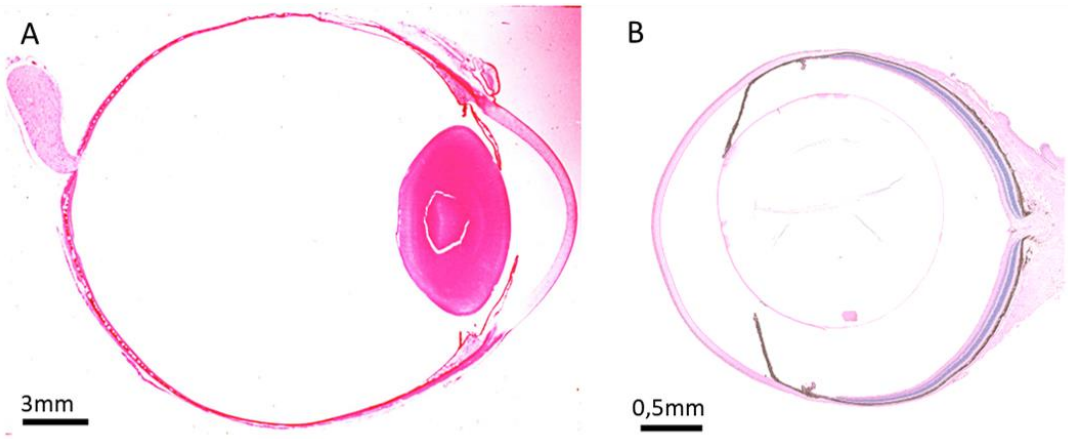

Figure 22. Comparative histological section of a human and a mouse eye
Though the global structure remains similar between the two species, it appears clearly that the anterior segment displays different features. The human lens (**A**) is small and ellipsoidal, while the mouse lens (**B**) is bigger in proportion to the globe size, and spherical. The global shape of the mouse eye is also rounder, and the anterior chamber is less prominent.

It is interesting to note that some bigger mammals, such as dogs, cattle, and even primates (Freddo, 1984), are also of high interest in the genetic field, and so some species might have been used to study ocular defects, whether to put them in parallel with human common diseases, as basic research work, or to better understand and treat their pathologies. In particular, many dog breeds are affected with specific ocular disorders, as for Beagle dogs, which frequently suffer from congenital stationary blindness. Therefore, this common breed constitutes a natural study model for the disease, and is often used in laboratories (Oh et al., 2018).

1.5.2. *In vitro* approaches

In recent years, many ethical questions have arisen from the use of animals in research. Therefore, complementary models have been designed to replace needed animals and reduce their numbers. In the field of ocular research, many cancerous cell lines have existed for a long time, and some are of common use today. These commercialized lines derive from samples collected in patients affected with uveal melanoma (*eg* OCM1, OCM3, MUM2B (Griewank et al., 2012)), retinoblastoma (*eg* Y79, RB355, RB166 (Madreperla et al., 1991)) or sarcoma (neuronal Schwann cell). However primary cell culture is always preferred, as they offer a more accurate model than cell lines, although their harvest might represent a great challenge.

1.5.2.1. Anterior segment

Lens epithelium and corneal layers (epithelium, endothelium and stroma) are quite easy to dissect and often used in cell culture. These primary cells are of high importance in the understanding the proteins involved in their development (Ibaraki et al., 1998) and the common pathologies of those tissues, such as cataract formation (Reddy et al., 1988), keratoconus (Sharif et al., 2019) and corneal fibrosis (Karamichos et al., 2010). A great work has also been performed on the cultivation of TM cells. The methods of collection and harvest of those cells have been perfected through years (Johnson and Tschumper, 1986), to design a model that fits the biological reality of this complex tissue (Keller et al., 2018; Yemanyi et al., 2020). Human TM primary cells are a great tool to study the deposition of extracellular matrix (ECM) *in vitro*, and get a better understanding of the etiology of glaucoma (Raghunathan et al., 2023).

Iris epithelium, however, is more delicate to obtain due to the tight junctions maintaining all layers together. First attempts to cultivate human iris epithelium started sixty years ago (Tenenbaum and Kornblueth, 1958), but it took decades for the methods to be perfected to harvest pure epithelium cells (Hu et al., 1992; Tang et al., 2014). However, obtaining clonal cell lines from primary cells remains a great challenge to this day (Johnen et al., 2011), and therefore limits the use of these cells, their immortalization often emerging as the best solution.

1.5.2.2. Retina

Due to their embryonic origin that makes them weakly attached to both the NR and the choroid, RPE cells are easy to dissect without any contamination of neighbouring tissue. Harvesting cells from the RPE of different species is possible and well-documented, although a commercial cell line, immortalized by telomerase reverse transcriptase (hTERT-RPE1, ATCC), is available. These cells are widely used in research to get a better understanding of many ocular retinal disease, such as age-related macular degeneration, from a difficultly accessible tissue (Fronk and Vargis, 2016). However, neuroretina is particularly hard to study *in vitro*, due to the various cell types that compose it. Despite the possibility to study retinal ciliopathies with the use of mice cones cell line 661W (Wheway et al., 2019) or fibroblast producing cilia under stress conditions to mimic photoreceptors cells (Gerard et al., 2012; Shimada et al., 2017), these models do not allow a global of the functioning of the retina, thus forcing researchers to develop more elaborate models.

1.5.2.3. Three-Dimensional models

More recently, new models have been designed to improve conventional cell culture in two dimensions. 3D organoids constitute a simplified version of an organ and the most accurate *in vitro* human model to this day. Early on, embryonic stem cells (ESc) were used to study the formation of human optic cup (Eiraku et al., 2011), but the recent discovery of induced pluripotent stem cells (IPSc) improved the method, allowing the use of patients cells to study a specific pathology (Boutin et al., 2019; Gupta et al., 2023). Optic cup and retinal organoids (Figure 23) can be harvested and provide a strong model to understand the first developmental stages of the eye (O'Hara-Wright and Gonzalez-Cordero, 2020), and develop therapies for retinal diseases (Parfitt et al., 2016).

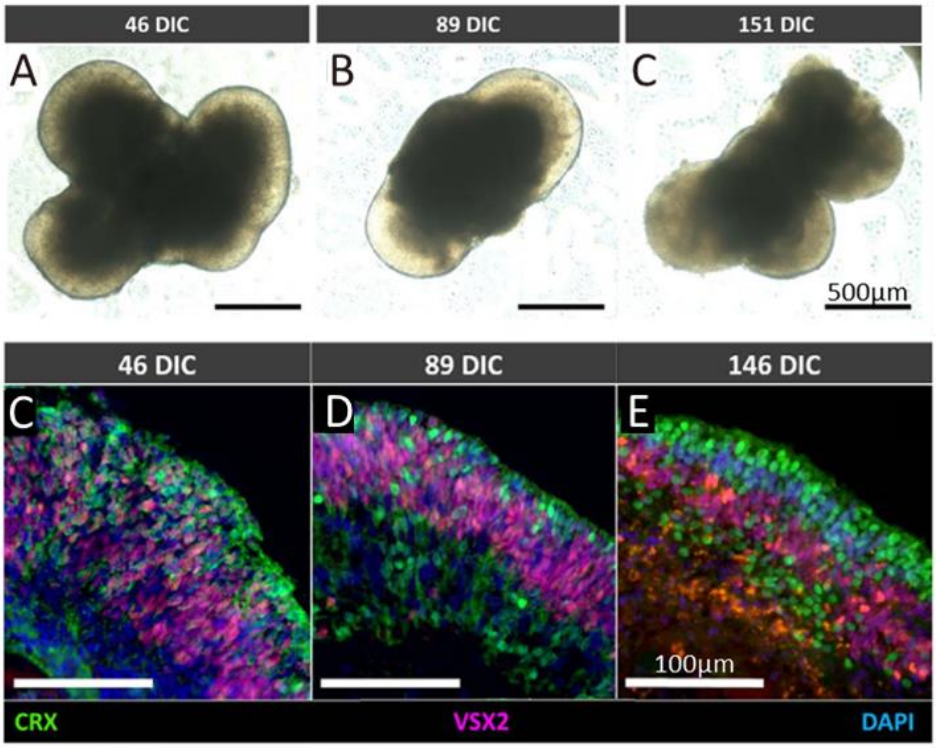

Figure 23. Example of retinal organoids derived from human embryonic stem cells
(**A-C**) Phase contrast microscopy of hESC-derived retinal organoids at different times of cultivation, showing limited microstructural details. (**D-F**) Immunofluorescence staining of retinal markers demonstrating a primitive, yet good organization of the retinal layers in these hESC-derived organoids. (Adapted from Browne *et al.* in *Retinal Cell Biology*, 2017) **DIC**: Days in culture.

Some 3D models of the eye anterior segment have also been designed using cell aggregates from animal ocular tissues. The creation of a 3D *in vitro* lens allowed studies on the regenerative process of IPE cells from newt irises (Hoffmann et al., 2014), and recent techniques of 3D TM culture might open new insight in understanding the etiology of glaucoma.

Although these methods offer new perspectives on fundamental studies and drug testing, respecting the ethical view of animal experimentation, they are still incomplete and fail to entirely reproduce the accurate organ and its environment. Notably, optic cups organoids lack the POM that is necessary for the formation of anterior eye elements, and are therefore restricted to the earliest stages of development. Organoids are also very restrictive and constitute a very expensive technique for most laboratories, both in time and money, therefore their use is still not widely spread, though they remain a good model to complete *in vivo* studies.

Objectives

Ocular malformations can severely impact vision, in particular when associated with an early onset glaucoma (GLC) that require a lifelong treatment to avoid blindness. Understanding the molecular basis of these defects seems essential to provide better diagnostic and counseling for the patients. The work presented here aimed to resolve the molecular etiology and physiopathology of ocular malformations affecting various developmental stages and includes:

I. Deciphering the molecular mechanisms underlying congenital microcoria through:
   - conducting a comprehensive review encompassing both the clinical and genetic aspects of MCOR
   - Describing the phenotype of the mouse model
   - Investigating the link between MCOR and GLC
   - Unraveling the molecular mechanisms of a disrupted TAD

II. Characterizing a candidate non-coding variant in a case of complex microphthalmia by:
   - Creating a *Foxe3* Knock-out mouse model
   - Studying the molecular phenotype of the mouse model
   - Discovering new TFs implicated in microphthalmia

III. Describing the genetic architecture of pediatric retinal diseases in Chile and identifying new causal genes, using:
   - High throughput DNA sequencing
   - Functional validation

Part I: Deciphering the molecular mechanisms underlying congenital microcoria

2.1. Review of the literature (First Publication)

The COVID-19 pandemic led to a national lockdown requiring the cessation of all experimental work in 2020. In this exceptional context, we decided to assemble all available data from the literature reporting isolated congenital miosis cases to provide the first review ever on this disease since its original description in 1862. The objective of this work, aside from providing the first comprehensive work on this subject, was to find leads to explain the etiology of glaucoma (GLC) and myopia, both frequently associated with the iris condition. We gathered all information from a total of 122 patients, described across 37 papers published between 1862 and 2020. Of note: publications reporting Pierson syndrome cases were excluded from this survey, as this syndrome associates renal defects to the pupillary default. We extracted all accessible data on patients, with a great attention drawn to the refraction error, the age of onset of GLC, the intraocular pressure (IOP), and whenever available, the histology of the iridocorneal angle.

This review offers a comprehensive survey of dilator muscle anomalies, as well as other associated features and explores their interconnections. This survey supports the following findings:

- The dilator muscle exhibits diverse anomalies among patients, ranging from well-developed muscle patches to the absence of myofibrils.
- Immaturity of the chamber angle, iridocorneal spicules, and a high insertion of the iris root into the scleral spur are nearly constant findings.
- The disease is significantly associated with refractive errors, including astigmatism and high myopia.
- High-pressure juvenile open-angle glaucoma develops in approximately half of myopic individuals, with those who develop GLC exhibiting higher levels of myopia compared to those who do not.

- Individuals with no chamber angle immaturity (only a few reported cases) seem to have no -or a lower risk of- developing GLC.

- All tested individuals bear structural variations on the 13q32.1 locus, and the size of these variations does not impact the presentation of the disease. The variations include both deletions and a reciprocal duplication of the locus region supporting a disease mechanism that involves deregulation of the 3D regulatory architecture of the region.

Together, these findings demonstrate substantial variability of disease expression. It suggests that chamber angle anomalies and high axial myopia may play a role in occurrence of GLC which itself influence myopia severity, but they are not the sole factors. The observed variability in both clinical features and dilator muscle anomalies within the tissue together suggests the involvement of stochastic processes in addition to genetic and malformative factors in the etiology.

This review was published in Genes in April 2021.

genes

MDPI

Review

Congenital Microcoria: Clinical Features and Molecular Genetics

Clémentine Angée, Brigitte Nedelec, Elisa Erjavec, Jean-Michel Rozet and Lucas Fares Taie *

Laboratory of Genetics in Ophthalmology (LGO), INSERM UMR1163, Institute of Genetic Diseases, Imagine and Paris Descartes University, 75015 Paris, France; clementine.angee@institutimagine.org (C.A.); brigitte.nedelec@inserm.fr (B.N.); elisa.erjavec@institutimagine.org (E.E.); jean-michel.rozet@inserm.fr (J.-M.R.)
* Correspondence: lucas.fares-taie@inserm.fr

Abstract: Iris integrity is required to regulate both the amount of light reaching the retina and intraocular pressure (IOP), with elevated IOP being a major risk factor for glaucoma. Congenital microcoria (MCOR) is an extremely rare, autosomal dominant disease affecting iris development and hindering both of these functions. It is characterized by absent or underdeveloped dilator muscle fibers and immaturity of the iridocorneal angle—where the aqueous humor is drained—which play a central role in IOP regulation. The dilator muscle anomaly is manifested in pinhole pupils (<2 mm) and thin transilluminable irises, causing both hemeralopia and photoaversion. Axial myopia and juvenile open-angle glaucoma are very frequent (80% and 30% of all cases, respectively). It has been suggested that the immaturity of the chamber angle contributes to glaucoma, and myopia has been ascribed to photoaversion and elevated IOP. Though possible, these mechanisms are insufficient. The disease has been tied to chromosome 13q32.1 structural variations. In addition to compromising iris development, modification of the 13q32.1 architecture could alter signaling pathways for axial ocular length and IOP regulation. Here, we summarize the clinical, histological, and molecular features of this disease, and we discuss the possible etiology of associated anomalies.

Keywords: congenital microcoria; congenital miosis; dilator muscle; glaucoma; myopia; chromosome 13q32.1 structural variants

Citation: Angée, C.; Nedelec, B.; Erjavec, E.; Rozet, J.-M.; Fares Taie, L. Congenital Microcoria: Clinical Features and Molecular Genetics. *Genes* **2021**, *12*, 624. https://doi.org/10.3390/genes12050624

Received: 10 March 2021
Accepted: 19 April 2021
Published: 22 April 2021

1. Introduction

The iris (Figures 1 and 2) is a flat ring-shaped ocular membrane located between the cornea and the lens. Its root is attached to the corneoscleral junction on the anterior side and the ciliary body on the posterior side, next to the lens, and its center is perforated to form the pupil. The iris is composed of a stroma, bilayer epithelium, and two smooth muscles that work in opposition to adapt the pupil aperture to light intensity [1]. The circular sphincter muscle lies within the stroma, near the pupil margin, and can constrict the pupil in miosis [2]. The dilator muscle extends longitudinally within the stroma, from the iris root to below the midpoint of the sphincter [3], and can contract to expand the pupillary aperture in mydriasis [1]. The dilator muscle originates from the anterior iris epithelium, composed of a single layer of myoepithelial cells, the basal portion of which consists in elongated smooth muscle processes [4]. The ciliary body is an extension of the iris, with which it is continuous. It produces a fluid known as aqueous humor that provides nourishment to eye structures. The aqueous humor flows between the iris and lens, through the pupil to the anterior part of the iris, where it is drained through the trabecular meshwork (TM), a sieve-like structure lying at the juncture of the corneoscleral region with the iris periphery [1]. Aqueous humor drainage is required to regulate IOP, which, when elevated, is a major risk factor for optic nerve damage (glaucoma) [5,6].

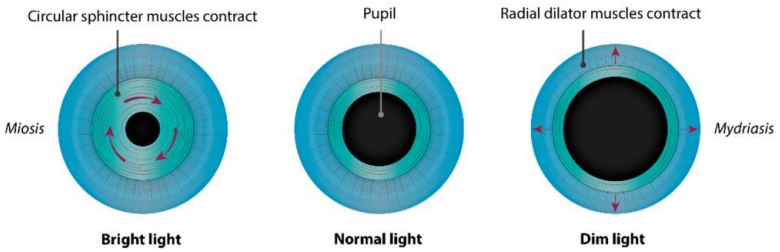

Figure 1. Muscles of the iris and adaptation of pupil aperture to light intensity. The circular sphincter muscle, or pupillary constrictor, near the pupil margin is composed of smooth muscle cells, which can constrict the pupil (*miosis*) when exposed to bright light. It works in opposition to the radial dilator muscle fibers, whose contraction expands the pupillary aperture (*mydriasis*) in a dim environment. The sphincter and dilator muscles are innervated by the parasympathetic and sympathetic nervous systems, respectively.

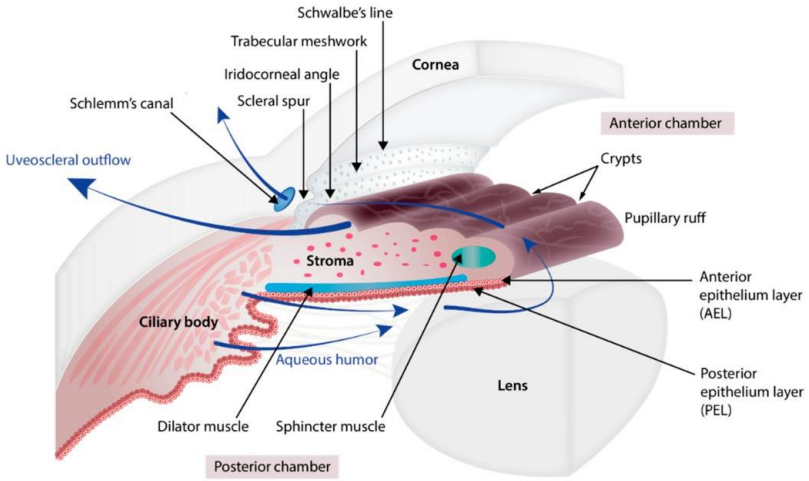

Figure 2. Anatomy of the iris, ciliary body, and aqueous humor pathway. The iris is organized into four layers (from the visible surface layer to the posterior region next to the lens): anterior border layer, stroma, and sphincter muscle, the lightly pigmented anterior epithelium layer (AEL) and dilator muscle, and the heavily pigmented posterior epithelium layer (PEL). The circular sphincter muscle lies within the stroma. The anterior iris epithelium is composed of a single layer of myoepithelial cells. The basal portion of these cells consists in elongated smooth muscle processes forming 3 to 5 layers of radial dilator muscle fibers. The iris root is attached to the ciliary body and to the corneoscleral junction (iridocorneal angle). Near the root, the anterior border layer, stroma, and bilayer epithelium of the iris form finger-shaped processes and become the ciliary body, the anterior and posterior epithelium layers of which are heavily and lightly pigmented, respectively. The aqueous humor that provides nourishment to eye structures is produced by the ciliary body. It flows between the iris and lens, through the pupil, and to the anterior part of the iris, where it runs (i) across the iris and anterior face of the ciliary body, and out through the sclera (uveoscleral pathway) and (ii) through the trabecular meshwork (at the corneoscleral junction with the iris periphery) and out along the inner wall of Schlemm's canal.

Congenital microcoria, also known as congenital miosis, is an iris malformation that affects both the regulation of the amount of light reaching the retina and the IOP. It is characterized by partial or total absence of dilator muscle fibers and manifested in pinhole

pupils (<2 mm), iris hypopigmentation, and transillumination (Figure 2), causing both hemeralopia and light hypersensitivity [7–12]. Juvenile-onset glaucoma, axial myopia, and astigmatism are frequently associated with this condition, which can lead to visual dysfunction or blindness [8]. MCOR is a purely ocular disease. The presence of extraocular symptoms should evoke a differential diagnosis [13,14].

This is a very rare disease. Worldwide, some fifty families have been reported as having the disease, since its first mention about 150 years ago [15]. These cases describe autosomal dominant inheritance, and a unique locus has been mapped and ascribed to 13q32 submicroscopic chromosomal rearrangements [7].

Despite some recent progress, the exact cause of congenital miosis remains elusive, as is the etiology of the associated refraction errors and glaucoma, which is the topic of much discussion. Here, we will review the clinical and histological features of this disease and discuss its possible physiopathology as well as associated anomalies.

2. Embryology of the Chamber Angle and Iris

The development of the eye involves the coordinated development of the neuroectoderm, surface ectoderm, and neural crest cell-derived mesenchyme.

The eye begins to develop as a pair of optic vesicles on each side of the forebrain around 3 weeks of gestation [16]. They extend from the forebrain toward the surface ectoderm through the adjacent mesenchyme. The contact of the optic vesicle with the surface ectoderm induces the thickening of the ectoderm, creating the lens placode which invaginates and detaches from the surface ectoderm to form the lens vesicle which will give rise to the lens. Mesenchyme cells begin to migrate into the space between the anterior epithelium of the lens vesicle and the surface ectoderm. The migration continues until the cells condense to form all the layers of the future cornea. The primitive corneal endothelial layer and future trabecular meshwork are formed from posterior mesenchyme cells whereas the surface ectoderm that covers the anterior side of the mesenchyme will become the corneal epithelium. In between, the mesenchyme cells differentiate to form the corneal stroma. During differentiation of the corneal endothelium, the lens detaches from the future cornea, creating the anterior chamber cavity [17].

Whilst the lens vesicle is forming, the optic vesicle also invaginates to form the double-walled optic cup. This iris and ciliary body derive from both the neuroectoderm and mesenchyme [18]. The epithelial layers of the iris and ciliary body, like the retina, develop from the third month of gestation as an outgrowth of the optic cup whilst the lens and the cornea are being formed. The outer wall produces pigment and forms the retinal pigment epithelium (RPE) and the inner wall differentiates to form the neural retina. The developing RPE and retina meet at the anterior rim of the optic cup, close to the lens vesicle which induces the differentiation of the cells of the inner wall of the anterior optic cup into the posterior pigmented epithelium of the iris (continuous with the developing retina) and the cells of the outer wall form the anterior iris epithelium (continuous with the developing RPE) [19]. At the root of the iris, the epithelium layers fold and the cells differentiate further to form the ciliary process epithelium [1]. The stroma of the iris and ciliary body arise from mesenchymal cells that migrate to the angle between the future cornea and the anterior edge of the optic cup which begins to extend to form the iris. The cells proliferate and migrate along the iris and ciliary body epithelial layers in formation and differentiate into stromal cells. Within the stroma of the iris, the sphincter pupillae and dilator pupillae muscles develop from optic cup neuroectodermal cells, contrasting with the ciliary muscle which derives from the mesenchyme [2]. The sphincter muscle arises from outer wall of the rim of the optic cup [20]. A group of cells characterized by diminished melanogenesis are distinguishable and indicate the future sphincter which begins to develop at 4 months and is well formed by 6 months [21]. The dilator pupillae also develops from the outer wall of the optic cup, but in a slightly more peripheral location than the sphincter. At the 6th month, myofilaments of the dilator muscles began to appear in the cytoplasm of the

peripheral anterior pigment epithelium layer, with villous protrusions toward the stroma. The dilator muscle is fully formed histologically in human fetuses at eight months [22].

In parallel to the formation of the iris, the mesenchyme cells that migrated at the chamber angle separate from each other, generating small open spaces filled with extracellular fibers which will further organize into trabecular beams and vessels form close to the sclera which will ultimately form Schlemm's canal [17]. Just posterior to the canal, tissue condenses to form the scleral spur that is composed of collagen and is continuous with that of the trabecular beams [5,23]. Between the trabecular beams and Schlemm's canal, some mesenchymal cells differentiate into endothelial cells and fibroblasts which are embedded in a matrix of collagen, elastic-like fibers, and ground substance, forming the juxtacanalicular tissue [24]. While the TM is forming, the anterior chamber expands and its peripheral margin slides posteriorly, exposing the TM to the chamber cavity. The structures involved in aqueous humor drainage develop late, being mature around birth, and the anterior chamber is defined at 5 months of gestation [17].

3. Disease Description

The first mention of the disease dates back to 1862, when W. R. Wilde reported a series of three unrelated individuals displaying pinhole pupils without neurological problems, a condition he called "miosis congenita" [15]. In the following years, a dozen similar observations were reported by a few other ophthalmologists [25,26], some of whom described weakened pupil response to mydriatics [27]. To the best of our knowledge, a total of 160 affected individuals from 49 families have to date been reported with a bilateral disease characterized by partial or total absence of pupil dilation, even after mydriatic treatment [8,9]. A featureless surface with poorly developed collarette and crypts, reduced iris pigmentation, iris stroma thinning, and visible transillumination are typical of the disease [9,28–32].

Defective development of the iris musculature was suspected early on, as indicated by the phrases "fault of development" and "feeble development of the iris musculature" found in initial descriptions of the disease [16,17]. This was substantiated in 1923 by a Norwegian ophthalmologist and pathologist, who provided a detailed clinical description of the ocular phenotype in three siblings combined with a post mortem anatomical analysis of the eyes of two of them who had died of apoplexia cerebri [33]. This study, along with subsequent post mortem analyses of irises and iridectomy specimens from 25- to 72-year-old individuals, revealed significant iris thinning with atrophy of the stroma, displaying a normal ultrastructure and abundant collagen fibrils but greater numbers of fibroblasts and melanocytes in the ground substance [11,28,32,34–37]. Consistent with the observation of partial or total dilation inability among affected individuals, varying dilator muscle anomalies have also been described—from peripheral to generalized dearth or absence of stromal contractile processes of the anterior iris epithelium [8–11,21,34,35,38,39]. Existing myofibrils can be normal in appearance, particularly behind the sphincter muscle and in the intermediary region [33], or greatly disordered and lack myofilaments and desmin [9,28,33–35,37]. Thickened fibrobrotic and vacuolated dilator muscle can be observed [37]. The sphincter muscle and the ciliary body are normal, as are the innervation and vasculature [32,34,40]. In humans, the iris and ciliary body epithelia develop from the third month of gestation as an outgrowth of the anterior margins of the neuroectoderm-derived optic cup [41,42]. At 16 weeks of gestation, there is a distinct pigmented bilayer epithelium at the site that will later accommodate the adult iris. Myofilaments appear in the posterior iris epithelium near the presumptive pupillary margin in the 10th week, and in the cytoplasm of the peripheral anterior pigment epithelium in the 6th month, forming histologically recognizable sphincter and dilator muscles in the 6th and 8th months, respectively [43,44]. Differentiation of the anterior layer of the iris epithelium is manifested by the expression of α smooth muscle actin in the 28th week, and desmin intermediate filaments in dilator fibers by the 37th week [45]. Histological observations of all dilator muscle developmental stages, sometimes for the same iris [33]—ranging from a normal structure

behind the sphincter, through poor differentiation with sparse and highly disordered fibers lacking myofilaments and intermediate filaments [9,10,37,46], down to complete growth inhibition [11,34]—suggest anomalies in the terminal stages of anterior iris pigment epithelium differentiation. Furthermore, this observation, which correlates with the variability of dilation phenotypes (partial or absent dilation ability), suggests that the genetic defect underlying the disease has a stochastic effect on development of the eye.

3.1. Associated Signs

3.1.1. Glaucoma

Cases of glaucoma in individuals with congenital miosis were sporadically reported in 1949 and the following decades [40,46–48]. Studying over 40 members of a Breton family spanning five generations—the oldest of whom were evaluated in the 1960s [49], Toulemont and coll. Toulemont, P.J. et al.showed that glaucoma was significantly associated with microcoria, having been observed in seven out of 23 microcoric individuals, but none of the unaffected relatives (Fisher's exact test: $p = 0.001$) [8]. Similar observations were made for a four-generation Indian pedigree comprising 18 individuals with congenital miosis, 11 of whom had glaucoma [30] and a three-generation Japanese family of which four out of five members had glaucoma [9]. In total, glaucoma or high IOP has been reported in association with congenital miosis in 36 individuals from eight families [8–10,30,31,40,46–48,50–52], whereas absence of glaucoma is mentioned in 71 patients. Diagnoses were made as early as ages seven [8,10] and 12 [30], but mostly in individuals in their early twenties [8–10,30,31,50] or thirties [9,30,47,51] (median age at diagnosis = 25 years). Glaucoma has been reported in some older persons, including two relatives aged 40 and 55 belonging to the second generation of the four-generation Indian pedigree. In this family, nine other individuals with congenital miosis had glaucoma in their second or third decade, suggesting late diagnosis in earlier generations. Late-onset glaucoma has been described in a 64-year-old from a three-generation family including eight individuals with congenital miosis [46]. This individual may have had chronic simple glaucoma, as seen in another case involving a 59-year-old [40].

Typically, glaucoma in this condition is characterized by elevated IOP, up to 60 [8] and 70 mm Hg [9] (mean: 29 mm Hg, SEM: 2.43 mm Hg versus 16.3 mm Hg, SEM: 0.62 in counterparts with no glaucoma [8,9,30,40,50]; unilateral *t*-test: $p < 0.00001$). Several authors have emphasized the difficulty of monitoring glaucomatous damage to the optic nerve due to pupillary miosis, which complicates fundus examination, and high myopia, which modifies the shape of the optic disk [8,28].

The etiology of glaucoma in congenital miosis is obscure. Occasionally, gonioscopic examination has revealed shallow anterior chambers and narrow angles, which might contribute to glaucoma [40,47]. The vast majority of individuals with both congenital miosis and glaucoma display wide-open chamber angles, although with prominent iris processes expanding over the TM and, in most cases, a high insertion of the iris root into Schwalbe's line, the TM, or the scleral spur [8,9,46,50,51]. Prominent iris processes are not uncommon in the general population and are not believed to have any influence on IOP regulation [30,31]. However, some authors consider that the additional chamber anomalies might compromise aqueous humor outflow, and they describe open-angle goniodysgenetic [46] or developmental glaucoma [9]. These designations have been widely debated because—as mentioned by Toulemont and colleagues [8]—the chamber angle anomaly associated with congenital miosis cannot be categorized into a known iris dysgenesis subclass of the Anatomical Classification of the Developmental Glaucomas by Hoskins et al. [53]. More importantly, it should be noted that the same gonioscopic anomalies are very common in microcoric individuals with normal IOP, even at advanced ages (seven out of eight [46]; 16 out of 27 [8]). In the absence of precise information on etiology, the term *childhood-onset*, or *juvenile glaucoma* is preferable [8,51].

A normal chamber angle is rather uncommon in individuals with congenital miosis. However, it is interesting to note that the review of these cases highlights the consistent

absence of glaucoma [11,21,32,34,38,54]. This observation suggests that angle anomalies are necessary but not sufficient to trigger IOP elevation and glaucoma. The extracellular matrix (ECM) of the TM is thought to have an important role in the regulation of IOP [55]. Interestingly, histopathologic examination of TM biopsies from two brothers with elevated IOP belonging to the three-generation Japanese MCOR family showed thickened and fibrotic connective tissue in the juxtacanalicular region, with accumulations of ECM [9]. This observation suggests a role of ECM homeostasis in congenital miosis-associated glaucoma.

3.1.2. Axial Myopia

Myopia as another contributing factor for developing or aggravating glaucoma in congenital microcoria is possible. Population-based studies indicate that myopia is strongly associated with glaucoma in both adults [56] and children [57] and that the risk of glaucoma increases with an increasing degree of myopia [56,58,59]. Furthermore, some studies have demonstrated that elevated IOP during postnatal eye growth can increase the length of the eye [8,60].

Axial myopia is extremely frequent in congenital miosis. It was mentioned in the initial description of the disease by R. Wilde, who noted that one of those studied was "remarkably near-sighted" [15]. In 1986, Mazzeo and colleagues reported several cases of individuals with congenital miosis and myopia, but they were born from a myopic mother, which casts doubt on an association between the traits [46]. Like glaucoma, myopia was demonstrated to be correlated with congenital miosis in the multigenerational Breton family (Fisher's exact test: $p < 0.0001$) and was also prevalent in the Indian (15 out of 18 microcoric individuals were myopic [30]) and Japanese (five out of five considered [9]) families. The review of all the cases indicates that at least 70% of individuals displaying congenital microcoria were myopic, half of whom suffered from glaucoma, knowing that 95% of individuals suffering glaucoma were myopic [21,30,33,35,39,49]. Of note, in the three-generation Indian family [29,30], glaucomatous subjects displayed higher refraction errors (mean: −12.5 Diopters (D); SEM: 4.67 D) than their counterparts with normal IOP (mean: −2 D; SEM: 0.41 D; Wilcoxon test: $p = 0.040$). Similarly, Toulemont and colleagues noted that, in the five-generation Breton family, microcoric individuals with glaucoma had high myopia, ranging from −4 to −19 diopters [8]. Elevated IOP in some of these cases may play a role in axial elongation of the eye. However, myopia is also frequent in individuals with congenital miosis and normal ocular tension (57% of the cases for whom both IOP and refraction information were available) [21,30,33,35,39,49]. For example, an individual from the multiplex family that was described by Holth and Berner in 1923 presented with high myopia at age 30 (−7 D, −8 D) and an even higher refraction error at age 52 (−15 D, −16 D) but normal IOP, leaving the mechanisms behind axial length elongation in congenital miosis an open question [33].

Some authors have proposed that propensity to close the eyelids to reduce glare caused by iris transillumination in congenital miosis could elicit a form-deprivation myopia. Indeed, monoocular myopia in infants with unilateral eyelid closure [61–63] and axial myopia following surgical eyelid closure at various points of postnatal development in primates and mice have demonstrated that ocular occlusion can increase the axial length of the eye [64–66]. However, the lack of correlation between myopia and oculocutaneous albinism, where iris transillumination and photoaversion are major symptoms, challenges these assumptions.

3.1.3. Astigmatism and Other Corneal Anomalies

Corneal anomalies have been reported by several authors, the most frequent being astigmatism, present in 51 subjects with congenital miosis, among the 63 whose data are available from the literature [8,9,12,21,28,33,35,36,39,40,46,54,67]. Of these individuals, data available for 16 of them indicated the pattern of astigmatism as being with-the-rule (WTR) astigmatism in the majority of eyes (73%) and against-the-rule (ATR) astigmatism in 19% of eyes [12,28,33,35,36,39,40,46]. The association is statistically significant in the

five-generation Brittany family: an anterior corneal astigmatism of >0.5 D was observed in 20 out of 23 microcoric individuals—1.75 to 4.00 D for 12 of these 20 (52%)—compared with only 20% of control subjects (Fisher's exact test: $p < 0.0001$) [8].

Other corneal anomalies described include corneal edema [9,40] and megalocornea [21,39]. Megalocornea has reportedly affected all microcoric subjects from two-generation (two subjects) and three-generation (six subjects) pedigrees [21], a two-generation family (two subjects) [39], and a sporadic case [68]. Although rather infrequent (11 individuals in four families), the association of the two ocular anomalies may not be random. It would be interesting to determine whether the molecular cause of the disease in these subjects differed from that for affected individuals in other families.

3.1.4. Cataract

There have been 12 cases of late-onset or senile cataracts [11,21,28,67] and two cases of congenital cataracts [25,34] reported in individuals with congenital miosis. Their occurrence is likely coincidental considering that neither senile nor congenital cataracts are more prevalent in microcoric subjects than in the general population.

4. Genetics

At least 24 multigenerational pedigrees (>100 cases in total) have been reported, while there have only been a dozen sporadic cases. Dominant transmission was first proposed in 1949 [69] and further supported by the initial description of the Breton pedigree [49]. Retrospective analysis of published pedigrees reveals a moderate predominance of affected males (84 men, 63 females; M/F ratio: 1.3), but there is no difference in clinical presentation between the sexes. The disease is transmitted equally by males and females, and father-to-son transmission is not uncommon (at least 25 occurrences [10,29,61]), demonstrating autosomal inheritance. In multigenerational pedigrees, segregation analysis indicates the absence of disease transmission through unaffected obligate carriers, suggesting complete penetrance of the disease [8–10,29,30]. It should be noted that, in 1979, Polomeno and Milot suggested autosomal recessive transmission in two sporadic cases concerning individuals born to consanguineous parents [21]. However, today it is well known that dominant de novo mutations are not uncommon in consanguineous families [70,71].

In the late 1990s, Rouillac and colleagues applied whole genome-linkage analysis to the five-generation Breton family, mapping the disease locus to chromosome 13q31-32, in an 8 cM interval flanked by markers D13S1239 proximally and D13S1280 distally [10]. Analysis of the large four-generation Indian pedigree matched the region of interest to a 4 Mb interval between markers D13S265 and D13S1280 [30]. The genetic heterogeneity of the disease has been hypothesized on the basis of primary mapping analysis in two unrelated British families, one of which reportedly did not exhibit a defect at this locus [38]. However, as highlighted by Ramprasad and colleagues in 2005, the markers at or flanking the locus were not analyzed, and therefore linkage cannot be ruled out [30].

The very high LOD score obtained by primary mapping for the five-generation Breton family ($Z_{max} = 9.79$) unambiguously mapped the disease to 13q31-32 [10]. Yet, Sanger-based mutational screening of genes lying within the genetic interval failed to detect the disease-causing mutation [7]. Thus, array comparative genomic hybridization was used to search for structural variations, revealing a submicroscopic 54.8 kb heterozygous deletion in the family, as well as 79.9 kb, 72.6 kb, 35.2 kb, 79.9 kb, and 73.1 kb overlapping deletions in the three-generation Mexican [28] and Japanese [9] pedigrees and three previously unreported families of French, Mexican, and Japanese origin, respectively [7]. Subsequently, four additional structural variations involving the same region were published. Deletions of lengths 69, 82, and 46 kb were reported in multigenerational families from the UK [31], Switzerland [32], and Saudi Arabia [67], respectively. In the British family, which comprised five affected subjects over three generations, iridocorneal angle anomalies were reported to affect at least three individuals aged >40, of whom two (mother and son) had juvenile glaucoma [31]. In the other two families, disease description was limited to a mother and two

children. All were described as having normal chamber angle and early onset myopia [32] or minimal hyperopic astigmatism [67]. The mother in the Saudi family reportedly suffered bilateral senile cataract [67]. All the deletions except the one identified in Mexican families differ from each other, which suggests independent events [7]. Extensive bioinformatic analysis of deletion breakpoints and surrounding genomic architecture has identified a duplicated sequence prone to recurrent nonallelic homologous recombination in one case. The others likely involve nonrecurrent microhomology-mediated rearrangement [7]. Analysis of the positions of the deletions, which range in size from 35 kb to 85 kb, places the critical congenital miosis-causing deletion in a 31.8 kb interval (Figure 3). Although variable in size, the deletions encompassed or interrupted the tail-to-tail genes *TGDS* and *GPR180*.

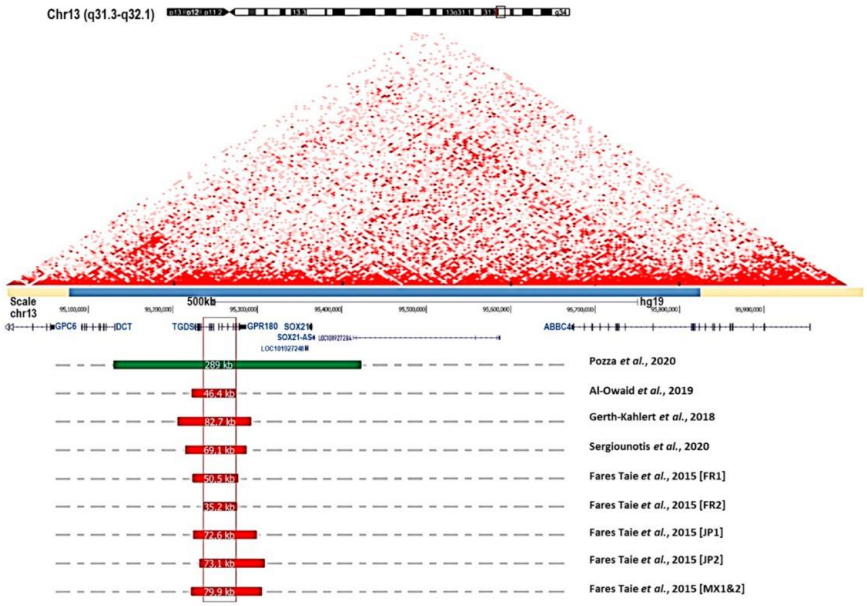

Figure 3. Summary of 13q32.1 structural variations associated with congenital microcoria. The two-dimensional heat map representing normalized Hi-C sequencing visualization in HMEC with the 3D Genome Browser is shown [72]. The topologically associating domain (TAD) encompassing the MCOR region and spanning 600 kb is indicated with a light blue bar (chr13:95,075,000–95,825,000, Hg19 and 5 kb resolution). Gene organization at chromosome 13q32.1, and position and size of structural variations (deletions in red; duplication in green) reported in individuals suffering from congenital microcoria [7,31,32,67]. The critical deletion (shown in red frame) responsible for MCOR spans 31.8 kb (hg19, chr13: 95,241,606–95,273,292). The reciprocal duplication encompasses 7 genes: *DCT, TGDS, GPR180, LOC101927248, SOX21, SOX21-AS*, and *LOC101927284* [12].

Recessive mutations in *TGDS*—encoding TDP-glucose 4,6-dehydratase—cause malformations of the mouth, face, and digits (Catel–Manzke syndrome (CATMANS); MIM: 616145). Ophthalmologic examination of individuals with *TGDS*-associated CATMANS at Necker Hospital (Paris, France) revealed no iris anomalies, suggesting *TGDS* does not play a role in MCOR. *GPR180*—encoding G protein-coupled receptor 180—is involved in the regulation of smooth muscle cell growth. However, analysis of knockout mice and individuals from a two-generation family carrying a heterozygous *GPR180* nonsense mutation failed to detect any iris dilator muscle anomaly. Yet, those family members (aged 16 to 62) harboring the *GRP180* loss-of-function mutation displayed prominent iris processes in the chamber angle expanding over the TM, and normal IOPs [7]. This observation suggests that *GRP180* loss-of-function may compromise iris development, but is not sufficient to

cause congenital miosis. The disease likely involves the loss of elements regulating the expression of genes neighboring the deletions. The deleted sequences are contained in a topologically associated domain (TAD) spanning 600 kb on chromosome 13q32.1. The deletions may change the enhancer dosage, resulting in the loss of function of one or more of the 8 genes in the TAD or result in upregulation or tissue-specific misexpression [12]. *DCT* encoding daupachrome tautomerase is among the genes of interest. It is involved in the biosynthesis of eumelanin [73]. Recently, biallelic loss-of-function mutations in *DCT* have been described in oculocutaneous albinism (OCA8) [74]. Misexpression of this gene may contribute to the disease or at least the excessively light pigmentation of the iris reported in subjects with congenital miosis. *SOX21* encodes a transcription factor of the SRY-related HMG-box (SOX) family which is transiently expressed during the early phases of optic vesicle morphogenesis in chicks and during specification in the lens and retina but is switched of afterwards, i.e., before the iris starts developing [75]. Its loss of function in chicks, as in zebrafish, interferes with normal lens development [76]. Ectopic expression during iris development could be induced by 13q32.1 deletions and therefore compromise the development of the iris and chamber angle. Finally, *ABCC4* (*MRP4*) immunoreactivity has been demonstrated throughout the aqueous outflow pathway, including the trabeculum meshwork, Schlemm's canal, and juxtacanalicular tissue [77]. This gene has been suggested to regulate intracellular cAMP and cGMP levels in the TM and IOP, possibly through the regulation of ECM homeostasis. Whether misexpression of this gene contributes to congenital miosis-associated glaucoma merits consideration. However, in the five-generation Breton family, 29 of the 31 MCOR patients shared a 4 Mb haplotype encompassing the 600 kb TAD (markers D13S1300 and D13S154) at the 13q32 locus [10]. As myopia and glaucoma were not consistent features among the 29 haploidentical individuals, and as crossovers are highly unlikely in a 4 Mb interval, it is unlikely that structural variants are directly involved.

Interestingly, a recent study has reported a reciprocal 289 kb duplication encompassing seven genes (including *TGDS* and *GPR180*)—identified in a mosaic mother and her daughter with congenital miosis and a normal anterior chamber angle [12]. From this observation, the authors attributed the chamber angle dysgenesis identified in families carrying 13q32.1 deletions to partially non-functional GPR180. However, this is challenged by the report of normal chamber angles in the Swiss and Saudi Arabian families carrying deletions encompassing *GPR180* [32,67] (Figure 3). The duplication is contained in the 600 kb TAD and may result in dose-dependent upregulation or tissue-specific misexpression [12].

5. Discussion

Congenital microcoria was initially described over 150 years ago and, as cases were reported, additional ocular anomalies were noted. While the rarest of these may be coincidentally present, others like myopia, astigmatism, and glaucoma are correlated. Thus far, the identification of structural variations as the cause of the disease has not made it possible to unravel the mechanisms underlying the observed iris developmental defects. The association with refraction errors or glaucoma appears to be independent of the size or type of structural variation, and whether they are secondary to the iris anomalies or the modification of the regulatory architecture of chromosome 13q32.1 remains a mystery. This review suggests that the combination of iris and chamber angle dysgenesis and genetic anomalies is necessary for glaucoma to occur in congenital microcoria. Photoaversion and immaturity of the chamber angle could contribute to myopia and elevated IOP, which may itself aggravate myopia. However, the absence of an increased prevalence of deprivation myopia in oculocutaneous albinism and the higher prevalence of myopia among individuals with normal IOP make the causative mechanism uncertain. This review highlights that chamber angle anomaly is common both in glaucomatous and nonglaucomatous individuals. Yet, while all glaucomatous individuals display angle anomalies, none of the few people with normally developed chamber angles had glaucoma, suggesting that the angle anomaly is necessary but insufficient to trigger glaucoma. The report of ECM

accumulation in the TM of two siblings may provide a clue. There is increasing evidence that ECM accumulation in the juxtacanalicular region, the deepest part of the TM, is a main trigger of open-angle glaucoma, including primary open-angle glaucoma. It reduces the filtering capacity of the TM and increases aqueous humor outflow resistance, leading to elevated IOP and, ultimately, the death of retinal ganglion cells, whose axons form the optic nerve [24,78]. It is probable that high IOP in congenital miosis is due to the combination of chamber angle anomalies and deregulated ECM homeostasis. In addition to compromising the proper development of the iris, it is possible for 13q32.1 structural variations to deregulate signaling pathways important for axial length control and for ECM turnover in the TM.

6. Conclusions

Despite the identification of chromosomal rearrangements in individuals suffering from congenital miosis, the mechanisms underlying the defective development of the iris and chamber angle and the cause of associated glaucoma and refraction errors remain elusive. Further studies, including whole-genome sequencing with Hi-C sequencing in multigenerational families in the search for genetic factors increasing susceptibility to glaucoma and myopia, will hopefully shed light on the intriguing mechanisms behind these ocular anomalies and how they are linked to each other.

Author Contributions: C.A., B.N., E.E. and L.F.T. extracted and analyzed data from the literature and drafted the manuscript; L.F.T. and J.-M.R. revised and edited the draft manuscript. All authors have read and agreed to the published version of the manuscript.

Funding: The research of the authors on congenital microcoria was funded by grants from the Agence Nationale de la Recherche (ANR) (MCORGLAUC_WP09T162F), the Institut National de la Santé et de la Recherche Médicale (INSERM), the Université de Paris, the Fondation VISIO, and the Association Retina France.

Institutional Review Board Statement: Not applicable.

Informed Consent Statement: Not applicable.

Data Availability Statement: Not applicable.

Acknowledgments: Not applicable.

Conflicts of Interest: The authors declare no conflict of interest.

References

1. Davis, N.; Ashery-Padan, R. Iris Development in Vertebrates; Genetic and Molecular Considerations. *Brain Res.* **2008**, *1192*, 17–28. [CrossRef]
2. Bloom, J.; Motlagh, M.; Czyz, C.N. Anatomy, Head and Neck, Eye Iris Sphincter Muscle. In *StatPearls*; StatPearls Publishing: Treasure Island, FL, USA, 2021.
3. Uvea. Clinical Gate 2015. Available online: https://clinicalgate.com/the-uveal-tract/ (accessed on 8 March 2015).
4. Forrester, J.; Dick, A.; McMenamin, P.; Roberts, F.; Pearlman, E. *The Eye*; Elsevier: Amsterdam, The Netherlands, 2016; ISBN1 978-0-7020-5554-6. Available online: https://www.sciencedirect.com/book/9780702055546/the-eye (accessed on 19 February 2015).
5. Abu-Hassan, D.W.; Acott, T.S.; Kelley, M.J. The Trabecular Meshwork: A Basic Review of Form and Function. *J. Ocul. Biol.* **2014**, *2*, 1–22. [CrossRef]
6. Goel, M.; Picciani, R.G.; Lee, R.K.; Bhattacharya, S.K. Aqueous Humor Dynamics: A Review. *Open Ophthalmol. J.* **2010**, *4*, 52–59. [CrossRef]
7. Fares-Taie, L.; Gerber, S.; Tawara, A.; Ramirez-Miranda, A.; Douet, J.-Y.; Verdin, H.; Guilloux, A.; Zenteno, J.C.; Kondo, H.; Moisset, H.; et al. Submicroscopic Deletions at 13q32.1 Cause Congenital Microcoria. *Am. J. Hum. Genet.* **2015**, *96*, 631–639. [CrossRef]
8. Toulemont, P.J.; Urvoy, M.; Coscas, G.; Lecallonnec, A.; Cuvilliers, A.F. Association of Congenital Microcoria with Myopia and Glaucoma. *Ophthalmology* **1995**, *102*, 193–198. [CrossRef]
9. Tawara, A.; Itou, K.; Kubota, T.; Harada, Y.; Tou, N.; Hirose, N. Congenital Microcoria Associated With Late-Onset Developmental Glaucoma. *J. Glaucoma* **2005**, *14*, 409–413. [CrossRef]

10. Rouillac, C.; Roche, O.; Marchant, D.; Bachner, L.; Kobetz, A.; Toulemont, P.-J.; Orssaud, C.; Urvoy, M.; Odent, S.; Le Marec, B.; et al. Mapping of a Congenital Microcoria Locus to 13q31-Q32. *Am. J. Hum. Genet.* **1998**, *62*, 1117–1122. [CrossRef] [PubMed]
11. Simpson, W.A.C. The Ultrastructural Pathological Features of Congenital Microcoria: A Case Report. *Arch. Ophthalmol.* **1989**, *107*, 99. [CrossRef] [PubMed]
12. Pozza, E.; Verdin, H.; Deconinck, H.; Dheedene, A.; Menten, B.; De Baere, E.; Balikova, I. Microcoria Due to First Duplication of 13q32.1 Including the GPR180 Gene and Maternal Mosaicism. *Eur. J. Med. Genet* **2020**, *63*, 103918. [CrossRef] [PubMed]
13. Pierson, M.; Cordier, J.; Hervouuet, F.; Rauber, G. An Unusual Congenital and Familial Congenital Malformative Combination Involving the Eye and KidneY. *J. Genet Hum.* **1963**, *12*, 184–213.
14. Zenker, M.; Aigner, T.; Wendler, O.; Tralau, T.; Müntefering, H.; Fenski, R.; Pitz, S.; Schumacher, V.; Royer-Pokora, B.; Wühl, E.; et al. Human Laminin B2 Deficiency Causes Congenital Nephrosis with Mesangial Sclerosis and Distinct Eye Abnormalities. *Hum. Mol. Genet.* **2004**, *13*, 2625–2632. [CrossRef]
15. Wilde, W.R. *An Essay on the Malformations and Congenital Diseases of the Organs of Sight/by W. R. Wilde*; John Churchill: London, UK, 1862.
16. Edward, D.P.; Kaufman, L.M. Anatomy, Development, and Physiology of the Visual System. *Pediatr. Clin. N. Am.* **2003**, *50*, 1–23. [CrossRef]
17. Cvekl, A.; Tamm, E.R. Anterior Eye Development and Ocular Mesenchyme. *Bioessays* **2004**, *26*, 374–386. [CrossRef]
18. Bales, T.R.; Lopez, M.J.; Clark, J. Embryology, Eye. In *StatPearls*; StatPearls Publishing: Treasure Island, FL, USA, 2021.
19. Graw, J. Eye Development. *Curr. Top. Dev. Biol.* **2010**, *90*, 343–386. [CrossRef]
20. Ruprecht, K.W.; Wulle, K.G. Light and electron microscopic studies on the development of the human pupillary sphincter muscle. *Albrecht Graefes Arch. Klin. Exp. Ophthalmol. Albrecht Graefe's Arch. Clin. Exp. Ophthalmol.* **1973**, *186*, 117–130. [CrossRef]
21. Polomeno, R.C.; Milot, J. Congenital Miosis. *Can. J. Ophthalmol.* **1979**, *14*, 43–46.
22. Mann, I.C. Notes on the Anatomy of the Living Eye, as Revealed by the Gullstrand Slitlamp. *J. Anat.* **1925**, *59*, 155–165.
23. Anderson, D.R. The Development of the Trabecular Meshwork and Its Abnormality in Primary Infantile Glaucoma. *Trans. Am. Ophthalmol. Soc.* **1981**, *79*, 458–485. [PubMed]
24. Vranka, J.A.; Kelley, M.J.; Acott, T.S.; Keller, K.E. Extracellular Matrix in the Trabecular Meshwork: Intraocular Pressure Regulation and Dysregulation in Glaucoma. *Exp. Eye Res.* **2015**, *133*, 112–125. [CrossRef] [PubMed]
25. Treacher Collins, E.; Mayou, M.S. *Pathology and Bacteriology in Ophthalmic Practice*; William Heinemann: London, UK, 1911; pp. 64, 82.
26. Wood, C.A. Fully Illustrated; Lenicet to Muscles, Ocular (Classic Reprint). In *The American Encyclopedia and Dictionary of Ophthalmology*; Forgotten Books: London, UK, 1917; Volume 10, ISBN 1396359575 (ISBN13: 9781396359576).
27. Truc and Valude. *Nouveaux Éléments d'Ophtalmologie*; Maloine: Paris, France, 1896; p. 475.
28. Ramirez-Miranda, A.; Paulin-Huerta, J.M.; Chavez-Mondragón, E.; Islas-de la Vega, G.; Rodriguez-Reyes, A. Ultrabiomicroscopic-Histopathologic Correlations in Individuals with Autosomal Dominant Congenital Microcoria: Three-Generation Family Report. *Case Rep. Ophthalmol.* **2011**, *2*, 160–165. [CrossRef] [PubMed]
29. Saxena, S.; Saxena, R.C. Congenital Microcoria: A Study in Three Generations. *Indian J. Ophthalmol.* **1993**, *41*, 130.
30. Ramprasad, V.L.; Sripriya, S.; Ronnie, G.; Nancarrow, D.; Saxena, S.; Hemamalini, A.; Kumar, D.; Vijaya, L.; Kumaramanickavel, G. Genetic Homogeneity for Inherited Congenital Microcoria Loci in an Asian Indian Pedigree. *Mol. Vis.* **2005**, *11*, 934–940.
31. Sergouniotis, P.I.; Ellingford, J.M.; O'Sullivan, J.; Fenerty, C.H.; Black, G.C. Genome Sequencing Identifies a Large Deletion at 13q32.1 as the Cause of Microcoria and Childhood-Onset Glaucoma. *Acta Ophthalmol.* **2017**, *95*, e249–e250. [CrossRef] [PubMed]
32. Gerth-Kahlert, C.; Maggi, J.; Töteberg-Harms, M.; Tiwari, A.; Budde, B.; Nürnberg, P.; Koller, S.; Berger, W. Absence of Goniodysgenesis in Patients with Chromosome 13Q Microdeletion-Related Microcoria. *Ophthalmol. Glaucoma* **2018**, *1*, 145–147. [CrossRef]
33. Holth, S.; Berner, O. Congenital miosis or pinhole pupils owing to developmental faults of the dilatator muscle. *Br. J. Ophthalmol.* **1923**, *7*, 401–419. [CrossRef] [PubMed]
34. Butler, J.M.; Raviola, G.; Miller, C.D.; Friedmann, A.I. Fine Structural Defects in a Case of Congenital Microcoria. *Graefes Arch. Clin. Exp. Ophthalmol.* **1989**, *227*, 88–94. [CrossRef]
35. Ferreira, B.F.D.A.; Schmidt, M.B.; Barbosa, L.J.; Oyamada, M.K.; Carricondo, P.C. Phacoemulsification and 1% Atropine Eye Drops for Treatment of Antimetropic Congenital Microcoria Associated with Cataracts. *Arq. Bras. Oftalmol.* **2019**, *82*. [CrossRef] [PubMed]
36. Lambert, S.R.; Amaya, L.; Taylor, D. Congenital Idiopathic Microcoria. *Am. J. Ophthalmol.* **1988**, *106*, 590–594. [CrossRef]
37. Pietropaolo, A.; Corvino, C.; DeBlasi, A.; Calabrò, F. Congenital Microcoria: Case Report and Histological Study. *J. Pediatr. Ophthalmol. Strabismus.* **1998**, *35*, 125–127. [CrossRef] [PubMed]
38. Bremner, F.D.; Houlden, H.; Smith, S.E. Genotypic and Phenotypic Heterogeneity in Familial Microcoria. *Br. J. Ophthalmol.* **2004**, *88*, 469–473. [CrossRef]
39. Meire, F.M.; Delleman, J.W. Autosomal Dominant Congenital Miosis with Megalocornea. *Ophthalmic Paediatr. Genet.* **1992**, *13*, 123–129. [CrossRef] [PubMed]
40. Hyams, S.W.; Neumann, E. Congenital Microcoria and Combined Mechanism Glaucoma. *Am. J. Ophthalmol.* **1969**, *68*, 326–327. [CrossRef]
41. Imaizumi, M.; Kuwabara, T. Development of the Rat Iris. *Investig. Ophthalmol.* **1971**, *10*, 733–744.

42. Jensen, A.M. Potential Roles for BMP and Pax Genes in the Development of Iris Smooth Muscle. *Dev. Dyn.* **2005**, *232*, 385–392. [CrossRef] [PubMed]
43. Thumann, G. Development and Cellular Functions of the Iris Pigment Epithelium. *Surv. Ophthalmol.* **2001**, *45*, 345–354. [CrossRef]
44. Mann, I.C. The Development of the Human Iris. *Br. J. Ophthalmol.* **1925**, *9*, 495–512. [CrossRef]
45. Uusitalo, M.; Kivelä, T. Development of Cytoskeleton in Neuroectodermally Derived Epithelial and Muscle Cells of the Human Eye. *Investig. Opthalmol. Vis. Sci.* **1995**, *36*, 2584–2591.
46. Mazzeo, V.; Gaiba, G.; Rossi, A. Hereditary Cases of Congenital Microcoria and Goniodysgenesis. *Ophthalmic Paediatr. Genet.* **1986**, *7*, 121–125. [CrossRef]
47. Veirs, E.R. Congenital Miosis: Associated with a Narrow Angle of the Anterior Chamber and Abnormally Placed Iris Tissue. *Arch. Ophthalmol.* **1961**, *65*, 59. [CrossRef]
48. Heatley, J. Miosis Congenita Familiar. *Soc. Mex. Oftalmol.* **1948**, *22*, 141–148.
49. Ardouin, M.; Urvoy, M.; Lefranc, J. Microcorie Congenitale. *Bull. Mem Soc. Fr. Ophtalmol.* **1964**, *77*, 356.
50. Stabilization of Glaucoma Associated with Microcoria | Semantic Scholar. Available online: https://www.semanticscholar.org/paper/Stabilization-of-Glaucoma-Associated-with-Ngabou/6ade8acf89a87b9afe174a5c2f10d7702229fcc4 (accessed on 9 March 2021).
51. Sahori, A.; Katsumori, O.K. Congenital Miosis Associated with Juvenile Glaucoma. *Folia Ophthalmol. Jpn.* **1987**, *38*, 853–857.
52. Coulon, G.; Delbosc, B.; Jeffredo, Y.; Viennet, G.; Oppermann, A.; Royer, J. Congenital microcoria: A case report with histopathological study. *J. Fr. Ophtalmol.* **1986**, *9*, 35–39.
53. Hoskins, H.D.; Shaffer, R.N.; Hetherington, J. Anatomical Classification of the Developmental Glaucomas. *Arch. Ophthalmol.* **1984**, *102*, 1331–1336. [CrossRef] [PubMed]
54. Agoston, I.; Gróf, P. La Miose Congénitale et l'albinisme. *OPH* **1968**, *155*, 399–408. [CrossRef] [PubMed]
55. Acott, T.S.; Kelley, M.J. Extracellular Matrix in the Trabecular Meshwork. *Exp. Eye Res.* **2008**, *86*, 543–561. [CrossRef] [PubMed]
56. Mitchell, P.; Hourihan, F.; Sandbach, J.; Wang, J.J. The Relationship between Glaucoma and Myopia: The Blue Mountains Eye Study. *Ophthalmology* **1999**, *106*, 2010–2015. [CrossRef]
57. Quinn, G.E.; Berlin, J.A.; Young, T.L.; Ziylan, S.; Stone, R.A. Association of Intraocular Pressure and Myopia in Children. *Ophthalmology* **1995**, *102*, 180–185. [CrossRef]
58. Chen, S.-J.; Lu, P.; Zhang, W.-F.; Lu, J.-H. High Myopia as a Risk Factor in Primary Open Angle Glaucoma. *Int. J. Ophthalmol.* **2012**, *5*, 750–753. [CrossRef] [PubMed]
59. Sommer, A.; Tielsch, J.M. Risk Factors for Open-Angle Glaucoma: The Barbados Eye Study. *JAMA Ophthalmol.* **1996**, *114*. [CrossRef]
60. Schmid, K.L.; Hills, T.; Abbott, M.; Humphries, M.; Pyne, K.; Wildsoet, C.F. Relationship between Intraocular Pressure and Eye Growth in Chick. *Ophthalmic Physiol. Opt.* **2003**, *23*, 25–33. [CrossRef] [PubMed]
61. Hoyt, C.S.; Stone, R.D.; Fromer, C.; Billson, F.A. Monocular Axial Myopia Associated with Neonatal Eyelid Closure in Human Infants. *Am. J. Ophthalmol.* **1981**, *91*, 197–200. [CrossRef]
62. Rabin, J.; Sluyters, R.C.V.; Malach, R. Emmetropization: A Vision-Dependent Phenomenon. *Investig. Opthalmol. Vis. Sci.* **1981**, *20*, 561–564.
63. Johnson, C.A.; Post, R.B.; Chalupa, L.M.; Lee, T.J. Monocular Deprivation in Humans: A Study of Identical Twins. *Investig. Opthalmol. Vis. Sci.* **1982**, *23*, 135–138.
64. Raviola, E.; Wiesel, T.N. An Animal Model of Myopia. *N. Engl. J. Med.* **1985**, *312*, 1609–1615. [CrossRef]
65. Pardue, M.T.; Faulkner, A.E.; Fernandes, A.; Yin, H.; Schaeffel, F.; Williams, R.W.; Pozdeyev, N.; Iuvone, P.M. High Susceptibility to Experimental Myopia in a Mouse Model with a Retinal ON Pathway Defect. *Investig. Opthalmol. Vis. Sci.* **2008**, *49*, 706–712. [CrossRef]
66. Schaeffel, F.; Feldkaemper, M. Animal Models in Myopia Research. *Clin. Exp. Opt.* **2015**, *98*, 507–517. [CrossRef]
67. Al-Owaid, A.; Alarfaj, M.; Al-Qahtani, A.; Al-Arfaj, K. Congenital Microcoria in a Saudi Family. *Ophthalmic Genet.* **2019**, *40*, 578–580. [CrossRef]
68. Vail, D.T., Jr. Adult Hereditary Anterior Megalophthalmus Sine Glaucoma: A Definite Disease Entity: With Special Reference To The Extraction Of Cataract. *Arch. Ophthalmol.* **1931**, *6*, 39–62. [CrossRef]
69. Van Leeuwen, M.A. La Microcorie Congenitale Hereditaire. *Bull Soc Belge Ophtalmol* **1949**, *91*, 118–136.
70. Castilla-Vallmanya, L.; Gürsoy, S.; Giray-Bozkaya, Ö.; Prat-Planas, A.; Bullich, G.; Matalonga, L.; Centeno-Pla, M.; Rabionet, R.; Grinberg, D.; Balcells, S.; et al. De Novo PORCN and ZIC2 Mutations in a Highly Consanguineous Family. *Int. J. Mol. Sci.* **2021**, *22*, 1549. [CrossRef] [PubMed]
71. Perrault, I.; Hanein, S.; Gerber, S.; Barbet, F.; Dufier, J.-L.; Munnich, A.; Rozet, J.-M.; Kaplan, J. Evidence of Autosomal Dominant Leber Congenital Amaurosis (LCA) Underlain by a CRX Heterozygous Null Allele. *J. Med. Genet.* **2003**, *40*, e90. [CrossRef]
72. Wang, Y.; Song, F.; Zhang, B.; Zhang, L.; Xu, J.; Kuang, D.; Li, D.; Choudhary, M.N.K.; Li, Y.; Hu, M.; et al. The 3D Genome Browser: A Web-Based Browser for Visualizing 3D Genome Organization and Long-Range Chromatin Interactions. *Genome Biol.* **2018**, *19*, 151. [CrossRef] [PubMed]
73. Costin, G.-E.; Valencia, J.C.; Wakamatsu, K.; Ito, S.; Solano, F.; Milac, A.L.; Vieira, W.D.; Yamaguchi, Y.; Rouzaud, F.; Petrescu, A.-J.; et al. Mutations in Dopachrome Tautomerase (Dct) Affect Eumelanin/Pheomelanin Synthesis, but Do Not Affect Intracellular Trafficking of the Mutant Protein. *Biochem. J.* **2005**, *391*, 249–259. [CrossRef] [PubMed]

74. Pennamen, P.; Tingaud-Sequeira, A.; Gazova, I.; Keighren, M.; McKie, L.; Marlin, S.; Halem, S.G.; Kaplan, J.; Delevoye, C.; Lacombe, D.; et al. Dopachrome Tautomerase Variants in Patients with Oculocutaneous Albinism. *bioRxiv* **2020**. [CrossRef]
75. Uchikawa, M.; Kamachi, Y.; Kondoh, H. Two Distinct Subgroups of Group B Sox Genes for Transcriptional Activators and Repressors: Their Expression during Embryonic Organogenesis of the Chicken. *Mech. Dev.* **1999**, *84*, 103–120. [CrossRef]
76. Pauls, S.; Smith, S.F.; Elgar, G. Lens Development Depends on a Pair of Highly Conserved Sox21 Regulatory Elements. *Dev. Biol.* **2012**, *365–248*, 310–318. [CrossRef]
77. Pattabiraman, P.P.; Pecen, P.E.; Rao, P.V. MRP4-Mediated Regulation of Intracellular CAMP and CGMP Levels in Trabecular Meshwork Cells and Homeostasis of Intraocular Pressure. *Investig. Opthalmol. Vis. Sci.* **2013**, *54*, 1636. [CrossRef]
78. Carreon, T.; van der Merwe, E.; Fellman, R.L.; Johnstone, M.; Bhattacharya, S.K. Aqueous Outflow—A Continuum from Trabecular Meshwork to Episcleral Veins. *Prog. Retin. Eye Res.* **2017**, *57*, 108–133. [CrossRef]

2.2. Description of the mouse phenotype (Second publication)

In an effort to comprehend how structural variations involving chromosome 13q32.1 in individuals affected with MCOR impact iris development and lead to abnormal eye growth and glaucoma, we considered using the CRISPR-Cas9 technology to target and remove the minimal 35 Kb disease-causing deletion in the mouse genome.

In this publication, we report our analysis of the 3D structure and organization of the genomic region containing the MCOR locus, alongside a comparison with the corresponding 14qE4 region in the mouse genome. We demonstrate, through the use of HIC-seq data, the existence of two significant interacting topologically associated domains (TADs) within the 13q32.2 region, with one containing a cluster of three subTADs. We show that the MCOR locus, defined by its outermost boundaries, is situated within the region created by two subTADs, roughly centered at the boundary between them. Finally, upon analyzing the syntenic region in mice, we demonstrated that there exist a strikingly high conservation of both gene content and organizational structure. This finding underscores the significance of deleting the critical MCOR-causing region in the mouse genome as a mean to faithfully model the disease.

We present the phenotypes of the mouse model harboring the critical MCOR deletion in homozygosity and single heterozygosity. We unveil that homozygosity for the deletion is embryolethal in mice. Conversely, heterozygous mice were viable and underwent normal development. Remarkably, however, their irises exhibited a statistically significant moderate reduction in pupil size that correlated with a decrease in desmin mRNA abundance, as determined by pupillometry and RNAseq analysis respectively.

The transcriptome analysis further revealed the expression of the *Sox21* transcription factor (TF) in heterozygous irises, while it remained undetected in wildtype irises. A detailed examination of the spatiotemporal pattern of *Sox21* mRNA and protein expression during normal eye development, conducted through high-resolution RNAscope analysis, demonstrated that *Sox21* is neither expressed in adult nor in

developing eyes. Absence of *Sox21* expression during mouse eye development contrasts with data from zebrafish and chick studies where it is detected in the lens (Pauls et al., 2012). This lack of *Sox21* expression in the developing mouse eye aligns with the absence of ocular defects observed in the *Sox21*-/- mouse (Kiso et al., 2009). In mutant MCOR mice, *Sox21* exhibited expression in the outer layer of the optic cup, forming the retinal pigment epithelium (RPE), the anterior epithelium of the ciliary body, and the anterior epithelium of the iris, from which the dilator muscle develops. Notably, this expression pattern coincided with that of *Dct*, which encodes dopachrome tautomerase, a marker of pigmented tissues. *Dct* is positioned just upstream of the MCOR locus, while *Sox21* is located downstream of the locus in the next subTAD, suggesting that ectopic expression of *Sox21* is induced by the adoption of *Dct* enhancers by its promoter.

Of particular interest, we report the binding of SOX21 to a consensus sequence located in the first intron of the *Tgfb2* gene in mutant irises. This finding is especially significant since we observed elevated expression of *Tgfb2* in heterozygous irises and accumulation of TGFB2 in the aqueous humor of a MCOR patient, as determined by transcriptome analysis and ELISA assay, respectively. This observation, combined with data from the literature correlating elevated TGFB2 concentration in the aqueous humor with the accumulation of extracellular matrix proteins in the trabeculum meshwork and the development of open-angle glaucoma, suggests a pivotal role of SOX21-TGFB2 signaling in glaucoma among MCOR patients. Evidence of extracellular matrix (ECM) accumulation in the trabeculum of a MCOR case, whose iris was sampled during trabeculectomy surgery (Tawara et al., 2005), further support this hypothesis.

In summary, our research suggests that MCOR results from TAD disruption, leading to the ectopic expression of *Sox21*. This deregulation of *Sox21* contributes to iris development failure and may trigger glaucoma, likely through the dysregulation of the TGFB2 signaling cascade. Additionally, a proposed correlation between TGFB2 and eye elongation further support these findings. Collectively, these observations suggest that SOX21 dysregulation may serve as a unifying link among MCOR symptoms.

This extensive work constitutes the core of my thesis and has been presented at multiple events. We are currently preparing the paper for submission to Genes & Development.

Poster presentations:

- *Expression ectopique de Sox21 par adoption d'un enhancer de Dct chez la souris modèle de la microcorie congénitale liée aux délétions du chromosome 13q32.1.* **C Angée**, B. Nedelec, P. David, S. Gerber, S. Crippa, B. Passet, J.-L. Vilotte, N. Chassaing, J. Kaplan, D. Lupiañez, C. Kostic, P. Calvas, J.-M. Rozet & L. Fares Taie. **Assises de Génétique Humaine**, *January 2020*, Tours (France).

- *A Common type glaucoma TGFb2 signaling pathway is involved in congenital microcoria-associated glaucoma challenging a malformative origin*. **C. Angée**, B. Nedelec, P. David, S. Gerber, S. Creuzet, S. Crippa, B. Passet, J.-L. Vilotte, N. Chassaing, J. Kaplan, C. Kostic, P. Calvas, J.-M. Rozet & L. Fares Taie. **American Society of Human Genetics (ASHG)**, *October 2020*, Virtual meeting.

Oral communications:

- *Ablation of the congenital microcoria (MCOR) critical region on 13q32.1 activates common-type glaucoma signaling pathways challenging a developmental etiology of MCOR-associated glaucoma.* **C. Angée**, B. Nedelec, P. David, S. Gerber, S. Crippa, B. Passet, J.-L. Vilotte, N. Chassaing, J. Kaplan, C. Kostic, P. Calvas, J.-M. Rozet & L. Fares Taie. **European Society of Human Genetics (ESHG) 2.0**, *June 2020,* Virtual meeting.

- *Congenital microcoria: a suitable model to study common glaucoma.* **C. Angée,** B. Nedelec, P. David, S. Creuzet, S. Gerber, S. Crippa, B. Passet, J.-L. Vilotte, N. Chassaing, J. Kaplan, C. Kostic, P. Calvas, J.-M. Rozet & L. Fares Taie. **Swiss Eye Research Meeting (SERM)**, *January 2022*, Lowenberg (Switzerland).

- *Understanding the mechanisms underlying ectopic expression of Sox21 in Congenital.* **C. Angée,** E. Erjavec, B. Nedelec, P. David, S. Creuzet, D. Hadjadj, S. Crippa, B. Passet, J.-L. Vilotte, N. Chassaing, J. Kaplan, C. Kostic, P. Calvas, J.-M. Rozet & L. Fares Taie. **Genetics of Ocular Development (GoOD) Meeting**, *May 2023*, Toulouse (France).

Modeling the critical MCOR-causing deletion in mouse unveils aberrant *Sox21* expression in developing and adult iris and ciliary body, and implicates *Tgfb2* in MCOR-associated glaucoma and myopia.

Clémentine Angee[1#], Elisa Erjavec[1#], DJihad Hadjadj[2], Bruno Passet[3], Pierre David[4], Corinne Kostic[5], Emmanuel Dodé[6], Nicolas Cagnard[7], Brigitte Nedelec[1], Sylvain Crippa[5], Christine Bole-Feysot[8], Mohammed Zarhrate[8], Jean-Luc Vilotte[3], Julie Plaisancié[9], Nicolas Chassaing[9], Josseline Kaplan[1], Jean-Michel Rozet[1]*, Lucas Fares Taie[1]*

1. Laboratory of Genetics in Ophthalmology (LGO), INSERM UMR1163, Institute of Genetic Diseases, Imagine and Université Paris Cité; Paris, France.
2. Institut Cochin, Inserm U1016, CNRS UMR8104, UFR de Pharmacie de Paris, Université Paris Cité, CARPEM; Paris, France.
3. University of Paris-Saclay, INRAE, AgroParisTech, UMR1313 GABI; Jouy-en-Josas, France
4. Transgenesis Platform, Laboratoire d'Expérimentation Animale et Transgenèse (LEAT), Imagine Institute, Structure Fédérative de Recherche Necker INSERM US24/CNRS UMS3633; Paris, France
5. Group for Retinal Disorder Research, Department of Ophthalmology, University of Lausanne, Jules-Gonin Eye Hospital, Fondation Asile des Aveugles; Lausanne, Switzerland
6. Institut Ophtalmologique de L'Ouest-Clinique Jules VERNE; Nantes, France.
7. Université Paris Cité, Bioinformatics Core Facility, Imagine Institute, INSERM UMR 1163; Paris, France
8. Université Paris Cité, Genomics Platform, Imagine Institute, INSERM UMR 1163; Paris, France
9. Centre de Référence pour les Affections Rares en Génétique Ophtalmologique (CARGO), CHU Toulouse; Toulouse, France

# These authors contributed equally to this work

*__Correspondence:__ lucas.fares-taie@inserm.fr, jean-michel.rozet@inserm.fr

ABSTRACT

Congenital microcoria (MCOR) is a rare hereditary developmental defect of the iris dilator muscle, frequently associated with high axial myopia and high intraocular pressure (IOP) glaucoma. The condition is caused by submicroscopic rearrangements of chromosome 13q32.1. However, the mechanisms underlying the failure of iris development and the origin of associated features remain elusive. Here, we present a 3D architecture model of the 13q32.1 region, demonstrating that MCOR-related deletions consistently disrupt the boundary between two interacting Topologically Associating Domains (TADs). Deleting the critical MCOR-causing region in mice reveals ectopic *Sox21* expression precisely aligning with *Dct*, each located in one of the two TADs. This observation is consistent with the TADs' boundary alteration and adoption of *Dct* regulatory elements by the *Sox21* promoter. Additionally, we identify *Tgfb2* as a target gene of SOX21 and show TGFB2 accumulation in the aqueous humor of a MCOR-affected patient. Accumulation of TGFB2 is recognized for its role in glaucoma and potential impact on axial myopia. Our results highlight the importance of SOX21-TGFB2 signaling in iris development and control of eye growth and IOP. Insights from congenital microcoria studies may provide therapeutic avenues for this condition but also for glaucoma and high myopia conditions, impacting millions.

INTRODUCTION

The iris is a remarkable ocular structure, serving a dual purpose by finely tuning the amount of light that reaches the retina and regulating intraocular pressure (IOP). It comprises a stroma, a double epithelium layer and two dynamic muscles, the dilator and the sphincter, that work together to adjust the size of the pupil and hence the light intensity for optimal vision. The iris is rooted to both the corneal-scleral junction and the ciliary body (CB), whose stroma and epithelial layers are continuous with those of the iris. This structural arrangement creates an open space known as the irido-corneal angle where the aqueous humor (AH) produced by the CB to nourish ocular tissues is drained out, playing a vital role in maintaining intraocular pressure (Davis-Silberman and Ashery-Padan 2008). An increase in IOP is a prominent risk factor for optic nerve damage and glaucoma (GLC) (Gould et al. 2004).

Congenital microcoria (MCOR, MIM#156600) is an extremely rare autosomal dominant condition affecting both of these functions. It is characterized by the partial or complete absence of the iris dilator muscle, which normally originates from the anterior part of the epithelial layer (AEL) and extends along its stroma. The sphincter muscle near the pupil's edge retaining full functionality. The absence of dilator muscle fibers is evident in the presence of pinhole-sized pupils (< 2mm) that exhibit minimal or no dilation, even when mydriatic drugs are used. This also leads to the iris thinning and atrophy of the stroma, particularly in the dilator muscle region, which permits light to pass through, inducing iris transillumination (Simpson and Parsons 1989; Ramirez-Miranda et al. 2011). In the vast majority of the cases, this abnormal development of the iris does not affect the chamber angle that is wide-open although prominent iris processes and a higher insertion of the iris root in the angle have been typically described. Alongside dilation problems, individuals with MCOR are at a substantially increased risk of developing high axial myopia, affecting 70% of cases. Among those with high myopia, half also experience juvenile-onset high IOP glaucoma, an unusually high prevalence compared to the general population, which stands at 34% of all MCOR cases (reviewed in Angée et al. in 2021). The underlying causes of these associated features is highly debated. It has been suggested that the tendency to close the eyelids to reduce the glare caused by iris transillumination in MCOR could lead to form-deprivation myopia. However, the absence of a clear link between myopia and oculocutaneous albinism, which shares similar symptoms of iris transillumination and light sensitivity, challenges this notion (Angée et al. 2021). In relation to glaucoma, high axial myopia, a known contributor to the condition, and the anatomical features of microcoric chamber angles, which may affect AH flow, may play a contributory role but are not solely sufficient. This is evident from the fact that although all individuals with

glaucoma exhibit these anomalies, only about a third of those with these anatomical variations actually develop glaucoma.

The disease has been ascribed to submicroscopic rearrangement of chromosome 13q32.1, particularly deletions and a reciprocal duplication, suggesting that the disease is linked to an alteration of the regulatory landscape of the region (Fares-Taie et al. 2015; Sergouniotis et al. 2017; Pozza et al. 2020).

Here, we provide a 3D architecture model of the 13q32.1 region which suggest that MCOR-related deletions consistently alter the boundary between two interacting Topologically Associating Domains (TADs) in the 13q32.1 region. Deleting the critical 30 Kb MCOR-causing region in mice leads to aberrant *Sox21* (MIM*604974) expression in developing and adult iris and CB, aligning precisely with *Dct* (MIM*191275), located in the adjacent TAD. This suggests ectopic *Sox21* expression may stem from *Dct* regulatory element adoption, supporting the alteration of TAD boundaries.

Additionally, we identify *Tgfb2* (MIM*190220) as a SOX21 target gene and TGFB2 accumulation in the aqueous humor of a MCOR-affected patient. This accumulation, known for its role in glaucoma and potential impact on axial myopia, underscores the significance of SOX21-TGFB2 signaling in these ocular anomalies and iris development. Insights from congenital microcoria studies may offer therapeutic avenues for individuals with this condition, as well as those with primary open-angle glaucoma (POAG) and high myopia, affecting millions.

RESULTS

MCOR-causing deletions are predicted to alter the boundary between two interacting topologically associated domains on chromosome 13q32.1

The MCOR locus, defined by its most distant deletion boundaries, spans 99.8 Kb base pairs on chromosome 13q32.1 (chr13: 95 209 609 - 95 309 380; Angée et al. 2021). According to Hi-C sequencing data available on the 3D Genome Browser, this locus was originally situated within a 1 megabase (Mb) TAD, encompassing the genomic region extending from the *DCT* (MIM*191275) to the *UGGT2* (MIM*605898) genes. Utilizing higher-resolution Hi-C sequencing data obtained from mouse neural progenitor cells, we refined the structural organization of the 13q32.1 region through the detection of two interacting TADs of 1.2 (TAD1) and 1.5 Mb (TAD2), respectively (**Figure 1A, B**). TAD2 which comprises the original 1 Mb TAD comprises at three interacting sub-TADs of 0.2 (TAD2.1), 0.5 (TAD2.2), and 0.2 (TAD2.3) Mb, respectively. Remarkably, all documented deletions associated with MCOR, as

reported by Angée et al. in 2021, exhibit modifications at the interface between TAD2.1 and TAD2.2, along with alterations within the regions of both TADs that engage in mutual interactions (**Figure 1A, 1B**). This underscores the significance of the boundary between TAD2.1 and TAD2.2 and emphasizes the intricate interplay within these topologically associating domains in the context of MCOR. None of the reported deletions have an impact on TAD1 or subTAD2.3 (**Figure 1A, 1B**).

The human MCOR locus at 13q32.1 aligns with a broad syntenic region on mouse 14qE4, covering TADs 1 and 2

Through a comparison of human and mouse genomic sequences, we demonstrate that TADs 1 and 2 reside within a large block of synteny shared by human chromosome 13q32.1 and mouse chromosome 14qE4, with minimal changes in gene composition and organizational structure occurring outside the subTADs 2.1 and 2.2 (**Figure 1C, 1D**). Based on the observed synteny, we generated c57B6J transgenic mice (B6.cΔMCOR) by using the CRISPR-Cas9 methodology to specifically delete the critical MCOR sequence. This approach was undertaken to investigate its regulatory architecture and to gain insights into its role in iris development, as well as its potential connections to glaucoma and high myopia.

Homozygosity for the critical MCOR causing deletion is lethal in C57B6J mice

Mating of heterozygous B6.cΔMCOR/+ failed to produce homozygous B6.cΔMCOR/cΔMCOR animals. To understand this observation, we collected embryos from 8.5 to 10.5 embryonic days (E) and observation showed that homozygous animals ceased developing around E8.5 and regressed by E9.5 (not shown). Further analysis of E9 embryos revealed that homozygous mutants displayed noticeable abnormalities, including smaller size, varying degrees of cardiac hypertrophy, and one individual exhibited pericardial effusion consistent with compromised cardiac function. Additional anomalies included hypoplastic optic and otic vesicles, enlargements in specific facial structures, and irregularities along the body axis (**Figure S1A**).

For in-depth analysis of these abnormalities in homozygous embryos, serial histological sections were conducted (**Figure S1B**). Mutant embryos exhibited pyknotic nuclei in key regions, including the neural tube, hindbrain, and neural crest-derived tissues such as branchial arches and spinal primordia. Massive pyknosis was notably observed in these neural crest-derived tissues. Additionally, scattered pyknotic cells were found in mesenchyme, neural tube, and endodermal regions throughout the embryos (**Figure S1B)**.

Although the mutant embryos displayed a well-regionalized and differentiated heart, a notable finding was the presence of red blood cells in the pericardium, potentially indicating myocardium issues. While the myocardium in mutants was thinner compared to controls, their developmental delay complicated conclusive assessments of abnormal differentiation (**Figure S1B)**. Of note, placenta sections showed no apparent differences between mutants and controls (not shown), suggesting that observed cardiovascular abnormalities are not linked to placental defects.

Together these observations, in particular the pattern of pyknosis in mutant embryos, support defective neural crest migration and differentiation.

Heterozygosity for the critical MCOR causing deletion cause reduced pupil size

In contrast to homozygous animals, heterozygous littermates (B6.cΔMCOR/+; referred to thereafter as the MCOR-mouse model) developed normally (**Figure S1A**). Pupillometry analysis in adult animals revealed a moderate but statistically significant ($p<0.01$) reduction in base-line pupil size compared to B6.WT littermates (**Figure 2**). Exposure to mydriatic drugs enabled pupil dilation in both B6.cΔMCOR/+ and B6.WT animals **(Figure 2**). B6.cΔMCOR/+ irises were not transilluminable.

***Sox21* in TAD2.2 and its product are ectopically expressed in iris tissue of the MCOR mouse model**

To examine the impact of the deletion of the critical MCOR-causing deletion on gene expression in iris tissue, we performed transcriptome sequencing on newborn B6.cΔMCOR/+ and B6.WT irises. Consistent with heterozygosity for the deletion which alters *Tgds* (MIM*616146) and *Gpr180* (MIM*607787), the mRNA levels of these two genes in B6.cΔMCOR/+ animals were approximately half of those found in B6.WT specimens (0.49 and 0.60, respectively; $p < 10e-4$).Further analysis of the genes within the three predicted interacting subTAD within TAD2 revealed *Sox21* expression in irises from B6.cΔMCOR/+, while no expression was observed in B6.WT littermates ($p < 10e-9$). This observation strongly suggests that the critical MCOR-causing deletion induces ectopic expression of *Sox21*, a gene encoding a transcription factor belonging to the SRY-related HMG-box family located in subTAD2.2, approximately 50 Kb downstream of the 3'MCOR locus boundary (**Figure 1**). The expression of the other genes located in the interacting TADs displayed comparable expression in mutant and wildtype irises (not shown).

RT-qPCR and Western blot analyses were conducted on iris RNA and protein extracts from adult mice using specific primers for *Sox21* and a highly specific SOX21 antibody (Matsuda et al. 2012), respectively. These analyses confirmed the sustained ectopic expression of *Sox21* in adulthood (**Figure 3A**) and disclosed the presence of a protein product in B6.cΔMCOR/+ mice, conspicuously absent in B6.WT littermates (**Figure 3B and C**).

Sox21 is detected specifically in DCT-expressing cells from the iris and ciliary body of the MCOR-mouse model

Immunohistochemistry (IHC) analysis of the iris in C57BL6J animals is challenging due to the high pigmentation of the tissue. To circumvent potential alterations to iris integrity caused by depigmentation protocols, we opted to generate albino cΔMCOR/+ and WT lines by mating B6.cΔMCOR/+ animals with tyrosinase (TYR, MIM*606933)-negative Swiss albino (CFW) mice. RT-qPCR analysis of *Sox21* expression in irises of 2-month-old animals from the resulting lines, referred to as SW.cΔMCOR/+ and SW.WT, revealed continued ectopic expression, despite the inactivation of tyrosinase (data not shown). We performed IHC analysis on iris and CB sections from adult animals using antibodies specific to SOX21 and DCT antibodies, respectively. DCT, also recognized as TYRP2, encodes the dopachrome tautomerase and operates as a melanogenic enzyme located just downstream of tyrosinase. It serves as a distinctive marker for melanocyte lineages, encompassing the pigmented epithelium layers of the iris and CB, specifically the iris posterior and CB anterior layers. The *Dct* gene is positioned in TAD2.1 and a mere 75 Kb upstream of the 3'-boundary of the MCOR locus (**Figure 1A and B**). IHC exhibited robust staining of DCT in both the iris posterior and CB anterior epithelia in both SW.cΔMCOR/+ and SW.WT animals (**Figure 3C**). This observation indicates that neither the deletion of the critical MCOR region nor the inactivation of tyrosinase has any discernible effect on the expression of the *Dct* gene in albino mices. Interestingly, in SW.cΔMCOR/+ animals, *Sox21* expression was limited to *Dct*-expressing epithelium layers of the iris and CB (**Figure 3C**). At this age, we observed no SOX21 staining in the anterior layer of the iris, which is the region from which the dilator muscle forms during the embryonic life (**Figures 3C**). Consistent with the ectopic expression of *Sox21* in mutant mice, SOX21 was undetectable in the iris and CB of SW.WT littermates (**Figure 3C**).

Combining RNAscope™ *In Situ* Hybridization (ISH) of *Sox21* mRNA and immune staining of DCT, we investigated their spatio-temporal pattern of expression from 10 embryonic days (E) to birth (postnatal day 0, P0) in SW.WT and SW.cΔMCOR/+ eyes (**Figure 4**). In wildtype eyes, *Sox21* mRNA was detected in the proximal part of the optic vesicle (OV)

at E10 and in the dorsal neuroectoderm at E10.5 and E11. However, from E11.5 onwards, although the DCT protein became evident, Sox21 mRNA was no longer detectable, except in the surface ectoderm forming the eyelid and hair follicles, beginning around E15 (**Figure S2**). In mutant eyes, *Sox21* mRNA was initially detectable in the proximal part of the OV at E10 and in the dorsal neuroectoderm at E10.5 and E11, similar to its expression in wildtype littermates. However, from E10.5 onwards, *Sox21* mRNA was observed in the outer layer of the optic cup (OC) and later in the pigmented structures derived from this layer (**Figure 4A**). Notably, these pigmented structures in the developing eye include the retinal pigmented epithelium (RPE), as well as the iris anterior (reversed in adults) and CB anterior epithelia (**Figure 4B**). Notably, these structures consistently expressed the DCT protein, which became readily detectable from E11.5 onward (**Figure 4A and B**).

The absence of *Sox21* expression in the non-pigmented posterior epithelium layer of both the developing and adult CB, along with the loss of both *Sox21* and DCT expression in the adult anterior epithelium of irises compared to developing irises (Figures 3D and 4), further strengthens the evidence for the co-expression of *Sox21* and DCT in SW.cΔMCOR/+ eyes (**Figure 4A and B**).

Combined analysis of SOX21 targets and gene expression deregulation suggests perturbations in genes associated with iris development and MCOR-related symptoms in the MCOR-mouse model

We investigated the impact of the loss of the critical MCOR-causing region on the expression of genes lying outside of TADs 1 and 2 by analyzing RNAseq data from the new-born B6.cΔMCOR/+ and B6.WT. This study detected 2500 differentially expressed genes (DEG ≥1.5 fold, $p<0.05$; **Figure 5A**). Gene Ontology (GO) enrichment analysis revealed a significant enrichment of genes associated with crucial processes such as cellular commitment, development, differentiation, and migration, particularly in the context of neural and sensory systems. Notably, the top pathways identified include cell fate commitment, forebrain development, regulation of cell differentiation, retina morphogenesis, regulation of neuron differentiation, and neuron projection development (**Figure 5B**). An enrichment of genes related to the regulation of smooth muscle cell proliferation was also noted, albeit with a lower significance ranking (top 45; **Figure 5B**). The impact of the critical MCOR-causing deletion on the gene *Des* (MIM*125660), encoding desmin (DES) intermediate filaments, reported to be deficient in the iris anterior epithelium layer of MCOR-affected patients (Simpson and

Parsons 1989). This analysis showed reduced expression of the gene in the iris of B6.cΔMCOR/+ compared to B6.WT littermates (0.49, p = 0.012).

To investigate whether the diminished pupil size in B6.cΔMCOR/+ could be associated with a reduction in DES abundance, we conducted immunohistochemistry (IHC) on mouse iris sections using antibodies against DES and smooth muscle actin (SMA; not deregulated in RNAseq datasets) as control. While SMA stained both the sphincter and dilator muscle fibers (**Figure S2**), the available DES antibodies proved unsuccessful in detecting the protein in both B6.cΔMCOR/+ and B6.WT irises.

Further analysis to identify deregulated signaling pathways linked to iris development and MCOR disease symptoms unveiled an impact of the critical MCOR deletion on *Wtn2b* (MIM*601968; 2.35, $p < 0.01$) that is known to play an essential for the specification of iris progenitor cells toward myoepithelial fate, *Bmp7* (MIM*112267; 1.47, $p<0.05$) playing a role in iris smooth muscle generation (Davis-Silberman and Ashery-Padan 2008) and *Tgfb2* (MIM*190220; 1.6, $p<0.01$) known to be involved both in GLC (Prendes et al. 2013) and possibly high myopia (Jia et al. 2017).

Tgfb2 is a direct target of SOX21 in the iris of the MCOR-mouse model

To determine which of the deregulated genes were targets of SOX21, we conducted ChIP-seq analysis using the SOX21 antibody on irises from newborn B6.cΔMCOR/+ mice. This analysis revealed 25 DNA regions throughout the genome ($p \leq 0.1$), including 10 intragenic (all intronic) and 14 intergenic and 1 in promoter-TSS regions, respectively (**Table 1**). We conducted a search for deregulated (≥ 1.5 fold; $p \leq 0.05$) expression among these genes and nearest genes in cases where the binding occurred outside a gene, in RNA-seq datasets from B6.cΔMCOR/+ compared to B6.WT animals. This analysis identified a unique gene: *Tgfb2* (**Table 1**). The remaining genes either exhibited no expression or showed no deregulation in the iris of both B6.cΔMCOR/+ and B6.WT animals. Binding of SOX21 to *Tgfb2* as determined by CHIPSEQ was unambiguous ($p<0.0001$) and strongly supported by JASPAR analysis, which searches for a consensus SOX21-binding sequence in the 252 bp intronic region identified by ChIPseq (chr1:186,698,304-186,698,555; GRCm38/mm10 Assembly; 5.9 Kb downstream from the consensus donor splice-site of the 16 Kb-long intron 1; **Figure 5A**). This sequence is conserved in the human *TGFB2* intron 1 orthologous region, which comprises many potential transcription factor-binding sites (GRCh38; chr1:218,352,441-218,352,576; **Figure 5B**).

In line with the association between SOX21 and *Tgfb2*, RNAseq analysis revealed dysregulation of the TGFB2 signaling pathway in the iris of B6.cΔMCOR/+ compared to B6.WT littermates (**Figure 5C**).

TGFB2 concentration is elevated in the AH of a MCOR patient

The ectopic expression of *Sox21* in the ciliary body (CB), along with SOX21 binding to a regulatory region of the *Tgfb2* and its upregulation in B6.cΔMCOR/+ irises, prompted us to measure the TGFB2 concentration in the aqueous humor (AH) of 12-month-old B6.cΔMCOR/+ and B6.WT mice using an ELISA assay. The concentrations, measured from pooled AH from both eyes, exhibited high variability in both wild-type and mutant eyes. Analysis of a large number of samples revealed no statistical difference between the two groups (**Figure S3**).

However, when analyzing AH samples collected on the same day during cataract surgery in a 45-year-old non-glaucomatous adult MCOR individual from a large French pedigree (Rouillac et al. 1998), as well as in eleven non-MCOR and non-glaucomatous individuals, we observed a significant increase in TGFB2 levels in the patient's AH compared to the controls (**Figure 6**). Notably, the TGFB2 concentration was elevated as well in the AH sample collected during cataract surgery in the fellow eye of the MCOR individual, which occurred two weeks after the first eye surgery. This observation provides additional support for the connection between SOX21 and TGFB2, emphasizing the role of TGFB2 in MCOR.

DISCUSSION

Various anatomical analyses have been conducted on post-mortem eyes and iris specimens obtained during ocular surgery from adult individuals affected by congenital microcoria. These analyses revealed significant iris thinning, stromal atrophy, and a deficiency or absence of stromal contractile processes in the anterior iris epithelium, suggesting that the constitutive closure of the iris is linked to a defective development of the iris musculature. However, the mechanisms involved remain elusive, as does the reason why the disease is often associated with an abnormally long eye and high intraocular pressure (reviewed in Angée et al., 2021). We leveraged the recent identification of the genetic etiology of the disease and the accessibility of CRISPR-Cas9 technology to develop a mouse model of the disease, analysis of which provides support for the central role of the SOX21 transcription factor in the pathology. The role of SOX21 in eye development has been documented in the chick and zebrafish (Uchikawa et al. 1999; Lan et al. 2011) but not in the mouse. In the chick, *Sox21* has been

reported to be transiently activated during the early phases of optic vesicle morphogenesis and specification in the lens and retina but is no longer expressed afterward (Lan et al. 2011); *Sox21* expression in the eye ceases before the onset of iris development. Loss of Sox21 function in the chick, akin to findings in zebrafish, disrupts normal lens development (Pauls et al. 2012). In contrast, a *Sox21*-knockout mouse model has been reported (Kiso et al. 2009), which exhibited no ocular defects. This finding is consistent with our immunohistological analysis, which detected no expression of *Sox21* in the anterior segment of the developing mouse eye. In our study, we demonstrate that the deletion of the syntenic critical region in the mouse genome, responsible for congenital microcoria in humans, leads to a constitutive expression of *Sox21*. Remarkably, we observed colocalization of *Sox21* and the melanogenic marker DCT in both developing and adult eyes. This observation aligns with the predicted 3D structural organization of the region encompassing the MCOR locus, which situates *Dct* and *Sox21* in two adjacent interacting TADs, the integrity of which is consistently disrupted by MCOR-causing deletions. Importantly, the genes themselves remain unaltered by any of the MCOR-causing deletions. Disruptions in TADS have been shown to influence regulatory mechanisms during organogenesis, potentially leading to developmental defects (Lupiáñez et al. 2015). Within this framework, the loss of boundary between the two TADs in MCOR could instigate a comprehensive reorganization of the region and render *Dct* active enhancers available for *Sox21* expression. In this context, it is crucial to note that enhancer priming has been shown to precede the initiation of gene transcription (Panigrahi and O'Malley 2021; Reddington et al. 2020; Ghavi-Helm et al. 2014). This, coupled with the fact that our analysis focused on expression of the DCT protein rather than mRNA expression in irises from the mutant mouse, might account for the slight discrepancy observed in our experiments between the detection of *Sox21* mRNA (E10.5) and the detection of DCT protein (E11.5).

Consistent with the expression pattern of the melanogenic DCT protein, the ectopic expression of *Sox21* is detected in the pigmented posterior iris epithelium at the adult age in the MCOR-mouse model, while it is absent in the anterior epithelium responsible for dilator muscle formation (Lai 1972; Forrester et al. 2016). During embryonic development, however, the anterior iris epithelium is pigmented and expresses DCT. The literature lacks reports on the development of iris muscles in mice, but in rats, the dilator muscle begins development around E18.5 and continues postnatally (Lai 1972). In our study, at E18.5 and P0 in mice, we found that the anterior iris epithelium expresses DCT in the wildtype mouse and both DCT and *Sox21* in the MCOR-mouse model. This suggests that the abnormal expression of Sox21 in the anterior epithelium of the MCOR-mouse model coincides with the onset of dilator muscle

development and diminishes progressively during postnatal development, concurrent with the loss of DCT expression in the anterior epithelium (**Figure 4**). These findings could explain histological observations of microcoric irises, revealing anomalies ranging from poor differentiation and disordered fibers lacking myofilaments and intermediate filaments to complete growth inhibition, which point to anomalies in the terminal stages of anterior iris pigment epithelium differentiation (Reviewed in Angée et al. 2021). In the mouse, our histological analysis failed to detect such anomalies. This could be attributed to the minimal iris phenotype of the mutant mouse, potentially linked to weaker *Sox21* expression, divergent timelines in iris dilator muscle development, or dissimilarities in the 3D architecture of the region encompassing the MCOR locus between humans and mice. While the iris phenotype in the mutant mouse is minimal, it is noteworthy that we observed a reduced expression of desmin in the iris of newborn mutant mice. This finding aligns with studies on iris anatomy, which report the absence or severe reduction of desmin fibers in the anterior epithelium of microcoric irises (as reviewed in Angée et al., 2021).

The reduced expression of desmin was identified through RNAseq analysis, given the absence of suitable antibodies for immunocytochemistry analysis. Furthermore, RNAseq analysis revealed the deregulation of key genes known to be crucial in signalling pathways important for iris development. Notably, *Wnt2B*, a gene with significant roles in iris specification and morphogenesis (as reviewed in Noa Davis-Silberman and Ruth Ashery-Padan, Brain Research, 2008), was found to be significantly upregulated in mutant irises. This deregulation appears to be indirect to *Sox21* induction, as indicated by ChIPseq analysis which did not reveal binding of the SOX21 protein on *Wnt2b* regulatory sequences. Among the deregulated genes identified by RNAseq, *Tgfb2* is the sole gene found to bind SOX21 in mutant irises. This binding occurs through a consensus binding sequence located in intron 1. This observation aligns with a growing body of evidence across various organisms, suggesting that for a subset of genes, the critical sequences regulating expression are not primarily situated in the promoter but within introns within the first kilobase of transcribed sequences (Rose 2019). Remarkably, several studies have reported significantly elevated levels of TGFB2 in the aqueous humor of individuals with primary open-angle glaucoma (POAG), as well as in cultured glaucomatous cell strains and isolated human glaucomatous trabecular meshwork (TM) tissues (Wordinger et al. 2014; Agarwal et al. 2015). The cause and cellular source of TGFB2 in glaucomatous eyes remain elusive. However, studies have demonstrated that cells from the trabecular meshwork, through which aqueous humor is drained out at the iridocorneal angle, express an active TGF receptor complex and respond to exogenous TGFB2 (Medina-

Ortiz et al. 2013; Montecchi-Palmer et al. 2017). This has been reported to result in increased synthesis of extracellular matrix proteins (ECM), accumulation of which increases resistance to aqueous outflow, leading to elevated intraocular pressure and glaucoma in both human and mouse (Zeimer et al. 1998; Munemasa and Kitaoka 2012; Prendes et al. 2013; Oikawa et al. 2023).

This knowledge, combined with (i) the histopathologic examination of trabecular meshwork (TM) biopsies from two microcoric brothers with elevated IOP, revealing ECM accumulation (Tawara et al. 2005), and (ii) an elevated concentration of TGFB2 in the aqueous humor of an individual with MCOR, implies that glaucoma associated with MCOR may be initiated by SOX21. The strength of this inference is heightened by our findings, which provide evidence of ectopic *Sox21* expression in the ciliary body—where the aqueous humor is produced—specifically in the non-pigmented posterior epithelium (Skalicky 2016). Furthermore, a recent study has uncovered a significant correlation between elevated TGFB2 levels in the aqueous humor and axial elongation. This discovery not only suggests a connection between the protein and, by extension, SOX21 but also extends the potential link to high myopia (Jia et al. 2017).

Finally, we demonstrate that homozygosity for the critical MCOR-causing deletion is lethal in the mouse. While the possibility of *Sox21* playing a role cannot be ruled out, it is more likely that lethality results from the homozygous deletion of *Tgds*. Notably, biallelic mutations in *TGDS* have been documented to lead to a severe developmental disorder characterized by the Pierre Robin anomaly, known as Catel-Manzke syndrome (MIM# 616145). Intriguingly, to our knowledge, no instances of homozygosity or compound heterozygosity for loss-of-function alleles have been reported, suggesting that such a situation could be lethal.

In conclusion, our study demonstrates that the critical submicroscopic deletion associated with MCOR disrupts the 3D architecture of the region, leading to modified gene interactions. This alteration results in the ectopic expression of the Sox21 transcription factor in Dct-expressing pigmented cells within the iris and ciliary body of MCOR mice. Importantly, we posit that in MCOR, both GLC and high myopia stem directly from SOX21-mediated TGFB2 overexpression in the ciliary body, rather than arising due to abnormal iris development. Consequently, we propose that SOX21 serves as a crucial link, connecting iris malformation, high myopia, and glaucoma in congenital microcoria. This positions MCOR as an invaluable model for scrutinizing eye development and unraveling the underlying mechanisms of common myopia and primary open-angle glaucoma.

MATERIALS AND METHODS

Generation of a MCOR-mouse model

The B6.cΔMCOR strain utilized in this study was generated through CRISPR/Cas9 methodology at the Transgenesis Platform of the Animal Facility (LEAT) at the Imagine Institute (Paris). Animal procedures received approval from the French Ministry of Research and were conducted in compliance with the French Animal Care and Use Committee from the University of Paris Cité (APAFIS #14311-201801151627355). Two guide RNAs (sgRNAs, 5'-CTCACAGTTTGGTCCAGGCT-3' and 5'-ATTCCCCAGCAGAGAGGCGC-3') targeting the MCOR locus were designed using the CRISPOR web tool (http://crispor.tefor.net/). Deleterious alleles were induced via CRISPR/Cas9 ribonucleoprotein (RNP) complex microinjection into C57BL/6J mouse zygote pronuclei, as described by Ucuncu in 2020. Offspring were genotyped from genomic DNA through PCR amplification using appropriate primers (forward 5'-GGATGTGCGTTCAAATCCCAGTACC-3' and reverse 5'-TGTTCCCATGCAGTGTGGCAATG-3'). To eliminate potential off-target mutations, transgenic animals underwent multiple generations of backcrossing with C57BL/6J mice. SW.cΔMCOR/+ animals were obtained by crossing B6.cΔMCOR/+ with Swiss albino mice over several generations.

Pupillometry analysis

Two-month-old mice (8 B6.WT and 8 B6.cΔMCOR/+) underwent dark adaptation overnight, and pupillary responses were recorded following established protocols (Kostic et al. 2016). To avoid the potential effects of anesthesia, animals were not anesthetized. The baseline pupil diameter was defined as the mean pupil diameter during the 500 ms before light onset. Subsequently, all pupil sizes were normalized relative to this baseline value. The light stimulus sequence comprised 50 ms exposures to (-2.2, -1, and 0.5) log W/m2 white light and a 20s exposure to 0 log W/m2 blue light. Pupil diameter was automatically determined using Neuroptics A2000, Inc**.** software. One-way/two-way ANOVA analyses were employed to identify significant differences.

RNA extraction

Mice aged from 0 days postnatal (P0) to 12 months, were euthanized, and their eyes were enucleated. On ice, the eyes were dissected to collect the iris and ciliary body. Each eye was halved following the ora serrata, and after lens removal, the iris and ciliary body were extracted

from the anterior segment. Tissues from both eyes were pooled for total RNA extraction using the RNAeasy MiniKit (Qiagen, Hilden, Germany), following the manufacturer's instructions, post-mechanical tissue disruption. RNA quality and concentration were assessed through optical density measurements (Nanodrop, Thermo Fisher Scientific, Waltham, MA, USA), and RNA integrity was analyzed using capillary electrophoresis with a Tape Station (Agilent, Santa Clara, CA, USA) and High Sensitivity RNA Screen Tape.

RNAseq analysis

The Ovation Mouse RNA-Seq System from NuGEN (Tecan Genomics, Leek, NL) was employed to prepare RNA-seq libraries using 25 ng of total RNA, following the manufacturer's recommendations. This kit enables strand-specific RNA-Seq library construction using 10 to 100 ng of total RNA and utilizes the Insert Dependent Adaptor Cleavage (InDA-C) technology to eliminate ribosomal RNA transcripts. An equimolar pool of the final indexed RNA-Seq libraries was sequenced on an Illumina HiSeq 2500, targeting a sequencing depth of approximately 30 million paired-end reads per library. On average, 28 million reads were obtained. FASTQ files were mapped to the ENSEMBL Mouse (MM10) reference using Hisat2 and counted by feature. Counts from the Subread R package. Read count normalizations and group comparisons were conducted using three independent and complementary statistical methods (Deseq2, edgeR, LimmaVoom). Flags were generated from counts normalized to the mean coverage, where counts <20 were considered as background (flag 0) and counts >=20 were considered as signal (flag=1). P50 lists, utilized for statistical analysis, grouped genes showing flag=1 in at least half of the compared samples. Results from the three methods were filtered at p-value <= 0.05 and fold changes of 1.2/1.5/2, and grouped by Venn diagram. Cluster analysis employed hierarchical clustering with the Spearman correlation similarity measure and ward linkage algorithm. Heat maps were generated using the R package ctc: Cluster and Tree Conversion and visualized with Java Treeview software. Functional analyses were conducted using Ingenuity Pathway Analysis (IPA, Qiagen).

RT-qPCR analysis

cDNA was synthesized using the cDNA Verso reverse transcription kit (Thermo Fisher Scientific). Quantitative RT-PCR (RT-qPCR) was conducted using SYBR Green (Sso Advanced Universal SybrGreen Supermix, Bio-Rad, Hercules, CA, USA), with *B2m*, *Tbp*, *Gusb* and *Hprt* as reference genes. The primer sequences for qPCR were as follows: *Sox21* forward 5'-AGCCTGTGGACCACGTCAA-3' and reverse 5'-

CCGACTCGGTGAGCAGCTT; *Dct* forward 5'-AGATTGTGTGCGACAGCTTG-3' and reverse 5'-AAGGGAGGGCTGTCAAACTT-3'; *B2m* forward 5'-CCTGTATGCTATCCAGAAAACCCCT-3' and reverse 5'-CGTAGCAGTTCAGTATGTTCGGCTT-3'; *Tbp* forward 5'-TGACCTAAAGACCATTGCACTTCGT-3' and reverse 5'-CTGCAGCAAATCGCTTGGGA-3'; *Gusb* forward 5'-CTGGGGTTGTGATGTGGTCTGT-3' and reverse 5'-TGTGGGTGATCAGCGTCTTAAAGT-3'; *Hprt* forward 5'-GTTGGTACAGGCCAGACTTTGTT-3' and reverse 5'-AAACGTGATTCAAATCCCTGAAGTA-3'. The relative expression of *Sox21* and Dct was calculated using the method described in Vandesompele et al., 2002.

Western blot analysis

The western blots were performed using 40 µg of total iris protein lysates. The following antibodies were used in this study: SOX21 (AF3538, R&D Systems, Minneapolis, MN, USA) and beta-Actin (ab8227, Abcam, Cambridge, UK). Secondary antibodies, goat IgG or mouse IgG HRP (Thermo Fisher Scientific) were used at a 1:10000 dilution. Western blot membranes were developed using the Clarity Western ECL substrate (Bio-Rad), and the signal was detected with a Chemidoc MP Imaging System (Bio-Rad).

ChIPseq analysis

The irises of 24 newborns (P0), including both B6.cΔMCOR/+ and B6.WT mice, were collected for ChIP-seq analysis. Three samples were prepared for B6.cΔMCOR/+ mice and three for B6.WT mice, with each sample comprising 16 irises. The ChIP assay was performed on all samples using 2 µg of chromatin.

Cells were crosslinked with 1% formaldehyde for 10 minutes at room temperature. ChIP was carried out using the iDeal ChIP-seq kit for Transcription Factors (C01010055, Diagenode, Liege, Belgium), following the provided protocol. Immunoprecipitation utilized an anti-SOX21 antibody (AF3538, R&D Systems). Sequencing was performed on an Illumina HiSeq 4000, running HiSeq Control Software HD version 3.4.0.38. Quality control of sequencing reads was conducted using FastQC. Reads were aligned to the reference genome (MM10) from the UCSC genome browser using BWA software v.0.7.5a. All samples were filtered using a list of genomic regions created from the two input samples. Subsequently, samples were deduplicated using SAMtools version 1.3.1. Alignment coordinates were converted to BED format using BEDTools v.2.17, and peak calling was performed using MACS2.

ELISA assay

Mice were euthanized at 5, 6, and 12 months old, and aqueous humor (AH) was collected from both eyes using a 27G-syringe inserted at the ora serrata (around 5 µL per eye). The AH from both eyes was pooled, and TGFB2 proteins from the samples were activated using one volume of HCl and two volumes of NaOH, as per the manufacturer's instructions (Mouse TGF-beta 2 Quantikine ELISA Kit, R&D Systems). The samples were diluted (1:80), and the quantity of total inactive TGFB2 protein was measured using the Quantikine kit.

Human AH was collected from ten patients undergoing cataract surgery at Clinique Jules Verne, Nantes, France. The mean age of the nine controls was 76.7 ± 5 years old, while the MCOR patient was the youngest at 44 years old. All samples were collected with the written and informed consent of the patients. TGFB2 dosage in each eye (13 controls + 2 cases) was conducted with the Human TGF-beta 2 Quantikine ELISA kit (R&D Systems), following the provided instructions.

Immunofluorescence and RNAscope analysis

Pregnant mice were euthanized to collect embryos at various stages, from E10.5 to P0. Accurate embryonic stages were assigned post-cutting by consulting established atlases due to variations in early embryo development within littermates. Embryo heads were fixed with 4% Paraformaldehyde (PFA), and fixed heads as well as fresh adult eyes were embedded in Optimal Cutting Temperature (OCT) compound and frozen in liquid nitrogen for rapid tissue freeze. OCT blocks were stored at -80°C and brought up to -20°C prior to cutting (CM3050S, Leica, Wetzlar, Germany). Frozen tissue sections (14µm thickness) were collected at the level of the pupillary aperture, air-dried, and stored at -80°C.

Frozen sections were rinsed in PBS to remove surrounding OCT, and antigen retrieval was performed using Citrate Buffer (pH 6.0) in a 95°C water bath for 30 minutes. Slides were then cooled for 30 minutes at room temperature. Tissues were blocked for 1 hour in PBS with 1% bovine serum albumin (BSA), labeled with primary antibodies anti-SOX21 (AF3538, R&D Systems), anti-DCT (ab74073, Abcam), and Cy3-coupled anti-alpha Smooth Muscle Actin (C6198, Sigma-Aldrich, Saint-Louis, MO, USA), followed by appropriate secondary antibodies. Slides were counterstained with DAPI and mounted with Fluoromount medium (Sigma-Aldrich).

For mRNA detection, slides were processed using the RNAscope Multiplex Fluorescent v2 Assay, and subsequent immunohistochemistry was performed. All images were acquired with a Spinning Disk Confocal microscope (Carl Zeiss, Oberkochen, Germany), capturing whole

sections with a 10X objective and specific areas of interest (iris, ciliary body, and margins of the optic cup) with a 40X oil-objective. Raw images were converted to TIFF for further analysis using Fiji (v1.53t).

Statistical analysis

Unpaired bilateral Student's t-test was used for two-group analyses. Two-way ANOVA analysis was used for multigroup analyses (GraphPad Prism, ver. 10.0.3). Data are presented as the mean ± SEM; $p<0.05$ was considered significant.

CONFLICT OF INTEREST

The SOX21-TGFB2 pathway in iris development, axial myopia, and glaucoma has been officially patented under the title: "Methods and pharmaceutical compositions for treating ocular diseases" (WO/2021/245224). The inventors of this groundbreaking patent are JMR, LFT, BN, CA, and JK.

ACKNOWLEDGEMENTS

This research has been generously supported by grants from the Agence Nationale de la Recherche (ANR# -20-CE 12-0019-01), the Institut Nationale de la Santé et de la Recherche Médicale (INSERM), MSD Avenir (DEVO-DECODE program), the Fondation Vision, and the Association Retina France.

AUTHOR CONTRIBUTIONS

JK, JMR and LFT designed the project. BP, JLV and PD generated the MCOR mice. CA and EE performed and interpreted the molecular, histological and imaging experiments. DH analyzed the Hi-Cseq data. CK and SC performed the pupillometry experiments. ED, JK, JP and NCh provided clinical data. MZ and CBF performed sequencing of the RNA samples. NCa performed bioinformatic analyses. BN provided technical assistance. CA wrote the manuscript and prepared the figures with contributions from all coauthors. JM and LFT reviewed all of the data and edited the manuscript.

REFERENCES

Agarwal P, Daher AM, Agarwal R. 2015. Aqueous humor TGF-β2 levels in patients with open-angle. *Mol Vis*.

Angée C, Nedelec B, Erjavec E, Rozet J-M, Fares Taie L. 2021. Congenital Microcoria: Clinical Features and Molecular Genetics. *Genes* **12**: 624.

Davis-Silberman N, Ashery-Padan R. 2008. Iris development in vertebrates; genetic and molecular considerations. *Brain Res* **1192**: 17–28.

Fares-Taie L, Gerber S, Tawara A, Ramirez-Miranda A, Douet J-Y, Verdin H, Guilloux A, Zenteno JC, Kondo H, Moisset H, et al. 2015. Submicroscopic Deletions at 13q32.1 Cause Congenital Microcoria. *Am J Hum Genet* **96**: 631–639.

Forrester JV, Dick AD, McMenamin PG, Roberts F, Pearlman E. 2016. Chapter 2 - Embryology and early development of the eye and adnexa. In *The Eye (Fourth Edition)* (eds. J.V. Forrester, A.D. Dick, P.G. McMenamin, F. Roberts, and E. Pearlman), pp. 103-129.e8, W.B. Saunders https://www.sciencedirect.com/science/article/pii/B9780702055546000022 (Accessed September 13, 2023).

Ghavi-Helm Y, Klein FA, Pakozdi T, Ciglar L, Noordermeer D, Huber W, Furlong EEM. 2014. Enhancer loops appear stable during development and are associated with paused polymerase. *Nature* **512**: 96–100.

Gould DB, Smith RS, John SWM. 2004. Anterior segment development relevant to glaucoma. *Int J Dev Biol* **48**: 1015–1029.

Jia Y, Yue Y, Hu D-N, Chen J-L, Zhou J-B. 2017. Human aqueous humor levels of transforming growth factor-β2: Association with matrix metalloproteinases/tissue inhibitors of matrix metalloproteinases. *Biomed Rep*. http://www.spandidos-publications.com/10.3892/br.2017.1004 (Accessed August 26, 2022).

Kiso M, Tanaka S, Saba R, Matsuda S, Shimizu A, Ohyama M, Okano HJ, Shiroishi T, Okano H, Saga Y. 2009. The disruption of Sox21-mediated hair shaft cuticle differentiation causes cyclic alopecia in mice. *Proc Natl Acad Sci* **106**: 9292–9297.

Kostic C, Crippa SV, Martin C, Kardon RH, Biel M, Arsenijevic Y, Kawasaki A. 2016. Determination of Rod and Cone Influence to the Early and Late Dynamic of the Pupillary Light Response. *Invest Ophthalmol Vis Sci* **57**: 2501–2508.

Lai Y-L. 1972. The development of the dilator muscle in the iris of the albino rat. *Exp Eye Res* **14**: 203–207.

Lan X, Wen L, Li K, Liu X, Luo B, Chen F, Xie D, Kung H. 2011. Comparative analysis of duplicated sox21 genes in zebrafish. *Dev Growth Differ* **53**: 347–356.

Lupiáñez DG, Kraft K, Heinrich V, Krawitz P, Brancati F, Klopocki E, Horn D, Kayserili H, Opitz JM, Laxova R, et al. 2015. Disruptions of topological chromatin domains cause pathogenic rewiring of gene-enhancer interactions. *Cell* **161**: 1012–1025.

Matsuda S, Kuwako K, Okano HJ, Tsutsumi S, Aburatani H, Saga Y, Matsuzaki Y, Akaike A, Sugimoto H, Okano H. 2012. Sox21 Promotes Hippocampal Adult Neurogenesis via the Transcriptional Repression of the Hes5 Gene. *J Neurosci* **32**: 12543–12557.

Medina-Ortiz WE, Belmares R, Neubauer S, Wordinger RJ, Clark AF. 2013. Cellular fibronectin expression in human trabecular meshwork and induction by transforming growth factor-β2. *Invest Ophthalmol Vis Sci* **54**: 6779–6788.

Montecchi-Palmer M, Bermudez JY, Webber HC, Patel GC, Clark AF, Mao W. 2017. TGFβ2 Induces the Formation of Cross-Linked Actin Networks (CLANs) in Human Trabecular Meshwork Cells Through the Smad and Non-Smad Dependent Pathways. *Invest Ophthalmol Vis Sci* **58**: 1288–1295.

Munemasa Y, Kitaoka Y. 2012. Molecular mechanisms of retinal ganglion cell degeneration in glaucoma and future prospects for cell body and axonal protection. *Front Cell Neurosci* **6**: 60.

Oikawa K, Torne O, Sun D, Moon AKB, Kiland JA, Trane RM, McLellan GJ. 2023. Aqueous Humor TGF-β2 and Its Association With Intraocular Pressure in a Naturally Occurring Large Animal Model of Glaucoma. *Invest Ophthalmol Vis Sci* **64**: 18.

Panigrahi A, O'Malley BW. 2021. Mechanisms of enhancer action: the known and the unknown. *Genome Biol* **22**: 108.

Pauls S, Smith SF, Elgar G. 2012. Lens development depends on a pair of highly conserved Sox21 regulatory elements. *Dev Biol* **365**: 310–318.

Pozza E, Verdin H, Deconinck H, Dheedene A, Menten B, De Baere E, Balikova I. 2020. Microcoria due to first duplication of 13q32.1 including the GPR180 gene and maternal mosaicism. *Eur J Med Genet* **63**: 103918.

Prendes MA, Harris A, Wirostko BM, Gerber AL, Siesky B. 2013. The role of transforming growth factor β in glaucoma and the therapeutic implications. *Br J Ophthalmol* **97**: 680–686.

Ramirez-Miranda A, Paulin-Huerta JM, Chavez-Mondragón E, Islas-de la Vega G, Rodriguez-Reyes A. 2011. Ultrabiomicroscopic-histopathologic correlations in individuals with autosomal dominant congenital microcoria: three-generation family report. *Case Rep Ophthalmol* **2**: 160–165.

Reddington JP, Garfield DA, Sigalova OM, Karabacak Calviello A, Marco-Ferreres R, Girardot C, Viales RR, Degner JF, Ohler U, Furlong EEM. 2020. Lineage-Resolved Enhancer and Promoter Usage during a Time Course of Embryogenesis. *Dev Cell* **55**: 648-664.e9.

Rose AB. 2019. Introns as Gene Regulators: A Brick on the Accelerator. *Front Genet* **9**. https://www.frontiersin.org/articles/10.3389/fgene.2018.00672 (Accessed November 11, 2023).

Rouillac C, Roche O, Marchant D, Bachner L, Kobetz A, Toulemont PJ, Orssaud C, Urvoy M, Odent S, Le Marec B, et al. 1998. Mapping of a congenital microcoria locus to 13q31-q32. *Am J Hum Genet* **62**: 1117–1122.

Sergouniotis PI, Ellingford JM, O'Sullivan J, Fenerty CH, Black GC. 2017. Genome sequencing identifies a large deletion at 13q32.1 as the cause of microcoria and childhood-onset glaucoma. *Acta Ophthalmol (Copenh)* **95**: e249–e250.

Simpson WA, Parsons MA. 1989. The ultrastructural pathological features of congenital microcoria. A case report. *Arch Ophthalmol Chic Ill 1960* **107**: 99–102.

Skalicky SE. 2016. The Ciliary Body and Aqueous Fluid Formation and Drainage. In *Ocular and Visual Physiology: Clinical Application* (ed. S.E. Skalicky), pp. 67–83, Springer, Singapore https://doi.org/10.1007/978-981-287-846-5_5 (Accessed August 25, 2023).

Tawara A, Itou K, Kubota T, Harada Y, Tou N, Hirose N. 2005. Congenital microcoria associated with late-onset developmental glaucoma. *J Glaucoma* **14**: 409–413.

Uchikawa M, Kamachi Y, Kondoh H. 1999. Two distinct subgroups of Group B Sox genes for transcriptional activators and repressors: their expression during embryonic organogenesis of the chicken. *Mech Dev* **84**: 103–120.

Ucuncu E, Rajamani K, Wilson MSC, Medina-Cano D, Altin N, David P, Barcia G, Lefort N, Banal C, Vasilache-Dangles M-T, et al. 2020. MINPP1 prevents intracellular accumulation of the chelator inositol hexakisphosphate and is mutated in Pontocerebellar Hypoplasia. *Nat Commun* **11**: 6087.

Vandesompele J, De Preter K, Pattyn F, Poppe B, Van Roy N, De Paepe A, Speleman F. 2002. Accurate normalization of real-time quantitative RT-PCR data by geometric averaging of multiple internal control genes. *Genome Biol* **3**: research0034.1-research0034.11.

Wordinger R, Sharma T, Clark A. 2014. The Role of TGF-β2 and Bone Morphogenetic Proteins in the Trabecular Meshwork and Glaucoma. *J Ocul Pharmacol Ther Off J Assoc Ocul Pharmacol Ther* **30**.

Zeimer R, Asrani S, Zou S, Quigley H, Jampel H. 1998. Quantitative detection of glaucomatous damage at the posterior pole by retinal thickness mapping. A pilot study. *Ophthalmology* **105**: 224–231.

Gene	Gene Description	Chr	Peak Score	Annotation	Distance to TSS	Nearest PromoterID	RNAseq
Hipk2	Homeodomain interacting protein kinase 2	chr6	104.51 /26.18	intron (NM_010433, intron 2 of 14)	76864	NM_001136065	
Gm13580	Predicted gene 13580	chr2	46.62	Intergenic	-8724	NR_046065	
Gm17644	Predicted gene 17644	chr1	43.95	Intergenic	-22756	NR_045297	
Tgfb2	Transforming growth factor, beta 2	chr1	40.86	intron (NM_009367, intron 1 of 6)	7563	NM_009367	1,6 Up Regulated in HT
Mydgf	Myeloid derived growth factor	chr17	40.64	intron (NM_172624, intron 10 of 20)	-16198	NM_080837	
Olfr854	Olfactory receptor 854	chr9	37.19	Intergenic	-8090	NM_146522	
Tex14	Testis expressed gene 14	chr11	24.63	intron (NM_031386)	-4435	NM_001199293	
Gm4736	Predicted gene 4736	chr6	21.86	Intergenic	-99620	NM_053251	
Sjf1	SMC5-SMC6 complex localization factor 1	chr13	20.03	intron (NM_134071, intron 5 of 20)	25853	NM_134071	
4930521E06Rik	RIKEN cDNA 4930521E06 gene	chr1	18.78	Intergenic	-206375	NR_040602	
Ctdsp1	C-terminal domain small phosphatase 1	chr1	17.45	Intergenic	-4548	NM_153088	
Myo7a	Myosin VIIA	chr7	16.1	intron (NM_001256081, intron 39 of 48)	49182	NM_001256083	
AA545190	EST AA545190	chr6	15.75	Intergenic	788031	NR_033776	
Popdc3	Popeye domain containing 3	chr10	15.56	Intergenic	-109987	NM_024286	
Gdnf	Glial cell line derived neurotrophic factor	chr15	14.96	Intergenic	-113169	NM_001301332	
1700128A07Rik	RIKEN cDNA 1700128A07 gene	chr14	14.8	Intergenic	-588884	NR_045938	
Pcdh9	Protocadherin 9	chr14	14.16	Intergenic	1798871	NM_001081377	
Adgrl4	Adhesion G protein-coupled receptor L4	chr3	14.16	Intergenic	-303096	NM_133222	
Nsmce2	Non-SMC element 2 homolog (MMS21)	chr15	14.11	intron (NM_026746)	51552	NM_026746	
Wls	Wntless homolog (Drosophila)	chr3	13.73	intron (NR_037590)	12420	NR_037590	
Nrarp	Notch-regulated ankyrin repeat protein	chr2	12.17	promoter-TSS (NM_025980)	-24	NM_025980	
Cpa6	Carboxypeptidase A6	chr1	11.31	intron (NM_177834)	208422	NM_001289497	
Llph	LLP homolog, long-term synaptic facilitation factor	chr10	11.22	Intergenic	51806	NM_025431	
Cartpt	CART prepropeptide	chr13	10.95	Intergenic	-2410	NM_001081493	
2810404M03Rik	RIKEN cDNA 2810404M03 gene	chr8	10.1	intron (NR_045497)	143286	NR_045497	

Table 1. DNA regions identified by ChIPseq analysis for SOX21 binding in the iris of B6.cΔMCOR/+ mice. The genes listed in this table are restricted to those associated with a Peak score greater than 10, corresponding to a p-value of 0.1 or higher. The peak location is presented relative to the genomic distance from the transcription start site (TSS). Specifically, the 25 sites from the SOX21 ChIP sequencing data were identified in one or more samples, each of which comprised 16 irises.

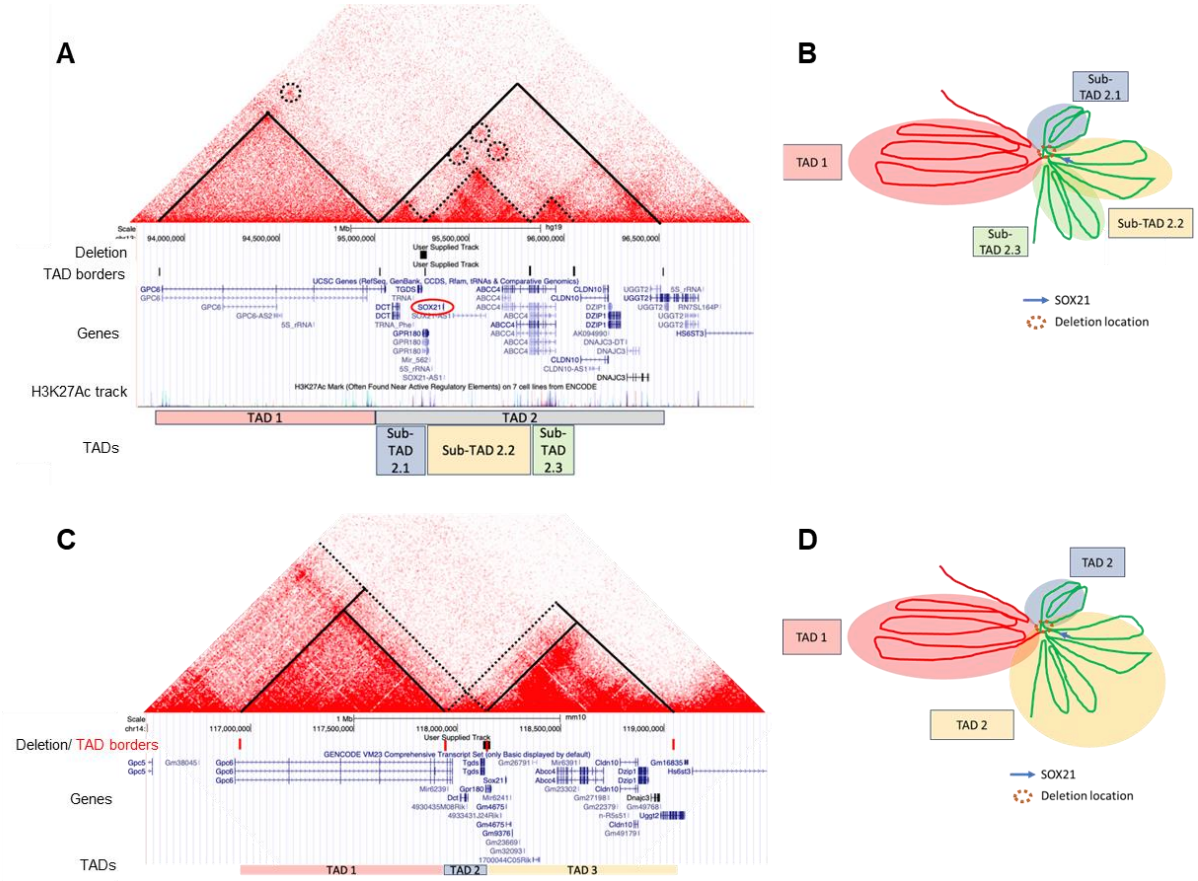

Figure 1: Organization of the MCOR Region in the human and syntenic mouse genomes. A) The 13q32.1 MCOR locus in humans (hg19) is depicted. Based on HiC-seq data from human neural progenitor cells, the region consists of two topologically-associated domains (TADs) spanning 1.2 Megabases (Mb) and 1.5 Mb (in pink and grey, respectively). These TADs are demarcated by black straight lines on the interaction frequency map, with TAD borders indicated in the second track under the interaction map. TAD 2 further reveals at least three discernible sub-TADs: Sub-TAD 2.1 (in blue) covering 0.2 Mb, Sub-TAD 2.2 (in yellow) spanning 0.5 Mb, and Sub-TAD 2.3 (in green) covering 0.2 Mb. Sox21 is located within Sub-TAD 2.2, and the deletion affects the boundary between Sub-TAD 2.1 and Sub-TAD 2.2. Circled dashed lines highlight direct and robust interactions between the deleted region and other regions in various TADs and sub-TADs. **B)** The schematic representation illustrates the chromatin organization at the 13q32.1 locus. TAD 1 and the three Sub-TADs are emphasized in their respective colors. A dashed brown circle line denotes the location of the MCOR deletion, while the blue arrow highlights the Sox21 gene's position in Sub-TAD 2.2. **C)** and **D)** depict the predicted 3D structure of the mouse syntenic region on chromosome 14. This structure closely mirrors the human configuration, demonstrating a high degree of similarity between the two species.

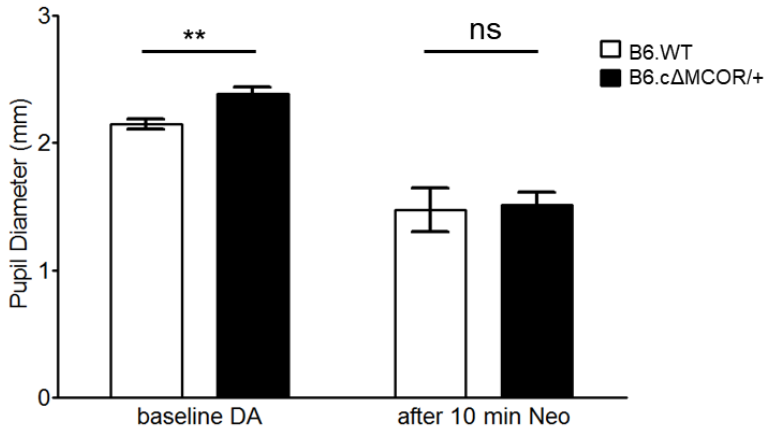

Figure 2: Pupillary Response of cΔMCOR Mice. Pupillometry was employed to assess pupil diameter in B6.cΔMCOR/+ mice, revealing a moderate but statistically significant basal reduction in pupil size compared to B6.WT animals (**: $p<0.01$, $n = 8$ animals per group). Following mydriatic administration (neosynephrin, 10 min), pupil size exhibited no significant difference between the two mouse lines (ns: not significant).

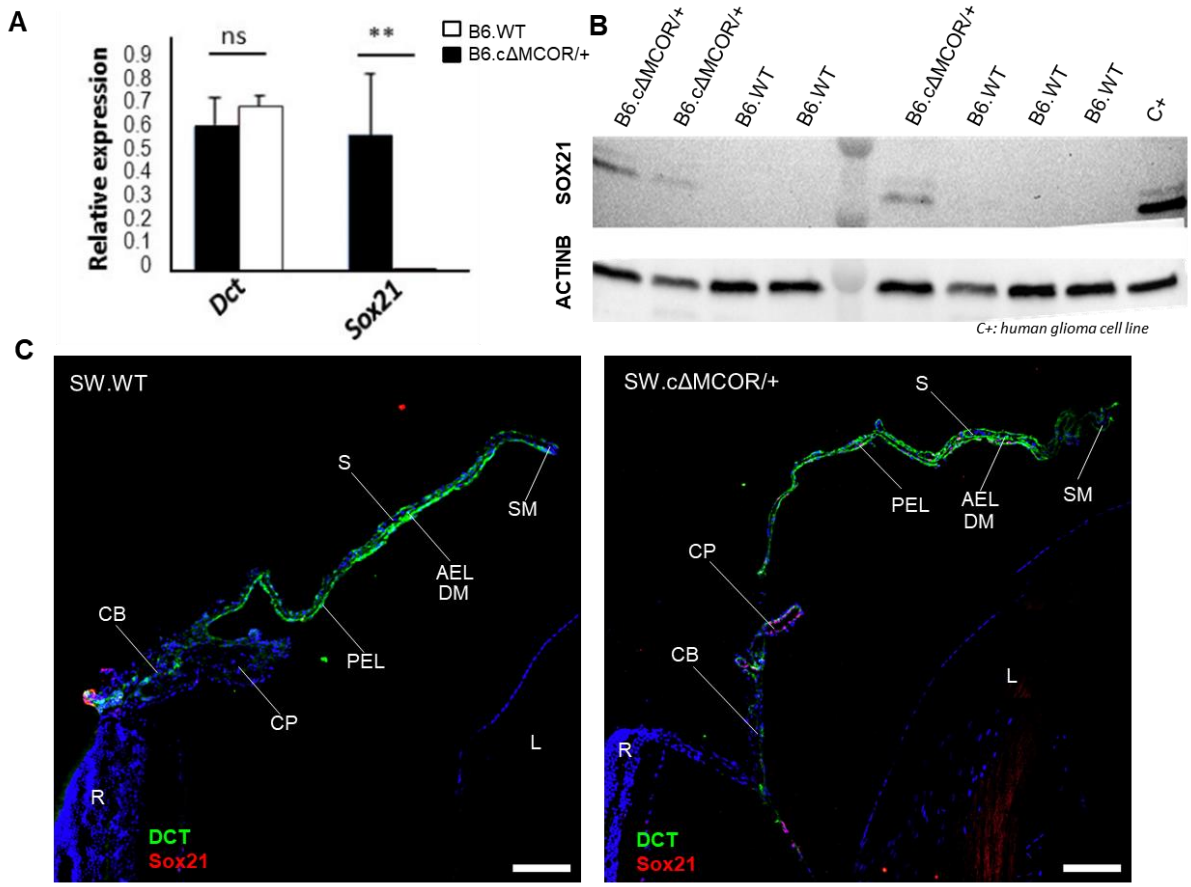

Figure 3: Expression Level Analysis at the 1Mb-TAD, RTqPCR, WB, and HiC Analysis of *Sox21* and its protein product in cΔMCOR and WT Animals. A) RTqPCR analysis of *Dct* and *Sox21* abundance in iris/ciliary body RNA extracts from newborn B6.cΔMCOR/+ and B6.WT mice (n = 5, each group). **B**) Western blot analysis of iris protein extracts reveals the presence of SOX21 in B6.cΔMCOR/+ but not in B6.WT counterparts. ActinB serves as the loading control, and C+ denotes glial cells expressing endogenous SOX21. **C**) Immunohistochemistry (IHC) analysis of iris and ciliary body in newborn B6.cΔMCOR and B6.WT mice, illustrating the detection of SOX21 and DCT in the PEL layer. AEL - iris anterior epithelium layer, **CB**: ciliary body, **CP**: ciliary process, **DM:** dilator muscle, **L:** lens, **PEL:** iris posterior epithelium layer, **R:** retina, **S:** iris stroma, **SM:** sphincter muscle. (Scale bars: 100 μm).

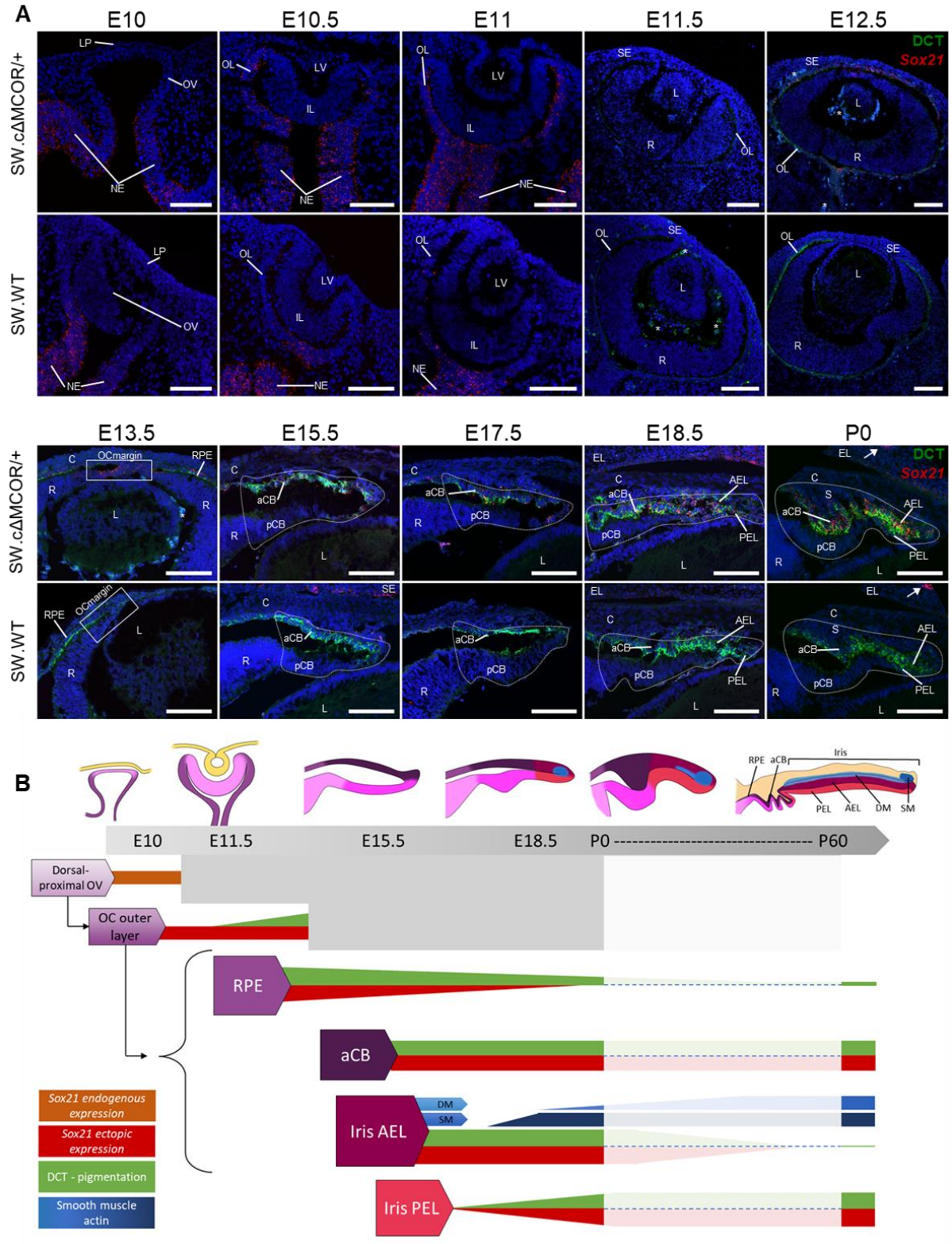

Figure 4. Expression pattern of *Sox21* and DCT during eye development. The spatio-temporal pattern of expression of Sox21 and DCT was assessed using in situ hybridization (ISH) combined with immunofluorescence (IF) on multiple heads at various developmental stages, spanning from the invagination of the optic vesicle into the optic cup to the formation of the iris and ciliary body (**A**). In the images, Sox21 mRNA is stained in red, DCT in green, and autofluorescence, predominantly caused by blood vessels, is visible in cyan (white asterisks).

The overall expression dynamics of Sox21 and DCT during iris development are summarized in the scheme below (**B**). Sox21 is naturally expressed in the proximal region of the developing optic vesicle (OV) (depicted by the orange bar) at embryonic day 10 (E10) and is absent during the subsequent stages of optic cup formation. Around E15.5, endogenous Sox21 is also observed in the eyelid and hair follicles (white arrows). In SW.cΔMCOR/+ animals, Sox21 ectopic expression emerges from E10.5, encompassing the entire outer layer of the optic cup (OC) in red. This layer gives rise to the retinal pigment epithelium (RPE), and the anterior epithelium of both the ciliary body (CB) and iris at its margin (outlined by white dotted lines), around E15.5. Intriguingly, Sox21 misexpression precedes the appearance of DCT (green) in the developing eye. As the RPE differentiates, the reduction in DCT is accompanied by a decline in Sox21 during the late stages of development. The expression of both genes remains stable in the anterior CB epithelium from its development to maturation. Concurrently, the evolution in iris pigmentation aligns with the change in Sox21 expression: the iris anterior epithelium layer (AEL) is initially heavily pigmented (rich in DCT) and loses its melanin, along with Sox21, during postnatal maturation. The posterior epithelium layer (PEL) progressively gains melanin in a centrifugal manner during development, becoming fully pigmented in adulthood, while also expressing Sox21. Notably, the sphincter and dilator muscles (depicted in blue) begin forming around E17.5 and E18.5, respectively, with the dilator maturing long after birth. The shaded box indicates the period from birth to the age of 2 months, during which we currently lack information regarding iris anterior epithelium layer (AEL) pigmentation and the precise stages of dilator muscle (DM) development. **aCB:** anterior ciliary body epithelium, **AEL:** iris anterior epithelium layer, **C:** cornea, **DM:** dilator muscle, **EL:** eyelid, **IL:** optic cup inner layer, **L:** lens, **LP:** lens placode, **LV:** lens vesicle, **NE:** neuroectoderm, **OC:** optic cup, **OL:** optic cup outer layer, **OV:** optic vesicle, **pCB:** posterior ciliary body epithelium, **PEL:** iris posterior epithelium layer, **R:** retina, **RPE:** retinal pigment epithelium, **S:** iris stroma, **SE:** surface ectoderm, **SM:** sphincter muscle. Scale bars: **100µm**.

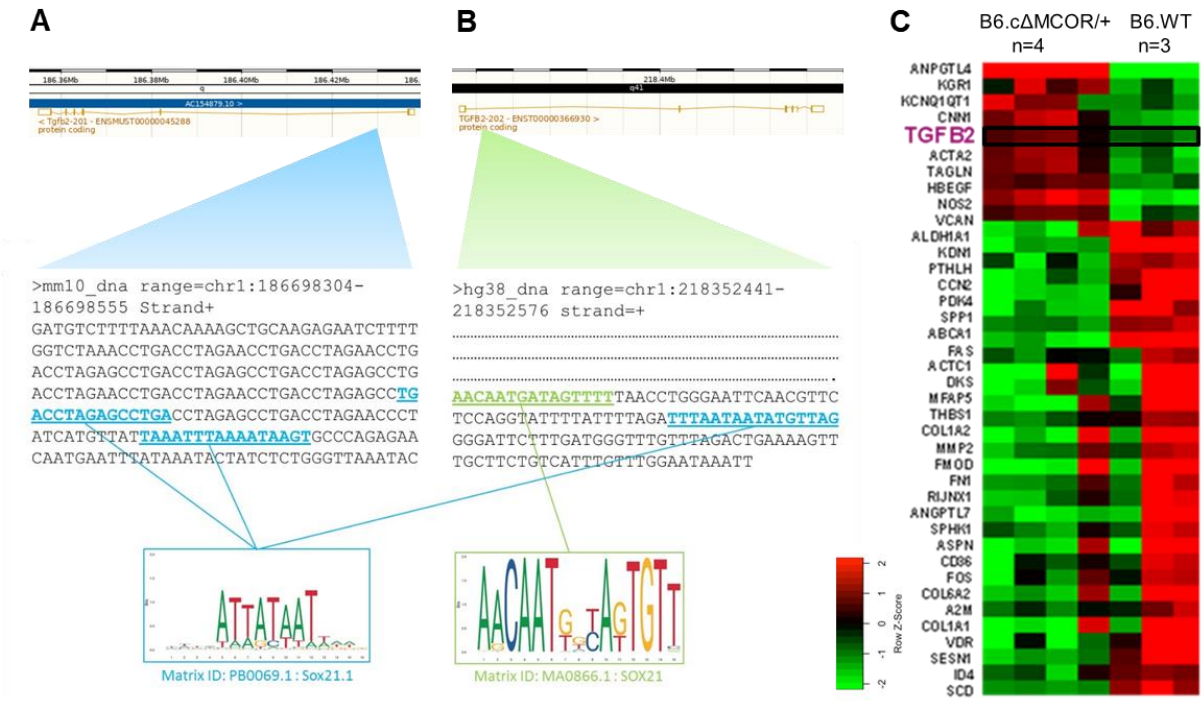

Figure 5. SOX21 consensus binding sequences in mouse and human *TGFB2* gene and RNA-seq analysis of the *Tgfb2* signaling pathway in the B6.cΔMCOR/+ mouse as compared to B6.WT counterparts. A) ChIP-seq experiment reveals the DNA sequence binding to SOX21 in the mouse, particularly in the first intron of the *Tgfb2* gene. **B**) The syntenic sequence from the human genome assembly GRCh38, situated in the first intron of the TGFB2 gene, is presented. The SOX21-consensus motif, according to the JASPAR database, is displayed at the bottom of the figure. The mouse binding sequence (PB006.1) of SOX21 is highlighted in blue, found in both the human and mouse sequences in the intron. The human motif (MA0866.1), shown in green, is also present in the *TGFB2* intron 1, suggesting a potential binding of SOX21 in this location. **C**) The RNA-seq heatmap shows genes of the TGFB pathway. While some variations are observable among individuals within the same group, *Tgfb2* is consistently overexpressed in all four cΔMCOR/+ irises.

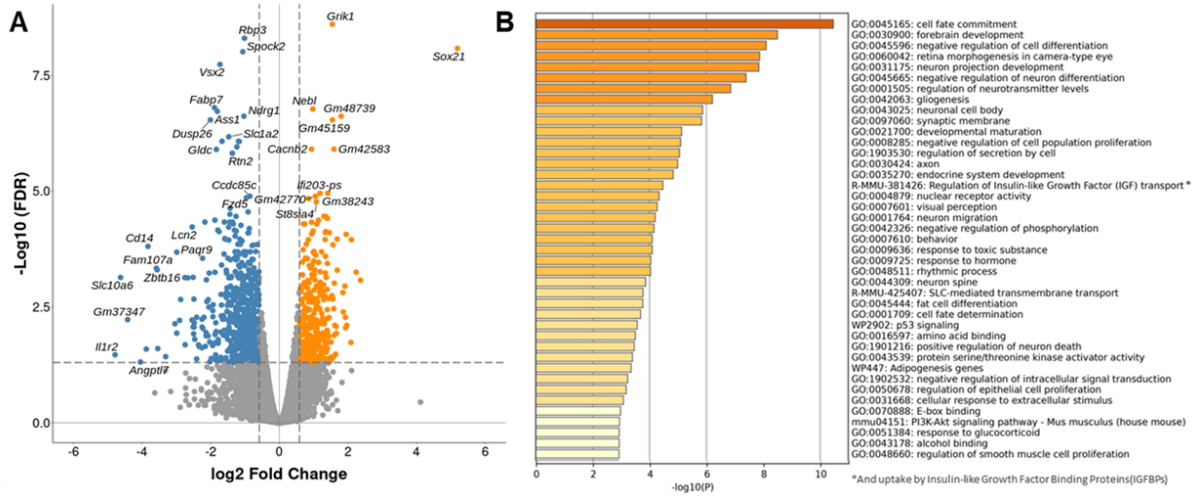

Figure 6. Comparative analysis of gene expression in the iris of B6.cΔMCOR/+ versus B6.WT littermates. A) Volcano plots of the most differentially expressed genes (DEGs) from RNAseq data of B6.WT ($N = 3$) and B6.cΔMCOR/+ ($N = 4$) irises at P0. On the x-axis (log2 scale), the difference in gene expression Fold Change (FC) is displayed and False Discovery Rate (FDR) adjusted significance is plotted on the y-axis (log10 scale). Negative values indicate down regulation; positive values indicate up regulation. **B**) Enrichment analysis in the category Biological Processes for most relevant DEGs using Metascape. The input DEGs lists are shown in a heatmap with enriched terms, which are colored by p-values.

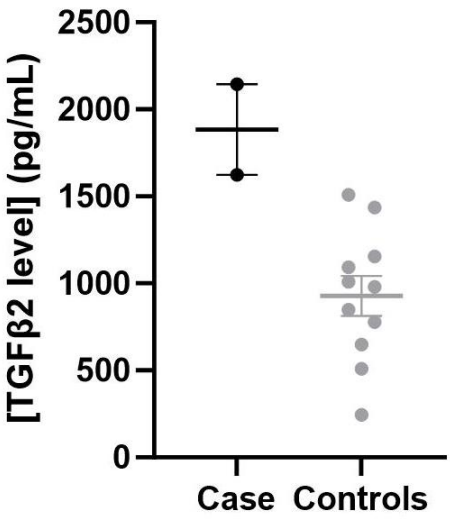

Figure 7. Analysis of TGFB2 concentration in the aqueous humor of a MCOR patient and controls. The ELISA dosage of TGFB2 in human samples reveals an accumulation of the protein in the MCOR patient analyzed, contrasting with 11 controls. Each data point on the graph represents the dosage value from the aqueous humor of an individual eye.

SUPPLEMENTARY FIGURES

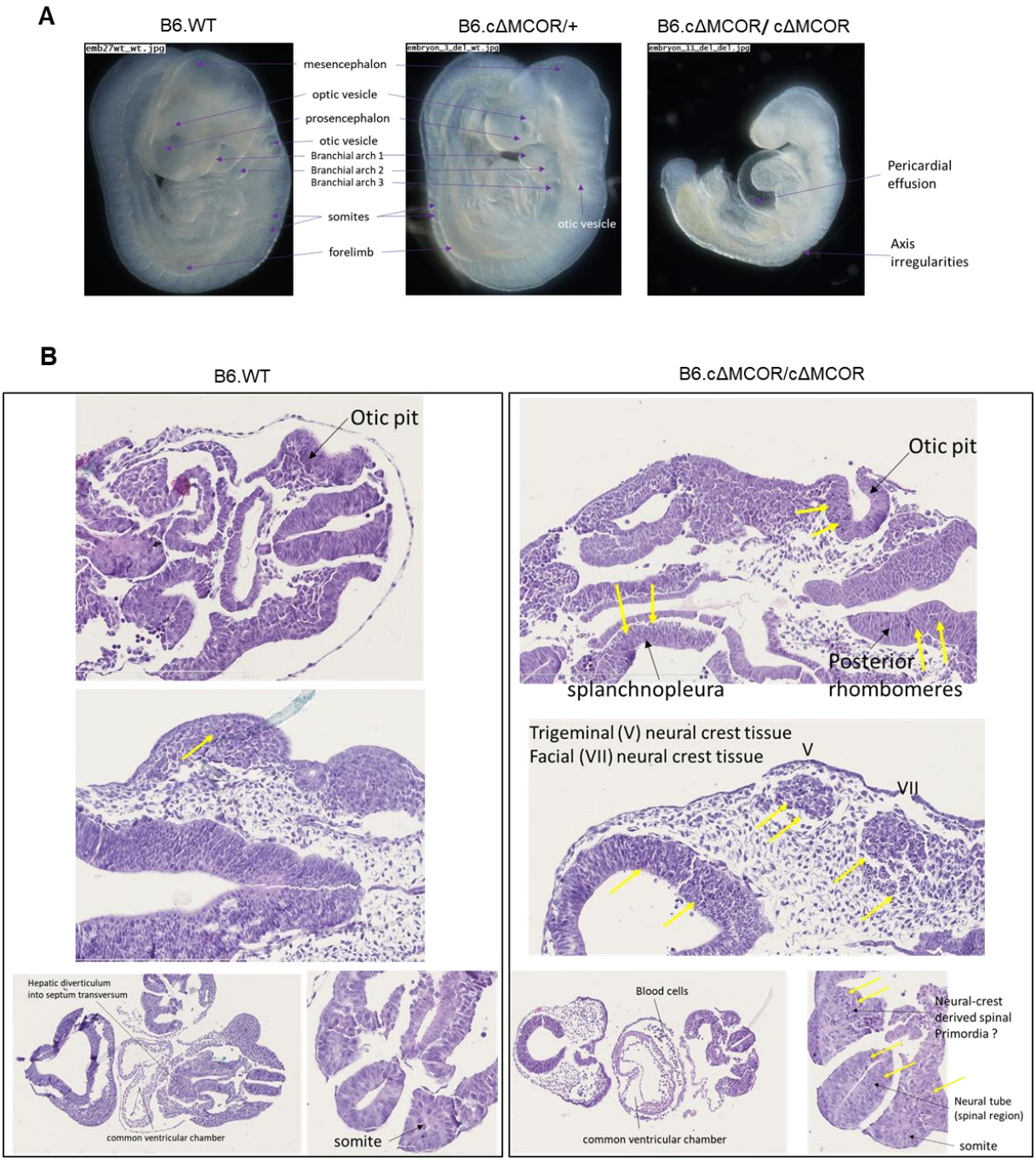

Figure S1. Lethality studies. A) Magnified pictures of embryos collected at 9.5 embryonic days. Genotyping was performed using the placenta. All individuals carrying the deletion in homozygosity presented a similar phenotype, with a smaller size and varying degrees of cardiac hypertrophy. Heterozygous and WT embryos presented no developmental defects. **B**) Histological analysis of homozygous embryos (E9.5) and comparison with WT counterparts. Mutant embryos exhibit an abnormal amount of pyknotic nuclei (yellow arrows) in numerous regions. Some pyknotic nuclei were found scattered in the neural tube and others were focalized as packets in particular regions such as for example posterior rhombomeres of the hindbrain, spinal region of the neural tube, and region of the optic vesicle. In the control embryo, some pyknotic nuclei can be observed in the neural tube but never at this amount. Packets of pyknotic nuclei were detected in the mesenchyme adjacent to the neural tube-containing pyknosis and near the somites, this region may represent neural-crest derived spinal primordia. Pyknosis was also observed in the splanchnopleura tissue.

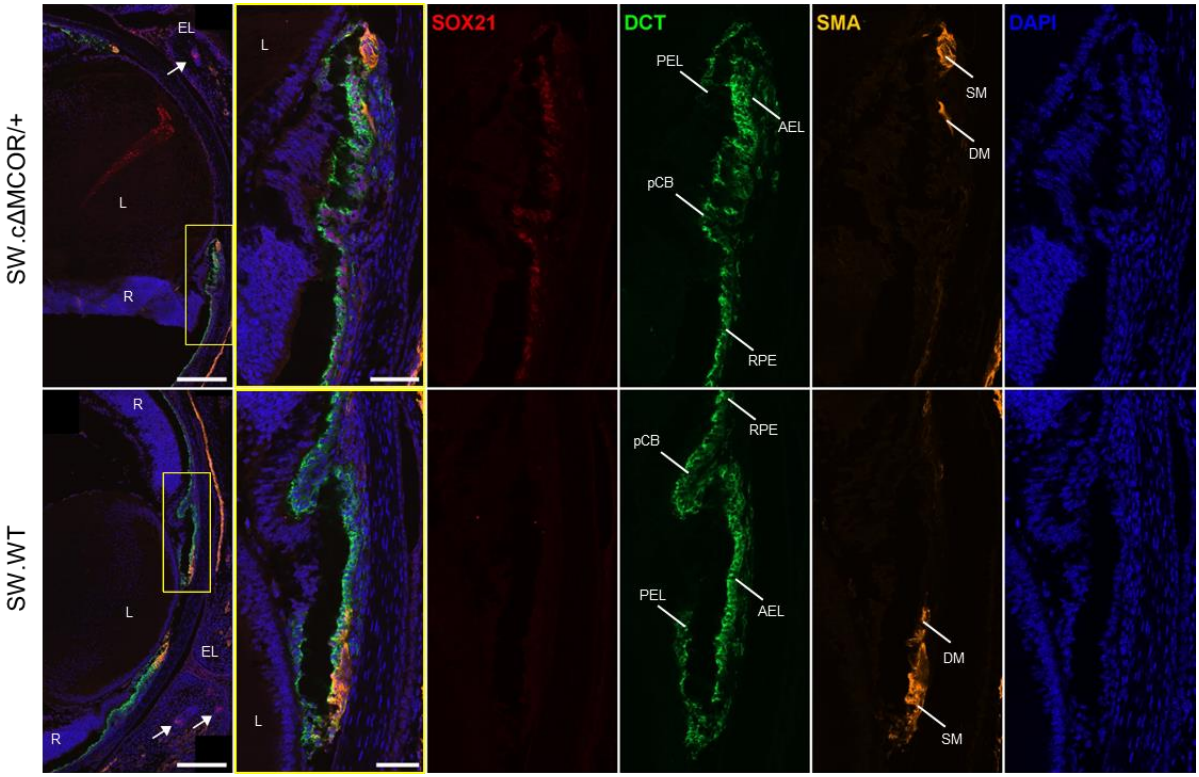

Figure S2. Expression of SOX21, DCT and SMA at E18.5. Global view of the anterior segment of the eye at late embryonic stage E18.5 (left) reveals the endogenous expression of *Sox21* in the eyelid and in hair follicles (white arrows). The yellow frame is represented with higher magnification on the right. In SW.cΔMCOR/+ eye, colocalization of SOX21 and DCT appears clearly in pigmented epithelia of the eye, namely the RPE, aCB, iris AEL and PEL. The SMA staining show the apparition of the first DM fibers behind the SM that developed earlier. No difference in both muscles were observed between SW.cΔMCOR/+ and WT counterparts. **AEL:** iris anterior epithelium layer, **DM:** dilator muscle, **EL:** eyelid, **L:** lens, **pCB:** posterior ciliary body epithelium, **PEL:** iris posterior epithelium layer, **R:** retina, **RPE:** retinal pigment epithelium, **S:** iris stroma, **SM:** sphincter muscle. Scale bars: **200µm** (left) and **50µm** (right zoom).

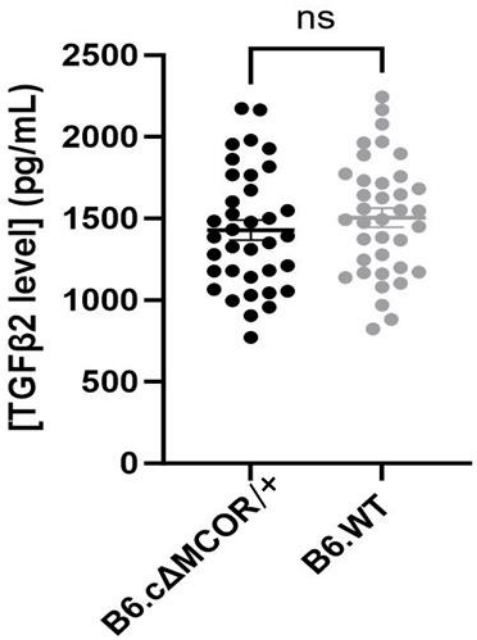

Figure S3. Analysis of TGFB2 concentration in the mouse aqueous humor. The ELISA dosage of TGFB2 in the aqueous humor (AH) of one-year-old mice utilized twenty animals for each genotype, with each dot on the graph representing an individual (AH from both eyes pooled due to limited sample quantity). The dosage results exhibit considerable variability in the measured TGFb2 levels in mouse AH. Notably, no significant (ns) difference was observed between the two groups.

Part II: Characterizing a candidate non-coding variant in a case of complex microphthalmia

3.1. Results (Third publication)

This project originated from the identification of a single patient with unilateral complex microphthalmia, accompanied by a Peters anomaly and cataract. Initial gene panel sequencing, focusing on 119 genes associated with ocular developmental defects, revealed a single nonsense variant in *FOXE3*. However, this variant alone did not seem to account for the patient's phenotype. Further investigation to find a second genetic event led to the discovery of an unreferenced single nucleotide variant (SNV) in the 5' UTR region of *FOXE3*.

In vitro luciferase assay analysis of this SNV indicated its potential effect on gene expression regulation. To validate this hypothesis, we generated mouse models that carried the variants found in both the *Foxe3* coding (KO) and non-coding (KI) regions in single heterozygosity, homozygosity, and in compound heterozygosity (mimics the patient's genotype), respectively. Analysis of these mouse models provided compelling evidence of a significant impact of the non-coding SNV on *Foxe3* expression. Heterozygous mice showed no notable phenotype, while homozygous Foxe3 KO mice exhibited microphthalmia, as expected. In contrast, homozygous KI animals displayed reduced levels of both mRNA and protein in the lens, with even greater diminution of FOXE3 in the lens of compound heterozygous mice.

In addition, we conducted DNA pull-down assays to identify proteins that exhibit preferential binding to the mutant and wild-type 5'UTR sequences, respectively. This study revealed differential binding patterns for three proteins. Analysis of these findings is expected to shed light on the regulation of Foxe3 expression and its significance in lens development. Furthermore, it may offer valuable insights for identifying potential genes in the diagnosis of microphthalmia

Collectively, our findings strongly substantiate the pathogenic impact of the SNV identified in the 5'UTR region of the FOXE3 gene. Furthermore, this discovery highlights a novel cis-regulatory element (CRE) that should be taken into consideration in the molecular diagnosis of ocular developmental defects.

I have presented this work at the 2022 Young Researchers of Imagine Institute (YR2I) Congress. It will be submitted for publication to the American Journal of Human Genetics by the end of 2023.

Oral communication:

- *Implication of a non-coding variation of FOXE3 in an individual displaying complex microphtalmia*. J. Plaisancié, **C. Angée**, N. Chassaing, L. Fares Taie, J.-M. Rozet & P. Calvas. **Young Researchers of Imagine Institute (YR2I) Congress**, *June 2022*, Paris, France.

Characterization of the upstream transcriptional network of the *FOXE3* gene involved in complex microphthalmia by lens degeneration

Julie Plaisancié[1,2,3*], Clémentine Angée[4*], Elisa Erjavec[4], Isabelle Raymond-Letron[5], Jean-Yves Douet[6,7], Mathilde Goetz[6], Catherine Vincent-Delorme[8], Ino Karemaker[9], Marijke Baltissen[9], Leonardo Valdivia[10], Yanad Abou Monsef[5], Faouzi Lyazrhi[5], Patrick Calvas[2], Jean-Michel Rozet[4], Nicolas Chassaing[1,2*], Lucas Fares-Taie[4]**

1 Laboratoire de Référence (LBMR) des anomalies malformatives de l'œil, Institut Fédératif de Biologie (IFB), CHU de Toulouse, Toulouse, France
2 Centre de Référence des Affections Rares en Génétique Ophtalmologique (CARGO), site constitutif, CHU de Toulouse, Toulouse, France
3 Molecular, Cellular and Developmental Biology Unit (MCD), Centre de Biologie Intégrative (CBI), Université de Toulouse, CNRS, UPS, 118 route de Narbonne, 31062 Toulouse, France.
4 Laboratoire de Génétique Ophtalmologique, INSERM U1163, Institut Imagine, Paris, France
5 Ecole Nationale Vétérinaire de Toulouse (ENVT), Toulouse, France
6 CHUVAC, Université de Toulouse, ENVT, Toulouse, France
7 IHAP, Université de Toulouse, INRAE, ENVT, Toulouse, France
8 Service de Génétique Médicale, CHU de Lille, Lille, France
9 Department of Molecular Biology, Faculty of Science, Radboud Institute for Molecular Life Sciences, Oncode Institute, Radboud University Nijmegen, Nijmegen, The Netherlands.
10 Center for Integrative Biology, Facultad de Ciencias, Universidad Mayor, Santiago, Chile
* Those authors contributed equally to this work

***Corresponding author:**
Dr Lucas Fares-Taie
Laboratoire de Génétique Ophtalmologique, INSERM U1163, Institut Imagine, Paris, France
E-mail: lucas.fares-taie@inserm.fr

Conflict of Interest: the authors declare no conflict of interest.
Funding: RETINA 2019

Abstract

FOXE3 encodes a transcription factor (TF) whose expression is extremely conserved throughout species that use vision. It plays a role in the development of the lens, the integrity of which is required to allow proper development of the eye. Accordingly, biallelic truncating *FOXE3* mutations cause complex microphthalmia with anterior segment and lens anomalies.
Studying a patient affected with complex microphthalmia, we identified a heterozygous nonsense variant in *FOXE3*. In the hypothesis of an autosomal recessive inheritance, a search for a second hit in *trans* was undertaken leading to the identification of a previously unreported single nucleotide variant (SNV) in an upstream conserved non-coding region 3Kb distant from the gene.
In vivo genetically engineered mice were generated *and in vitro* experiments were designed to study the deleterious effect of the non-coding variant on *FOXE3* function. Luciferase transactivation assay was performed and revealed a statistically significant impact of the non-coding variant on gene reporter expression as compared to the wild-type counterpart ($p<0.01$). This result led us to generate mouse lines carrying the non-coding variant (KI) or a frameshift mutation (KO) in homozygosity (KI/KI and KO/KO, respectively). The two lines were crossed to obtain compound heterozygous KI/KO animals (mimicking our patient genotype). Phenotype analysis (slit lamp, OCT, ocular size measurements) showed a spectrum of eye growth, cornea, anterior segment and lens abnormalities of increasing severity in the KI/KI, KI/KO and KO/KO lines, respectively. These anomalies were reminiscent of *FOXE3*-associated phenotypes in human. Intriguingly, the phenotype observed in KO/KO adult mice was severe bilateral microphthalmia with small or absent lens, contrasting with the observation of a correct organization of the basic ocular structures during the ocular development. The underlying mechanism of this putative degenerative process of the eye was thus studied in those animals, bringing further evidence for a mechanism of lens degeneration leading to microphthalmia, whose pathophysiology still remains largely unknown.
Finally, to dissect the mechanisms by which the non-coding variant contributes to an ocular developmental defect, we performed DNA pull-down coupled with mass spectrometry experiments using two mouse ESC lines and one human line of immortalized epithelial lens cells, searching for differentially bound transcription factors (TF). In total, we identified 34 candidate TFs, three of which were common between the threecells lines: *Cnbp, Usf,* and *Gabpa*. The spatiotemporal expression pattern of those candidates was studied during mice ocular development by using RNAscope studies.
In conclusion, this work expands the mutational landscape of *FOXE3*-associated ocular developmental defects. Furthermore, it shows the contribution of unsolved cases to dissect the regulatory landscapes of genes and identify novel candidate genes in ocular malformations.

Keywords: Microphthalmia, Peters' Anomaly, Anterior Segment Dysgenesis, FOXE3, non-coding, mouse, lens degeneration

Introduction

Eye morphogenesis is a highly evolutionary conserved and complex process among vertebrates, requiring coordinated interactions between several tissues of different embryonic origins. Precision of tissue patterning is genetically controlled during time and space and all the basic structures of the eye are established very early during the development in vertebrates [Cardozo MJ, 2023]. In particular, correct development of the lens is crucial for proper development of the eye and several ocular defects are thought to be the consequence of a defect in lens development [Cardozo MJ, 2023; Casey M, 2023]. Major steps of ocular development are mainly under the control of transcription factors that act during all the eye formation, from eyefield specification to maturation processes of ocular structures. Most of these transcription factors are conserved between species that use vision and their mutations are responsible for ocular malformations in humans as well as in vertebrate or even invertebrate species [Washington N, 2009]. These malformations consist in defects in eye growth and formation such as micro-anophthalmia and coloboma (MAC) but also in anterior segment dysgeneses (ASD) such as Peters' anomaly, Axenfeld-Rieger anomaly and aniridia. The causes of these ocular malformations are various and complex but they are mainly of genetic origin [Plaisancié J, 2019]. For each of those clinical entities, there is a wide genetic heterogeneity as many genes are involved. There is also a large clinical heterogeneity and several phenotypes can be associated with the mutations of one of those genes. For most of them, there is a wide allelic heterogeneity and for some of them the variants have even been associated with different inheritance pattern and phenotypes [Islam L, 2015; Chou CM, 2015; Zazo Seco C, 2018]. This is the case for the *FOXE3* gene, for which a genotype-phenotype correlation has been described [Plaisancié J, 2018].

FOXE3 is an intronless gene coding for a 319 amino acids protein that belongs to the forkhead family of transcription factors, characterized by a distinct forkhead domain to bind DNA structures. The encoded protein functions as a lens-specific transcription factor and plays an important role in vertebrate lens formation. In patients, several mutations of different nature have been described and associated with a wide range of phenotypes (from bilateral complex microphthalmia, aphakia to ASD and isolated cataract), with both autosomal dominant and recessive inheritance patterns. In previous works, we and others have shown that there was a correlation between the nature and localisation of the mutations, the inheritance pattern and the severity of the phenotype [Plaisancié J, 2018; Reis LM 2021]. Briefly, the truncating and missense pathogenic variations are responsible for a recessive ocular phenotype usually severe and bilateral (microphthalmia, aphakia) while the dominant forms are consisting in milder ocular phenotypes (ASD, cataract) secondary to mutations responsible for a C-terminal extension of the FOXE3 protein.

Accordingly, biallelic truncating *FOXE3* mutations cause a bilateral and severe ocular phenotype such as complex microphthalmia with anterior segment and lens anomalies. Studying a patient affected with a bilateral and severe ocular phenotype, we identified a heterozygous nonsense variant (p.Cys240*) in the *FOXE3* gene. This variant is a recurrent pathogenic variant that has always been described in recessive forms [Plaisancié J, 2018; Reis LM 2021]. Given the phenotype that can be considered as severe and the presence of a recessive allele in our patient, we hypothesize that the second allele might affect the *FOXE3* expression. After using targeted and whole genome sequencing, we focused on a non-coding variant in a conserved region near the *FOXE3* locus. Here, we report the results of *in vitro* and *in vivo* experiments bringing evidence of the deleterious effect of a non-coding variant on *FOXE3* function.

Materials and methods

1-Clinical and genetic data in the patient

This study was designed in compliance with the tenets of the Helsinki Declaration and informed consent was obtained from the patient and the members of her family. Full medical and familial history was collected. Patient underwent detailed general and ophthalmological examination with slit lamp examination, gonioscopy, ocular ultrasound, fundus examination and optical coherence tomography (OCT). Brain MRI was performed to investigate visual tract and intracerebral structures. Ultrasound was used to investigate cardiac and kidney structures. The patient benefited from the analysis of 119 ocular development genes through the use of a customized NGS panel whose method was detailed in previous works [Chesneau B, 2022], allowing both the detection of SNV (Single Nucleotide Variant) and Copy Number Variation (CNV). Variants were classified according to the ACMG guidelines [Richards S, 2015]. All variants were confirmed by Sanger sequencing. CGH-array (BlueGnome, UK, 44k) and Whole Genome Sequencing (WGS) were also performed in the proband to look for genomic rearrangements and discard other genetic causes.

2- WGS

Whole-genome sequencing was performed by the *Centre National de Recherche en Génomique Humaine* (CNRGH) in Evry. Genomic DNA (1 µg) was used to prepare a library for WGS, using the Illumina TruSeq DNA PCR-Free Library Preparation Kit (Illumina Inc.) according to the manufacturer's instructions. Qualified libraries were sequenced on a NovaSeq 6000 platform from Illumina (Illumina Inc.), as paired-end 150 bp reads. Samples were pooled on a NovaSeq 6000 S4 flowcell to target a minimal average sequencing depth of 30x. After demultiplexing, sequences were aligned to the reference human genome hg19 using the Burrows-Wheeler Aligner. Downstream processing was carried out with the Genome Analysis Toolkit (GATK), SAMtools and Picard following documented best practices

(http://www.broadinstitute.org/gatk/guide/topic?name=best-practices). Variant calls were made with the GATK Haplotypecaller version 4. The Large Variants calls (CNV and SV) were made by a combination of three different software, WiseCondor, Canvas and Manta.

3-Luciferase assay

Construction of the recombinant pGL4.24 vector (Figure 1)

The luciferase reporter system (i.e the pGL4.24 expression plasmid, Promega, USA) was used in this study. The pGL4.24 plasmid was first subjected to digestion with the enzyme BglI, allowing the opening of the latter and the creation of two ends with non-complementary cohesive ends, in order to carry out the oriented ligation of our fragment of interest in this vector. Our fragment of interest consisted in a 81bp-sequence of the 5' upstream conserved region of the *FOXE3* gene (hg19: chr1:47877964-47878774) centred on the identified G>A variant (rs745674596). Two versions of this fragment were therefore generated, a wild-type (WT) version and a mutated (MT) version. These two generated fragments were then each inserted into a pGL4.24 vector (previously digested) using a T4 ligase (NEB, UK). The vectors were propagated in a competent bacterial strain of E. coli (OneShot TOP10, Thermo Fisher Scientific, USA) then extracted and purified by Miniprep (Qiagen, Germany). The insertion and orientation of our two fragments of interest were checked by direct and reverse sequencing of the plasmid vectors.

CCE-Rx cell model: Cell Culture and transfection protocol

In order to evaluate the impact of the rs745674596 variant in *FOXE3* expression, we used embryonic stem cells (ESC) of murine origin, established in line (CCE), genetically modified (overexpressing the *Rax* gene) called CCE-Rx (a kind gift from Pr. S. Watanabe). Overexpression of *Rax* allows their differentiation into retinal cells [Tabata Y, 2004].The undifferentiated CCE-Rx are cultured in culture dishes 10 cm in diameter coated with gelatin (Biocoat, USA) in 6 ml of medium containing DMEM pyruvate 4.5 g/L of Glutamax glucose, LIF, β-mercaptoethanol (0.1M), MEM non-essential amino acids (1%), Pen-Strept and Fetal Calf Serum (special ES FCS) (15%). CCE-Rx cells are maintained in a humidified incubator at 37°C and 5% CO_2 in air. The culture medium is changed daily. The undifferentiated CCE-Rx are adherent and are subcultured every 48 hours. For the formation of embryoid bodies (cells in the process of differentiation), the CCE-Rx are cultured in suspension in non-adherent plastic Petri dishes 6 cm in diameter with 4ml of culture medium. The culture medium differs from that of undifferentiated cells: the FCS concentration is 10% and there is no LIF. The cells grow in suspension and form cellular aggregates, the embryoid bodies.

The transfection protocol was adapted from the transfection protocol described for these cells (Ko BS, 2009). Adherent undifferentiated CCE-Rx cells are detached by

trypsinization and 1.2 10^6 cells are seeded in a 6 cm non-adherent dish. For transfection, there are no antibiotics in the medium. Transfection uses Effectene (Qiagen, Germany) and allows high transfection efficiency. For each of the transfections, 1 µg of recombinant vector DNA and 100 µg of Renilla vector (ratio optimized at 100:1 in the case of our experimental conditions) was associated with 3.2 µl of enhancer and 8 µl of Effectene according to the manufacturer's protocol and added directly at the time of inoculation into non-adherent Petri dishes for the formation of embryoid bodies.
In this work, we therefore compared 4 conditions. Each condition was tested three times (i.e. three transfections per condition) to check the reproducibility of the results (**Figure S1**): **1)** the unmodified pGL4.24 vector (negative control), **2)** the recombinant vector pGL4.24 containing the WT cis-regulatory sequence upstream of the minimal luciferase promoter, **3)** the recombinant vector pGL4.24 containing the mutated cis-regulatory sequence upstream of the minimal promoter, **4)** the non-transfected CCE-Rx cells (negative control to estimate the background noise).

Assay of luciferase activity and calculation of ratios
The luciferase activity assay is an *in vitro* method that requires prior cell lysis. Thus, 48h after transfection, the embryoid bodies are harvested, freed from their medium and washed with 1X PBS. The addition of 400 µl of PLB (Promega, USA) allows cell lysis. Lysates are stored at least once at -20°C. Each sample is deposited in triplicate (20 µl/well) in the wells of an opaque white 96-well plate. The results were generated in absolute values by the luminometer. For each well, two absolute values are obtained, the one corresponding to the Firefly expression and the other corresponding to the Renilla expression. This allows to calculate a Firefly/Renilla ratio for each sample. The 9 ratios obtained for the 3 transfections of each condition are then averaged. Finally, the average ratios between the different conditions tested were compared. Under our experimental conditions, the final ratio of our negative control (the unmodified pGl4.24) was normalized to 1 in order to express a relative variation of our recombinant vectors.

4-DNA pull-down and mass spectrometry (Figure 2)

Nuclear extract preparation (CCE-RAX and murine ESC lines)
Nuclear extractions were performed essentially as described (Dignam JD, 1983). Briefly, cells were harvested with trypsin, washed twice with PBS and spun down for 5 min at 400g at 4°C. Cells were resuspended in five volumes of buffer A (10 mM Hepes KOH pH 7.9, 1.5 mM MgCl2, 10 mM KCl), incubated for 10 min on ice and then centrifuged for 5 min at 400 g at 4°C. Cells were resuspended in two volumes of buffer A with EDTA-free complete protease inhibitors (CPI) (Roche) and 0.15% NP40 and transferred to a Dounce homogeniser. After lysis with 40 strokes of a type B pestle, the suspension was centrifuged for 15 min at 3,200 g at 4°C. The nuclear pellet was washed with PBS, centrifuged for 5 min at 3,200 g at 4°C and then resuspended in two volumes of buffer C (420 mM NaCl, 20 mM Hepes KOH pH 7.9, 20% (v/v) glycerol,

2 mM MgCl2, 0.2 mM EDTA, 0.1% NP40, CPI, 0.5 mM DTT). This suspension was rotated for 1 h at 4°C and subsequently centrifuged for 45 min at 20,800 g at 4°C. The supernatant was collected, aliquoted, snap-frozen in liquid nitrogen and stored at -80°C.

Whole cell lysate preparation from immortalized human epithelial lens cells

To specifically study the set of transcription factors expressed in human lens cells, we bought the HLEpiC cells from InnoProt (https://innoprot.com/product/human-lens-epithelial-cells/) with the specific medium culture (Epithelial Cell Medium, EpiCM) sold by this supplier. We then immortalized the cells by using the SV40 viral vector. For whole cell lysate preparation, cell pellets were resuspended in five volumes of cell lysis buffer (150 mM NaCl, 1% NP40, 50 mM Tris pH 8.0, CPI), rotated for 1,5 h at 4°C, and subsequently centrifuged for 20 min at 18,000 g at 4˚C. The supernatant was collected, aliquoted, snap-frozen in liquid nitrogen and stored at -80°C.

DNA pull-downs

Per DNA pull-down, 20 µl of Streptavidin Sepharose High Performance 50% bead slurry (GE Healthcare Life Sciences) was used. Beads were washed once with PBS containing 0.1% NP40 and once with DNA binding buffer (DBB: 1 M NaCl, 10 mM Tris pH 8.0, 1 mM EDTA, 0.05% NP40). Probes (1 µg per pull-down) were diluted to a total volume of 400-600 µl with DBB and rotated with the beads for 30 min at 4°C. Coupling of DNA to the beads was verified by agarose gel electrophoresis. Beads were washed once with DBB and twice with protein incubation buffer [PIB: 150 mM NaCl, 50 mM Tris pH 8.0, 0.25% NP40, 1 mM DTT and CPI). Nuclear extract (150 □g) or whole cell lysate (1.5 mg) and competitors (5 µg poly-dIdC (Sigma, P4929), 5 µg poly-dAdT (Sigma, P0883) and 5 µg tRNA (Sigma, R5636)] were diluted to a total volume of 600 µl with PIB and rotated with the beads for 90 min at 4°C. After beads were washed thrice with PIB and twice with PBS, all supernatant was removed using a 30-G syringe. Beads were then resuspended in 50 µl elution buffer (EB: 2 M urea, 100 mM ammonium bicarbonate, 10 mM DTT) and incubated for 20 min in a thermoshaker at 1,400 rpm at room temperature. After addition of 50 mM iodoacetamide (IAA), beads were incubated for 10 min at 1,400 rpm at room temperature in the dark. Proteins were then on-bead digested into tryptic peptides by addition of 0.25 µg trypsin and subsequent incubation for 2 h at 1,400 rpm at room temperature. The supernatant was transferred to new tubes and further digested overnight at room temperature with an additional 0.1 µg of trypsin. Tryptic peptides were purified on C18-StageTips [Rappsilber J, 2003], followed by on-StageTip dimethyl labelling. StageTips were loaded with 300 µl labelling buffer (2% of either CH2O (light) or CD2O (medium) in 10 mM NaH2PO4, 35 mM Na2HPO4, 0.6 M NaBH3CN) and centrifuged. Each pull-down was performed in duplicate, in which label-swapping was performed between the replicates to eliminate labelling bias. Finally, StageTips were washed with buffer A (0.1% formic acid) and stored at 4°C (**Figure S2**).

LC-MS/MS measurements and data analysis

Tryptic peptides were eluted from StageTips and the respective light- and medium-labelled samples were combined into a forward and a reverse reaction. Peptides were then separated on an Easy-nLC 1000 (Thermo) connected online to an LTQ-Orbitrap Fusion Tribrid mass spectrometer (Thermo) or an Exploris 480 mass spectrometer (Thermo), using a 2h or 1h linear gradient of acetonitrile, respectively (**Figure S2**). For samples measured on the Fusion, scans were collected in data-dependent top-speed mode of a 3-s cycle with dynamic exclusion set at 60 s. For samples measured on the Exploris, scans were collected in data-dependent top-20 mode with a 45 s dynamic exclusion. Peptides were searched against the UniProt mouse or human proteome with MaxQuant v1.5.1.0 (Cox J, 2008), using default settings, the appropriate dimethyl labels, and re-quantify enabled. Data were analysed with Perseus version 1.4.0.0 and in-house R scripts.

5-Generation of CRISPR-Cas9 murine models

FOXE3 KI (rs745674596 variant) and KO (c.82_92del; p.Gly28Argfs*112) mice were generated within the Transgenesis platform of the LEAT Facility at the Imagine Institute (Paris) by using a CRISPR/Cas9 system. Animal procedures were performed with approval from the French Ministry of Research, in compliance with the French Animal Care and Use Committee from the Paris Descartes University (APAFIS# 31491). The two guide RNAs (sgRNAs) targeting the regulatory region surrounding the KI variant (ATGCTCAGCCGCATCACGTC) and the KO variant (CTCCGGTTCGCGCCCCGGTT) of the gene *Foxe3* were designed and selected with CRISPOR web tool (http://crispor.tefor.net/). The HR (Homologous Recombination) template to introduce the KI variant (nucleotide in bold) was the ssODN [Integrated DNA technologies] with phosphorothioate modifications at 3' and 5' ends (*):
5'A*T*CCAGGCCCATGAGAAAGGGGCCACCTTCACTGGCCGTCTTATGCCCGGA
TGCTCAGCCGCATCAC**A**TCCGGCCCAGGGCCTGTGAAAAGAGGGCCCAGCCA
CGCTGAAAACGCGGA*T*T3'

The KI and KO alleles were generated through CRISPR/cas9 ribonucleoprotein (RNP) complex microinjection in C57BL/6J mouse zygotes pronuclei as described by Ucuncu E [2020]. The offspring were genotyped from genomic DNA by PCR amplification followed by Sanger sequencing using appropriate primers (**Table S1**).
Before intercrossing, these mutant mice were backcrossed to C57BL/6J mice for several generations to remove potential off-target mutations. Backcrossed heterozygous mice were then intercrossed to obtain the 6 different genotypes including WT/WT, KO/WT, KI/WT, KI/KI, KI/KO and KO/KO.

6- Study of the mice ocular phenotype during embryonic development and adulthood

Ocular phenotype analysis in adult mice

Mice were slightly anesthetized with a mix of ketamine and xylazine and examined by slit lamp and Optical Coherence Tomography (OCT) (Envisu R-class, Leica).

Section preparation for histological analyses

After ophthalmological examination, adult mice were euthanatized and enucleated. Both eyes of each mouse were measured using a caliper then paraffin-embedded after immersive fixation in a Davidson solution. The eye tissues sections were stained with Hematoxylin and Eosin.

To observe the ocular structures during development, in particular those of KO/KO mutants, mice were bred at 6 pm and separated 16h later. If a vaginal plug was present, the female was weighed 7 days later. If the weight gain was superior to 3g, the female was euthanatized at chosen stages (12.5, 13.5, 14.5 or 18.5 embryonic days) to collect the embryos. Some were collected at birth (P0). The heads were cut and fixed for 24h in 4%-PFA at 4°C. The eye tissues sections were stained with Hematoxylin and Eosin.

Statistical approach

Statistical analyses were performed using R software, version 2022.12.00. Logistic regression was used to describe associations between genotype and phenotype. The dependent variable “phenotype” was a binary variable (lack of phenotype/presence of phenotype) and the independent variable “genotype” was a factor with 5 levels (WT/WT, KO/WT, KI/WT, KI/KI, KI/KO). The corresponding odds ratios (OR) were computed as well as the 95% confidence intervals. The OR of the KO/KO genotype was not estimable because 100% of individuals with such a genotype had a phenotype. The same was done to assess the associations between genotype and severity of the phenotype. The dependent variable “severity of phenotype” was a binary variable (lack of phenotype or moderate phenotype/severe phenotype) and the independent variable “genotype” was a factor with 5 levels. Similarly, the WT/WT genotype was excluded from the analysis given that all individuals with such a genotype had a phenotype considered as non-severe. Statistical significance was defined as p-value <0.05. Statistical analyses were also performed to assess the absence of effect of the age as well as the gender on the phenotype occurrence.

7-RNA studies

RNA extraction

Mice (ranging from 2 to 5 months of age) were euthanatized and enucleated. The eyes were dissected on ice to collect the lens epithelium. Briefly, eyes were opened following the ora serrata, the lens was removed then carefully incised to isolate the capsule from the fibers. Epithelia of both eyes were pooled together to perform RNA extraction by using the RNAeasy MiniKit (Qiagen) according to the manufacturer's instructions.

RT-qPCR

The RNA concentration of each sample was estimated using a spectrophotometer (Nanodrop), allowing to perform the retro-transcription (RT) of total mRNAs with 35 ng of template (cDNA verso kit, Thermofisher). Semi-quantitative real-time PCR (**Table S2**) using Sso Advandced Universal SYBR Green Supermix (BioRad) was performed with the Mastercycler ep realplex (Eppendorf). *Foxe3* relative expression was calculated following the methods described by Vandesompele et al [2002] with *Tbp* and *Hprt as* the best two housekeeping genes.

Sections preparation for RNAscope studies

Mice were bred at 6 pm and separated 16h later. If a vaginal plug was present, the female was weighed 7 days later. If the weight gain was superior to 3g, the female was euthanatized at E12.5 to collect the embryos. The heads were cut and fixed for 24h in 4%-PFA at 4°C. After 3 washes in PBS, the heads were dried with absorbing paper, then bathed in OCT-compound. Heads were embedded in a mold containing OCT-compound in liquid nitrogen, allowing a fast freezing of the tissue. Embedded heads were stored at -80°C, then brought up to -20°C 1h prior to cutting. The cryostat (Leica CM3050 S) temperatures were set at -20°C (object) and -18°C (chamber). Frontal sections of the embryos head (or sagittal sections of the adult eyes) of 14 µm were collected at the level of the pupillary aperture. Sections were air dried (1-2 hours), then stored at -80°C.

RNAscope *in situ* hybridization

Prior to the RNAscope (ACDbio) signal amplification, slides were treated according to the manufacturer's instructions, following the corresponding protocol (FFPE for paraffin-embedded eyes sections; Fresh frozen for embryos). Briefly, sections were dehydrated in EtOH baths, dried and treated with H2O2 for 10 minutes at RT. FFPE sections only underwent target retrieval incubation in a 98°C water bath for 1 min. Proteinase digestion was performed the next day, using the Protease + for 30 minutes at 40°C (FFPE sections) or Protease IV for 20 minutes at room temperature (Frozen sections).

All sections were incubated for 2h at 40° with a mix of 3 probes (**Table 3**). The RNAscope signal amplification, consisting in a series of amplificators, HRP activators and blockers, and fluorophores incubations at 40°C, was done following the instructions of the kit (ACDbio). Opals (Akoya Bioscience) were diluted at 1:1500 in TSA buffer. Each Opal (570, 690, 520) were attributed to the same channel (C1, C2 and C3 respectively), independently of the probe mix.

Sections were counterstained with DAPI for 30 seconds and finally mounted with Fluoromount and stored at -20°C at least 12h prior to image acquisition. All images

were acquired with a Zeiss Spinning Disk Confocal. Whole sections were scanned using a 10X objective, and lens epithelium were captured with a 40X or 63X objective with oil, as a maximal projection of 10 or 30 stacks covering 1.89 µm or 6.09 µm (FFPE or frozen sections resp.). Images were acquired as .czi file and converted to a TIFF format to perform the analysis.

Quantitative image analysis.

Image analysis was performed using Fiji (v. 1.53t) and CellProfiler (v. 4.2.1) softwares. Frozen embryos (Fiji): following the analysis method suggested by the manufacturer, the presumptive lens was manually defined as the ROI. The integrated intensity of the ROI was measured for each channel, along with the area covered by the DAPI-signal. For each channel, 25 spots were measured to determine the average intensity value of one mRNA spot, and 25 nuclei were delimited to measure the average area of one nucleus. Dividing the integrated intensity of the ROI by the average dot intensity estimates the total dots of mRNA in the region, and this value can be reported to the number of nuclei, resulting in a mean value of dots/nuclei.

FFPE adult eyes (CellProfiler): due to their lower quantity, the nuclei and RNAscope signal are easier to identify in the mature anterior lens epithelium. Therefore, the method of analysis slightly differs. Briefly, the algorithm determines the nuclei in each picture and estimates the cells as an expansion of 100px from the nuclei. The RNAscope signal from each probe is enhanced as speckle features, and each speckle is identified as a single mRNA and related to a parent-cell to determine precisely the number of mRNA of each target per cell.

8- Western blot

Western blots were performed using 70 µg of total lens capsule protein lysates. The following antibodies were used in this study: FOXE3 (Santa Cruz Biotechnologies, sc-377465) and Vinculin (Abcam, ab91459). Secondary antibodies, mouse IgG or rabbit IgG HRP (Thermo Scientific) were used at a 1:8000 dilution. Western blot membranes were developed using the Clarity Western ECL substrate (Bio-Rad), and the signal was detected with a Chemidoc MP Imaging System (Bio-Rad). Protein quantification was done with the gel analysis tool from Fiji (v. 1.53t) software.

Results

Clinical and genetic data in the patient

The proband is a 11-year-old girl with left complex microphthalmia with Peters' anomaly and a right polar cataract (**Figure 1A**). She has no other notable medical history. She is the first child of young parents of Caucasian origin, with no personal nor familial medical history.

The targeted sequencing using a 119 genes panel approach allows to identify the heterozygous c.720C>A pathogenic variant responsible for the p.Cys240* protein change leading to a premature stop codon in the *FOXE3* gene (NM_012186.3). This nonsense variant is a recurrent well-known pathogenic variant in *FOXE3* [Reis LM, 2021]. This mutation has been reported several times in the literature, always associated with a second mutation on the other allele and not pathogenic in heterozygotes [Plaisancie J, 2018; Reis LM, 2021]. This pathogenic variant was inherited from her asymptomatic father. The heterozygous nature of this variant made it possible to eliminate a deletion on the other allele, but left the possibility of a rearrangement in the non-coding regions. We tested by array-CGH (44k) the adjacent region. No rearrangement was highlighted, in particular in the 1p33 region containing *FOXE3*. A transcripts' analysis in search for elements in favour of a second pathogenic variation not identified by sequencing, could not be carried out due to the lack of available tissues expressing this gene.

We therefore sequenced in the proband a region relatively conserved during evolution, located approximately 3Kb upstream of the *FOXE3* gene (chr1:47877964-47878774 according to the GRCh37/hg19 assembly) previously involved in the mouse with complex microphthalmia and cataract [Wada K, 2011] (**Figure 1B**). Sequencing of this conserved region revealed two variations: the homozygous G>C at position chr1:47878626 (rs10399673) and the heterozygous G>A at position chr1:47878428 (rs745674596). The G>C variation (rs10399673) is considered to be a benign variant because it is found in the general population with an allelic frequency of 45% (GnomAD). It is found in the heterozygous state in both parents. The G>A variation (rs745674596) is an extremely rare variation for which there are only 4 heterozygous individuals reported (no homozygous) in the GnomAD database (allelic frequency of 0.01%). This rare variant was found heterozygous in the proband's mother, herself asymptomatic.

This segregation analysis was thus compatible with a recessive biparental transmission given that the previously identified nonsense variation was inherited from the father (**Figure 1B**).

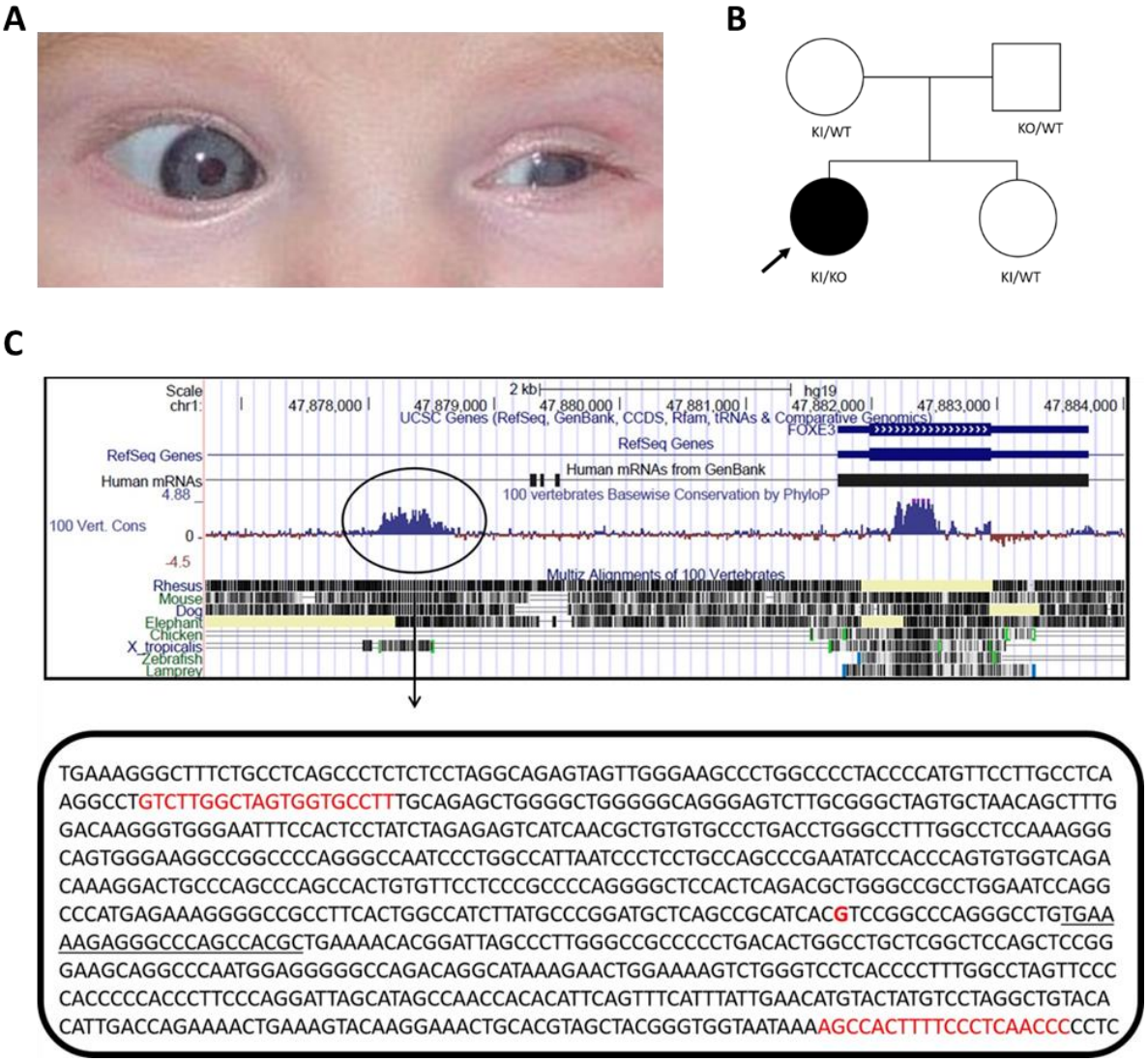

Figure 1: Clinical and genetic features of the proband case. A: Clinical picture of the proband affected by left complex microphthalmia and right polar cataract. **B**: Pedigree of the family and segregation analysis. **C**: In the upper part of the figure (UCSC screenshot), is encircled the conserved region of interest located around 3Kb upstream the *FOXE3* coding sequence. Its nucleotide sequence is shown in the lower part of the figure. In red, forward and reverse primers used for PCR amplification as well as the candidate G>A variation (rs745674596). This substitution is located a few bases from the 22 bp homozygous deletion (underlined) identified by Wada K [2011] in mice.

Whole Genome Sequencing (WGS) ruled out **i)** the presence of a rearrangement (copy number and structural variants) involving the *FOXE3* locus, **ii)** the presence of other candidate variants in conserved regions around the *FOXE3* gene and **iii)** the presence of other pathogenic variations (affecting other genes) that could explain the ocular phenotype in the patient.

Luciferase assay

Luciferase assays revealed **(i)** a 10-fold relative increase ($p<0.05$) in the luciferase expression under the control of the wild-type cis-regulatory sequence and **(ii)** a 45-fold increase ($p<0.01$) in the luciferase expression under the control of the mutated cis-regulatory sequence compared to the unmodified vector. Thus, the variation identified in this conserved region affect the regulation of the reporter expression when compared with the wild-type sequence. In this model, the luciferase expression is 4.5 times stronger when its promoter is under the control of the mutated sequence than the wild-type sequence (**Figure S3**).

DNA pull down and mass spectrometry

Nuclear extracts were obtained from the CCE-RAX line, the murine ESC cell line and whole lysate from immortalized human epithelial lens cells (HLEpiC cells from InnoProt). A total of 34 candidate transcription factors (**Figure 2**) were found differentially bound between WT and mutant oligonucleotides, three of which were common between the murine and human cells lines: GABPA (and its cofactor GABPB1), USF2 and CNBP (**Figure 2**). GABPA is binding solely the mutant version while USF2 and CNBP are binding only the wild-type version. Of note, we were also interested in the ZIC5 factor because, while it was found only in the two murine lines, its mutations are responsible for microphthalmia in mouse [Furushima K, 2005].

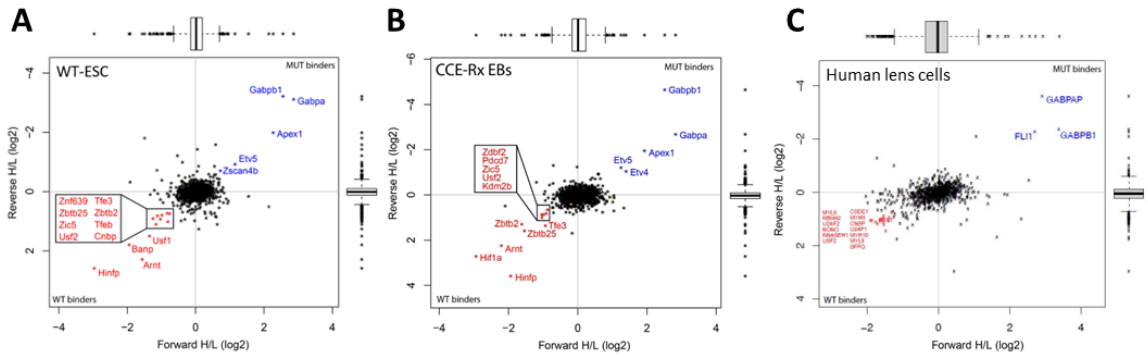

Figure 2 showing the results of the combined DNA-PD and mass spectrometry approach applied in the murine WT-ESC cells (**A**), CCE-Rx cells (**B**) and immortalized human epithelial lens cells (**C**). In red, factors that preferentially bind the wild-type (WT) oligonucleotide with statistically significant difference ($p<0.05$). In blue, factors that that preferentially bind the mutant (MT) oligonucleotide with statistically significant difference ($p<0.05$).

FOXE3 murine model

From a C57BL/6 strain we generated two gene-edited lines in the *Foxe3* region. The first one, here after called KI, was carrying the variant in the regulatory region (introduced by knock-In) and the second one was the KO model bearing a frameshift variant in the coding *Foxe3* region (**Figure 3A**). After several crossing we managed to

obtain the 6 different genotypes with around 25 mice per group, aged between 4 and 11 months with female as much as male per group of age. Then, we performed ophthalmological examination of 157 mice using slit lamp and OCT. After examination, mice were euthanized and enucleated to measure the ocular globe size by using a calliper. A total of 314 eyes were thus analysed.

First, we obtained from this study basic information about the eye size in WT mice (C57BL/6 strain). Of note, the eye still continues to grow until 3 months of age [Tkatchenko TV, 2010]. All the WT mice (total of 24 mice) have an antero-posterior ocular diameter comprised between 3.5 and 4 mm after 3 months of age that was defined as the normal range. Microphthalmia was considered when this diameter was ≤ 3 mm.

Phenotype analysis of the mutant lines showed a spectrum of eye growth, cornea, anterior segment and lens abnormalities of increasing frequency and severity in the homozygous KI/KI, compound heterozygous KI/KO and homozygous KO/KO lines, respectively (**Figure 3B**).

Heterozygous mice (KI/WT or KO/WT) show no phenotypic difference compared to the wild-type mice (WT vs KI/WT 0.139 [0.013;0.87] p=0.055; WT vs KO/WT 0.22 [0.021;1.7] p=0.16) and presented occasionally mild ocular phenotype, often unilateral, such as cataract (**Figures 3C, S4-S7**). This is in correlation with the sporadic occurrences of corneal opacity or even microphthalmia that have been described among some mice strains [Pierro LJ and Spiggle J, 1967].

36% of the homozygous KI mice (KI/KI) and 50% of the compound heterozygous mice (KI/KO) display bilateral cataract, corneal opacity and iridocorneal adherences (**Figures 3C, S8-S12**).

All homozygous KO mice (KO/KO) display complex microphthalmia, with severe anomalies in the anterior segment such as corneal opacities, central pit, iridocorneal adherences, lens adherences and anomalies (mainly cataract and microphakia) (**Figures 3C, S13-S15**). A small pyramidal pigmentary and vascular formation was also frequently visible, from the posterior lens capsule to the retina, highly evocative of a persistent fetal vasculature (PFV). In almost all the eyes, the retina was anteriorly displaced, invading the anterior segment, while the composition of its layers appeared relatively preserved.

The proportion of symptomatic mice (penetrance, all ocular defects combined) was increasing from WT (9%), KO/WT (14%), KI/WT (18%), KI/KI (36%), KI/KO (50%) and KO/KO (100%) with a statistically significant difference (WT vs KI/KO 0.038 [0.004;0.183] p=0.0041; WT vs KI/KI 0.12 [0.016;0.566] p=0.015; KI vs KI/KO 0.27 [0.07;0.84] p=0.031 ; KO vs KI/KO 0.17 [0.035;0.62] p=0.013; KI/KI vs KI/KO 0.32 [0.10;0.92] p=0.04).

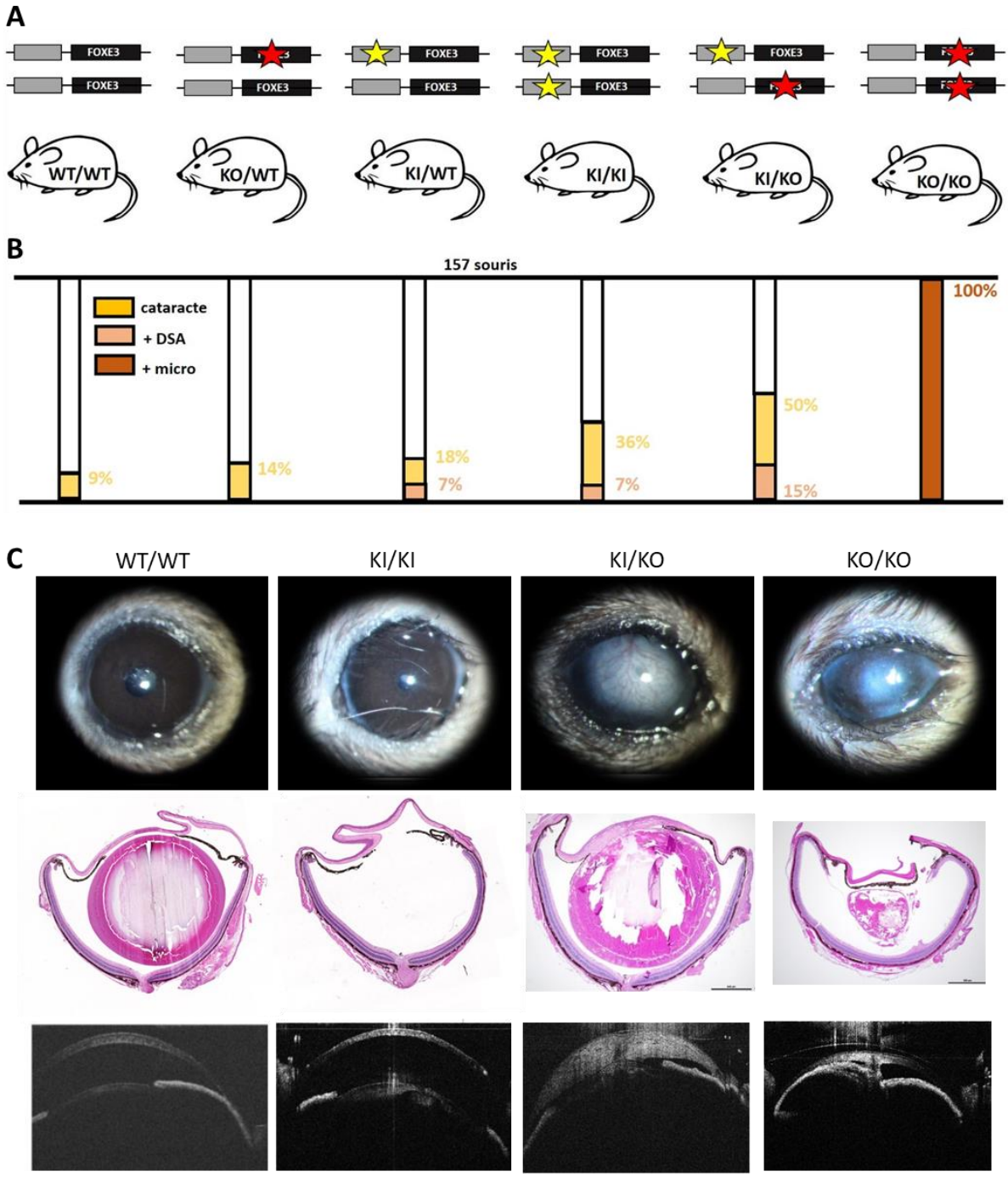

Figure 3: The different mice genotypes and their corresponding phenotype. A: Scheme of the six different genotypes studied here. **B:** Around 25 mice per genotype underwent complete eye examination. Ocular defects were observed in mutant mice with a frequency correlating with the severity of the genotype. **C:** Comparative pictures of the phenotypic analysis (live picture, histological section and OCT) between (1) a sane, WT/WT eye, (2) a KI/KI eye with a cataract, (3) a KI/KO eye with a retrocorneal lens and small anterior chamber and microphthalmic KO/KO eye.

*

The proportion of severe phenotype (clinical variability) was increasing from KI/KI (7%), KI/KO (15%) and KO/KO (100%) with a statistically significant difference for the KO/KO compared to the other lines ($p<0.05$).

Study of ocular development in mice embryos

To understand the pathological mechanism in homozygous KO mice (KO/KO), we studied ocular structures at different embryonic stages of development until birth (E12.5, E13.5, E14.5, E18.5, P0) by using histological colorations on embryos heads sections (3 heads/6 eyes per genotype). Strikingly, we observed in KO/KO embryos that at the E12.5 stage all the primary structures of the eye were in place: the lens vesicle, the future cornea and the two optic cup layers (future RPE and retina). The only thing which was observable at E12.5 on those mutant mice compared to WT individuals, was the persistence of a central lenticulo-corneal epithelial connection and an anterior lens epithelium displaying a certain degree of disorganization (**Figure 4**).

At E13.5, we observed that this anterior epithelial layer can be more disorganized with even the disappearance of the cells at the place where persists the lenticulo-corneal connection. The lens is abnormally close to the future cornea compared to WT, with sometimes the impression of an opened lens on its anterior pole, pouring proteic material into the mesenchyme of the future cornea. Mild vacuolization and swelling of the lens fibers are also observed from this embryonic stage and these abnormalities will gradually worsen through the various successive stages. Adherent or abnormally close to the cornea, the lens will progressively loose its anterior epithelium layer, become microphakic with lower number of vacuolized degenerative lens fibers. Despite this lens changes, we see that at E18.5 the eyes have kept their normal size. We also inconstantly observed a kind of fibrotic phenomenon of the primary vascularization of the vitreous (from the posterior lens pole to the retina).

In KI/KO, we observed that the development of ocular structures is nearly normal. Although in some cases was observed a persistence of the central lenticulo-corneal epithelial connection, the space between the lens vesicle and the cornea was conserved as well as the anterior epithelium of the lens. The only microscopic finding observed is a slight vacuolization of the lens fibers just posteriorly of the anterior epithelium that could be compatible with the predominant phenotype of cataract observed in non-KO/KO mutant mice.

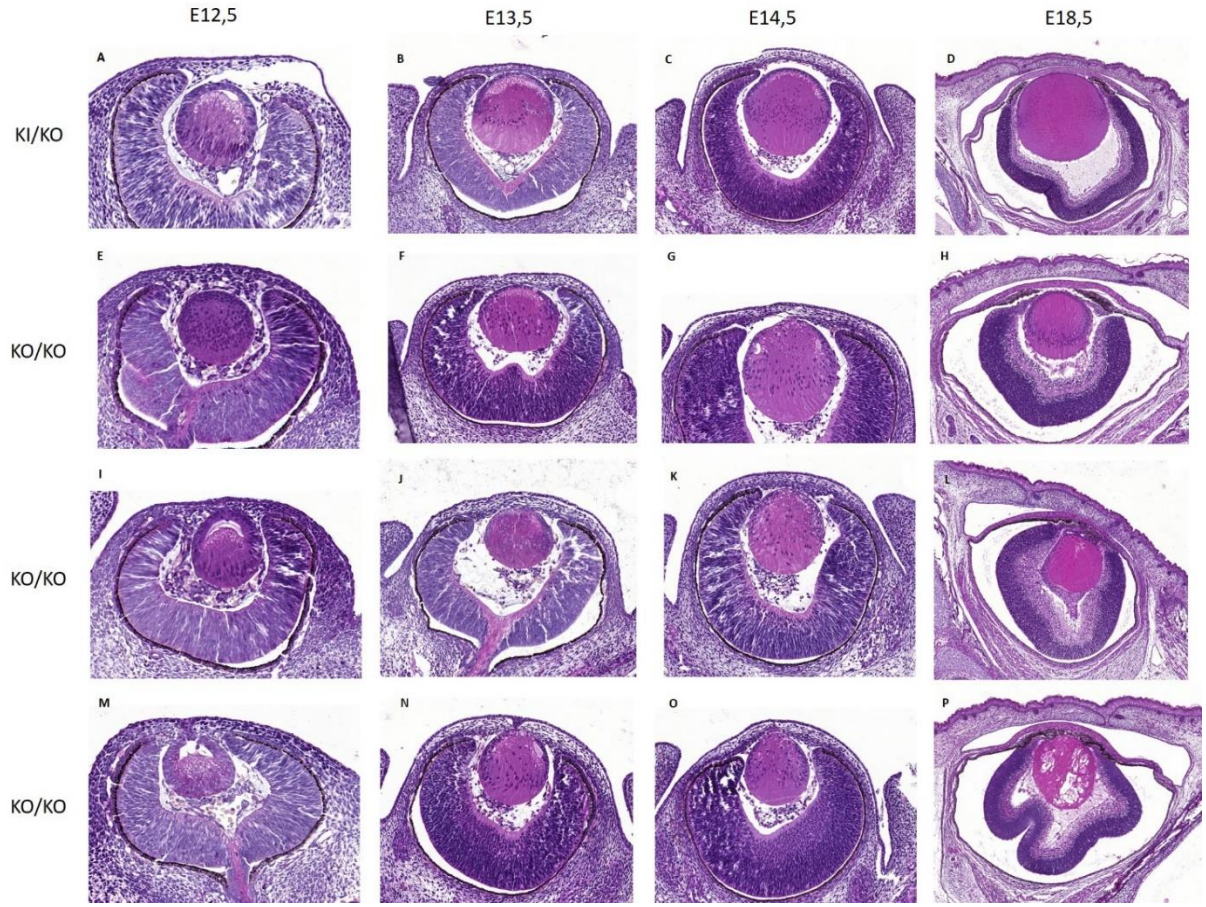

Figure 4: early ocular development through different embryonic stages (E12.5, E13.5, E14.5, E18.5). **A-D**: Ki/KO embryos with relatively normal development of the eye. **E-H**: KO/KO embryos with normal development; **I-L**: KO/KO embryos with normal development and subtle changes such as disorganised anterior lens epithelium or reduced space between lens and cornea; In the **L** individual we can see a dense fibrovascular tissue in perilenticular position also extending from the posterior lens pole to the central retina. **M-P:** KO/KO embryos showing persistent lenticulo-corneal epithelial connection and increasing number of lens vacuolation and lens fibers degeneration. Of note, some genotype (WT/WT) and stage (P0) will be included soon in the figure as some individuals missing to illustrate all the stages are currently being analysed.

RNA studies

RT-qPCR, RNA-seq and RNAscope

To further understand the impact of the KI mutation over the expression of *Foxe3*, we quantified its mRNA in the anterior lens epithelium. The lens capsules of 6 animals from each genotype were collected, excepted KO/KO animals whose microphakic eyes did not allow proper dissection of the lens. *Foxe3* mRNA expression was determined in these tissues by RT-qPCR and we observed a significant 50% reduction of *Foxe3* in the anterior lens epithelium of KI/KI mice (P<0.01), as compared to wild-type littermates. The expression was slightly reduced among the KI/WT animals and increased in KO/WT and KI/KO mice (**Figure 5A**).

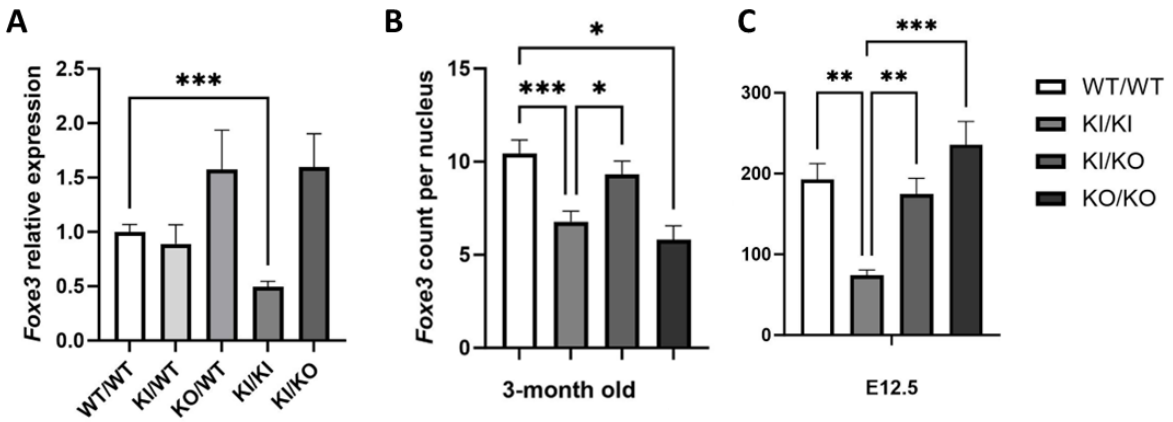

Figure 5: RNA quantification in of *Foxe3* in the anterior lens epithelium. A: Relative expression of *Foxe3* as determined by RT-qPCR. **B**-**C**: Total *Foxe3* mRNA count per nucleus estimated from RNAscope analysis, in adult anterior epithelium lens (**B**) and developing lens vesicle at E12.5 (**C**). Only significant relations are shown.

RNAscope *in situ* hybridization was performed on lens sections obtained from the eyes of WT/WT, KI/KI, KI/KO and KO/KO mice at E12.5 and at 3 months of age. Although this method offers a quantitative mRNAs detection in tissue sections, the designed probes do not allow differentiating the wild-type *Foxe3* mRNA from the one bearing the frameshift variant produced by the KO allele. The *Foxe3* quantification at adulthood showed no significant difference between the compound heterozygotes animals and their wild-type counterpart, with the KI/KO lenses displaying a varying expression of the gene among the individual of same genotype, and throughout the lens capsule (**Figure S16**). KO/KO animals showed no expression of *Foxe3* but no lens capsule could be seen. RNAscope signal was significantly decreased in the lens of KI/KI animals, with an average of 5 mRNA per cell, against 11 mRNA molecules counted within the WT/WT animals (**Figure 5B**). The same observations were made from the presumptive lens at E12.5, with a stronger decrease in *Foxe3* expression associated with a KI/KI genotype (50 vs 200 counts per cell in WT/WT embryos, **Figure 5C**). Interestingly, the KO/KO presumptive lens also showed a high expression (230 counts/cell) of *Foxe3*, and no anomaly was still observed in these animals (**Figure S17**).

RNAscope *in situ* hybridization was also performed on lens sections obtained from the eyes of WT/WT at E12.5 to ckeck the DNA-PD candidates' expression during development (**Figure 6**). The absence of *Zic5* in the developing lens excluded this gene from our candidates. The three other genes, *Cnbp*, *Usf2* and *Gabpa* all appeared ubiquitous, hence supposing a colocalization of *Foxe3* in the lens anterior epithelium.

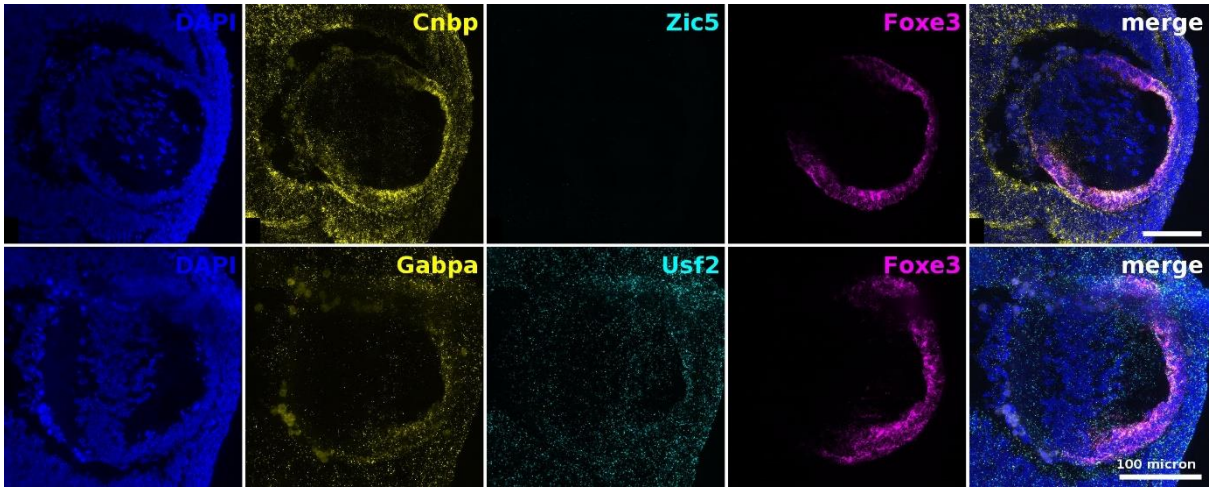

Figure 6: *Foxe3* expression at E12.5 is restricted to the anterior layer of the presumptive lens, while *Cnbp, Gabpa* and *Usf2* seem to be ubiquitous. No signal was observed for *Zic5*.

Western blot

As RNA studies did not allow the differentiation of the *Foxe3* alleles, we studied the impact of the KI mutation on the abundancy of the protein in the lens epithelium by western blot (**Figure 7A**). Analysis of the assay revealed a significant decrease of FOXE3 in the KI/KI lenses (50%, $p<0.01$), consistent with the mRNA observations. More interestingly, the quantity of the protein was drastically reduced in the lens of compound animals compared to KO heterozygous littermates (33%, $p<0.05$), showing that the KI mutation heavily impacts the production of the protein (**Figure 7B**). Overall, the quantity of FOXE3 positively correlates with the observed severity of the phenotype (**Figure 3B**).

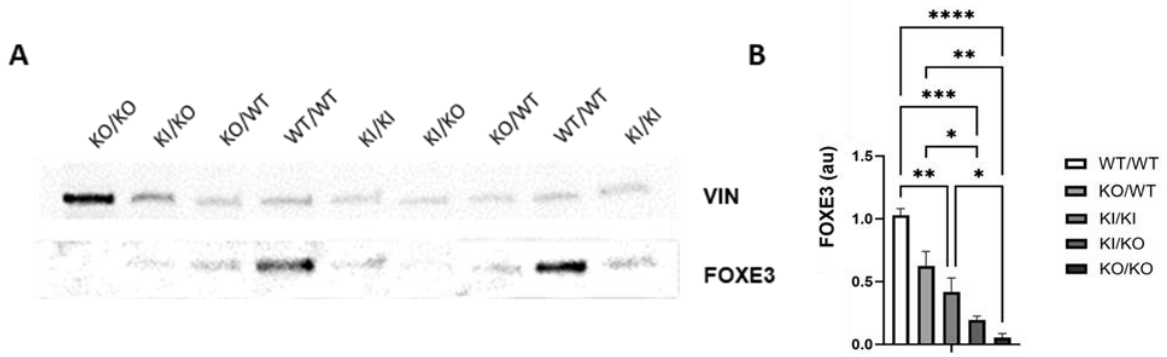

Figure 7: FOXE3 protein abundancy in the lens epithelium as determined by western blot. A: Picture of a western blot, showing a very weak FOXE3-signal for compound lenses, and no signal in KO homozygous animals. **B:** Quantification of western blot signal indicates a strong decrease of FOXE3 in the lens epithelium with the KI mutation. Only significantly different relations are shown.

Discussion

Identification and validation of a second event in our patient

The *FOXE3* locus (around 40Kb) in the 1p33 region contains several sequences conserved during the evolution of the species, all upstream of the gene. One of them, located 3Kb upstream the *FOXE3* gene (chr1:47877964-47878774 according to the GRCh37/hg19 assembly) was previously implicated in the *Foxe3* expression regulation. Indeed, the team of Wada K. [2011] showed that the homozygous deletion of a part of this conserved element (22 bp deletion) was responsible for mild microphthalmia with cataract in mice (rct mutant that arose spontaneously in a SJL/J strain) and associated with a decrease in *Foxe3* expression. This region displays several features suggesting a regulatory role in the locus. It is a known open chromatin region with no CPG island and with DNase hypersensitive areas. Several works have also shown the binding of several transcription factors in this region, some of them (SOX2, PAX6, PITX3 and TFAP2A) playing a role in ocular development [Zhao Y, 2019]. This putative enhancer was therefore a good candidate to harbor a pathogenic variation in a patient with only one heterozygous variant identified after screening of the coding sequence.

Thus, we screened by sanger sequencing this 800 bp region in our patient and found an extremely rare variant (0,01%) : chr1:47878428 G>A (hg19). This allele was also found heterozygous in the asymptomatic mother of the proband, fitting with our putative model of recessive biparental transmission (the previously identified nonsense variation was inherited from the father). Scores such as GERP (3.5799) and CADD (18.83) at this position were in favor of a possible deleterious effect.

We therefore looked for further arguments to demonstrate that this variation could be the second event detected in *Trans* with the nonsense mutation identified on the other *FOXE3* allele in our patient.

Analysis of the data available on the UCSC database (https://genome.ucsc.edu/) enabled us to see that there was no CTCF protein binding site, nor any regulatory RNA located that could be affected by this variant. Thus, we consider two possible scenarios. First, the regulatory variant prevents or reduces the binding of a transcription factor involved in the positive control of *FOXE3* expression, or secondly, the regulatory variant leads to the binding of a novel transcription factor that negatively regulates *FOXE3* expression or induces its ectopic expression.

Combination of several database available on the UCSC site (CHIP-seq data from the ENCODE project, JASPAR predicted transcription factors binding sites) does not indicate relevant candidate transcription factors in this variant-centered region. Having no strong criteria to study a factor in particular, we decided to first carry out a simple approach based on a transactivation test using the luciferase reporter system. Thus, we cloned in a pGL4 vector, upstream of the minimal promoter of the firefly, either the

wild-type cis-element either its mutated counterpart. However, somewhat unexpectedly, the mutated version strongly increased the transcription of the reporter gene compared to the wild-type version. Indeed, we rather expected the opposite effect, that is to say a loss-of-function effect from the mutated element by considering animal models or functional studies carried out by Islam L [2015]. Nevertheless, this is an *in vitro* test, which may only partially reflect what is happening *in vivo* during early ocular development in embryos. It is known that the regulation of gene expression can vary according to time and tissue and it is possible that *in vivo*, this variant leads to a decrease in *FOXE3* expression during early ocular development. Thus, this first approach allowed to show that this conserved region is clearly playing a role in gene expression regulation since, regardless of the condition tested (wild-type or mutant), its presence upstream of a minimal promoter enhances the expression of the reporter gene. Thus, in view of these data and those obtained by the team of Wada K [2011], the expression of the *FOXE3* gene could probably be dependent on this cis-regulatory element and it is likely that the mutation identified in this regulatory sequence is involved in *FOXE3* expression regulation and may thus correspond to the second pathogenic variation of the recessive model assumed in our patient.

We decided to carry out further studies in order to understand the role of this variation and the molecular interactions and mechanisms involved in this patient. We then generated different mouse mutant lines to study the variant under *in vivo* conditions.

Phenotype analysis of the different mutant mice showed a spectrum of eye growth, cornea, anterior segment and lens abnormalities of increasing frequency and severity in the homozygous KI/KI, compound heterozygous KI/KO and homozygous KO/KO lines, respectively (**Figure 3**). These anomalies were reminiscent of the *FOXE3*-associated phenotypes in human [Plaisancié J, 2018; Reis LM, 2019]. As in humans, we showed that there was a significant correlation between the occurrence and the severity of the phenotype and the nature and the number of the mutation in the *Foxe3* locus. The non-coding variant seems to act here as an hypomorphic allele. Several examples in literature show in humans that, when combined with a loss-of-function variant or a deletion, hypomorphic alleles result in a recessive disease (e.g., in thrombocytopenia-absent radius syndrome [Boussion S, 2020], Stargardt disease [Zernant J, 2022] and spondylocostal dysostosis [Takeda K, 2017]). These results allowed us to confirm the implication of the non-coding variant in the phenotype of our patient, crucial for diagnosis and genetic counselling in this family.

A particular attention will be paid to this particular region in future patients with severe ocular phenotype and one recessive *FOXE3* allele on genetic analyses.

Although the implication of the non-coding variant was demonstrated by the phenotypic analyses of the mutant mice, we wanted to study the impact of those two different alleles (KI and KO) on the *Foxe3* expression. Thus, we performed both RT-qPCR in adult eyes and RNAscope studies in embryonic and adult eyes among the different lines.

Through these different RNA studies, we consistently showed that the KI/KI genotype is associated with a drastic reduction of the *Foxe3* expression from early development (**Figure 5C**) to adulthood (**Figures 5B**). This confirms that the studied variation has a negative regulatory impact on the *Foxe3* expression and can be consider as a pathogenic variation.

For the KI/KO and KO/KO, we observed varying levels of *Foxe3* expression depending on the stage and/or the method used. In the KI/KO mice, the *Foxe3* expression was slightly reduced in embryos RNAscope (**Figure S17**) and in adults RNAscope (**Figure S16**) but drastically increased in RT-qPCR (**Figure 5A**). In the KO/KO mice, the *Foxe3* expression was conserved in KO/KO embryos (**Figure S17**) then undetectable in adults due to the microphakic lens in adult eyes (**Figure S16**).

Concordant with this observation, the protein was not found in KO/KO adult lens. However, quantification of the protein FOXE3 revealed a significant decrease of the protein in the eyes of adult KI/KO mice, while the reduction was moderate in KO/WT lens and intermediary for compound lens (**Figure 7**). Overall, the decrease of the protein strongly correlates with the graded severity of the ocular phenotypes (**Figure 3**).

In view of these results, one possible explanation is that the *Foxe3* mRNA carrying the KO allele escapes the nonsense-mediated mRNA-decay (NMD) (given *Foxe3* is an intronless gene) explaining why it is thus detected at normal level. Despite normal mRNA level and given the genotype of the KO/KO mice (p.Gly28Argfs*112), the FOXE3 protein is however unlikely to be functional and is secondarily degraded.

Understanding the role of *Foxe3* in ocular development

FOXE3 is a transcription factor that controls lens epithelial cell growth through regulation of proliferation, apoptosis and cell cycle [Wang Y, 2012; Islam I, 2015]. During lens development, it controls lens vesicle closure and subsequent separation of the lens vesicle from ectoderm. Then, it controls the ratio of the lens fiber cells to the cells of the anterior lens epithelium by regulating the rate of proliferation and differentiation. From our RNA studies and literature data [Blixt A, 2000], we know that *Foxe3* is expressed during normal ocular development initially in lens placode (E10.5), in lens vesicle (E12.5) and then its expression is confined to the anterior lens epithelium that is conserved into adulthood (**Figure S16**).

In this work, clinical and histological analyses of the KO/KO adults showed consistent results among the 20 analyzed eyes: all, except one, were microphthalmic (of note this eye presented buphthalmia which might have artificially normalized the eye size). No “true” anophthalmia was observed. Besides the constant microphthalmia, all eyes were presenting common severe anomalies consisting in **i)** anterior chamber lesions (corneal opacities, central pit of the cornea, irido-corneal and irido-lenticular adherences), **ii)** lens anomalies (microphakia with severe cataractic lesions), **iii)**

posterior segment anomalies with lesions evocative of a persistent fetal vasculature and anteriorly extended retina.

To better understand the genesis of these lesions, we performed histological analyses in several embryonic stages (E12.5, E13.5, E14.5, E18.5) to compare the establishment of the different ocular structures during eye formation between WT, KI/KO and KO/KO embryos until birth (P0). Strikingly, in KO/KO mice embryos, eye structures were forming correctly until E12.5 (**Figure 4**) and the mutant *Foxe3* mRNA was detected (**Figure S17**). From E13.5 to E14.5 (**Figure 4**), we observe **i)** a delay in the lens vesicle detachment from the cornea in all the eyes that was also visible in some KI/KO eyes, **ii)** a progressive disorganization/loss of the anterior lens epithelium, **iii)** a mild vacuolization of the lens fibers and **iv)** an abnormal position of the lens too close to the cornea. From E18.5, the KO/KO lenses are microphakic and the overall size of the eyeball seems to be preserved (**Figure 4**).

Apoptotic events in KO/KO embryos.

These results are in correlation with the *Foxe3* mutant lines described in the literature respectively carrying homozygous missense mutation [Sanyal and Hawkins, 1979; Blixt A 2000] and null mutations [Medina-Martinez O, 2005; Blixt A 2007]. The former is the dyl/dyl mutant that arose spontaneously in Balb/c mice [Sanyal and Hawkins, 1979] whose genetic cause (the *Foxe3* gene) has been elucidated by Blixt A [2000] and whose phenotype was further analyzed by the same team [Ormestad M, 2002; Blixt A 2007]. The latter is the genetically engineered *Foxe3* null mutant by two different teams in two different backgrounds, 129×C57Bl/6 [Medina-Martinez O, 2005] and Balb/c mice [Blixt A 2007]. If some slight differences were observed in the phenotype (that was always restricted to the eye) between those lines, all the biallelic *Foxe3* mutant lines displayed severe lens abnormalities and eye growth defects (i.e., microphthalmia). Of note, Ormestad M [2002] revealed that approximately 40% of mice heterozygous for *Foxe3* dyl have also mild corneal and lenticular defects (central corneal opacity, keratolenticular adhesion, anterior polar cataract). The most striking phenotype between those mutant lines, was the persistent connection between the lens and the cornea, which results from failure or a delay of the lens vesicle to close and separate from the ectoderm. Reduced size, irregular shape and disorganized structure with large vacuoles are other characteristics of the lenses of those mutant mice. It was shown that lens fiber elongation and expression of crystallins were initiated in an apparently normal way, but the number of fibers were drastically reduced, resulting in a diminutive, irregular and cataractic lens where lens fiber material is sometimes expelled to the exterior through the persistent ectodermal connection, a finding that we also observed in our KO/KO mutants. In mutant lenses [Medina-Martinez O, 2005; Blixt A 2007], the epithelial layer is formed during lens vesicle polarization, but then gradually become disorganised and with lower cell density by the time of birth, leaving a cataractic lens. In both type of mutants, the lens epithelium fails to proliferate (BrDU incorporation and proliferative markers) and the

lens fiber cells fail to differentiate [Medina-Martinez O, 2005; Blixt A 2007]. Moreover, those mutant lenses had many apoptotic cells in the anterior part of the epithelium at E14.5 whereas no signs of apoptosis could be detected in wild-type at the same stage.

Furthermore, similar results were obtained in the rct/rct mice [Maeda YY, 2001] genetically characterized by Wada K [2011] with a non-coding 22bp deletion in the regulatory region of *Foxe3*. This mutant line presented with mild microphthalmia and marked degeneration of the lens, including loss of the fine structure of the lens fibers and swelling of epithelial cells with vacuoles of various sizes in the cortex. There was also evidence of disorganization in the anterior epithelium of the lens in the rct/rct mice compared to wild-type mice that progressively worsen through the embryonic development and in postnatal rct/rct mice.
Thus, as we observed similar marked degenerative process in our KO/KO mice as in other *Foxe3* reported lines [Blixt A 2000; Maeda YY, 2001; Medina-Martinez O, 2005; Blixt A 2007; Wada K, 2011], the central question emerging from this study is how the growth defect of the eye (microphthalmia) observed in all the KO/KO individuals could happen while all the eye structures fall into place normally during early embryonic development.

The first recognizable phenotypic deviation was the failure or delay of the lens vesicle to separate from the ectoderm, visible from the E12.5 stage onwards. However, the starting point of the pathological process seems rather to be the progressive disorganization of the anterior lens epithelium (in which is precisely expressed *Foxe3*) that is ending by a whole degeneration of the lens. But how this degenerative lens will lead to microphthalmia remains unknown.

Several explanations can be formulated. First, in mice, unlike in humans, the lens occupies a larger portion of the eye, thus we can intuitively say that its absence (due to degeneration) will lead to collapse of the eye, this resulting in microphthalmia. However, several patients with aphakia have been reported without microphthalmia [Reis LM, 2021]. Secondly, it could be argued that the persistent ectodermal connection facilitates expulsion of lens tissue and thereby reduces intraocular pressure, which in turn may result in smaller eyes because optimum pressure is necessary for the growth of the eyeball. However, this persistent connection is also present in some KI/KO individuals that are not microphthalmic. Finally, this *Foxe3* mutant model is strangely evocative of the cavefish (the blind cave-dwelling morph of the Astyanax Mexicanus) whose lens, from approximately 30 hours postfertilization (hpf), enters massive apoptosis [Rétaux S, 2022; Yamamoto and Jeffery, 2000; Alunni et al., 2007], which will trigger the progressive and total loss of eye by degeneration. In adults, the residual cyst is covered with skin, invisible and non-functional. The "instructive" role of the lens in triggering this degeneration has been shown by elegant embryo transplantation experiments: a cavefish lens transplanted at 24 hpf into the optic cup of a river-dwelling surface embryo form causes its degeneration, while a river-dwelling surface lens transplanted at 24 hpf in the optic cup of a cavefish embryo “saves” the eye of the cavefish [Yamamoto and Jeffery, 2000]. The genetic defect that

causes apoptosis of the lens is unknown, but it seems that a deregulation and a defect in the expression of the alpha-A crystallin, the small anti-apoptotic chaperone, participate in the process [Hinaux H, 2015].

In all vertebrate species, the folding of optic vesicle happens concomitantly to the lens vesicle formation and their reciprocal interaction seem to be necessary for the formation of a proper 3D shaped eye, according to several studies [Casey MA, 2023]. Lens-retina crosstalk is mediated by many transcription factors and signaling pathways (BMP, FGF and Wnt) and is decisive for correct morphogenesis of the eyes [Casey MA, 2023]. Many studies have tried to disentangle these complex interactions and dissect the role and interactions of each of these structures on each other (lens placode/optic vesicle, lens vesicle/optic cup, lens/retina) and also with the peri-ocular mesenchyme and the neural crest cells. For example, several studies have convincingly demonstrated a cell autonomous requirement for PAX6 in the surface ectoderm for lens placode development, but showed it to be dispensable for the inductive capacity of the optic vesicle [Collinson JM, 2000; Davis-Silberman N, 2005; Dimanlig PV, 2001].

What constitutes the so-called "induction" hypothesis formulated by Spemann H [1901] is actually questioned following the demonstration of optic cup formation without any lens induction through several experiments in different models [Cardozo MJ 2023] and as illustrated by the presence of optic cup in patients with aphakia [Valleix S, 2006]. This is emphasized by the fact that the lens, a structure that appears secondarily during eye evolution, would only have a role in optimizing optic cup invagination and formation [Cardozo MJ, 2023]. Our work described for the first time a model of eye growth defect in which the initial instructions for the growth and 3D organization of the basic ocular structures are given but, at a certain point of the embryonic development (here E18.5) the “inductive” processes are replaced by “involutive” processes, i.e., the progressive degeneration of the lens impacting the ocular growth and formation. Strikingly, some structures such as the retina seem to be relatively preserved from those “involutive” orders and conversely will expand rather abnormally. Indeed, abnormal retina was observed in our KO/KO mice as well as the Foxe3 null mice described by Medina-Martinez [2005]. Moreover, in the Aey69 mutant line [Vetrivel S, 2019] a phenotype of microphthalmia with both aphakia and retinal hyperproliferation, was reported due to mutation in the *Hist2h3c1* gene. Detailed analysis of eye development in this homozygous mutant mouse documented a perturbed lens development starting from the lens vesicle stage including decreasing expression of crystallins as well as of lens-specific transcription factors such as *Pitx3* and *Foxe3*. In contrast, they observed an early expression of retinal progenitor cells characterized by several markers including *Brn3* (retinal ganglion cells) and *Otx2* (cone photoreceptors). The changes in the retina at the early embryonic stages of E11.5-E15.5 happened in parallel with apoptotic processes in the lens at the respective stages.

Thus, different degrees of eyeball degeneration due to lens degeneration are observed: the one leading to a complete involution of the eye (as observed in the cavefish) and another one leading to incomplete involution (microphthalmia) with hyperproliferation of the retina (as observed in different mouse models, including ours). The question is to what extent it is the same mechanism or rather two different pathological processes, ending both with eyeball degeneration.

Dissecting the regulatory landscapes of *Foxe3* and identification of candidate genes in ocular malformations

After confirming the role of this regulatory variant in the phenotype, we wanted to go further in dissecting the molecular mechanisms by which the non-coding variant contributes to an ocular developmental defect. Thus, we performed DNA-PD and mass spectrometry experiments on two different mouse ESC and one immortalized human epithelial lens cells, in search for differentially bound transcription factors. In total, we identified 34 candidate TF, whose binding appears or disappears in presence of the mutation (**Figure 2**). Three of which were common between the three cell lines: CNBP (knock-out mice present microphthalmia phenotype, [Chen W, 2003]), USF2 and GABPA. In addition, the ZIC5 factor caught our attention because its mutations cause microphthalmia in mice, even though it was only found in two murine lines (CCE-RAX and ESC lines).

By RNAscope (**Figure 6**), we showed that those three candidates were well expressed during early eye formation in the mouse, concomitantly with *Foxe3*. As this result does not help us to select one candidate among those three, other experiments need to be performed.

Conclusion

Enhancers generally consist in evolutionary conserved regions with characteristic features such as specific Histone marks, absence of CpG island, DNase hypersensitivity sites. These enhancers can be intragenic but more frequently located few Kb around the gene they drive and sometimes at several megabases far away from it [Schoenfelder S, 2019]. Generally, a gene is holding a set of cis-regulatory regions, each of them driving a specific expression pattern of this gene. Variants within enhancers can affect the dynamics of gene expression of the genes they regulate and can lead to a phenotype reminiscent of the mutation gene spectrum. Screening patients for mutations in regulatory sequences is such an approach to resolve unsolved genetic cases of developmental diseases.
However, despite these hallmarks that make these regions potentially recognizable, we are still far from being able to phenotype those regions and characterize the effect of variants inside, as witnessed by the rarity of examples in literature.
Our work demonstrates the difficulty to elucidate the effect of one variant in a non-coding region. Besides progresses that need to be made on non-coding variant

interpretation, our work illustrates the importance of the knowledge of phenotypes and the establishment of genotype-phenotype correlations in patients that is crucial for interpreting non-coding variants.

Beyond the medical interest, brought by the modelisation of variants, this work shows the contribution of pathogenic regulatory variations to dissect the regulatory landscapes of genes and identify novel candidate genes for genetic diseases.

Furthermore, this work allows to describe for the first time a novel mechanism of microphthalmia, by degeneration of the lens. This is an important point to consider in view of developing therapeutic approaches. Indeed, the possibility of treatment was thought to be limited by an early defect of the developing ocular structures (between 4^{th} and 7^{th} weeks of gestation). A degenerative mechanism may be more subject to allow therapeutic approaches as it will begin later in the pregnancy.

REFERENCES

Alunni A, Menuet A, Candal E, Pénigault JB, Jeffery WR, Rétaux S. Developmental mechanisms for retinal degeneration in the blind cavefish Astyanax mexicanus. J Comp Neurol. 2007 Nov 10;505(2):221-33.

Blixt A, Mahlapuu M, Aitola M, Pelto-Huikko M, Enerback S, Carlsson P. A forkhead gene, FoxE3, is essential for lens epithelial proliferation and closure of the lens vesicle. Genes Dev 2000;14(2):245-54.

Blixt A, Landgren H, Johansson BR, Carlsson P. Foxe3 is required for morphogenesis and differentiation of the anterior segment of the eye and is sensitive to Pax6 gene dosage. Dev Biol. 2007 Feb 1;302(1):218-29.

Boussion S, Escande F, Jourdain AS, Smol T, Brunelle P, Duhamel C, Alembik Y, Attié-Bitach T, Baujat G, Bazin A, Bonnière M, Carassou P, Carles D, Devisme L, Goizet C, Goldenberg A, Grotto S, Guichet A, Jouk PS, Loeuillet L, Mechler C, Michot C, Pelluard F, Putoux A, Whalen S, Ghoumid J, Manouvrier-Hanu S, Petit F. TAR syndrome: Clinical and molecular characterization of a cohort of 26 patients and description of novel noncoding variants of RBM8A. Hum Mutat. 2020 Jul;41(7):1220-1225.

Cardozo MJ, Sánchez-Bustamante E, Bovolenta P. Optic cup morphogenesis across species and related inborn human eye defects. Development. 2023 Jan 15;150(2):dev200399.

Casey MA, Lusk S, Kwan KM. Eye Morphogenesis in Vertebrates. Annu Rev Vis Sci. 2023 Apr 11.

Chalupa LM, Williams RW. Eye, Retina, and Visual System of the Mouse. Cambridge, MA: MIT Press; 2008:xii, 754.

Chen W, Liang Y, Deng W, Shimizu K, Ashique AM, Li E, Li YP. The zinc-finger protein CNBP is required for forebrain formation in the mouse. Development. 2003 Apr;130(7):1367-79.

Chesneau B, Aubert-Mucca M, Fremont F, Pechmeja J, Soler V, Isidor B, Nizon M, Dollfus H, Kaplan J, Fares-Taie L, Rozet JM, Busa T, Lacombe D, Naudion S, Amiel J, Rio M, Attie-Bitach T, Lesage C, Thouvenin D, Odent S, Morel G, Vincent-Delorme C, Boute O, Vanlerberghe C, Dieux A, Boussion S, Faivre L, Pinson L, Laffargue F, Le Guyader G, Le Meur G, Prieur F, Lambert V, Laudier B, Cottereau E, Ayuso C, Corton-Pérez M, Bouneau L, Le Caignec C, Gaston V, Jeanton-Scaramouche C, Dupin-Deguine D, Calvas P, Chassaing N, Plaisancié J. First evidence of SOX2 mutations in Peters' anomaly: Lessons from molecular screening of 95 patients. Clin Genet. 2022 May;101(5-6):494-506.

Chou CM, Nelson C, Tarlé SA, Pribila JT, Bardakjian T, Woods S, Schneider A, Glaser T. Biochemical Basis for Dominant Inheritance, Variable Penetrance, and Maternal Effects in RBP4 Congenital Eye Disease. Cell. 2015 Apr 23;161(3):634-646.

Collinson JM, Hill RE, West JD. Different roles for Pax6 in the optic vesicle and facial epithelium mediate early morphogenesis of the murine eye. Development. 2000 Mar;127(5):945-56.

Davis-Silberman N, Kalich T, Oron-Karni V, Marquardt T, Kroeber M, Tamm ER, Ashery-Padan R. Genetic dissection of Pax6 dosage requirements in the developing mouse eye. Hum Mol Genet. 2005 Aug 1;14(15):2265-76.

Dimanlig PV, Faber SC, Auerbach W, Makarenkova HP, Lang RA. The upstream ectoderm enhancer in Pax6 has an important role in lens induction. Development. 2001 Nov;128(22):4415-24.

Furushima K, Murata T, Kiyonari H, Aizawa S. Characterization of Opr deficiency in mouse brain: subtle defects in dorsomedial telencephalon and medioventral forebrain. Dev Dyn. 2005 Apr;232(4):1056-61.

Hinaux H, Blin M, Fumey J, Legendre L, Heuzé A, Casane D, Rétaux S. Lens defects in Astyanax mexicanus Cavefish: evolution of crystallins and a role for alphaA-crystallin. Dev Neurobiol. 2015 May;75(5):505-21.

Islam L, Kelberman D, Williamson L, Lewis N, Glindzicz MB, Nischal KK, Sowden JC. Functional analysis of FOXE3 mutations causing dominant and recessive ocular anterior segment disease. Hum Mutat. 2015 Mar;36(3):296-300.

Maeda YY, Funata N, Takahama S, Sugata Y, Yonekawa H. Two interactive genes responsible for a new inherited cataract (RCT) in the mouse. Mamm Genome. 2001 Apr;12(4):278-83.

Medina-Martinez O, Brownell I, Amaya-Manzanares F, Hu Q, Behringer RR, Jamrich M. Severe defects in proliferation and differentiation of lens cells in Foxe3 null mice. Mol Cell Biol. 2005 Oct;25(20):8854-63.

Ormestad M, Blixt A, Churchill A, Martinsson T, Enerback S, Carlsson P. Foxe3 haploinsufficiency in mice: a model for Peters' anomaly. Invest Ophthalmol Vis Sci 2002;43(5):1350-7.

Pierro, L.J. and Spiggle, J., 1967]: Congenital eye defects in the mouse. I. Corneal opacity in C57 Black mice, J. Exp. Zool. 166:25, 1967

Plaisancié J, Ragge NK, Dollfus H, Kaplan J, Lehalle D, Francannet C, Morin G, Colineaux H, Calvas P, Chassaing N. FOXE3 mutations: genotype-phenotype correlations. Clin Genet. 2018 Apr;93(4):837-845.

Plaisancié J, Ceroni F, Holt R, Zazo Seco C, Calvas P, Chassaing N, et al. Genetics of anophthalmia and microphthalmia. Part 1: non-syndromic anophthalmia/microphthalmia. Hum Genet. 2019;138:799–830.

Reis LM, Tyler RC, Schneider A, Bardakjian T, Stoler JM, Melancon SB, Semina EV. FOXE3 plays a significant role in autosomal recessive microphthalmia. Am J Med Genet A 2010;152A(3):582-90.

Reis LM, Semina EV. Genetic landscape of isolated pediatric cataracts: extreme heterogeneity and variable inheritance patterns within genes. Hum Genet. 2019 Sep;138(8-9):847-863.

Reis LM, Sorokina EA, Dudakova L, Moravikova J, Skalicka P, Malinka F, Seese SE, Thompson S, Bardakjian T, Capasso J, Allen W, Glaser T, Levin AV, Schneider A, Khan A, Liskova P, Semina EV. Comprehensive phenotypic and functional analysis of dominant and recessive FOXE3 alleles in ocular developmental disorders. Hum Mol Genet. 2021 Aug 12;30(17):1591-1606.

Rétaux S. La boîte à outils de l'évolution développementale ou comment les poissons cavernicoles mexicains ont perdu leurs yeux [The toolbox of developmental evolution or how Mexican cave fishes lost their eyes]. Biol Aujourdhui. 2022;216(1-2):49-53. French.

Richards S, Aziz N, Bale S, Bick D, Das S, Gastier-Foster J, Grody WW, Hegde M, Lyon E, Spector E, Voelkerding K, Rehm HL; ACMG Laboratory Quality Assurance Committee. Standards and guidelines for the interpretation of sequence variants: a joint consensus recommendation of the American College of Medical Genetics and Genomics and the Association for Molecular Pathology. Genet Med. 2015 May;17(5):405-24.

Sanyal S, Hawkins RK. Dysgenetic lens (dyl)--a new gene in the mouse. Invest Ophthalmol Vis Sci. 1979 Jun;18(6):642-5.

Schoenfelder, S., Fraser, P. Long-range enhancer–promoter contacts in gene expression control. Nat Rev Genet 20, 437–455 (2019).

Spemann H. 1901. Ueber Korrelationen in der Entwicklung des Auges. Ver. Anat. Gesellsch. 15:61–79

Tabata Y, Ouchi Y, Kamiya H, Manabe T, Arai K, Watanabe S. Specification of the retinal fate of mouse embryonic stem cells by ectopic expression of Rx/rax, a homeobox gene. Mol Cell Biol 2004;24(10):4513-21.

Takeda K, Kou I, Kawakami N, Iida A, Nakajima M, Ogura Y, Imagawa E, Miyake N, Matsumoto N, Yasuhiko Y, Sudo H, Kotani T; Japan Early Onset Scoliosis Research Group; Nakamura M, Matsumoto M, Watanabe K, Ikegawa S. Compound Heterozygosity for Null Mutations and a Common Hypomorphic Risk Haplotype in

TBX6 Causes Congenital Scoliosis. Hum Mutat. 2017 Mar;38(3):317-323. doi: 10.1002/humu.23168. Epub 2017 Jan 18. PMID: 28054739.

Tkatchenko TV, Shen Y, Tkatchenko AV. Analysis of postnatal eye development in the mouse with high-resolution small animal magnetic resonance imaging. Invest Ophthalmol Vis Sci. 2010 Jan;51(1):21-7. Tümer Z, Bach-Holm D: Axenfeld-Rieger syndrome and spectrum of PITX2 and FOXC1 mutations. Eur J Hum Genet 2009; 17: 1527–1539

Ucuncu E, Rajamani K, Wilson MSC, Medina-Cano D, Altin N, David P, Barcia G, Lefort N, Banal C, Vasilache-Dangles MT, Pitelet G, Lorino E, Rabasse N, Bieth E, Zaki MS, Topcu M, Sonmez FM, Musaev D, Stanley V, Bole-Feysot C, Nitschké P, Munnich A, Bahi-Buisson N, Fossoud C, Giuliano F, Colleaux L, Burglen L, Gleeson JG, Boddaert N, Saiardi A, Cantagrel V. MINPP1 prevents intracellular accumulation of the chelator inositol hexakisphosphate and is mutated in Pontocerebellar Hypoplasia. Nat Commun. 2020 Nov 30;11(1):6087.

Valleix S, Niel F, Nedelec B, Algros MP, Schwartz C, Delbosc B, Delpech M, Kantelip B. Homozygous nonsense mutation in the FOXE3 gene as a cause of congenital primary aphakia in humans. Am J Hum Genet 2006;79(2):358-64.

Vandesompele J, De Preter K, Pattyn F, Poppe B, Van Roy N, De Paepe A, et al. Accurate normalization of real-time quantitative RT-PCR data by geometric averaging of multiple internal control genes. Genome Biol. 2002;3:research0034.1-research0034.11.

Vetrivel S, Tiso N, Kügler A, Irmler M, Horsch M, Beckers J, Hladik D, Giesert F, Gailus-Durner V, Fuchs H, Sabrautzki S, Hrabě de Angelis M, Graw J. Mutation in the mouse histone gene Hist2h3c1 leads to degeneration of the lens vesicle and severe microphthalmia. Exp Eye Res. 2019 Nov;188:107632.

Wada K, Maeda YY, Watanabe K, Oshio T, Ueda T, Takahashi G, Yokohama M, Saito J, Seki Y, Takahama S, Ishii R, Shitara H, Taya C, Yonekawa H, Kikkawa Y. A deletion in a cis element of Foxe3 causes cataracts and microphthalmia in rct mice. Mamm Genome. 2011 Dec;22(11-12):693-702.

Wang Y, Li W, Wang Y, Huang Y. Growth inhibition of human lens epithelial cells by short hairpin RNA in transcription factor forkhead box E3 (FOXE3). Graefes Arch Clin Exp Ophthalmol. 2012 Jul;250(7):999-1007.

Washington NL, Haendel MA, Mungall CJ, Ashburner M, Westerfield M, Lewis SE. Linking human diseases to animal models using ontology-based phenotype annotation. PLoS Biol. 2009 Nov;7(11):e1000247.

Yamamoto Y, Jeffery WR. Central role for the lens in cave fish eye degeneration. Science. 2000 Jul 28;289(5479):631-3. doi: 10.1126/science.289.5479.631. Erratum in: Science 2001 Mar 30;291(5513):2551.

Zazo Seco C, Plaisancié J, Lupasco T, Michot C, Pechmeja J, Delanne J, Cottereau E, Ayuso C, Corton M, Calvas P, Ragge N, Chassaing N. Identification of PITX3 mutations in individuals with various ocular developmental defects. Ophthalmic Genet. 2018 Jun;39(3):314-320.

Zernant J, Lee W, Wang J, Goetz K, Ullah E, Nagasaki T, Su PY, Fishman GA, Tsang SH, Tumminia SJ, Brooks BP, Hufnagel RB, Chen R, Allikmets R. Rare and common variants in ROM1 and PRPH2 genes trans-modify Stargardt/ABCA4 disease. PLoS Genet. 2022 Mar 30;18(3):e1010129.

Zhao Y, Zheng D, Cvekl A. Profiling of chromatin accessibility and identification of general cis-regulatory mechanisms that control two ocular lens differentiation pathways. Epigenetics Chromatin. 2019 May 3;12(1):27.

Supplementary data

KI FOXE3	Foxe3-F2	TATCCACCCAGTGTGGTCAG
	Foxe3-R2	AGGCCATGTGCATAGTCTGG
KO FOXE3	mFOXE3 R7	ATATAAGGCGAACCTGCGACC
	mFOXE3 F7	CACCACTTCCTCCGGTTCG

Table S1: primers used to check the introduction of the mutations in the locus of interest.

Foxe3 Forward primer	*5'-GCCGCCCTACTCATACATC-3'*
Foxe3 Reverse primer	*5'-ACAGTCGTTGAGGGTGAGG-3'*
Tbp Forward primer	*5'-TGACCTAAAGACCATTGCACTTCGT-3'*
Tbp Reverse primer	*5'-CTGCAGCAAATCGCTTGGGA-3'*
Hprt Forward primer	*5'-GTTGGTACAGGCCAGACTTTGTT-3'*
Hprt Reverse primer	*5'-AAACGTGATTCAAATCCCTGAAGTA-3'*

Table S2: primers' sequences used to perform RT-qPCR.

Set of probes	***Channel 1***	***Channel 2***	***Channel 3***
Positive control	*Polr2a*	*Ppib*	*Ubc*
Negative control	*DapB-C1*	*DapB-C2*	*DapB-C3*
Foxe3 – mix 1	*Mm-Foxe3*	*Mm-Zic5-C2*	*Mm-Cnbp-C3*
Foxe3 – mix 2	*Mm-Foxe3*	*Mm-Usf2-C2*	*Mm-Gabpa-C3*

Table S3: sets of probes used for RNAscope studies.

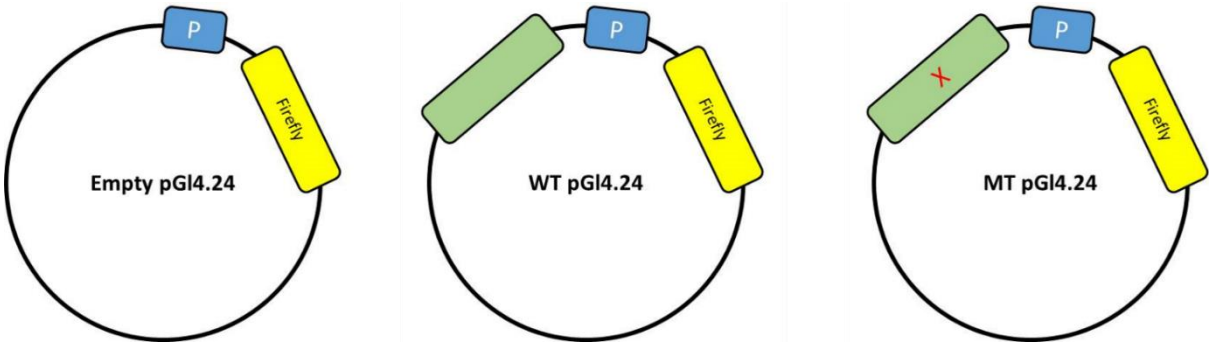

Figure S1 showing the different vectors constructed in this project. The pGL4.24 vector containing the firefly reporter gene (yellow box) under the control of a minimal promoter (blue box) and the two recombinant ones carrying the mutant or the wild-type cis-element (green box) upstream**.**

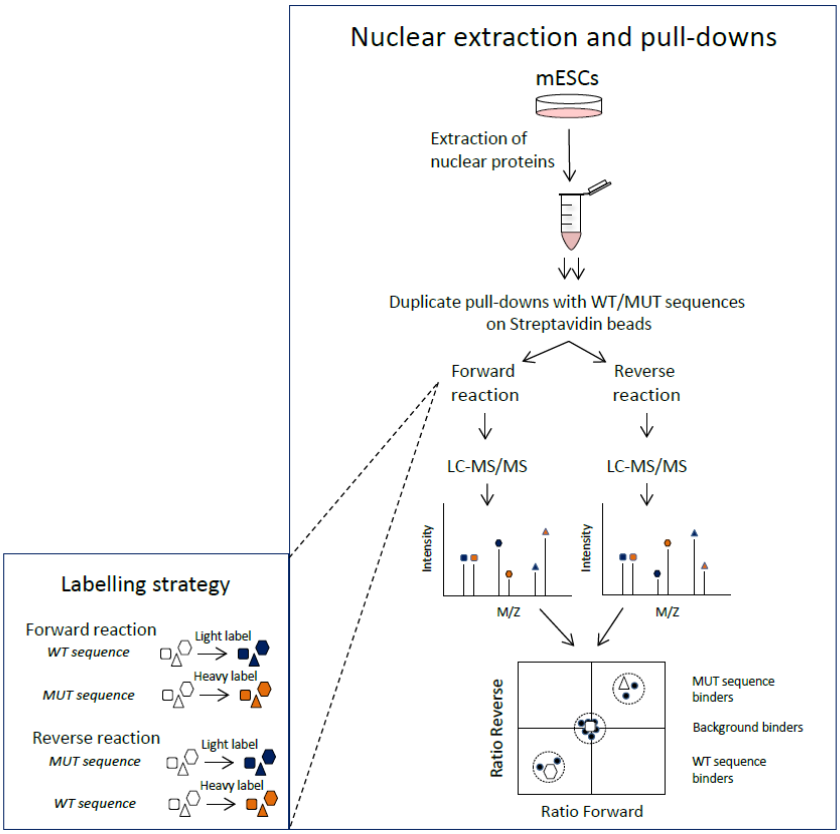

Figure S2: workflow of DNA pull-down and mass spectrometry followed in this study

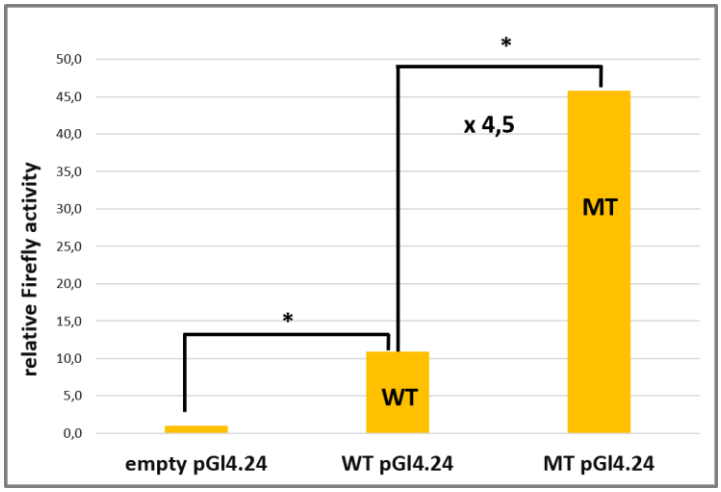

Figure S3: Results of the luciferase reporter assays

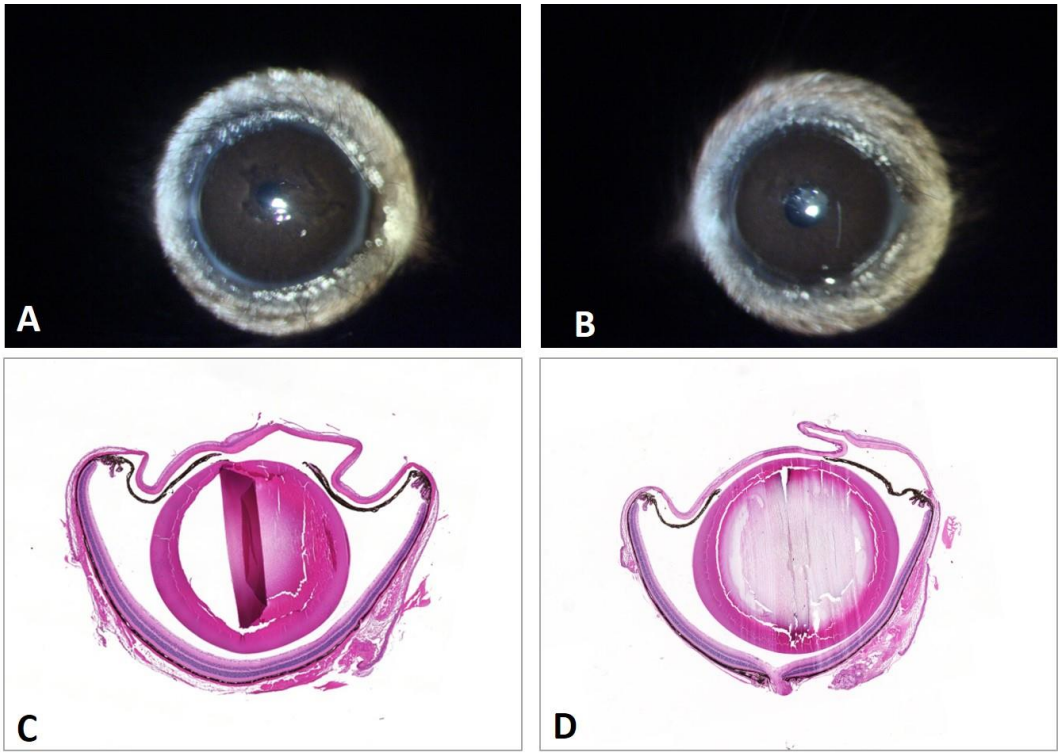

Figure S4: normal eyes of a WT/WT mouse (430) after slit lamp examination and histological analyses (**A/C right eye** and **B/D left eye**). It is important to note here that the mouse lens is rounder and occupies a larger portion of the eye than the human lens [Chalupa LM, 2008].

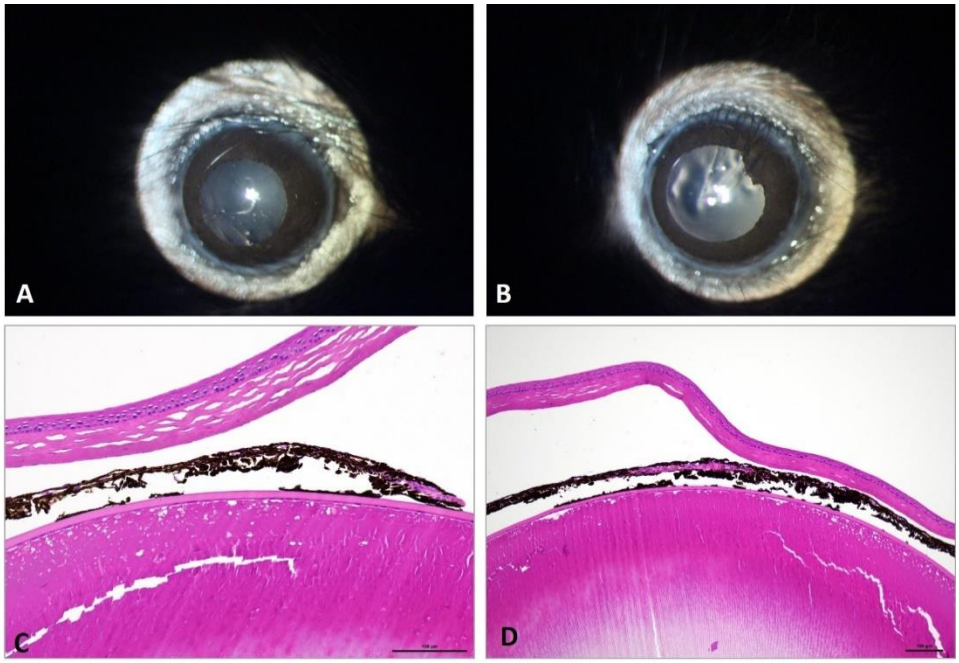

Figure S5: Clinical and histological phenotype of a KO/WT mouse (439) with unilateral phenotype. **A**: normal right eye after pharmacological mydriasis; **B**: clinical pictures of left eye after pharmacological mydriasis showing dyscoria and irido-lenticular adherences; **C and D**: histological analyses confirming the presence of an adherence between the iris (posterior face) and the lens in the left eye.

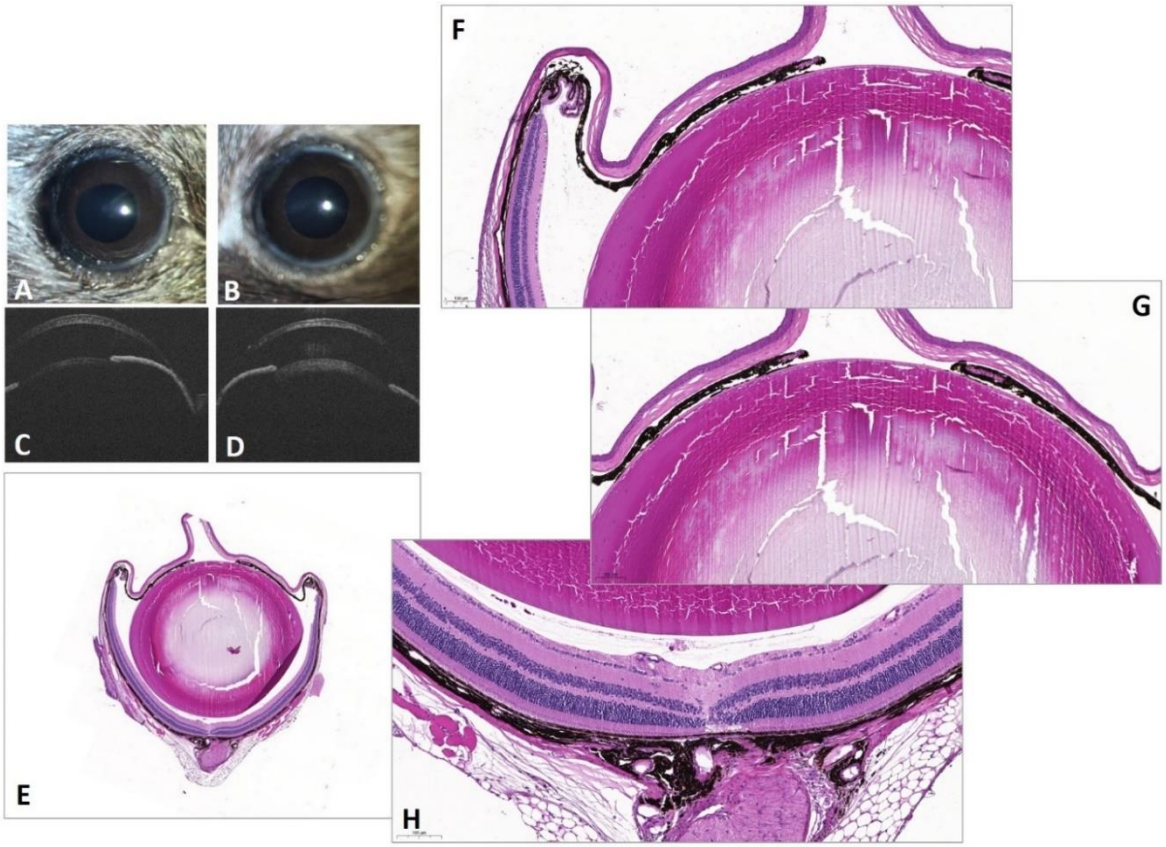

Figure S6: normal eyes structures of a KO/WT mouse (379) after clinical, imaging and histological studies

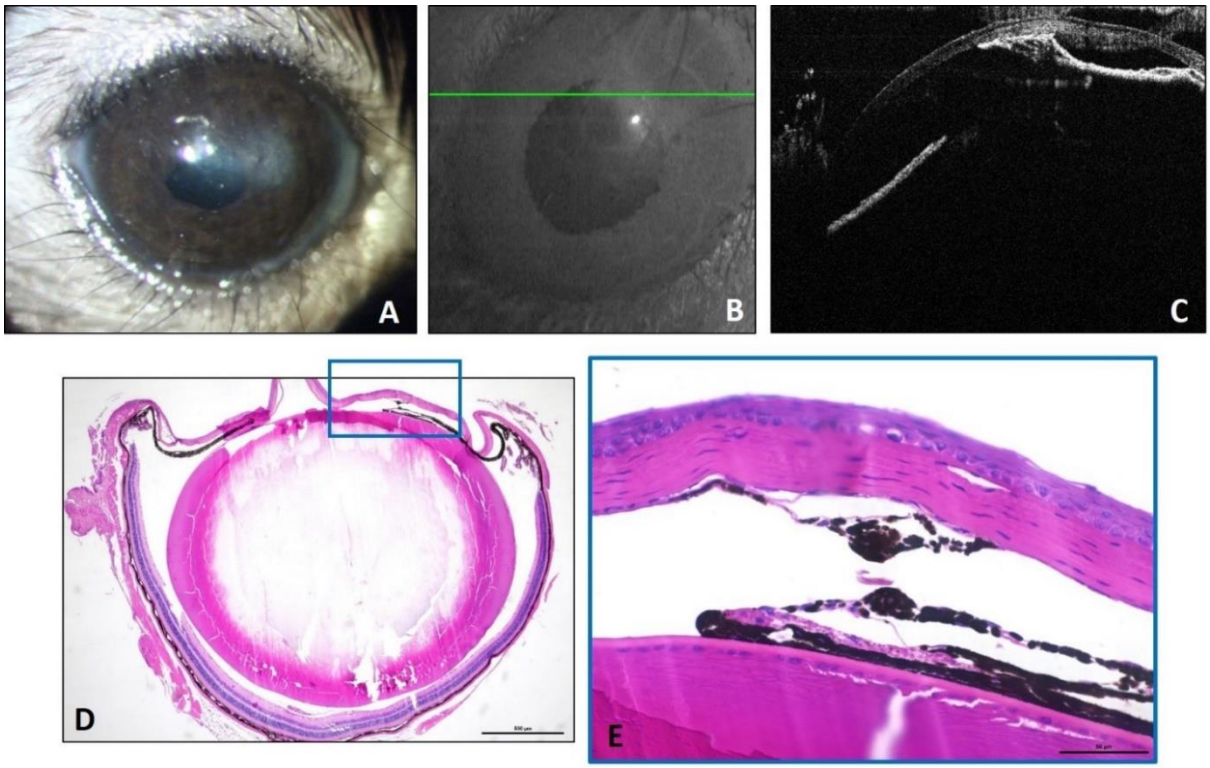

Figure S7: Clinical, Imaging and histological phenotype of a KI/WT mouse (452) **A**: clinical picture of the right eye showing corneal opacity due to iris adhesion; **B**: OCT in face view; **C**: OCT slide showing iris adhesion to cornea as well as closure of iridocorneal angle; **D and E** (zoom view): histological analyses illustrating irido-corneal focal extensive adhesion.

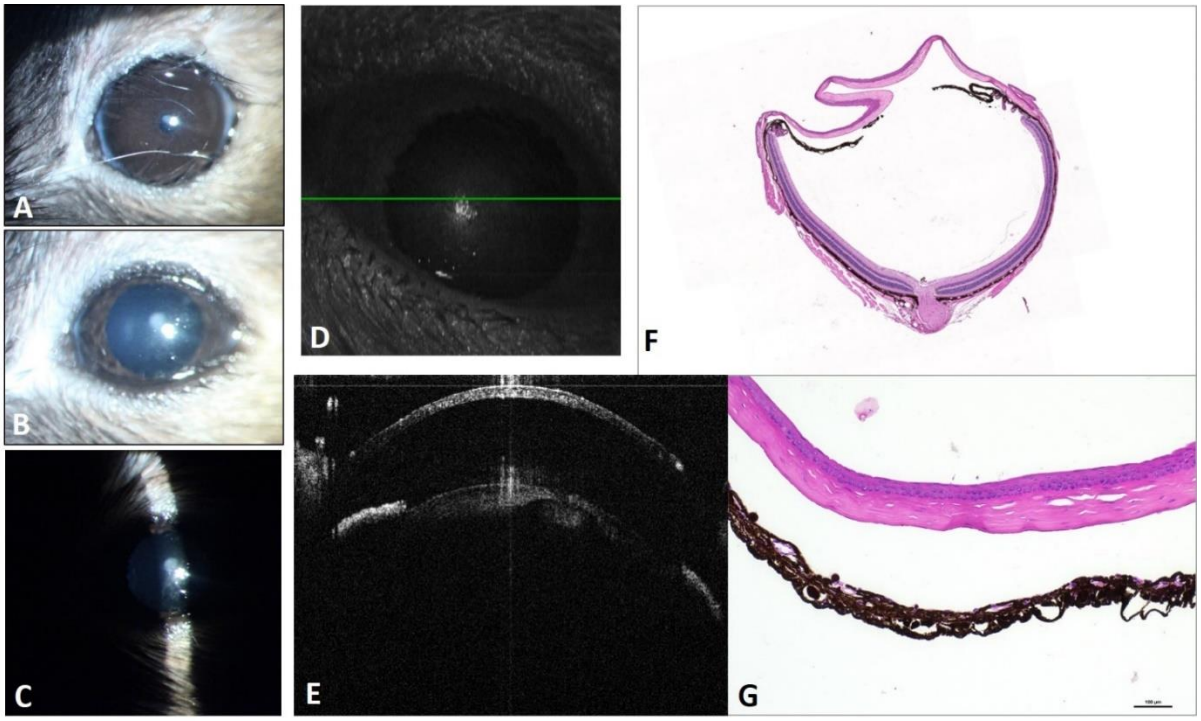

Figure S8: Clinical, imaging and histological analysis of a KI/KI mouse (350) **A**: clinical pictures (face view) of the left eye showing cataract; **B and C**: after pharmacological mydriasis; **D**: OCT in face view; **E**: OCT slide showing cataract; **F and G**: histological analyses showing normal ocular structure (lens is not visible). Technical artifact is visible by unspecific vacuolisation of the iris posterior epithelium.

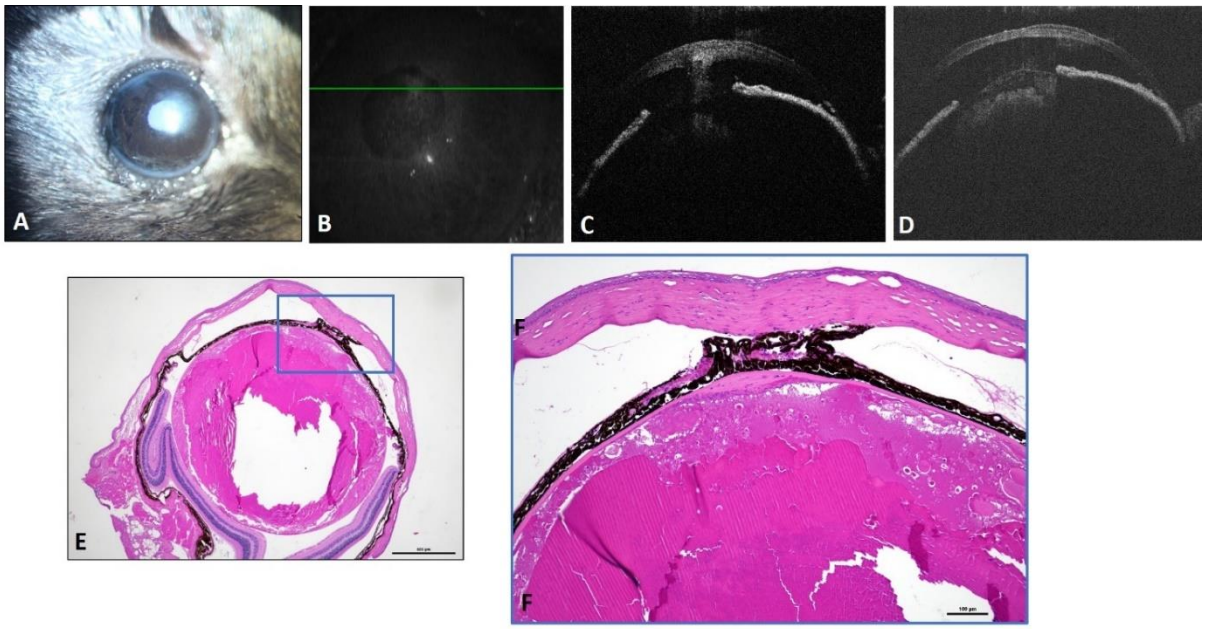

Figure S9: clinical, imaging and histological phenotype of a KI/KO mouse (328) **A**: clinical picture of right eye (face view) after pharmacological mydriasis showing cataract and irido-corneal adhesions; **B**: OCT in face view; **C and D**: OCT slide showing cataract and irido-

corneal adhesions; **E and F**: histological analyses confirming cataractic lens and focal extensive irido-lenticular and irido-corneal adhesions. The anterior lens capsule shows a focal fibrosis thickening at the adhesion site.

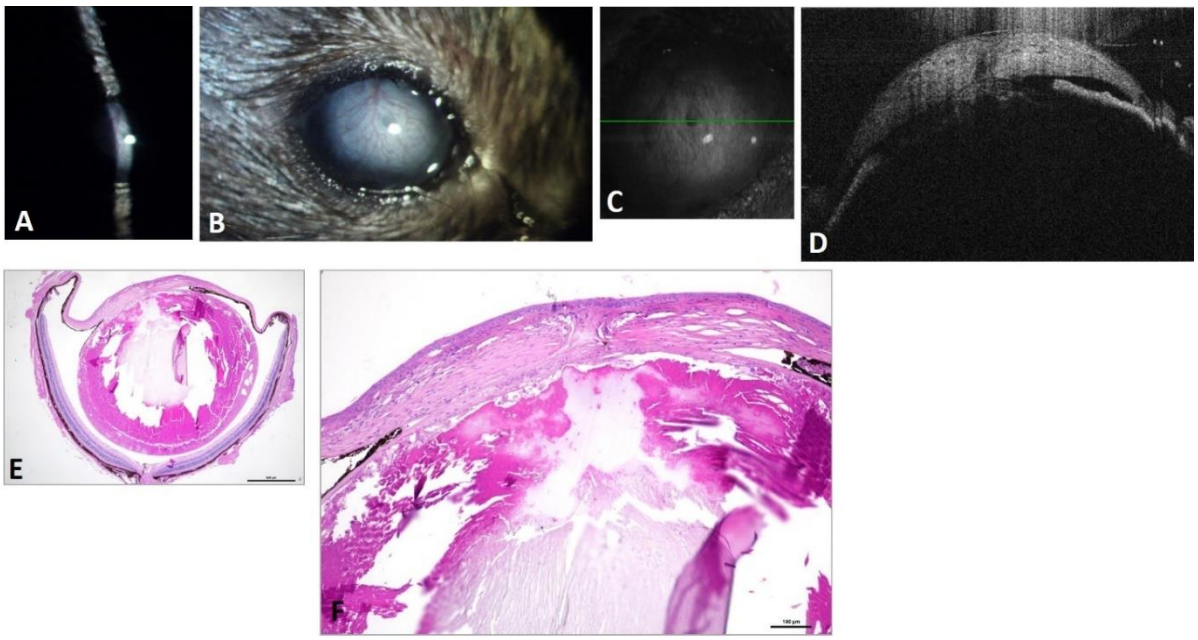

Figure S10: Clinical, imaging and histological phenotype of a KI/KO mouse (373) **A-B**: clinical pictures of right eye showing diffuse extensive keratitis with blood vessels, a central pit, a retrocorneal lens and small anterior chamber; **C**: OCT in face view; **D**: OCT slide showing the thicken cornea, the central pit with retrocorneal lens and the small anterior chamber; **E and F**: histological analyses showing the chronic keratitis, with a central focal transcorneal lesion and the focal fibrosis and adherence between the cornea and the anterior capsule of the cataractic lens.

Figure S11: Clinical and histological analysis of the right eye of a KI/KO mouse (393) showing dyscoria and irido-corneal and irido-lenticular adherences confirmed on histological analyses.

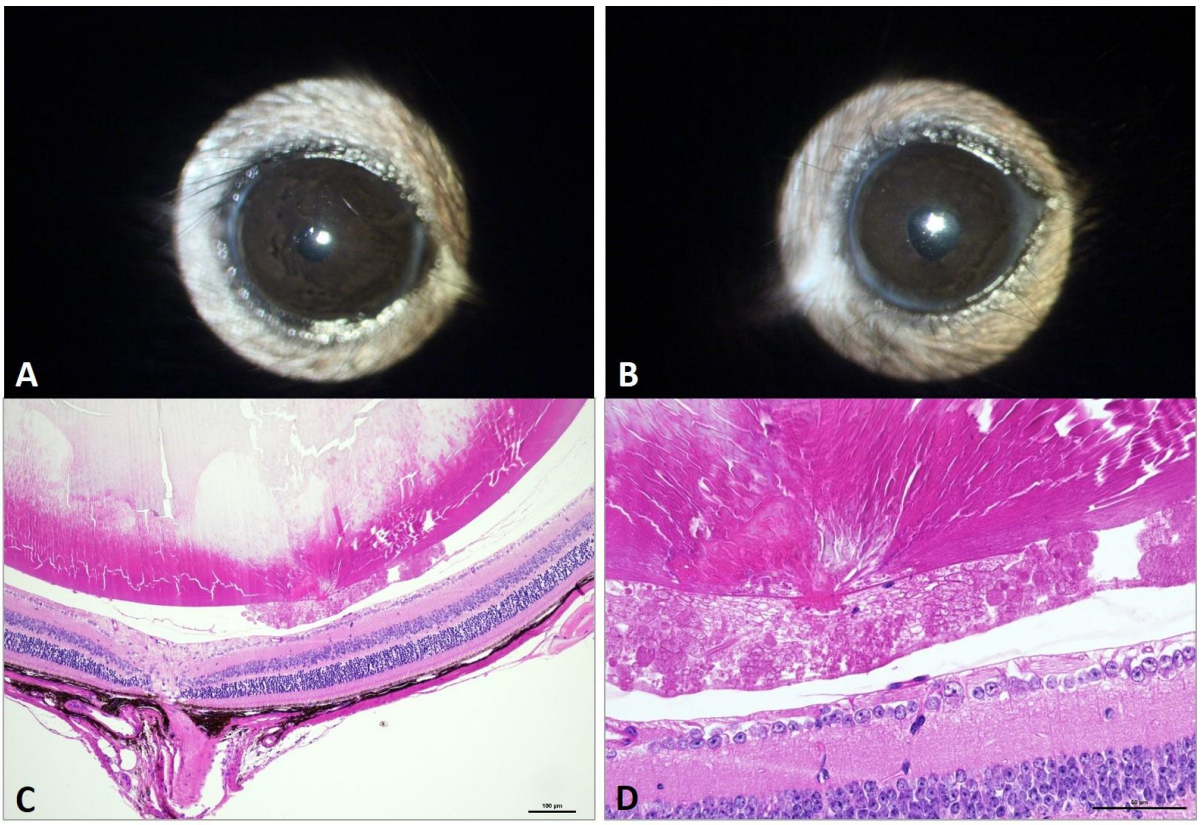

Figure S12: Clinical and histological phenotype of a KI/KO mouse (461) **A**: normal right eye; **B**: clinical pictures of left eye showing iris coloboma; **C and D** (zoom view): histological analyses showing posterior cataract and proteic leakage in the vitreous.

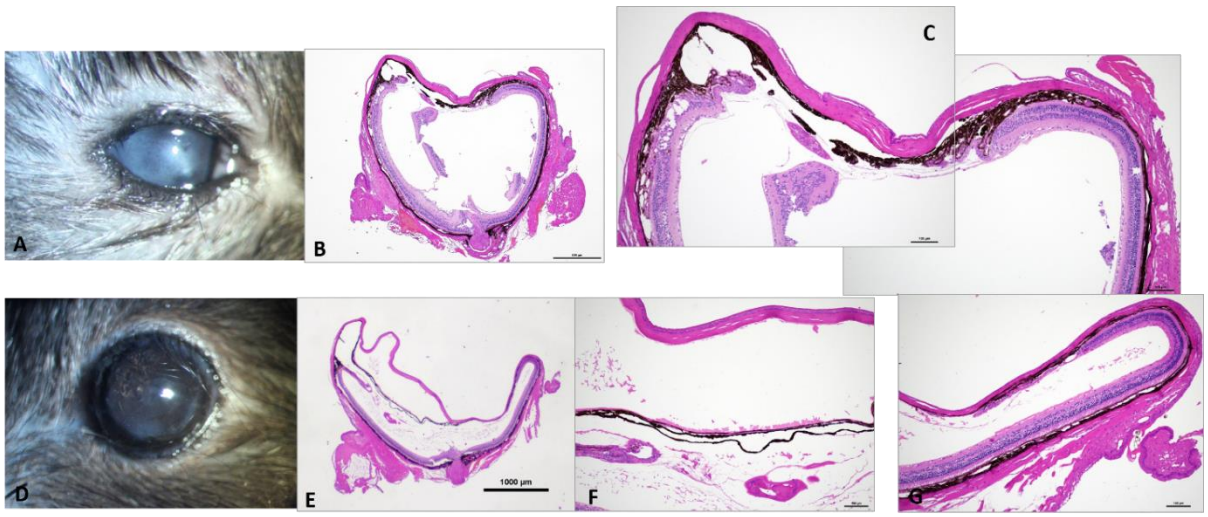

Figure S13: Clinical and histological phenotype of a KO/KO mouse (315) **A**: clinical picture of right eye showing severe microphthalmia, corneal clouding, athalamia. **B-C**: histological analyses the right eye showing, irido-corneal adherence, lens remnant, anteriorly displaced

retina, vascular membrane in the vitreous; **D**: clinical pictures of the left eye showing small pupil, pigmentary migration, angle anomaly, buphthalmia **E-G**: histological analyses of the left eye showing irido-corneal adherence, posterior iris cystic formation, lens remnant, proteic strands and flakes around the residual lens and in the vitreous.

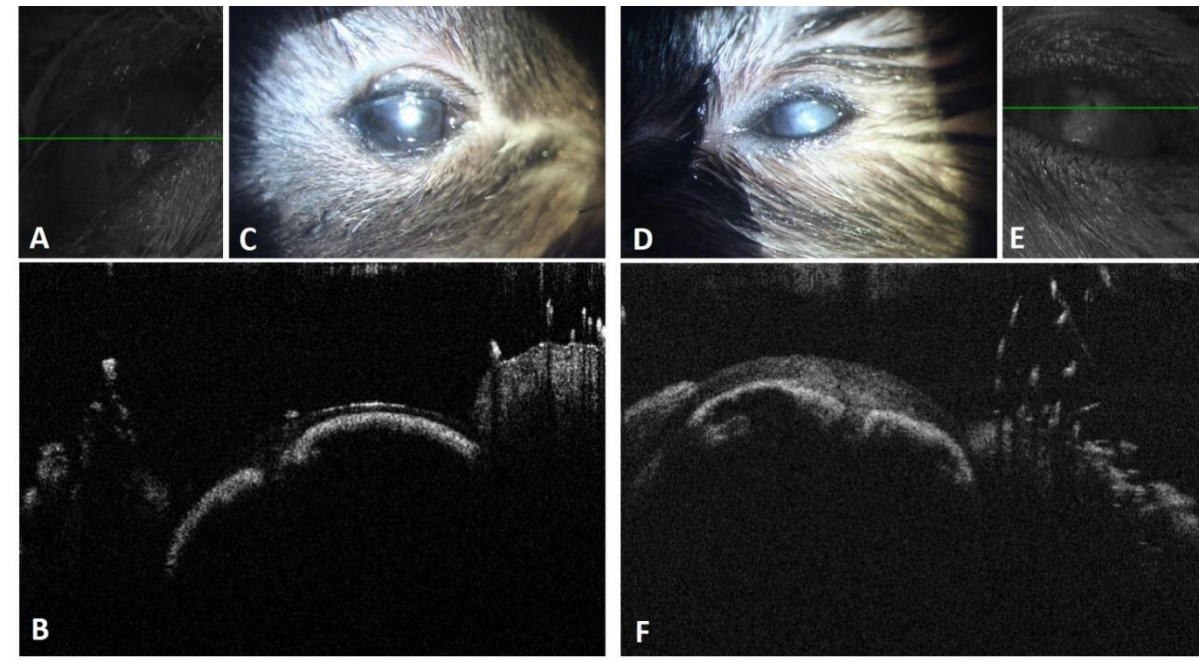
A
C
D
E
B
F

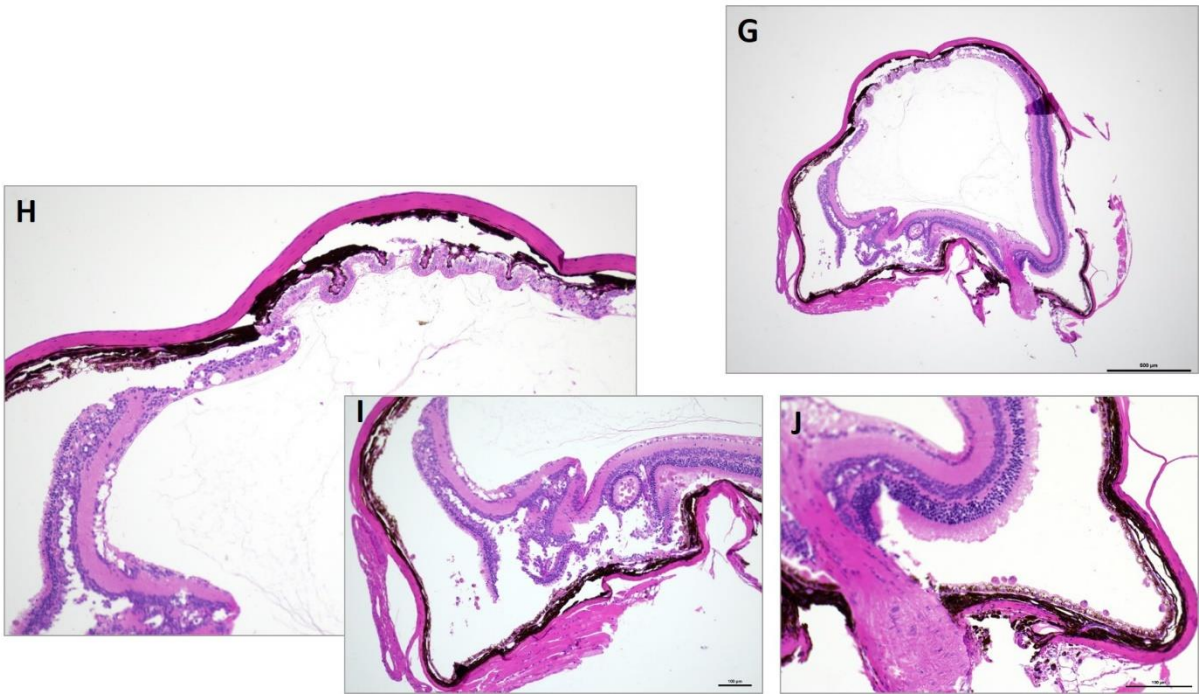
G
H
I
J

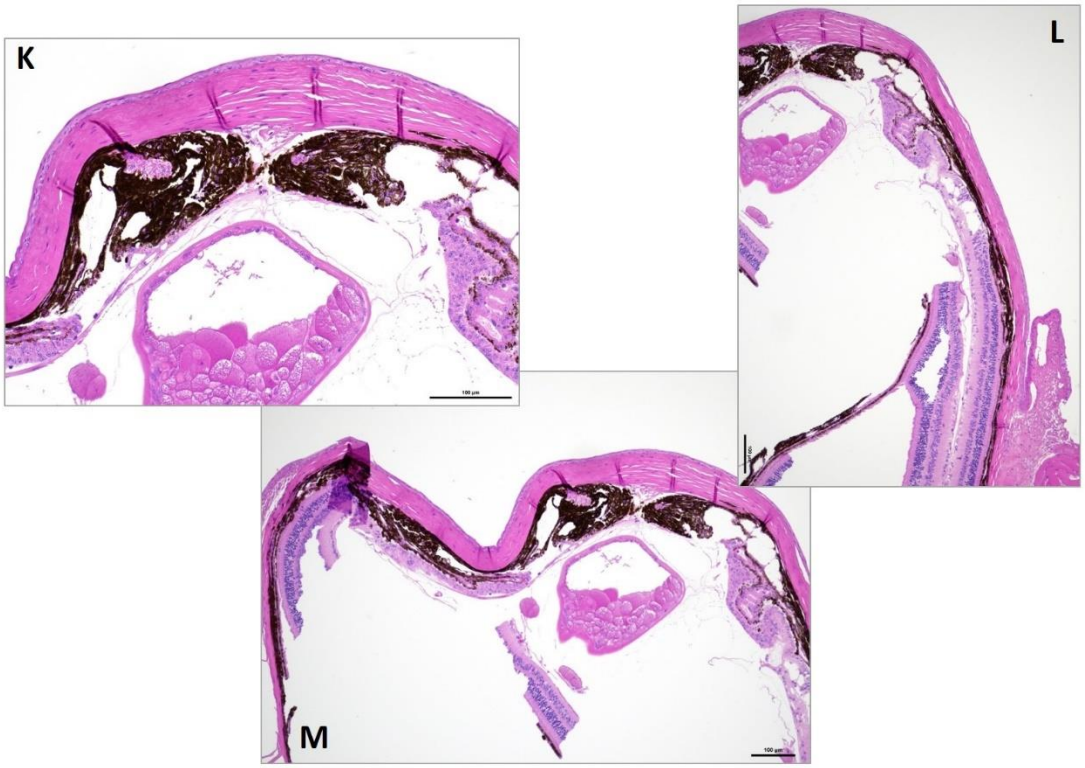

Figure S14: Clinical, imaging and histological phenotype of a KO/KO mouse (330) **A-C**: clinical and OCT picture of right eye showing severe microphthalmia, corneal clouding, athalamia. **G-J**: histological analyses of the right eye showing irido-ciliary and cornea adherences, absence of lens, anteriorly displaced retina with retinal detachment, rosette-like structures and tomb-stoning hypertrophy of the RPE (Retinal Pigmentary Epithelium). **D-F**: clinical pictures of left eye showing microphthalmia, corneal clouding, athalamia, no visible iris; **K-L**: histological analyses of left eye showing extensive fibrous adherences between cornea, iris and lens. The lens is small with irregular shape, prominent anterior empty vesicle and cataractic swollen fibers. The retina is anteriorly displaced.

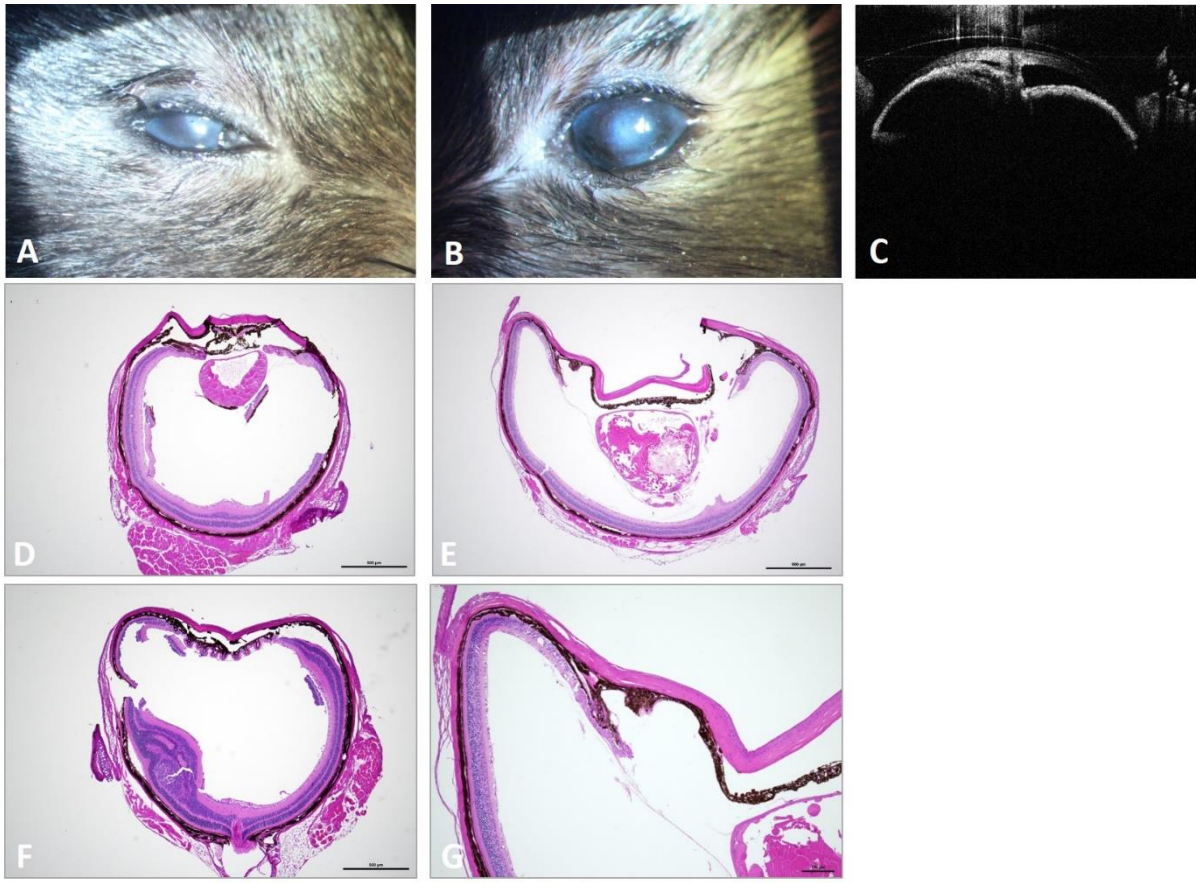

Figure S15: Clinical, imaging and histological phenotype of a KO/KO mouse (349) **A:** clinical picture of right eye showing microphthalmia, corneal clouding, central pit, athalamia. **D-F**: histological analyses of right eye showing extensive uveo-corneal adherences, triangle shaped small sized cataractic lens with large anterior vesiculation, anteriorly displaced retina with patches of retinal detachment and retinal folds; **B-C:** clinical and OCT pictures of left eye showing microphthalmia, corneal clouding, central pit, athalamia, **E-G**: histological analyses OG showing extensive uveo-corneal adherences, vacuolated triangle shaped small sized cataractic lens, anterior extension of the retina.

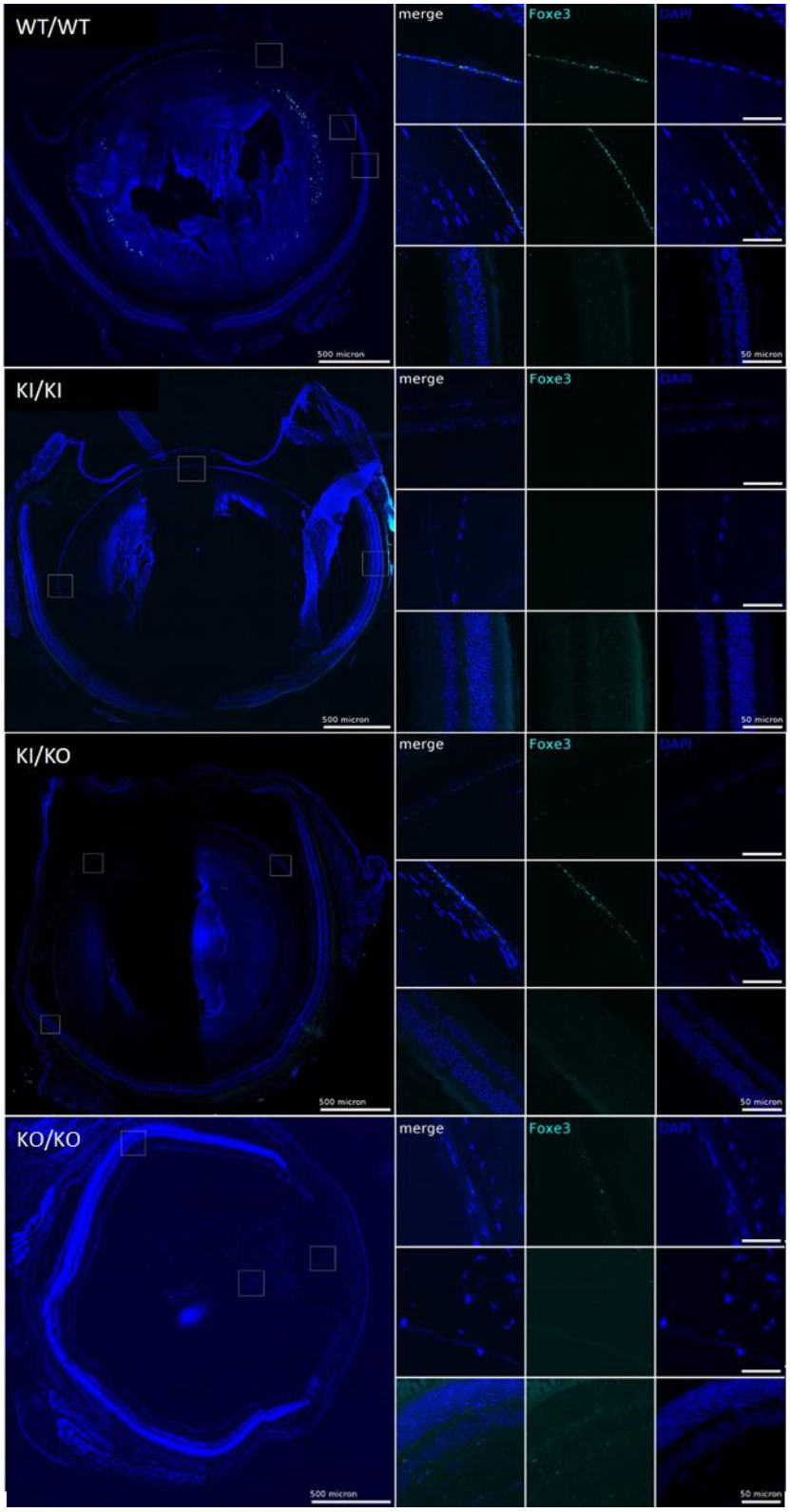

Figure S16: *Foxe3* expression study by RNAscope analysis in eyes of adult mice.

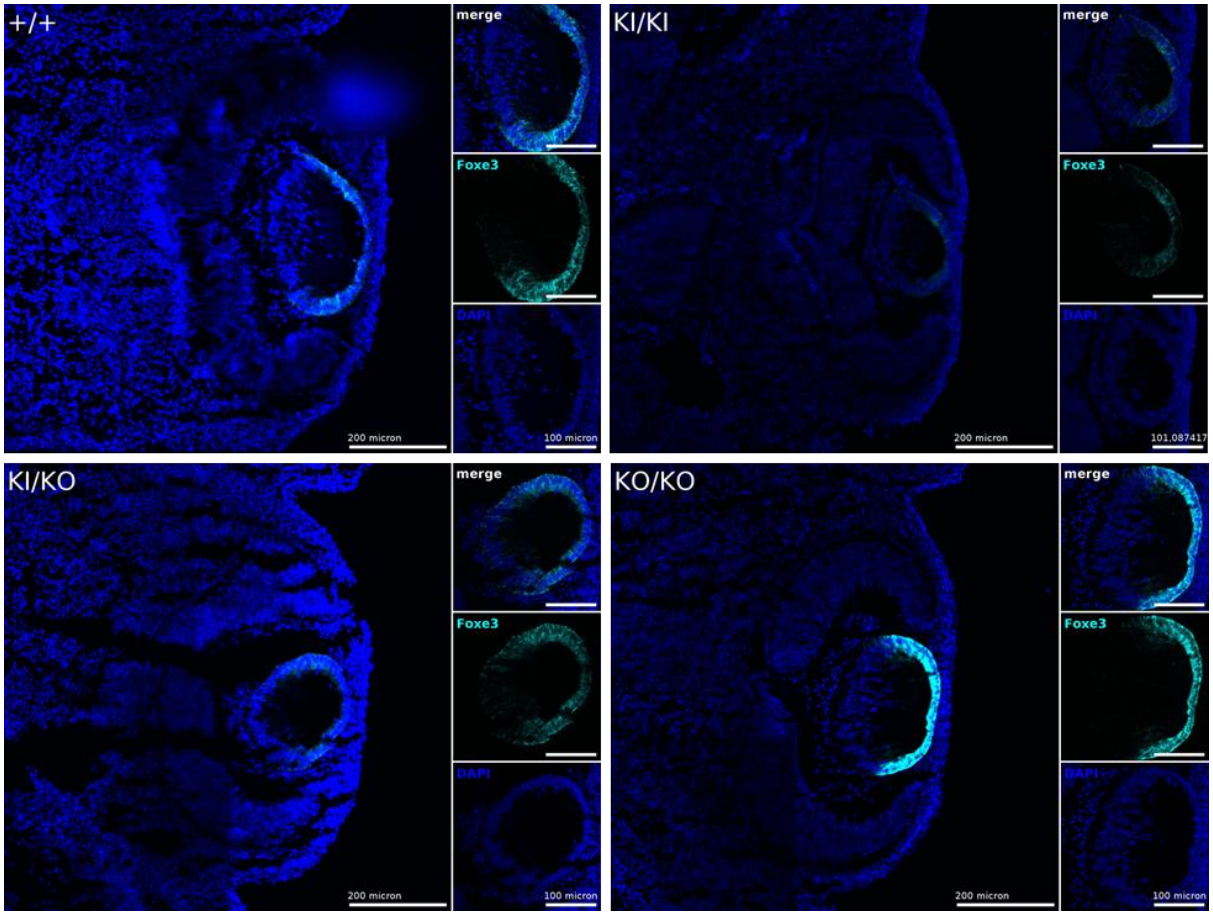

Figure S17: *Foxe3* expression study by RNAscope in the lens vesicle of embryos mice at E12.5

Part III: Describing the genetic architecture of pediatric retinal diseases in Chile

4.1. Results (Fourth publication)

As previously mentioned, inherited retinal dystrophies (IRDs) encompass a range of retinal disorders, traditionally considered degenerative. Yet, their frequent association with developmental genes prompts the question of eventual developmental defects in pediatric IRDs.

Here, we analyzed a cohort of 67 individuals with pediatric IRDs from the Hospital del Salvador in Chile to characterize the genetic landscape of pediatric IRDs in the country. Patients underwent thorough ophthalmological examinations and genetic testing, utilizing a panel of 212 IRD-related genes. Segregation of candidate variants with the disease was analyzed using Sanger sequencing.

This work successfully resolved 95% of the cases by identifying a limited number of genetic variants, with the majority being homozygous, highlighting a high rate of consanguinity or inbreeding. Several of these variants were unique to Chile, while others were most likely of Spanish origin. Although some cases had mutations in genes related to photoreceptor development, they were not prevalent. While the majority of the resolved cases carried mutations in genes known to cause pediatric IRDs, we also identified mutations in *RP1* and *ADAM9*, which involvement had only been suggested through the identification of candidate variants in unique pediatric cases.

This collaborative work, which constitutes the first global study of IRD genetics in Chile, was submitted to Human Mutation in August 2023 and is currently under review.

Four unique genetic variants in three genes account for 62.7% of pediatric retinal blindness in Chile: diagnostic and therapeutic consequences

Rene Moya[1*], Clementine Angee[2*], Sylvain Hanein[3], Fabienne Jabot-Hanin[3], Josseline Kaplan[2], Isabelle Perrault[2], Jean-Michel Rozet†[2], and Lucas Fares Taie†[2].

[1]Hospital del Salvador, Santiago, Chile

[2]Laboratory of Genetics in Ophthalmology (LGO), INSERM UMR1163, Institute of Genetic Diseases, Imagine and Paris Descartes University, 75015 Paris, France.

[3]Bioinformatic Platform, INSERM UMR1163, Institute of Genetic Diseases, Imagine and Paris Descartes University, 75015 Paris, France.

* These authors contributed equally to this work

†Correspondence to lucas.fares-taie@inserm.fr or jean-michel.rozet@inserm.fr; jean-michel.rozet@institutimagine.org

ABSTRACT

Leber congenital amaurosis (LCA) and early-onset retinal dystrophy (EORD) are the leading causes of incurable blindness in childhood. Clinical findings and molecular basis of syndromic and non-syndromic LCA/EORD in a Chilean cohort (67 patients/60 families) were studied. Panel Sequencing and variant filtering identified putative pathogenic variants in 64 cases, thereby leading to a detection rate of 95.5%. In this population, 17 genes and 126 variants, of which 32 were unique, were involved. *CRB1, LCA5* and *RDH12* accounted for the vast majority of the cases (46/64; 71.9%) *CRB1* being the most frequent of them (28/64; 43.8%). To note, four unique variants (*LCA5* p.Glu415*; *CRB1* p.Ser1049Aspfs*40 and p.Cys948Tyr and *RDH12* p.Leu99Ile) accounted for 62.7% of all disease alleles, the first two of these variants resulted from a founder effect. This observation suggests mutation-specific detection of the four major disease-causing variants as a first-tier analysis in Chilean patients. Furthermore, this study discloses a high degree of inbreeding in the Chilean families affected with pediatric retinal blindness, resulting in a very limited repertoire of mutations.

Additionally, the current study provides strong support to the phenotypic spectrum of *ADAM9*- and *RP1*-associated disease, and the genotypic spectrum of LCA/EOSRD.

Finally, the data presented here are valuable and crucial for counselling patients and families, as well as for the pharmaceutical industry in the progressing field of personalized medicine and for future enrollment in gene therapy-based treatments, knowing that therapeutic trials are either ongoing (*LCA5*) or advancing in preclinical developments (*CRB1* and *RDH12*).

INTRODUCTION

Inherited Retinal Dystrophies (IRDs) include a large and heterogeneous group of disorders in which rod and/or cone photoreceptors degenerate in a diffuse or regionalized manner, causing variable degree of visual handicap[1]. Leber congenital amaurosis (LCA, MIM PS204000) and early-onset severe retinal dystrophy (EOSRD) are the earliest and most severe of these diseases, manifesting in blindness or profound vision deficiency at birth or within the very first years of life[2]. The initial aspect of the retina is typically unremarkable but electroretinography (ERG) shows undetectable or deeply altered scotopic and photopic responses, in keeping with a profound dysfunction of rod and cone photoreceptors[3]. LCA/EOSRD are the most common causes of blindness or profound vision impairment in childhood, affecting 20% of children in Schools for the Blinds[4]. They are typically autosomal recessive diseases, although some dominant forms exist. They can occur as non-syndromic disorders or as the initial symptom in a range of devastating syndromes[2], in particular ciliopathies[5–9]. Some twenty and thirty genes have been involved in non-syndromic and syndromic LCA/EOSRD diseases, knowing that there is little genetic overlap between the two presentations [5,9]. Identifying the underlying genetic defect can aid in early differential diagnosis and tailor-made extraocular function follow-up, adding further value to the molecular diagnosis of these disease, which importance has increased with therapies on the market or in advanced clinical trials[10].

Here, we report the results of panel-based molecular diagnosis in a large Chilean cohort, which provide a comprehensive representation of the genetic landscape of LCA/EORD in Chile.

FAMILIES, MATERIALS AND METHODS

Subjects and clinical assessment

67 subjects from 60 Chilean families were recruited for LCA or EOSRD at the Department of Ocular Genetics of the Hospital del Salvador in Santiago, Chile between January 2018 and January 2022. The patients (mean age 29 ± 16 years; range 2 – 72; median 25.5) underwent a detailed medical history and, when feasible, a full ophthalmologic examination, including Best Corrected Snellen Visual Acuity (BCVA), cycloplegic refraction, slit lamp biomicroscopy, dilated ophthalmoscopy, digital fundus photography (*Optos PLC, Dumferline, Scotland UK*), full-field ERG (ERG system, Roland consult, Wiesbaden, Germany), SpectralDomain Optical Coherence Tomography (SD-OCT) obtained with the Heidelberg Spectralis

(Heidelberg Engineering, Heidelberg, Germany) and Fundus AutoFluorescence (FAF) Heidelberg Engineering (Heidelberg, Germany), depending on the patient age. The visual acuity (VA) was measured using a standardized Snellen chart (in decimals). Patients with very low vision were classified using the semiquantitative scale “counting fingers” (CF), “hand motion” (HM), “light perception” (LP), and “no light perception (NLP) ". The familial medical history was systematically recorded by interviewing the patients and/or parents and drawing a pedigree. The diagnosis was reviewed in three individuals from two families who had further developed extraocular symptoms consistent with Alström (ALMS, MIM# 203800) and SeniorLoken (SLNS, MIM# 266900) syndromes, respectively.

Genomic DNA from the patients and family relatives was extracted from peripheral blood using standard protocols or from saliva samples using Oragene-DNA (OG-500) Kit, according to the manufacturer protocol (DNA Genotek, Canada).

This study was approved by the local Bioethics Committee and by the *Comité de*

Protection des Personnes Ile–de–France II Institutional Review Board (CPP:2015-0303/DC2014-2272). Informed consent adhering to the tenets of the Declaration of Helsinki was received from all participants or their legal guardians.

Capture Panel Design and Library Preparation

A custom panel of 212 IRD genes was used, which includes non-syndromic and syndromic LCA and EOSRD genes and some differential diagnoses causal genes (Table S1). Libraries were generated from 2 µg of genomic DNA using the SureSelectXT Library Prep Kit (Agilent, Garches, France). Regions-of-interest were captured by hybridization using biotinylated complementary 120-bp RNA baits designed with the SureSelect SureDesign software and sequenced on an Illumina HiSeq2500 HT system (Illumina, Evry-Courcouronnes, France) to generate 130-bp paired-end reads with a minimum read depth of 200X.

Bioinformatic Analysis

Sequences were mapped on the hg19 build of the reference human genome (GRCh37) using the Burrows-Wheeler Aligner (BWA)[11] algorithm. Downstream processing was carried out with the Genome Analysis Toolkit (GATK)[12], SAMtools[13]. Single nucleotide variants and indels were called using the GATK Unified Genotyper based on the 72nd version of the ENSEMBL database. Copy number variations (CNV) were called using a specifically designed algorithm integrated to the *Imagine* PolyDiag interface[14]. Namely, copy numbers were given by the relative read count for each targeted region, determined by the ratio of the read count for that region divided by the total absolute read counts of all targeted regions of the design. The ratio of the relative read count of a region in a given individual over the average relative read counts in other individuals of the run provides an estimation of the copy number for that region

in that individual (method adapted from Goossens et al [15]). Gene variations were filtered using the PolyDiag interface for rarity and pathogenicity scores according to a large number of publically and *in-house* prediction softwares available through the Polydiag Interface [14]. The pathogenicity of variants was interpreted in accordance with the American College of Medical Genetics (ACMG) guidelines by using VarSome[16].

Sanger validation and segregation analysis

The presence of SNV and indels and their segregation with the disease were verified by Sanger sequencing using intronic primers (Table S2) and the BigDye® Terminator v3.1 on an ABI 3500XL Genetic Analyzer (Applied Biosystems, Thermo Fisher Scientific, Courtaboeuf, France). Data were analyzed using the ABI Sequencing Analysis 6 Software.

Haplotype analysis

SNPs around the *CRB1* c.3110_3143dup (Ser1049Aspfs*40) and *LCA5* c.1243G>T (p.Glu415*) variants were extracted from sequencing datasets and phased with the SHAPEIT2 software[17] to construct haplotypes. Common haplotypes among the subjects carrying the variants and flanking SNPs were then used to estimate the age of the most recent common ancestor using the ESTIAGE software[18], which implements a likelihood-based method. We used allele frequencies and genetic distances (cM) obtained from the 1000 Genomes Phase 3 data[19]. Positions absent from this map were interpolated. For simplicity, we considered a mutation rate of 0 at each marker taken into account in the model.

RESULTS

Data summary

Pathogenic or likely pathogenic variants were identified in 64/67 (95.5 %) individuals from 57/60 families (95 %), including the three subjects (2/57 families) with ALMS and SLNS (Table S3) and 61 individuals (55/57 families) with non-syndromic IRD. These latter individuals include 55 subjects (55/61, 90.2 % in 49/55, 89.1 % families) with mutations in LCA/EOSRD genes (*CRB1, CEP290*, *GUCY2D*, *LCA5, NMNAT1*, RDH12, *RPGRIP1*, *SPATA7, TULP1*: 54/55 recessive cases; *CRX:* 1/55 dominant case) and 6 subjects (6/61, 9.8 % in 6/55, 10.9 % families) with variants in other IRD genes *(ADAM9*, *NR2E3, RAB28*, *RP1*:5/6 recessive cases*; PRPF31:* 1/6 dominant case).

In total, we describe 124 recessive and 2 dominant disease alleles. Recessive alleles comprised missense (55/124, 44.4 %), frameshifting indel (34/124, 27.4 %), nonsense (23/124, 18.6 %), large deletion (4/124, 3.2 %), canonical or non-canonical splice-site (4/124, 3.2 %), large duplication (2/124, 1.6 %), and in-frame deletion (2/124, 1.6 %) changes **(**Table S3**)**. The 124 recessive alleles were made up of 30 unique variants, 14 of which were novel (14/30, 46.7 %). Homozygosity was frequent (84/124, 67.7% disease alleles in 42/62, 67.7 % subjects from 38/55, 69.1 % families), supporting high population inbreeding (Fig. 1A). Variants in *CRB1* made up the majority of disease alleles (56/124, 45.2 %), followed by changes in *RDH12* (18/124, 14.5 %) and *LCA5* (18/124, 14.5 %) and from a distance in *ADAM9, ALMS1, CEP290*, *GUCY2D*, *IQCB1, NMNAT1, NR2E3, RAB28, RP1, RPGRIP1, SPATA7* and *TULP1* (one or two cases each; Fig. 1B), respectively.

The two dominant alleles consisted of previously reported frameshift and nonsense variants in *CRX* [20] and *PRPF31*[21], respectively (Table S3).

Affected subjects with variants in LCA/EOSRD genes

Molecular results were consistent with the initial diagnosis of LCA/EOSRD in 90% of the solved cases (55/61; 49/55 families). 28/55 individuals (50.9%; 24/49, 49% families) carried mutant *CRB1* alleles, consisting in eight unique variants (3/8 reported and 5/8 novel variants). The reported c.2843G>A (p.Cys948Tyr) mutation[22] was the most common *CRB1* disease allele (31/56, 55.4%), identified in 21/28 subjects (75.0 %; 9/24, 79.2 % families). Ten of them (10/21, 47.6 %) were homozygous and 11/21 (52.4 %) were compound heterozygous with another reported mutation (c.3110_3143dup, p.Ser1049Aspfs*40 in 6 subjects from 4 families and c.2291G>A, p.Arg764His in 1 subject)[22] or an unreported variant (c.653-1G>A in 2 subjects and c.3827_3828del, p.Glu1276Valfs*4 and c.2466G>A, p.Trp822* in 1 individual each). The remaining 6/28 subjects (21.4%; 4/24, 16.7% families) carried the c.3110_3143dup (p.Ser1049Aspfs*40) in homozygosity (5/6 subjects) or compound heterozygosity with the novel nonsense mutation c.750T>A (p.Cys250*; 1/6 subject). In total, the c.3110_3143dup variant represented the second most common *CRB1* disease allele (17/56, 30.4%), identified in 12/28 individuals (42.9 %; 8/24, 33.3 % families) with a *CRB1*-associated disease. Haplotype analysis at the *CRB1* locus in 8 individuals carrying the c.3110_3143dup mutation in homozygosity or compound heterozygosity allowed the identification of a common haplotype of 110.5 kb, which could have appeared in a common ancestor 11 generations ago (confidence interval: 7-9 generations).

Together the c.2843G>A (Cys948Tyr) and c.3110_3143dup (Ser1049Aspfs*40) mutations accounted for 48/56 (85.7%) *CRB1* disease alleles, being identified in 27/28 subjects (96.4 %), of whom 6/28 (21.4 %; 4/24, 16.7 % families) carried the two mutations.

The last of the 28 individuals carried the novel c.750T>A (p.Cys250*) nonsense and the other unreferenced c.798_799del (p.Ala267Glnfs*18) truncating change.

All individuals presented with a typical *CRB1*-LCA phenotype consisting in congenital nystagmus, night blindness from early childhood, low vision progressing to blindness and in 50% or more of individuals, oculo-digital signs of Franceschetti, photoaversion and hyperopia. The fundus consistently showed macular and peripheral atrophy at the fundus with pseudocoloboma, nummular RPE pigmentation deposits and Preserved Para-arteriolar Retinal Pigment Epithelium (PPRPE; in a large majority of individuals. Detailed ophthalmological data is available in Table S3.

LCA5 variants were identified in 9/55 subjects (16.4 %; 8/49, 18.4% families), the all of whom carried the c.1243G>T (p.Glu415*) nonsense mutation in homozygosity (7/9, 77.8 %) or in compound heterozygosity with the novel c.1569_1582del (p.His523Glnfs*16) variant (2/9, 22.2 %). In total, the c.1243G>T (p.Glu415*) mutation accounted for 16/18 (88.9%) of *LCA5* disease alleles. Haplotype analysis at the *LCA5* locus in homozygous individuals identified a common haplotype of 442 kb which could have arisen in a common ancestor five generations ago (confidence interval: 2-21 generations). The nine individuals with *LCA5* variants manifested a profound visual deficiency at, or near birth. Typically individuals manifested a nystagmus and early-onset night blindness, whereas digito-ocular signs of Franceschetti and photophobia were rather infrequent. Patients displayed variable refraction deviations (from myopia to hypermetropia), very low, yet variable, visual functions and variable fundus aspect, which did not correlated to the age or genotype (Table S3).

Three unique and previously reported *RDH12* changes were identified in 9/55 subjects (16.4 %; 8/50, 16% families). The c.295C>A (p.Leu99Ile) substitution[23] made-up the majority of *RDH12* disease alleles (15/18, 83.3%), identified in homozygosity in 7/9 subjects (77.8%; 6/49, 12.2% families) and in compound heterozygosity with the c.716G>T (p.Arg239Leu) substitution[23]in 1/9 individuals (11.1%). The last of the 9 subjects carried a 1-bp duplication affecting the same Arg239 residue (c.715dup, p.Arg239Profs*34)[24] in homozygosity. Individuals carrying the p.Leu99Ile substitution in homozygosity manifested

visual symptoms at a very variable age (0 - 7 years). They manifested no nystagmus or digitoocular signs of Franceschetti but night blindness, photoaversion, mild hyperopia and poor visual function progressing to blindness were typical features. Wide spread pigmentary retinopathy with an early-onset central involvement were almost constant, in keeping with previous reports[24]. The disease presentation in individuals carrying the other two *RDH12* mutations was comparable except for an earlier and more severe onset with nystagmus.

Two individuals (2/55, 3.6 %; 2/49, 4.1% families) carried biallelic variations in *CEP290*, the mutations of which cause non-syndromic IRD or syndromic ciliopathies with IRD. Homozygous for the non-syndromic LCA-causing hypomorphic founder c.2991+1655A>G mutation[25] was identified in a nine-year old girl whose disease was unexpectedly mild: onset at 18 months, no nystagmus, oculo-digital sign or photophobia, moderate hyperopia, mild peripheral changes at the fundus and low but measurable BVCA at 9 years and severely altered, yet detectable, ERG responses. The second subject carried an unreferenced missense variant of uncertain significance c.38T>A (p.Val13Asp) in compound heterozygosity with the LCAcausing c.7341dup (p.Leu2448Thrfs*8) mutation reported in association with the c.2991+1655A>G variant [26]. This girl presented with nystagmus and oculo-digital sign of Franceschetti at birth and had a visual function limited to light perception but minor fundus changes which is typical of *CEP290* at the age of 8 years, supporting the pathogenicity of the missense change. Considering that *CEP290* missense changes are predicted hypomorphic, absence of further extraocular involvement can be anticipated.

Another 2/55 individuals (3.6 %; 2/49, 4.1% families) harbored the recurrent *NMNAT1* c.769G>A (p.Glu257Lys) missense mutation[27] in compound heterozygosity with the known c.364del (p.Arg122Glyfs*20)[23,27] and c.507G>A (p.Trp169*) loss-of-function mutations[21,27], respectively. The c.769G>A substitution has been reported a hypomorphic change causing LCA when in trans of a severe mutation [28]. Consistently, the individuals aged

3 and 35 years presented severe visual deficiency at birth with nystagmus and digito-ocular signs of Franceschetti. The youngest subject displayed the typical *NMNAT1*-associated central pseudocoloboma and peripheral atrophy at the fundus[27], whereas a bilateral cataract hampered fundus examination in the elder individual.

The remaining 5/55 (9.1%) individuals affected with a non-syndromic LCA carried variants in *GUCY2D*, *RPGRIP1*, *SPATA7*, *TULP1* and *CRX*, respectively (1.8% of individuals and 2% of families, each). *GUCY2D* was involved in a 3-year old individual carrying the previously reported c.389del (p.Pro130Leufs*36) and c.1343C>A (p.Ser448*) truncating mutations in compound heterozygosity (Table S3). The individual manifested a typical *LCA1*associated phenotype, consisting in profound visual deficiency from birth with nystagmus, digito-ocular signs of Franceschetti, photophobia, LP, hyperopia and unremarkable fundus aspect[29]. The *RPGRIP1* disease alleles consisted in the previously unreported *RPGRIP1* duplication involving exon 10 to 19, (estimated size 16 to 18 Kb). To our knowledge this is the largest *RPGRIP1* duplication reported thus far. The 27 year-old individual carrying the change in homozygosity manifested a *RPGRIP1*-associated phenotype [30], namely a severe visual deficit in the first year of life with nystagmus with dramatically poor vision and pigmentary retinopathy, with the exception of a unilateral myopia and night blindness symptoms which contrast with the moderate hyperopia and photoaversion that are typically associated with *RPGRIP1* mutations. One 42 year-old subject carried the *SPATA7* c.1171C>T (p.Arg391*) nonsense mutation in homozygosity. This mutation has been reported in homozygosity in a LCA case, but no clinical details were available[31]. The onset of the disease in our patient is not known but most recent examination are consistent with a very severe retinal disease as demonstrated by the presence of a nystagmus, a dramatically poor vision (LP and NLP) and a widespread pigmentary retinopathy. A 4 year-old individual was homozygous for a novel *TULP1* c.1149C>A (p.Asp383Glu) missense substitution classified as pathogenic in Varsome due to multiple lines of computational evidence, including the report of a RP-causing

missense mutation affecting the same residue [32]. Further consistent with pathogenicity, was the severe visual impairment in infancy with nystagmus, photoaversion, night blindness, poor vision (HM and CF), high myopia and widespread pigmentary retinopathy which is typical of *TULP1* involvement [33]. The last of the five individuals is a 31 year old woman who carried the *CRX* frameshifting 1-bp deletion c.434del (p.Pro145Leufs*42) in simple heterozygosity. This change was previously reported as a dominant mutation in a 15 year-old Japanese girl displaying myopia, night blindness, very reduced, yet measurable BVCA, paracentral scotoma without central scotoma, peripheral visual field defect and marked peripheral atrophy but rather preserved central retina at the fundus[34]. The Chilean patient presented with a more severe disease consisting in profound visual deficiency with nystagmus at birth, poor vision (CF and 0.025), night blindness in childhood and photophobia in teen age and widespread pigmentary retinopathy.

Subjects carrying mutations in other IRD genes

Among resolved non-syndromic LCA/ESORD cases, 6/61 (9.8 %) subjects carried variants in genes involved in other retinal diseases.

We identified homozygosity for an unreported *ADAM9* deletion encompassing exons 5 to 11 (26 to 40 Kb in size) in a male seen at the age of 9 months for a profound visual deficiency with nystagmus supporting a LCA disease, but ERG was not available for diagnosis. At the latest examination (age 26), the patient had a nystagmus, photoaversion, night blindness, extremely poor vision (LP, LRE) and widespread pigmentary retinopathy but central preservation at the fundus. This phenotype is more severe than the typical *ADAM9*-associated phenotype consisting in poor vision in childhood with no nystagmus and no photoaversion[35].

Two apparently unrelated subjects carried a novel *RP1* 1-bp deletion (c.5564del (p.Lys1855Argfs*42)) in homozygosity. *RP1* truncating mutations have been reported to cause

autosomal dominant or recessive retinal dystrophies, depending on the location of the variant. The dominant variants were reported to affect the middle of the protein and to cause RP whereas the recessive ones were present in the N- and C-terminal regions and caused more variable and severe phenotypes from RP, macular dystrophy, CRD to ESORD/LCA[36]. Accordingly, the two individuals homozygous for the p.Lys1855Argfs*42 variant which affects the C-terminal region were addressed in early childhood for a LCA disease. On recent examination (age 29 and 34 years, respectively) they presented a nystagmus, poor vision (HM and 0.33 and HM and LRE, respectively), widespread pigmentary retinopathy with macular atrophy at the fundus and, in the eldest individual, photophobia and high myopia.

Homozygosity for a founder *NR2E3* c.932G>A (p.Arg311Gln) mutation was identified in a female patient addressed for LCA. This mutation has been reported in a spectrum of retinal diseases, including Goldmann-Favre syndrome (GFS, MIM#268100) enhanced S-cone syndrome (ESCS, MIM# 268100), autosomal recessive or dominant RP (RP37, MIM# 611131). Getting back to the patient, she mentioned having experienced bilateral retinal detachment and vitrectomy at birth, strongly supporting a GFS rather than LCA.

Homozygosity for a likely pathogenic *RAB28* 3-bp deletion predicting the loss of the highly evolutionarily conserved (from human to *Caenorhabditis elegans*) Valine 111 (c.331_333del; p.Val111del) has been identified in a subject having a history of visual deficiency since the age of 16 months. At 55 years, he presented with low BVCA (0.1 and 0.1), nystagmus, photoaversion and widespread pigmentary retinopathy and macular atrophy. Mutations in *RAB28* have been reported to cause CORD18 (MIM# 615374) which can manifest as a childhood-onset cone-rod dystrophy with markedly reduced BVCA and dyschromatopsia, bull's eye maculopathy, foveal hyperpigmentation, peripapillary atrophy, extinguished photopic ERG responses and reduced scotopic ERG responses[37]. In the absence of initial ophthalmological data, specifically ERG recording and color vison, the diagnosis of CORD over LCA might be considered.

Finally, we identified the recurrent adRP-causing *PRPF31* variant c.1060C>T, p.(Arg354*)[21] in a 72 year-old individual presenting with LP, nystagmus, night blindness, photophobia and widespread pigmentary retinopathy who received an LCA diagnosis at the age of seven years. Consistent with this diagnosis is the description of two unrelated Chinese LCA subjects carrying the mutation[38,39].

Patients who developed additional symptoms consistent with a syndromic IRD

Three individuals (two brothers and a sporadic case) who were reported to manifest a profound visual deficiency with nystagmus near birth were included in this study and further developed extraocular symptoms consistent with ciliopathies. The brothers developed hearing loss, type 2 diabetes mellitus, arterial hypertension, and epileptic seizures in addition to earlyonset and severe visual disease, supporting ALMS. Consistently, the two of them were found to carry an *ALMS1* c.1092del (p.Asp365Ilefs*11; unreported previously) variant in homozygosity. Upon recent examination (47 and 49 years), they displayed extremely poor (LP) or absent (NLP) vision, night blindness, photophobia (eldest) and widespread pigmentary retinopathy.

The third subject presented a severe visual deficiency from birth with nystagmus, digitoocular signs, photophobia and LP consistent with LCA. He developed renal symptoms at the age 14 years. He was found to carry a previously unreported deletion encompassing the last exon (exon 15) of the *IQCB1* gene in homozygosity, leading to a reclassification of the initial diagnosis from LCA to SLNS. At the age of 17 years, the subject's vision was limited to LP and he manifested photoaversion. Macular and peripheral atrophy, which is frequently seen in *IQCB1*-associated individuals, were noted at the fundus.

DISCUSSION

Rare hereditary diseases can vary dramatically in prevalence, locus, and allelic heterogeneity depending on geographic region. The study aimed to determine the genetic architecture of severe pediatric IRDs in Chile by studying a cohort of individuals from across the country recruited between 2016 and 2022 at the Hospital El Salvador in the Capital City of Santiago. Sixty-seven individuals from 60 families were included. All were initially seen for a severe visual dysfunction consistent with a provisional clinical diagnosis of LCA or EOSRD. In two of these families, the diagnosis was secondarily reclassified in a syndromic ciliopathy. Molecular testing of a large panel of candidate genes yielded a 95 % of molecular diagnosis (57/60 families). Consistent with the typical recessive transmission of severe pediatric retinal dystrophies, biallelic variants were detected in 96.5% of the resolved families (55/57). Homozygosity was observed in two-thirds of these families, supporting high levels of inbreeding in the Chilean population.

In nearly 90% of solved families (49/55; excluding syndromic ciliopathies), the molecular diagnosis was consistent with the clinical diagnosis of LCA/EOSRD. This high diagnosis pick-up rate was associated with a limited locus heterogeneity. Only 10 among the twenty-some *LCA* genes were involved. *CRB1* and within a distance *RDH12* and *LCA5* were most prevalently implicated (44.4% and 14.3% each, respectively). The very high prevalence of *CRB1* variants in the Chilean pediatric IRD population is mostly due to the recurrence of the p.Cys948Tyr and p.Ser1049Aspfs*40 variants, which represent together 85.7% (48/56) of mutant *CRB1* alleles. The genome of Chilean individuals shows a mixture of European (57.2%), Native American (38.7%), and African (2.5%) ancestry[40]. *CRB1* variants are rather prevalent in Europe and the leading cause of severe pediatric IRDs in Spain, the largest source of European immigration to Chile[41]. Interestingly, the Cys948Tyr substitution that is the most prevalent disease allele in Chile (31/110, 28.2%, of all LCA alleles; 31/56, 55.4 % of mutant

CRB1 alleles) is described as the most frequent *CRB1* mutation in Spain (22% of *CRB1* alleles) [22]. This mutation most likely arrived to Chile through one or more European (Spanish) ancestors. The second most prevalent *CRB1* change, p.Ser1049Aspfs*40, representing 30.4% (17/56) of *CRB1* alleles has not been described previously, with the exception of a unique Chilean family[42]. Based on haplotype similarities among carriers, it is predicted that this mutation is the result of a founder effect that occurred in Chile 11 generations ago (CI: 7-9). Both *CRB1* variants most likely spread by inbreeding. The remaining six unique *CRB1* disease alleles identified in the Chilean cohort were less frequent (one or two families). The p.Arg764His is the only known variant, reported in populations from the Mediterranean region, including Spain, France, Tunisia, Turkey and in Brazil **(Table S3)**. The other substitutions have not been reported previously and, in the light of their scarcity, may have occurred more recently than the p.Ser1049Aspfs*40 change.

The prevalence of *RDH12* variants in the Chilean population is supported by the recurrence of the p.Leu99Ile allele (15/18, 83.3%) which was introduced to Chile possibly through Spain where it is described as the most frequent *RDH12* mutations[43]. In contrast, although *LCA5* mutations have been described as more frequent in Spain than in other countries[44], the prevalence of this gene in the Chilean population of pediatric IRDs is based on the p.Glu415* nonsense change (16/18, 88.9% of LCA5 alleles), identified solely in Chilean families[42]; this study] and which likely occurred five generations ago (CI: 2-21) in Chile.

Consistent with the high prevalence of *CRB1* p.Cys948Tyr and p.Ser1049Aspfs*40, *RDH12* p.Leu99Ile and *LCA5* p.Glu415* mutations, the allelic diversity in the Chilean population of pediatric IRDs was even more limited than the locus heterogeneity. Together these four variants contribute to the disease in more than three-fourths of the families (38/49, 77.6%).

The 20 other LCA-causing variants were private (one or two families; CRX excluded) and again largely homozygous. Ten of them were reported in patients from Europe and hence

were likely inherited from European individuals[26,27,31,45]. The remaining nine variants have not been reported yet (Table S3). Three of them were detected in unique families and may have emerged very recently. The three other ones were each identified in two unrelated families in compound heterozygosity, suggesting that they occurred earlier and have begun spreading in Chile.

Interestingly, some genes which are rather prevalently implicated in LCA/EOSRD in Western Europe, but not Spain such as *CEP290*[46] and *RPE65*[46] were only minimally (*CEP290)* or not at all (*RPE65*) involved in the Chilean cohort further supporting a Spanish origin of imported mutations.

Providing a final clinical diagnosis in pediatric retinal diseases can be difficult due to the need of sophisticated ophthalmological explorations and long-term follow-up of extraocular functions. Furthermore, the phenotype and genetic cause of LCA largely overlap those of other IRDs. Therefore, it may not be surprising that we found six subjects (6/64, 9.4%) carrying pathogenic variants in non-typical LCA/EOSRD genes (*ADAM9, RP1, NR2E3, RAB28* and *PRPF31*). We reassessed the clinical data of these patients and revisited the initial diagnosis in Goldmann-Favre syndrome, cone-rod dystrophy (CORD) and autosomal dominant RP in three of them, consistent with their *NR2E3, RAB28* and *PRPF31* genotypes, respectively.

On the contrary, we confirmed the diagnosis of LCA in three individuals harboring mutations in *ADAM9* (one case) and *RP1* (two cases). To date, biallelic *ADAM9* mutations have been involved in childhood-onset cone-rod dystrophy (CORD9), with one exception of a LCA proband harboring a truncating variant in homozygosity[47]. Regarding *RP1,* pathogenic variants have been largely associated with dominant RP and to some extent recessive RP. More rarely, biallelic *RP1* mutations have been described in LCA or EOSRD [38,48]. The addition of cases gives a strong support to *ADAM9* and *RP1* as rare causes of LCA/EOSRD.

Finally, consistent with their symptoms three individuals presented mutations in *ALMS1* (two cases) and *IQCB1* (1 case). Early diagnosis of ciliopathies is important but challenging

because many phenotypes do not occur in early childhood, but develop later on. Early molecular testing can certainly help anticipating the emergence of systemic clinical manifestations that could be under-diagnosed as families typically seek medical attention when symptoms worsen.

CONCLUSION

We demonstrate that *CRB1* is the most frequently mutated gene in pediatric retinal dystrophies in Chile and we disclose a high degree of inbreeding in affected families, which results in a very limited number of mutations. This may certainly be taken into consideration by health authorities to implement cost-effective molecular diagnosis of pediatric retinal diseases as well as to focus therapeutic efforts.

DATA AVAILABILITY

Unreferenced variants have been deposited in the CLINVAR database (submission ID SUB13723950).

CONFLICTS OF INTEREST

The authors declare no conflict of Interest.

FUNDING STATEMENT

The work presented here was supported by the Institut National de la Santé et de la Recherche Médicale (INSERM) and grants from the Association Retina France and the Foundation JED Belgique to IP.

ACKNOWLEDGMENTS

We thank the patients and their families for their participation to this study and Ms Allisson Audette for English editing.

REFERENCES

1. Georgiou M, Fujinami K, Michaelides M. Inherited retinal diseases: Therapeutics, clinical trials and end points—A review. Clinical & Experimental Ophthalmology. 2021;49:270–88.

2. Kumaran N, Moore AT, Weleber RG, Michaelides M. Leber congenital amaurosis/earlyonset severe retinal dystrophy: clinical features, molecular genetics and therapeutic interventions. Br J Ophthalmol. 2017;101:1147–54.

3. Hasan SM, Azmeh A, Mostafa O, Megarbane A. Coat's like vasculopathy in leber congenital amaurosis secondary to homozygous mutations in CRB1: a case report and discussion of the management options. BMC Research Notes. 2016;9:91.

4. Porto F, Jones E, Branch J, Soens Z, Maia I, Sena I, et al. Molecular Screening of 43 Brazilian Families Diagnosed with Leber Congenital Amaurosis or Early-Onset Severe Retinal Dystrophy. Genes. 2017;8:355.

5. Waters AM, Beales PL. Ciliopathies: an expanding disease spectrum. Pediatr Nephrol. 2011;26:1039–56.

6. Leroy BP, Birch DG, Duncan JL, Lam BL, Koenekoop RK, Porto FBO, et al. Leber congenital amaurosis due to *CEP290* mutations—severe vision impairment with a high unmet medical need: a review. retina. 2021;41:898–907.

7. Forsyth R, Gunay-Aygun M. Bardet-Biedl Syndrome Overview [Internet]. GeneReviews® [Internet]. University of Washington, Seattle; 2020 [cited 2022 Nov 18]. Available from: https://www.ncbi.nlm.nih.gov/books/NBK1363/

8. Marshall JD, Muller J, Collin GB, Milan G, Kingsmore SF, Dinwiddie D, et al. Alström Syndrome: Mutation spectrum of *ALMS1*. Hum Mutat. 2015;36:660–8.

9. Kaur A, Dhir SK, Goyal G, Mittal N, Goyal RK. Senior Loken Syndrome. J Clin Diagn Res. 2016;10:SD03–4.

10. Garafalo AV, Cideciyan AV, Heon E, Sheplock R, Pearson A, WeiYang Yu C, et al. Progress in treating inherited retinal diseases: Early subretinal gene therapy clinical trials and candidates for future initiatives. Prog Retin Eye Res. 2020;77:100827.

11. Li H, Durbin R. Fast and accurate short read alignment with Burrows-Wheeler transform. Bioinformatics. 2009;25:1754–60.

12. DePristo MA, Banks E, Poplin R, Garimella KV, Maguire JR, Hartl C, et al. A framework for variation discovery and genotyping using next-generation DNA sequencing data. Nat Genet. 2011;43:491–8.

13. Li H, Handsaker B, Wysoker A, Fennell T, Ruan J, Homer N, et al. The Sequence Alignment/Map format and SAMtools. Bioinformatics. 2009;25:2078–9.

14. Stoupa A, Al Hage Chehade G, Chaabane R, Kariyawasam D, Szinnai G, Hanein S, et al. High Diagnostic Yield of Targeted Next-Generation Sequencing in a Cohort of Patients

With Congenital Hypothyroidism Due to Dyshormonogenesis. Front Endocrinol (Lausanne). 2021;11:545339.

15. Goossens D, Moens LN, Nelis E, Lenaerts A-S, Glassee W, Kalbe A, et al. Simultaneous mutation and copy number variation (CNV) detection by multiplex PCR-based GS-FLX sequencing. Hum Mutat. 2009;30:472–6.

16. Kopanos C, Tsiolkas V, Kouris A, Chapple CE, Albarca Aguilera M, Meyer R, et al. VarSome: the human genomic variant search engine. Bioinformatics. 2019;35:1978–80.

17. Delaneau O, Howie B, Cox AJ, Zagury J-F, Marchini J. Haplotype estimation using sequencing reads. Am J Hum Genet. 2013;93:687–96.

18. Genin E, Tullio-Pelet A, Begeot F, Lyonnet S, Abel L. Estimating the age of rare disease mutations: the example of Triple-A syndrome. J Med Genet. 2004;41:445–9.

19. Auton A, Abecasis GR, Altshuler DM, Durbin RM, Abecasis GR, Bentley DR, et al. A global reference for human genetic variation. Nature. 2015;526:68–74.

20. Fujinami-Yokokawa Y, Fujinami K, Kuniyoshi K, Hayashi T, Ueno S, Mizota A, et al. Clinical and Genetic Characteristics of 18 Patients from 13 Japanese Families with CRXassociated retinal disorder: Identification of Genotype-phenotype Association. Sci Rep. 2020;10:9531.

21. Stone EM, Andorf JL, Whitmore SS, DeLuca AP, Giacalone JC, Streb LM, et al. Clinically Focused Molecular Investigation of 1000 Consecutive Families with Inherited Retinal Disease. Ophthalmology. 2017;124:1314–31.

22. Corton M, Tatu SD, Avila-Fernandez A, Vallespín E, Tapias I, Cantalapiedra D, et al. High frequency of CRB1 mutations as cause of Early-Onset Retinal Dystrophies in the Spanish population. Orphanet Journal of Rare Diseases. 2013;8:20.

23. Hanany M, Rivolta C, Sharon D. Worldwide carrier frequency and genetic prevalence of autosomal recessive inherited retinal diseases. Proc Natl Acad Sci U S A. 2020;117:2710–6.

24. Aleman TS, Uyhazi KE, Serrano LW, Vasireddy V, Bowman SJ, Ammar MJ, et al. RDH12 Mutations Cause a Severe Retinal Degeneration With Relatively Spared Rod Function. Invest Ophthalmol Vis Sci. 2018;59:5225–36.

25. Coppieters F, Lefever S, Leroy BP, De Baere E. CEP290, a gene with many faces: mutation overview and presentation of CEP290base. Hum Mutat. 2010;31:1097–108.

26. Feldhaus B, Weisschuh N, Nasser F, den Hollander AI, Cremers FPM, Zrenner E, et al. CEP290 Mutation Spectrum and Delineation of the Associated Phenotype in a Large German Cohort: A Monocentric Study. Am J Ophthalmol. 2020;211:142–50.

27. Perrault I, Hanein S, Zanlonghi X, Serre V, Nicouleau M, Defoort-Delhemmes S, et al. Mutations in NMNAT1 cause Leber congenital amaurosis with early-onset severe macular and optic atrophy. Nat Genet. 2012;44:975–7.

28. Eblimit A, Zaneveld SA, Liu W, Thomas K, Wang K, Li Y, et al. NMNAT1 E257K variant, associated with Leber Congenital Amaurosis (LCA9), causes a mild retinal degeneration phenotype. Exp Eye Res. 2018;173:32–43.

29. Hanein S, Perrault I, Gerber S, Tanguy G, Barbet F, Ducroq D, et al. Leber congenital amaurosis: comprehensive survey of the genetic heterogeneity, refinement of the clinical definition, and genotype-phenotype correlations as a strategy for molecular diagnosis. Hum Mutat. 2004;23:306–17.

30. Beryozkin A, Aweidah H, Carrero Valenzuela RD, Berman M, Iguzquiza O, Cremers FPM, et al. Retinal Degeneration Associated With RPGRIP1: A Review of Natural History, Mutation Spectrum, and Genotype–Phenotype Correlation in 228 Patients. Front Cell Dev Biol. 2021;9:746781.

31. Patel N, Alkuraya H, Alzahrani SS, Nowailaty SR, Seidahmed MZ, Alhemidan A, et al. Mutations in known disease genes account for the majority of autosomal recessive retinal dystrophies. Clin Genet. 2018;94:554–63.

32. Martin-Merida I, Avila-Fernandez A, Del Pozo-Valero M, Blanco-Kelly F, Zurita O, Perez-Carro R, et al. Genomic Landscape of Sporadic Retinitis Pigmentosa: Findings from 877 Spanish Cases. Ophthalmology. 2019;126:1181–8.

33. Jia D, Gao P, Lv Y, Huang Y, Reilly J, Sun K, et al. Tulp1 deficiency causes early-onset retinal degeneration through affecting ciliogenesis and activating ferroptosis in zebrafish. Cell Death Dis. 2022;13:962.

34. Sohocki MM, Sullivan LS, Mintz-Hittner HA, Birch D, Heckenlively JR, Freund CL, et al. A range of clinical phenotypes associated with mutations in CRX, a photoreceptor transcription-factor gene. Am J Hum Genet. 1998;63:1307–15.

35. Parry DA, Toomes C, Bida L, Danciger M, Towns KV, McKibbin M, et al. Loss of the metalloprotease ADAM9 leads to cone-rod dystrophy in humans and retinal degeneration in mice. Am J Hum Genet. 2009;84:683–91.

36. Wang J, Xiao X, Li S, Wang P, Sun W, Zhang Q. Dominant RP in the Middle While Recessive in Both the N- and C-Terminals Due to RP1 Truncations: Confirmation, Refinement, and Questions. Frontiers in Cell and Developmental Biology [Internet]. 2021 [cited 2023 May 18];9. Available from: https://www.frontiersin.org/articles/10.3389/fcell.2021.634478

37. Iarossi G, Marino V, Maltese PE, Colombo L, D'Esposito F, Manara E, et al. Expanding the Clinical and Genetic Spectrum of RAB28-Related Cone-Rod Dystrophy: Pathogenicity of Novel Variants in Italian Families. Int J Mol Sci. 2020;22:381.

38. Wang L, Zhang J, Chen N, Wang L, Zhang F, Ma Z, et al. Application of Whole Exome and Targeted Panel Sequencing in the Clinical Molecular Diagnosis of 319 Chinese Families with Inherited Retinal Dystrophy and Comparison Study. Genes (Basel). 2018;9:360.

39. Liu X, Tao T, Zhao L, Li G, Yang L. Molecular diagnosis based on comprehensive genetic testing in 800 Chinese families with non-syndromic inherited retinal dystrophies. Clin Exp Ophthalmol. 2021;49:46–59.

40. Homburger JR, Moreno-Estrada A, Gignoux CR, Nelson D, Sanchez E, Ortiz-Tello P, et al. Genomic Insights into the Ancestry and Demographic History of South America. PLOS Genetics. 2015;11:e1005602.

41. Gil FG. El sistema político de Chile. Andres Bello; 1969.

42. Zanolli M, Oporto JI, Verdaguer JI, López JP, Zacharías S, Romero P, et al. Genetic testing for inherited ocular conditions in a developing country. Ophthalmic Genet. 2020;41:36–40.

43. Valverde D, Pereiro I, Vallespín E, Ayuso C, Borrego S, Baiget M. Complexity of Phenotype–Genotype Correlations in Spanish Patients with RDH12 Mutations. Investigative Ophthalmology & Visual Science. 2009;50:1065–8.

44. Corton M, Avila-Fernandez A, Vallespín E, López-Molina MI, Almoguera B, MartínGarrido E, et al. Involvement of LCA5 in Leber congenital amaurosis and retinitis pigmentosa in the Spanish population. Ophthalmology. 2014;121:399–407.

45. Perrault I, Rozet JM, Calvas P, Gerber S, Camuzat A, Dollfus H, et al. Retinal-specific guanylate cyclase gene mutations in Leber's congenital amaurosis. Nat Genet. 1996;14:461–4.

46. Vallespin E, Lopez-Martinez M-A, Cantalapiedra D, Riveiro-Alvarez R, Aguirre-Lamban J, Avila-Fernandez A, et al. Frequency of CEP290 c.2991_1655A>G mutation in 175 Spanish families affected with Leber congenital amaurosis and early-onset retinitis pigmentosa. Mol Vis. 2007;13:2160–2.

47. Hull S, Arno G, Plagnol V, Robson A, Webster AR, Moore AT. Exome sequencing reveals ADAM9 mutations in a child with cone-rod dystrophy. Acta Ophthalmol. 2015;93:e392-393.

48. Georgiou M, Ali N, Yang E, Grewal PS, Rotsos T, Pontikos N, et al. Extending the phenotypic spectrum of PRPF8, PRPH2, RP1 and RPGR, and the genotypic spectrum of early-onset severe retinal dystrophy. Orphanet J Rare Dis. 2021;16:128.

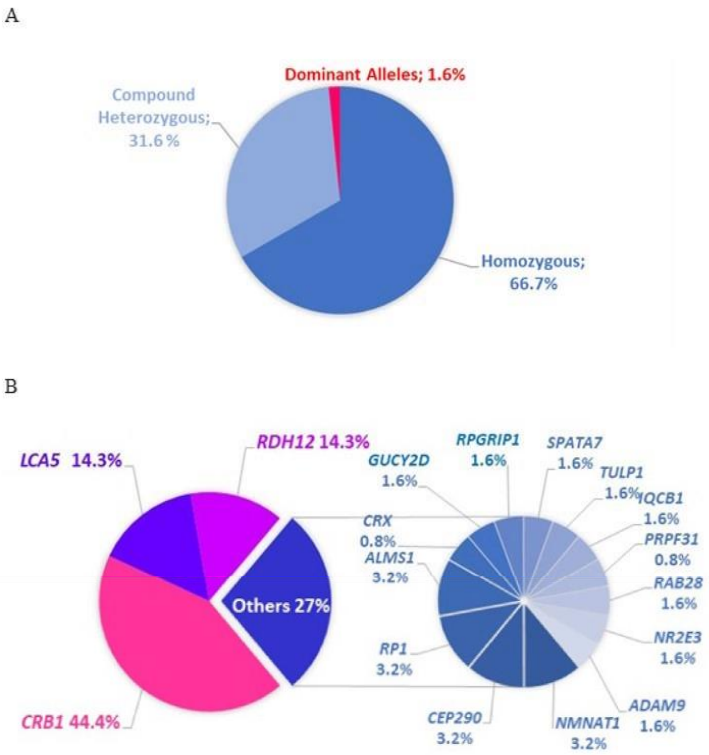

Figure 1. Genetic basis of LCA/EOSRD in the Chilean cohort: (A) Proportional identification of homozygous alleles versus compound heterozygous and dominant variants within 64 diagnosed cases. (B) Frequency of genes identified in 64 LCA/EOSRD cases. Mutations were identified in 17 genes, with 73% of the mutations found in the top three genes (*CRB1, LCA5, RDH12*).

Discussion and Perspectives

The success rate of molecular diagnosis, which relies on the analysis of the coding genome, varies significantly from one disease to another. It can be as high as 80% for pediatric IRDs and even higher in inbred populations, as demonstrated by our analysis in a Chilean cohort. Nevertheless, when it comes to ocular developmental defects (ODDs) in general, and specifically with MAC, the success rate typically stands at a modest 50%. This suggests that unsolved cases may involve novel genes, variants of uncertain significance, and non-coding variants. Currently, there is a significant acceleration in the identification of non-coding variations in diseases that affect vision, spanning from IRDs to ODDs. Recent studies utilizing genome sequencing have revealed novel non-coding variants, including variants that impact CREs. Notably, mutations in the regulatory region of *GUCY2D* was demonstrated to impact negatively its expression (Daich Varela et al., 2023). In a similar way, alterations of a co-repressor element of *CRX* and *OTX2* have been identified in patients exhibiting early-onset retinal degeneration (Langouët et al., 2022). In the case of ODDs, several mutations in *PAX6* regulatory elements have been linked to aniridia (Plaisancié et al., 2018).

This underscores the importance of delving into the non-coding genome, recognizing that investigating this long-neglected “junk” genome is crucial not only for improving diagnostic capabilities (Orozco et al., 2022) but also for advancing our understanding of gene regulation and ocular development, as demonstrated by our research on congenital microcoria and FOXE3-associated MAC.

While the majority of reviews on this topic concur that both iris muscles originate from the iris anterior epithelium (IAE), some theories propose an alternative perspective, suggesting that the sphincter muscle may develop from the posterior iris epithelium (IPE) (Thumann, 2001).

Another crucial question arises regarding the potential influence of pigmentation on iris muscle development. As evidenced by foveal hypoplasia observed in cases of oculocutaneous albinism (Grønskov et al., 2007), pigmentation indeed plays a crucial role in eye development, although the mechanisms behind

these retinal defects remain unknown. This consideration gains significance, given that the dilator muscle (DM) initiates its development from the IAE during a stage characterized by high pigmentation. Intriguingly, as development progresses, the DM undergoes a process of depigmentation while continuing its maturation. This intriguing aspect adds a layer of complexity to our understanding of iris muscle development. There is a notable dearth of literature regarding this important subject especially knowing that in MCOR, *Sox21* aberrant expression is likely driven by *Dct*.

Recent progress in comprehending the various elements of the iris has been achieved through single-cell RNA sequencing (van Zyl et al., 2020; J. Wang et al., 2021). Cutting-edge spatial single-cell genomics techniques would enhance this knowledge by enabling the generation of atlases of the iris during its development and thus help addressing these important questions.

While it is highly likely that the ectopic expression of Sox21 in MCOR irises is orchestrated by Dct regulatory elements, the precise mechanism remains elusive. Recent years have seen the emergence of groundbreaking techniques with the potential to unravel this mechanism by elucidating the intricate three-dimensional interactions within the genome. These methodologies include Chromosome Conformation Capture (3C), circularized 3C (4C), Carbon Copy 3C (5C) methodologies, and the most recently developed High-Throughput 3C (Hi-C) (Krijger et al., 2020). Continued progress in these methodologies is exemplified by the recent incorporation of HiChIP, which expertly integrates Hi-C with immunoprecipitation, opening new avenues to unravel intricate protein-DNA interactions. Additionally, the recent introduction of single-cell genomics has empowered researchers to explore the diversity of chromatin conformation among individual cells within a population. In the context of MCOR, the application of promoter Capture Hi-C (Schoenfelder et al., 2018), another valuable technique developed to resolve gene promoter interactions, holds promise for deciphering the regulation of ectopic *Sox21* expression. This capability provides invaluable insights into our understanding of the 3D genome architecture and its influence on gene regulation, development, and disease. However, it's crucial to note that these techniques come with certain limitations, including their cost and the substantial cell quantity often required, which may necessitate large-scale sampling of mouse irises, raising important ethical concerns.

Modeling the MCOR disease in mice raises additional questions. Although studies in mice have proven highly valuable in various areas of biology, they may not be the optimal choice for ocular research due to distinct physiological differences. In this thesis, we conducted two studies where we introduced the exact same SNP and SV responsible for complex microphthalmia or congenital microcoria, respectively. However, the resulting phenotype did not mirror that observed in humans. This observation suggests that despite the high degree of genomic conservation between the two species, non-coding variants may not have identical effects.

As mentioned earlier, disparities exist in mouse iris development compared to humans, especially regarding developmental timelines, with most structures maturing after birth in mice. Our study on *Sox21* expression during normal ocular development in mice revealed distinct differences, as its expression was confined solely to the proximal part of the optic vesicle, absent in the anterior segment at any developmental stage. Notably, previous research has emphasized the role of *Sox21* in lens development in chick and zebrafish. Some researchers propose that this requirement extends across all vertebrates, suggesting a universal aspect, given the presence of regulatory sequences for *Sox21* expression in the lens within a conserved non-coding element (Lan et al., 2011; Pauls et al., 2012). Along the same lines, our study on Foxe3 underscores the fact that, while CREs are highly evolutionarily conserved, variable genetic interactions exist across species.

As an alternative to mouse models, cell lines have emerged as a promising avenue for exploration in our research. To delve into the mechanisms underlying MCOR, we are cultivating cells obtained from the iris posterior epithelium of mice carrying the critical deletion. This approach will provide us with a sufficient quantity of nuclei, enabling us to achieve high-quality results using the high-throughput methods mentioned earlier. Our goal is to gain a deeper understanding of what triggers *Sox21* misexpression. Additionally, employing an *in vitro* model will allow us to further explore the involvement of SOX21 in the regulation of *Tgfb2* and potentially unveil the etiology of glaucoma in this rare iris disease. Concerning Foxe3, our research has identified a candidate protein with a preferential binding to the mutant version of the *Foxe3* CRE. This candidate may function as a novel repressor, potentially inhibiting *Foxe3* expression. In contrast, two other candidates have exhibited preferential binding to the

non-mutated *Foxe3* CRE. These factors are of significant interest, as they may serve as typical regulators of *Foxe3* expression, potentially playing a role in lens development and representing new genes of interest in microphthalmia. To test these hypotheses, we are currently harvesting cells from the anterior lens epithelium of wild-type and FOXE3-compound heterozygous animals, with the aim of silencing using siRNA the expression of the three identified candidate genes and observe their effects on *Foxe3* expression.

However, it is essential to acknowledge the numerous challenges associated with tissue culture, ranging from maintaining primary cell lines to simulating the complex in vivo microenvironment. A notable challenge specific to the iris epithelium is the dissociation of the two epithelia; despite the development of numerous methods, they do not always yield favorable results (Johnen et al., 2011). Successfully overcoming these obstacles will be crucial for unlocking the full potential of cell lines in ocular research. This significant effort is being led by another dedicated PhD student, and their work holds the potential to provide valuable insights into the questions raised in this study.

While the use of organoids shows significant progress and holds high value in ocular research, its application faces limitations when studying the iris. The development of this ocular structure requires the presence of periocular mesenchyme for proper growth. Consequently, current optic cup organoids are constrained to early developmental stages without differentiated margins (Vielle et al., 2021). To circumvent these challenges, an alternative approach involves the use of *ex vivo* ocular explants. This method has shown promising results in chick studies, enabling the successful differentiation of the iris (Alrajeh et al., 2019; Shirazi Fard et al., 2015).

In conclusion, the exploration of ocular genetics stands at a pivotal juncture, addressing questions surrounding undiscovered genes, non-coding variants, and the complexities inherent in ocular development. The advancing methods and models discussed above carry the potential to unveil the intricacies of ocular biology, promising advancements in diagnosis and treatment strategies for ocular disorders. This journey toward enlightenment not only holds the potential to benefit patients significantly but also to deepen our appreciation for the wonders of ocular development.

References

Acemel, R.D., Lupiáñez, D.G., 2023. Evolution of 3D chromatin organization at different scales. Curr. Opin. Genet. Dev. 78, 102019. https://doi.org/10.1016/j.gde.2022.102019

Adler, R., 2000. A model of retinal cell differentiation in the chick embryo. Prog. Retin. Eye Res. 19, 529–557. https://doi.org/10.1016/s1350-9462(00)00008-2

Ahmed, M.R., Sethna, S., Krueger, L.A., Yang, M.B., Hufnagel, R.B., 2022. Variable Anterior Segment Dysgenesis and Cardiac Anomalies Caused by a Novel Truncating Variant of FOXC1. Genes 13, 411. https://doi.org/10.3390/genes13030411

Alrajeh, M., Vavrusova, Z., Creuzet, S.E., 2019. Deciphering the Neural Crest Contribution to Cephalic Development with Avian Embryos. Methods Mol. Biol. Clifton NJ 1976, 55–70. https://doi.org/10.1007/978-1-4939-9412-0_5

Alward, W.L., 2000. Axenfeld-Rieger syndrome in the age of molecular genetics. Am. J. Ophthalmol. 130, 107–115. https://doi.org/10.1016/s0002-9394(00)00525-0

Angée, C., Nedelec, B., Erjavec, E., Rozet, J.-M., Fares Taie, L., 2021. Congenital Microcoria: Clinical Features and Molecular Genetics. Genes 12, 624. https://doi.org/10.3390/genes12050624

Arikawa, A., Yoshida, S., Yoshikawa, H., Ishikawa, K., Yamaji, Y., Arita, R.-I., Ueno, A., Ishibashi, T., 2010. Case of novel PITX2 gene mutation associated with Peters' anomaly and persistent hyperplastic primary vitreous. Eye Lond. Engl. 24, 391–393. https://doi.org/10.1038/eye.2009.114

Atik, S., Koc, F., Kaplan, Y.C., Yurtseven, S.G., 2014. Congenital Mydriasis: Diagnostic Challenge in a Case with Accompanying Neurologic Symptoms. Neuro-Ophthalmol. 38, 153–155. https://doi.org/10.3109/01658107.2014.894089

Bailey, T.J., El-Hodiri, H., Zhang, L., Shah, R., Mathers, E.H., Jamrich, M., 2004. Regulation of vertebrate eye development by Rx genes. Int. J. Dev. Biol. 48, 761–770. https://doi.org/10.1387/ijdb.041878tb

Baker, N.E., Li, K., Quiquand, M., Ruggiero, R., Wang, L.-H., 2014. EEye Development. Methods San Diego Calif 68, 252–259. https://doi.org/10.1016/j.ymeth.2014.04.007

Bakrania, P., Robinson, D.O., Bunyan, D.J., Salt, A., Martin, A., Crolla, J.A., Wyatt, A., Fielder, A., Ainsworth, J., Moore, A., Read, S., Uddin, J., Laws, D., Pascuel-Salcedo, D., Ayuso, C., Allen, L., Collin, J.R.O., Ragge, N.K., 2007. SOX2 anophthalmia syndrome: 12 new cases demonstrating broader phenotype and high frequency of large gene deletions. Br. J. Ophthalmol. 91, 1471–1476. https://doi.org/10.1136/bjo.2007.117929

Bardakjian, T.M., Schneider, A., 2011. The genetics of anophthalmia and microphthalmia. Curr. Opin. Ophthalmol. 22, 309–313. https://doi.org/10.1097/ICU.0b013e328349b004

Basharat, R., Rodenburg, K., Rodríguez-Hidalgo, M., Jarral, A., Ullah, E., Corominas, J., Gilissen, C., Zehra, S.T., Hameed, U., Ansar, M., de Bruijn, S.E., 2023. Combined Single Gene Testing and Genome Sequencing as an Effective Diagnostic Approach for Anophthalmia and Microphthalmia Patients. Genes 14, 1573. https://doi.org/10.3390/genes14081573

Behar-Cohen, F., Gelizé, E., Jonet, L., Lassiaz, P., 2020. Anatomie de la rétine. médecine/sciences 36, 594–599. https://doi.org/10.1051/medsci/2020094

Bhatia, S., Bengani, H., Fish, M., Brown, A., Divizia, M.T., de Marco, R., Damante, G., Grainger, R., van Heyningen, V., Kleinjan, D.A., 2013. Disruption of autoregulatory feedback by a mutation in a remote, ultraconserved PAX6 enhancer causes aniridia. Am. J. Hum. Genet. 93, 1126–1134. https://doi.org/10.1016/j.ajhg.2013.10.028

Biswas, P., Villanueva, A.L., Soto-Hermida, A., Duncan, J.L., Matsui, H., Borooah, S., Kurmanov, B., Richard, G., Khan, S.Y., Branham, K., Huang, B., Suk, J., Bakall, B., Goldberg, J.L., Gabriel, L., Khan, N.W., Raghavendra, P.B., Zhou, J., Devalaraja, S., Huynh, A., Alapati, A., Zawaydeh, Q., Weleber, R.G., Heckenlively, J.R., Hejtmancik, J.F., Riazuddin, S., Sieving, P.A., Riazuddin, S.A., Frazer, K.A., Ayyagari, R., 2021. Deciphering the genetic architecture and ethnographic distribution of IRD in three

ethnic populations by whole genome sequence analysis. PLoS Genet. 17, e1009848. https://doi.org/10.1371/journal.pgen.1009848

Blixt, Å., Landgren, H., Johansson, B.R., Carlsson, P., 2007. Foxe3 is required for morphogenesis and differentiation of the anterior segment of the eye and is sensitive to Pax6 gene dosage. Dev. Biol. 302, 218–229. https://doi.org/10.1016/j.ydbio.2006.09.021

Boutin, M.E., Hampton, C., Quinn, R., Ferrer, M., Song, M.J., 2019. 3D Engineering of Ocular Tissues for Disease Modeling and Drug Testing, in: Bharti, K. (Ed.), Pluripotent Stem Cells in Eye Disease Therapy, Advances in Experimental Medicine and Biology. Springer International Publishing, Cham, pp. 171–193. https://doi.org/10.1007/978-3-030-28471-8_7

Bremond-Gignac, D., 2019. [Congenital aniridia in children]. Rev. Prat. 69, 67–70.

Buffault, J., Labbé, A., Hamard, P., Brignole-Baudouin, F., Baudouin, C., 2020. The trabecular meshwork: Structure, function and clinical implications. A review of the literature. J. Fr. Ophtalmol. 43, e217–e230. https://doi.org/10.1016/j.jfo.2020.05.002

Cavodeassi, F., Bovolenta, P., 2014. New functions for old genes: Pax6 and Mitf in eye pigment biogenesis. Pigment Cell Melanoma Res. 27, 1005–1007. https://doi.org/10.1111/pcmr.12308

Chambers, T.M., Agopian, A.J., Lewis, R.A., Langlois, P.H., Danysh, H.E., Weber, K.A., Shaw, G.M., Mitchell, L.E., Lupo, P.J., 2018. Epidemiology of anophthalmia and microphthalmia: Prevalence and patterns in Texas, 1999-2009. Am. J. Med. Genet. A. 176, 1810–1818. https://doi.org/10.1002/ajmg.a.40352

Chang, B., 2013. Mouse models for studies of retinal degeneration and diseases. Methods Mol. Biol. Clifton NJ 935, 10.1007/978-1-62703-080–9_2. https://doi.org/10.1007/978-1-62703-080-9_2

Chassaing, N., Causse, A., Vigouroux, A., Delahaye, A., Alessandri, J.-L., Boespflug-Tanguy, O., Boute-Benejean, O., Dollfus, H., Duban-Bedu, B., Gilbert-Dussardier, B., Giuliano, F., Gonzales, M., Holder-Espinasse, M., Isidor, B., Jacquemont, M.-L., Lacombe, D., Martin-Coignard, D., Mathieu-Dramard, M., Odent, S., Picone, O., Pinson, L., Quelin, C., Sigaudy, S., Toutain, A., Thauvin-Robinet, C., Kaplan, J., Calvas, P., 2014. Molecular findings and clinical data in a cohort of 150 patients with anophthalmia/microphthalmia. Clin. Genet. 86, 326–334. https://doi.org/10.1111/cge.12275

Chen, L., Guo, W., Ren, Lili, Yang, M., Zhao, Yaofeng, Guo, Z., Yi, H., Li, M., Hu, Y., Long, X., Sun, B., Li, Jinxiu, Zhai, S., Zhang, T., Tian, S., Meng, Q., Yu, N., Zhu, D., Tang, G., Tang, Q., Ren, Liming, Liu, K., Zhang, S., Che, T., Yu, Z., Wu, N., Jing, L., Zhang, R., Cong, T., Chen, S., Zhao, Yiqiang, Zhang, Y., Bai, X., Guo, Y., Zhao, L., Zhang, F., Zhao, H., Zhang, Liang, Hou, Z., Zhao, J., Li, Jianan, Zhang, Lijuan, Sun, W., Zou, X., Wang, T., Ge, L., Liu, Z., Hu, X., Wang, J., Yang, S., Li, N., 2016. A de novo silencer causes elimination of MITF-M expression and profound hearing loss in pigs. BMC Biol. 14, 52. https://doi.org/10.1186/s12915-016-0273-2

Chesneau, B., Aubert-Mucca, M., Fremont, F., Pechmeja, J., Soler, V., Isidor, B., Nizon, M., Dollfus, H., Kaplan, J., Fares-Taie, L., Rozet, J.-M., Busa, T., Lacombe, D., Naudion, S., Amiel, J., Rio, M., Attie-Bitach, T., Lesage, C., Thouvenin, D., Odent, S., Morel, G., Vincent-Delorme, C., Boute, O., Vanlerberghe, C., Dieux, A., Boussion, S., Faivre, L., Pinson, L., Laffargue, F., Le Guyader, G., Le Meur, G., Prieur, F., Lambert, V., Laudier, B., Cottereau, E., Ayuso, C., Corton-Pérez, M., Bouneau, L., Le Caignec, C., Gaston, V., Jeanton-Scaramouche, C., Dupin-Deguine, D., Calvas, P., Chassaing, N., Plaisancié, J., 2022. First evidence of SOX2 mutations in Peters' anomaly: Lessons from molecular screening of 95 patients. Clin. Genet. 101, 494–506. https://doi.org/10.1111/cge.14123

Chow, R.L., Lang, R.A., 2001. Early Eye Development in Vertebrates. Annu. Rev. Cell Dev. Biol. 17, 255–296. https://doi.org/10.1146/annurev.cellbio.17.1.255

Chrystal, P.W., French, C.R., Jean, F., Havrylov, S., van Baarle, S., Peturson, A.-M., Xu, P., Crump, J.G., Pilgrim, D.B., Lehmann, O.J., Waskiewicz, A.J., 2021. The Axenfeld–

Rieger Syndrome Gene FOXC1 Contributes to Left–Right Patterning. Genes 12, 170. https://doi.org/10.3390/genes12020170
Conte, I., Hadfield, K.D., Barbato, S., Carrella, S., Pizzo, M., Bhat, R.S., Carissimo, A., Karali, M., Porter, L.F., Urquhart, J., Hateley, S., O'Sullivan, J., Manson, F.D.C., Neuhauss, S.C.F., Banfi, S., Black, G.C.M., 2015. MiR-204 is responsible for inherited retinal dystrophy associated with ocular coloboma. Proc. Natl. Acad. Sci. 112, E3236–E3245. https://doi.org/10.1073/pnas.1401464112
Cramer, P., 2019. Organization and regulation of gene transcription. Nature 573, 45–54. https://doi.org/10.1038/s41586-019-1517-4
Cuylen, S., Haering, C.H., 2010. A New Cohesive Team to Mediate DNA Looping. Cell Stem Cell 7, 424–426. https://doi.org/10.1016/j.stem.2010.09.006
Cvekl, A., Ashery Padan, R., 2014. The cellular and molecular mechanisms of vertebrate lens development. Dev. Camb. Engl. 141, 4432–4447. https://doi.org/10.1242/dev.107953
Cvekl, A., Tamm, E.R., 2004. Anterior eye development and ocular mesenchyme: new insights from mouse models and human diseases. BioEssays News Rev. Mol. Cell. Dev. Biol. 26, 374–386. https://doi.org/10.1002/bies.20009
Daich Varela, M., Bellingham, J., Motta, F., Jurkute, N., Ellingford, J.M., Quinodoz, M., Oprych, K., Niblock, M., Janeschitz-Kriegl, L., Kaminska, K., Cancellieri, F., Scholl, H.P.N., Lenassi, E., Schiff, E., Knight, H., Black, G., Rivolta, C., Cheetham, M.E., Michaelides, M., Mahroo, O.A., Moore, A.T., Webster, A.R., Arno, G., 2023. Multidisciplinary team directed analysis of whole genome sequencing reveals pathogenic non-coding variants in molecularly undiagnosed inherited retinal dystrophies. Hum. Mol. Genet. 32, 595–607. https://doi.org/10.1093/hmg/ddac227
Davis-Silberman, N., Ashery-Padan, R., 2008. Iris development in vertebrates; genetic and molecular considerations. Brain Res. 1192, 17–28. https://doi.org/10.1016/j.brainres.2007.03.043
de Bruijn, S.E., Fiorentino, A., Ottaviani, D., Fanucchi, S., Melo, U.S., Corral-Serrano, J.C., Mulders, T., Georgiou, M., Rivolta, C., Pontikos, N., Arno, G., Roberts, L., Greenberg, J., Albert, S., Gilissen, C., Aben, M., Rebello, G., Mead, S., Raymond, F.L., Corominas, J., Smith, C.E.L., Kremer, H., Downes, S., Black, G.C., Webster, A.R., Inglehearn, C.F., van den Born, L.I., Koenekoop, R.K., Michaelides, M., Ramesar, R.S., Hoyng, C.B., Mundlos, S., Mhlanga, M.M., Cremers, F.P.M., Cheetham, M.E., Roosing, S., Hardcastle, A.J., 2020. Structural Variants Create New Topological-Associated Domains and Ectopic Retinal Enhancer-Gene Contact in Dominant Retinitis Pigmentosa. Am. J. Hum. Genet. 107, 802–814. https://doi.org/10.1016/j.ajhg.2020.09.002
De Silva, Daham, Williamson, K.A., Dayasiri, K.C., Suraweera, N., Quinters, V., Abeysekara, H., Wanigasinghe, J., De Silva, Deepthi, De Silva, H., 2018. Gillespie syndrome in a South Asian child: a case report with confirmation of a heterozygous mutation of the ITPR1 gene and review of the clinical and molecular features. BMC Pediatr. 18, 308. https://doi.org/10.1186/s12887-018-1286-5
Dean, A., Larson, D.R., Sartorelli, V., 2021. Enhancers, gene regulation, and genome organization. Genes Dev. 35, 427–432. https://doi.org/10.1101/gad.348372.121
Dentici, M.L., Barresi, S., Nardella, M., Bellacchio, E., Alfieri, P., Bruselles, A., Pantaleoni, F., Danieli, A., Iarossi, G., Cappa, M., Bertini, E., Tartaglia, M., Zanni, G., 2017. Identification of novel and hotspot mutations in the channel domain of ITPR1 in two patients with Gillespie syndrome. Gene 628, 141–145. https://doi.org/10.1016/j.gene.2017.07.017
Doward, W., Perveen, R., Lloyd, I.C., Ridgway, A.E., Wilson, L., Black, G.C., 1999. A mutation in the RIEG1 gene associated with Peters' anomaly. J. Med. Genet. 36, 152–155.
Ducasse, A., 2004. Anatomie et physiologie de l'iris. EMC - Ophtalmol. 1, 1–7. https://doi.org/10.1016/S0246-0343(02)00069-2
Edén, U., Iggman, D., Riise, R., Tornqvist, K., 2008. Epidemiology of aniridia in Sweden and Norway. Acta Ophthalmol. (Copenh.) 86, 727–729. https://doi.org/10.1111/j.1755-3768.2008.01309.x

Eiraku, M., Takata, N., Ishibashi, H., Kawada, M., Sakakura, E., Okuda, S., Sekiguchi, K., Adachi, T., Sasai, Y., 2011. Self-organizing optic-cup morphogenesis in three-dimensional culture. Nature 472, 51–56. https://doi.org/10.1038/nature09941

Espana, E.M., Birk, D.E., 2020. Composition, Structure and Function of the Corneal Stroma. Exp. Eye Res. 198, 108137. https://doi.org/10.1016/j.exer.2020.108137

Fadool, J.M., Dowling, J.E., 2008. Zebrafish: a model system for the study of eye genetics. Prog. Retin. Eye Res. 27, 89–110. https://doi.org/10.1016/j.preteyeres.2007.08.002

Fahnehjelm, C., Dafgård Kopp, E., Wincent, J., Güven, E., Nilsson, M., Olsson, M., Teär Fahnehjelm, K., 2022. Anophthalmia and microphthalmia in children: associated ocular, somatic and genetic morbidities and quality of life. Ophthalmic Genet. 43, 172–183. https://doi.org/10.1080/13816810.2021.1989600

Fares-Taie, L., Gerber, S., Tawara, A., Ramirez-Miranda, A., Douet, J.-Y., Verdin, H., Guilloux, A., Zenteno, J.C., Kondo, H., Moisset, H., Passet, B., Yamamoto, K., Iwai, M., Tanaka, T., Nakamura, Y., Kimura, W., Bole-Feysot, C., Vilotte, M., Odent, S., Vilotte, J.-L., Munnich, A., Regnier, A., Chassaing, N., De Baere, E., Raymond-Letron, I., Kaplan, J., Calvas, P., Roche, O., Rozet, J.-M., 2015. Submicroscopic Deletions at 13q32.1 Cause Congenital Microcoria. Am. J. Hum. Genet. 96, 631–639. https://doi.org/10.1016/j.ajhg.2015.01.014

Farnung, L., Vos, S.M., 2022. Assembly of RNA polymerase II transcription initiation complexes. Curr. Opin. Struct. Biol. 73, 102335. https://doi.org/10.1016/j.sbi.2022.102335

Forrester, J.V., Dick, A.D., McMenamin, P.G., Roberts, F., Pearlman, E., 2016a. Chapter 1 - Anatomy of the eye and orbit, in: Forrester, J.V., Dick, A.D., McMenamin, P.G., Roberts, F., Pearlman, E. (Eds.), The Eye (Fourth Edition). W.B. Saunders, pp. 1-102.e2. https://doi.org/10.1016/B978-0-7020-5554-6.00001-0

Forrester, J.V., Dick, A.D., McMenamin, P.G., Roberts, F., Pearlman, E., 2016b. Chapter 2 - Embryology and early development of the eye and adnexa, in: Forrester, J.V., Dick, A.D., McMenamin, P.G., Roberts, F., Pearlman, E. (Eds.), The Eye (Fourth Edition). W.B. Saunders, pp. 103-129.e8. https://doi.org/10.1016/B978-0-7020-5554-6.00002-2

Freddo, T.F., 1984. Intercellular Junctions of the Iris Epithelia in Macaco Mulatta. Invest. Ophthalmol. 25, 11.

Fronk, A.H., Vargis, E., 2016. Methods for culturing retinal pigment epithelial cells: a review of current protocols and future recommendations. J. Tissue Eng. 7, 2041731416650838. https://doi.org/10.1177/2041731416650838

Fuhrmann, S., 2010. Eye morphogenesis and patterning of the optic vesicle. Curr. Top. Dev. Biol. 93, 61–84. https://doi.org/10.1016/B978-0-12-385044-7.00003-5

Gage, P.J., Rhoades, W., Prucka, S.K., Hjalt, T., 2005. Fate maps of neural crest and mesoderm in the mammalian eye. Invest. Ophthalmol. Vis. Sci. 46, 4200–4208. https://doi.org/10.1167/iovs.05-0691

Gerard, X., Perrault, I., Hanein, S., Silva, E., Bigot, K., Defoort-Delhemmes, S., Rio, M., Munnich, A., Scherman, D., Kaplan, J., Kichler, A., Rozet, J.-M., 2012. AON-mediated Exon Skipping Restores Ciliation in Fibroblasts Harboring the Common Leber Congenital Amaurosis CEP290 Mutation. Mol. Ther. Nucleic Acids 1, e29. https://doi.org/10.1038/mtna.2012.21

Gerber, S., Alzayady, K.J., Burglen, L., Brémond-Gignac, D., Marchesin, V., Roche, O., Rio, M., Funalot, B., Calmon, R., Durr, A., Gil-da-Silva-Lopes, V.L., Ribeiro Bittar, M.F., Orssaud, C., Héron, B., Ayoub, E., Berquin, P., Bahi-Buisson, N., Bole, C., Masson, C., Munnich, A., Simons, M., Delous, M., Dollfus, H., Boddaert, N., Lyonnet, S., Kaplan, J., Calvas, P., Yule, D.I., Rozet, J.-M., Fares Taie, L., 2016. Recessive and Dominant De Novo ITPR1 Mutations Cause Gillespie Syndrome. Am. J. Hum. Genet. 98, 971–980. https://doi.org/10.1016/j.ajhg.2016.03.004

Ghiasvand, N.M., Rudolph, D.D., Mashayekhi, M., Brzezinski, J.A., Goldman, D., Glaser, T., 2011. Deletion of a remote enhancer near ATOH7 disrupts retinal neurogenesis, causing NCRNA disease. Nat. Neurosci. 14, 578–586. https://doi.org/10.1038/nn.2798

Gillespie, F.D., 1965. Aniridia, cerebellar ataxia, and oligophrenia in siblings. Arch. Ophthalmol. Chic. Ill 1960 73, 338–341. https://doi.org/10.1001/archopht.1965.00970030340008
Glass, A.S., Dahm, R., 2004. The zebrafish as a model organism for eye development. Ophthalmic Res. 36, 4–24. https://doi.org/10.1159/000076105
Gould, D.B., Smith, R.S., John, S.W.M., 2004. Anterior segment development relevant to glaucoma. Int. J. Dev. Biol. 48, 1015–1029. https://doi.org/10.1387/ijdb.041865dg
Gräf, M.H., Jungherr, A., 2002. Congenital Mydriasis, Failure of Accommodation, and Patent Ductus Arteriosus. Arch. Ophthalmol. 120, 509–510.
Graw, J., 2010. Eye Development, in: Current Topics in Developmental Biology. Elsevier, pp. 343–386. https://doi.org/10.1016/S0070-2153(10)90010-0
Green, D.J., Lenassi, E., Manning, C.S., McGaughey, D., Sharma, V., Black, G.C., Ellingford, J.M., Sergouniotis, P.I., 2021. North Carolina Macular Dystrophy: Phenotypic Variability and Computational Analysis of Disease-Associated Noncoding Variants. Invest. Ophthalmol. Vis. Sci. 62, 16. https://doi.org/10.1167/iovs.62.7.16
Gregory-Evans, C.Y., Wang, X., Wasan, K.M., Zhao, J., Metcalfe, A.L., Gregory-Evans, K., 2014. Postnatal manipulation of Pax6 dosage reverses congenital tissue malformation defects [WWW Document]. https://doi.org/10.1172/JCI70462
Griewank, K.G., Yu, X., Khalili, J., Sozen, M.M., Stempke-Hale, K., Bernatchez, C., Wardell, S., Bastian, B.C., Woodman, S.E., 2012. Genetic and Molecular Characterization of Uveal Melanoma Cell Lines. Pigment Cell Melanoma Res. 25, 182–187. https://doi.org/10.1111/j.1755-148X.2012.00971.x
Grønskov, K., Ek, J., Brondum-Nielsen, K., 2007. Oculocutaneous albinism. Orphanet J. Rare Dis. 2, 43. https://doi.org/10.1186/1750-1172-2-43
Gupta, S., Lytvynchuk, L., Ardan, T., Studenovska, H., Sharma, R., Faura, G., Eide, L., Shanker Verma, R., Znaor, L., Erceg, S., Stieger, K., Motlik, J., Petrovski, G., Bharti, K., 2023. Progress in Stem Cells-Based Replacement Therapy for Retinal Pigment Epithelium: In Vitro Differentiation to In Vivo Delivery. Stem Cells Transl. Med. 12, 536–552. https://doi.org/10.1093/stcltm/szad039
Haddad, A., Ait Boujmia, O.K., El Maaloum, L., Dehbi, H., 2021. Meta-analysis of CYP1B1 gene mutations in primary congenital glaucoma patients. Eur. J. Ophthalmol. 31, 2796–2807. https://doi.org/10.1177/11206721211016308
Hanson, I.M., Fletcher, J.M., Jordan, T., Brown, A., Taylor, D., Adams, R.J., Punnett, H.H., van Heyningen, V., 1994. Mutations at the PAX6 locus are found in heterogeneous anterior segment malformations including Peters' anomaly. Nat. Genet. 6, 168–173. https://doi.org/10.1038/ng0294-168
Haug, P., Koller, S., Maggi, J., Lang, E., Feil, S., Wlodarczyk, A., Bähr, L., Steindl, K., Rohrbach, M., Gerth-Kahlert, C., Berger, W., 2021. Whole Exome Sequencing in Coloboma/Microphthalmia: Identification of Novel and Recurrent Variants in Seven Genes. Genes 12, 65. https://doi.org/10.3390/genes12010065
Heavner, W., Pevny, L., 2012. Eye Development and Retinogenesis. Cold Spring Harb. Perspect. Biol. 4, a008391. https://doi.org/10.1101/cshperspect.a008391
Hingorani, M., Hanson, I., van Heyningen, V., 2012. Aniridia. Eur. J. Hum. Genet. EJHG 20, 1011–1017. https://doi.org/10.1038/ejhg.2012.100
Hoffmann, A., Nakamura, K., Tsonis, P.A., 2014. Intrinsic Lens Forming Potential of Mouse Lens Epithelial versus Newt Iris Pigment Epithelial Cells in Three-Dimensional Culture. Tissue Eng. Part C Methods 20, 91–103. https://doi.org/10.1089/ten.tec.2013.0078
Holt, R.J., Young, R.M., Crespo, B., Ceroni, F., Curry, C.J., Bellacchio, E., Bax, D.A., Ciolfi, A., Simon, M., Fagerberg, C.R., van Binsbergen, E., De Luca, A., Memo, L., Dobyns, W.B., Mohammed, A.A., Clokie, S.J.H., Zazo Seco, C., Jiang, Y.-H., Sørensen, K.P., Andersen, H., Sullivan, J., Powis, Z., Chassevent, A., Smith-Hicks, C., Petrovski, S., Antoniadi, T., Shashi, V., Gelb, B.D., Wilson, S.W., Gerrelli, D., Tartaglia, M., Chassaing, N., Calvas, P., Ragge, N.K., 2019. De Novo Missense Variants in FBXW11 Cause Diverse Developmental Phenotypes Including Brain, Eye, and Digit Anomalies. Am. J. Hum. Genet. 105, 640–657. https://doi.org/10.1016/j.ajhg.2019.07.005

Holth, S., Berner, O., 1923. Congenital Miosis or pinhole pupils owing to developmental faults of the dilator muscle. Br. J. Ophthalmol. 7, 401–419. https://doi.org/10.1136/bjo.7.9.401
Honkanen, R.A., Nishimura, D.Y., Swiderski, R.E., Bennett, S.R., Hong, S., Kwon, Y.H., Stone, E.M., Sheffield, V.C., Alward, W.L.M., 2003. A family with Axenfeld-Rieger syndrome and Peters Anomaly caused by a point mutation (Phe112Ser) in the FOXC1 gene. Am. J. Ophthalmol. 135, 368–375. https://doi.org/10.1016/s0002-9394(02)02061-5
Hornby, S.J., Adolph, S., Gilbert, C.E., Dandona, L., Foster, A., 2000. Visual acuity in children with coloboma1: Clinical features and a new phenotypic classification system. Ophthalmology 107, 511–520. https://doi.org/10.1016/S0161-6420(99)00140-2
Hosseini, H.S., Tabber, L.A., 2018. How mechanical forces shape the developing eye. Prog. Biophys. Mol. Biol. 137. https://doi.org/10.1016/j.pbiomolbio.2018.01.004
Hu, D.N., Ritch, R., McCormick, S.A., Pelton-Henrion, K., 1992. Isolation and cultivation of human iris pigment epithelium. Invest. Ophthalmol. Vis. Sci. 33, 2443–2453.
Ibaraki, N., Chen, S.-C., Lin, L.-R., Okamoto, H., Pipas, J.M., Reddy, V.N., 1998. Human Lens Epithelial Cell Line. Exp. Eye Res. 67, 577–585. https://doi.org/10.1006/exer.1998.0551
Jat, N.S., Tripathy, K., 2023. Peters Anomaly, in: StatPearls. StatPearls Publishing, Treasure Island (FL).
Jean, D., Ewan, K., Gruss, P., 1998. Molecular regulators involved in vertebrate eye development. Mech. Dev. 76, 3–18. https://doi.org/10.1016/S0925-4773(98)00117-8
Jeon, C.J., Strettoi, E., Masland, R.H., 1998. The major cell populations of the mouse retina. J. Neurosci. Off. J. Soc. Neurosci. 18, 8936–8946. https://doi.org/10.1523/JNEUROSCI.18-21-08936.1998
Johnen, S., Wickert, L., Meier, M., Salz, A.K., Walter, P., Thumann, G., 2011. Presence of Xenogenic Mouse RNA in RPE and IPE Cells Cultured on Mitotically Inhibited 3T3 Fibroblasts. Investig. Opthalmology Vis. Sci. 52, 2817. https://doi.org/10.1167/iovs.10-6429
Johnson, D.H., Tschumper, R.C., 1986. Human Trabecular Meshwork Organ Culture 28, 9.
Kaplan, H.J., 2007. Anatomy and function of the eye. Chem. Immunol. Allergy 92, 4–10. https://doi.org/10.1159/000099236
Karaconji, T., Zagora, S., Grigg, J.R., 2022. Approach to childhood glaucoma: A review. Clin. Experiment. Ophthalmol. 50, 232–246. https://doi.org/10.1111/ceo.14039
Karamichos, D., Guo, X.Q., Hutcheon, A.E.K., Zieske, J.D., 2010. Human corneal fibrosis: an in vitro model. Invest. Ophthalmol. Vis. Sci. 51, 1382–1388. https://doi.org/10.1167/iovs.09-3860
Kaur, K., Gurnani, B., 2023. Primary Congenital Glaucoma, in: StatPearls. StatPearls Publishing, Treasure Island (FL).
Kaushik, S., Dubey, S., Choudhary, S., Ratna, R., Pandav, S.S., Khan, A.O., 2022. Anterior segment dysgenesis: Insights into the genetics and pathogenesis. Indian J. Ophthalmol. 70, 2293–2303. https://doi.org/10.4103/ijo.IJO_3223_21
Keehan, L., Jiang, M.-M., Li, X., Marom, R., Dai, H., Murdock, D., Liu, P., Hunter, J., Heaney, J.D., Robak, L., Emrick, L., Lotze, T., Blieden, L., Lewis, R.A., Levin, A.V., Capasso, J., Craigen, W., Rosenfeld, J.A., Lee, B., Burrage, L.C., 2021. A Novel De Novo Intronic Variant in ITPR1 Causes Gillespie Syndrome. Am. J. Med. Genet. A. 185, 2315–2324. https://doi.org/10.1002/ajmg.a.62232
Keller, K.E., Bhattacharya, S.K., Borrás, T., Brunner, T.M., Chansangpetch, S., Clark, A.F., Dismuke, W.M., Du, Y., Elliott, M.H., Ethier, C.R., Faralli, J.A., Freddo, T.F., Fuchshofer, R., Giovingo, M., Gong, H., Gonzalez, P., Huang, A., Johnstone, M.A., Kaufman, P.L., Kelley, M.J., Knepper, P.A., Kopczynski, C.C., Kuchtey, J.G., Kuchtey, R.W., Kuehn, M.H., Lieberman, R.L., Lin, S.C., Liton, P., Liu, Y., Lütjen-Drecoll, E., Mao, W., Masis-Solano, M., McDonnell, F., McDowell, C.M., Overby, D.R., Pattabiraman, P.P., Raghunathan, V.K., Rao, P.V., Rhee, D.J., Chowdhury, U.R., Russell, P., Samples, J.R., Schwartz, D., Stubbs, E.B., Tamm, E.R., Tan, J.C., Toris,

C.B., Torrejon, K.Y., Vranka, J.A., Wirtz, M.K., Yorio, T., Zhang, J., Zode, G.S., Fautsch, M.P., Peters, D.M., Acott, T.S., Stamer, W.D., 2018. Consensus recommendations for trabecular meshwork cell isolation, characterization and culture. Exp. Eye Res. 171, 164–173. https://doi.org/10.1016/j.exer.2018.03.001

Kha, C.X., Guerin, D.J., Tseng, K.A.-S., 2019. Using the Xenopus Developmental Eye Regrowth System to Distinguish the Role of Developmental Versus Regenerative Mechanisms. Front. Physiol. 10.

Khan, S.Y., Vasanth, S., Kabir, F., Gottsch, J.D., Khan, A.O., Chaerkady, R., Lee, M.-C.W., Leitch, C.C., Ma, Z., Laux, J., Villasmil, R., Khan, S.N., Riazuddin, S., Akram, J., Cole, R.N., Talbot, C.C., Pourmand, N., Zaghloul, N.A., Hejtmancik, J.F., Riazuddin, S.A., 2016. FOXE3 contributes to Peters anomaly through transcriptional regulation of an autophagy-associated protein termed DNAJB1. Nat. Commun. 7, 10953. https://doi.org/10.1038/ncomms10953

Kim, S., Yu, N.-K., Kaang, B.-K., 2015. CTCF as a multifunctional protein in genome regulation and gene expression. Exp. Mol. Med. 47, e166–e166. https://doi.org/10.1038/emm.2015.33

Kiso, M., Tanaka, S., Saba, R., Matsuda, S., Shimizu, A., Ohyama, M., Okano, H.J., Shiroishi, T., Okano, H., Saga, Y., 2009. The disruption of Sox21-mediated hair shaft cuticle differentiation causes cyclic alopecia in mice. Proc. Natl. Acad. Sci. 106, 9292–9297. https://doi.org/10.1073/pnas.0808324106

Krijger, P.H.L., Geeven, G., Bianchi, V., Hilvering, C.R.E., de Laat, W., 2020. 4C-seq from beginning to end: A detailed protocol for sample preparation and data analysis. Methods, Methods for Mapping Three-Dimensional Genome Architecture 170, 17–32. https://doi.org/10.1016/j.ymeth.2019.07.014

Kurilec, J.M., Zaidman, G.W., 2014. Incidence of Peters anomaly and congenital corneal opacities interfering with vision in the United States. Cornea 33, 848–850. https://doi.org/10.1097/ICO.0000000000000182

Kurtul, B.E., Özer, P.A., Çağlar, A.A., Kabataş, E.U., 2016. Bilateral congenital mydriasis in a child case. Turk. Arch. Pediatr. Pediatri Arş. 51, 176–177. https://doi.org/10.5152/TurkPediatriArs.2016.4194

Lan, X., Wen, L., Li, K., Liu, X., Luo, B., Chen, F., Xie, D., Kung, H., 2011. Comparative analysis of duplicated sox21 genes in zebrafish. Dev. Growth Differ. 53, 347–356. https://doi.org/10.1111/j.1440-169X.2010.01239.x

Landsend, E.C.S., Lagali, N., Utheim, T.P., 2021. Congenital aniridia - A comprehensive review of clinical features and therapeutic approaches. Surv. Ophthalmol. 66, 1031–1050. https://doi.org/10.1016/j.survophthal.2021.02.011

Langouët, M., Jolicoeur, C., Javed, A., Mattar, P., Gearhart, M.D., Daiger, S.P., Bertelsen, M., Tranebjærg, L., Rendtorff, N.D., Grønskov, K., Jespersgaard, C., Chen, R., Sun, Z., Li, H., Alirezaie, N., Majewski, J., Bardwell, V.J., Sui, R., Koenekoop, R.K., Cayouette, M., 2022. Mutations in BCOR, a co-repressor of CRX/OTX2, are associated with early-onset retinal degeneration. Sci. Adv. 8, eabh2868. https://doi.org/10.1126/sciadv.abh2868

Lenstra, T.L., Rodriguez, J., Chen, H., Larson, D.R., 2016. Transcription Dynamics in Living Cells. Annu. Rev. Biophys. 45, 25–47. https://doi.org/10.1146/annurev-biophys-062215-010838

Li, Z., Gu, S., Quan, Y., Varadaraj, K., Jiang, J.X., 2021. Development of a potent embryonic chick lens model for studying congenital cataracts in vivo. Commun. Biol. 4, 1–13. https://doi.org/10.1038/s42003-021-01849-0

Littink, K.W., Stappers, P.T.Y., Riemslag, F.C.C., Talsma, H.E., van Genderen, M.M., Cremers, F.P.M., Collin, R.W.J., van den Born, L.I., 2018. Autosomal Recessive NRL Mutations in Patients with Enhanced S-Cone Syndrome. Genes 9, 68. https://doi.org/10.3390/genes9020068

Love, S.L., Emerson, J.D., Koide, K., Hoskins, A.A., 2023. Pre-mRNA splicing-associated diseases and therapies. RNA Biol. 20, 525–538. https://doi.org/10.1080/15476286.2023.2239601

Lupiáñez, D.G., Kraft, K., Heinrich, V., Krawitz, P., Brancati, F., Klopocki, E., Horn, D., Kayserili, H., Opitz, J.M., Laxova, R., Santos-Simarro, F., Gilbert-Dussardier, B., Wittler, L., Borschiwer, M., Haas, S.A., Osterwalder, M., Franke, M., Timmermann, B., Hecht, J., Spielmann, M., Visel, A., Mundlos, S., 2015. Disruptions of topological chromatin domains cause pathogenic rewiring of gene-enhancer interactions. Cell 161, 1012–1025. https://doi.org/10.1016/j.cell.2015.04.004

Lutty, G.A., McLeod, D.S., 2018. Development of the hyaloid, choroidal and retinal vasculatures in the fetal human eye. Prog. Retin. Eye Res. 62, 58–76. https://doi.org/10.1016/j.preteyeres.2017.10.001

Macdonald, R., Barth, K.A., Xu, Q., Holder, N., Mikkola, I., Wilson, S.W., 1995. Midline signalling is required for Pax gene regulation and patterning of the eyes. Development 121, 3267–3278. https://doi.org/10.1242/dev.121.10.3267

Madreperla, S.A., Bookstein, R., Jones, O.W., Lee, W.H., 1991. Retinoblastoma cell lines Y79, RB355 and WERI-Rb27 are genetically related. Ophthalmic Paediatr. Genet. 12, 49–56. https://doi.org/10.3109/13816819109023085

Martinez-Morales, J.-R., Cavodeassi, F., Bovolenta, P., 2017. Coordinated Morphogenetic Mechanisms Shape the Vertebrate Eye. Front. Neurosci. 11, 721. https://doi.org/10.3389/fnins.2017.00721

Masland, R.H., 2001. The fundamental plan of the retina. Nat. Neurosci. 4, 877–886. https://doi.org/10.1038/nn0901-877

Matharu, N., Ahituv, N., 2015. Minor Loops in Major Folds: Enhancer–Promoter Looping, Chromatin Restructuring, and Their Association with Transcriptional Regulation and Disease. PLOS Genet. 11, e1005640. https://doi.org/10.1371/journal.pgen.1005640

McArthur, E., Capra, J.A., 2021. Topologically associating domain boundaries that are stable across diverse cell types are evolutionarily constrained and enriched for heritability. Am. J. Hum. Genet. 108, 269–283. https://doi.org/10.1016/j.ajhg.2021.01.001

McEntagart, M., Williamson, K.A., Rainger, J.K., Wheeler, A., Seawright, A., De Baere, E., Verdin, H., Bergendahl, L.T., Quigley, A., Rainger, J., Dixit, A., Sarkar, A., López Laso, E., Sanchez-Carpintero, R., Barrio, J., Bitoun, P., Prescott, T., Riise, R., McKee, S., Cook, J., McKie, L., Ceulemans, B., Meire, F., Temple, I.K., Prieur, F., Williams, J., Clouston, P., Németh, A.H., Banka, S., Bengani, H., Handley, M., Freyer, E., Ross, A., van Heyningen, V., Marsh, J.A., Elmslie, F., FitzPatrick, D.R., 2016. A Restricted Repertoire of De Novo Mutations in ITPR1 Cause Gillespie Syndrome with Evidence for Dominant-Negative Effect. Am. J. Hum. Genet. 98, 981–992. https://doi.org/10.1016/j.ajhg.2016.03.018

Michels, K., Bohnsack, B.L., 2023. Ophthalmological Manifestations of Axenfeld-Rieger Syndrome: Current Perspectives. Clin. Ophthalmol. Auckl. NZ 17, 819–828. https://doi.org/10.2147/OPTH.S379853

Miesfeld, J.B., Brown, N.L., 2019. Eye organogenesis: A hierarchical view of ocular development, in: Current Topics in Developmental Biology. Elsevier, pp. 351–393. https://doi.org/10.1016/bs.ctdb.2018.12.008

Mocan, M.C., Mehta, A.A., Aref, A.A., 2019. Update in Genetics and Surgical Management of Primary Congenital Glaucoma. Turk. J. Ophthalmol. 49, 347–355. https://doi.org/10.4274/tjo.galenos.2019.28828

Mui, S.H., Kim, J.W., Lemke, G., Bertuzzi, S., 2005. Vax genes ventralize the embryonic eye. Genes Dev. 19, 1249–1259. https://doi.org/10.1101/gad.1276605

Nabih, O., Hamdani, H., ELMaaloum, L., Allali, B., ELkettani, A., 2022. Gillespie syndrome: An atypical form and review of the literature. Ann. Med. Surg. 74, 103244. https://doi.org/10.1016/j.amsu.2022.103244

Nelson, L.B., Spaeth, G.L., Nowinski, T.S., Margo, C.E., Jackson, L., 1984. Aniridia. A review. Surv. Ophthalmol. 28, 621–642. https://doi.org/10.1016/0039-6257(84)90184-X

Nguyen, M.-T.T., Arnheiter, H., 2000. Signaling and transcriptional regulation in early mammalian eye development: a link between FGF and MITF. Development 127, 3581–3591. https://doi.org/10.1242/dev.127.16.3581

Nilsson, D.E., 2013. Eye evolution and its functional basis. Vis. Neurosci. 30, 5–20. https://doi.org/10.1017/S0952523813000035
Oh, A., Loew, E.R., Foster, M.L., Davidson, M.G., English, R.V., Gervais, K.J., Herring, I.P., Mowat, F.M., 2018. Phenotypic characterization of complete CSNB in the inbred research beagle: how common is CSNB in research and companion dogs? Doc. Ophthalmol. Adv. Ophthalmol. 137, 87–101. https://doi.org/10.1007/s10633-018-9653-y
O'Hara-Wright, M., Gonzalez-Cordero, A., 2020. Retinal organoids: a window into human retinal development. Dev. Camb. Engl. 147, dev189746. https://doi.org/10.1242/dev.189746
Orozco, G., Schoenfelder, S., Walker, N., Eyre, S., Fraser, P., 2022. 3D genome organization links non-coding disease-associated variants to genes. Front. Cell Dev. Biol. 10, 995388. https://doi.org/10.3389/fcell.2022.995388
Panigrahi, A., O'Malley, B.W., 2021. Mechanisms of enhancer action: the known and the unknown. Genome Biol. 22, 108. https://doi.org/10.1186/s13059-021-02322-1
Parfitt, D.A., Lane, A., Ramsden, C.M., Carr, A.-J.F., Munro, P.M., Jovanovic, K., Schwarz, N., Kanuga, N., Muthiah, M.N., Hull, S., Gallo, J.-M., da Cruz, L., Moore, A.T., Hardcastle, A.J., Coffey, P.J., Cheetham, M.E., 2016. Identification and Correction of Mechanisms Underlying Inherited Blindness in Human iPSC-Derived Optic Cups. Cell Stem Cell 18, 769–781. https://doi.org/10.1016/j.stem.2016.03.021
Patel, A., Sowden, J.C., 2019. Genes and pathways in optic fissure closure. Semin. Cell Dev. Biol., Craniofacial development 91, 55–65. https://doi.org/10.1016/j.semcdb.2017.10.010
Patel, N., Khan, A.O., Alsahli, S., Abdel-Salam, G., Nowilaty, S.R., Mansour, A.M., Nabil, A., Al-Owain, M., Sogati, S., Salih, M.A., Kamal, A.M., Alsharif, H., Alsaif, H.S., Alzahrani, S.S., Abdulwahab, F., Ibrahim, N., Hashem, M., Faquih, T., Shah, Z.A., Abouelhoda, M., Monies, D., Dasouki, M., Shaheen, R., Wakil, S.M., Aldahmesh, M.A., Alkuraya, F.S., 2018. Genetic investigation of 93 families with microphthalmia or posterior microphthalmos. Clin. Genet. 93, 1210–1222. https://doi.org/10.1111/cge.13239
Paulavičiūtė-Baikštienė, D., Baršauskaitė, R., Janulevičienė, I., 2013. New insights into pathophysiological mechanisms regulating conventional aqueous humor outflow. Med. Kaunas Lith. 49, 165–169.
Pauls, S., Smith, S.F., Elgar, G., 2012. Lens development depends on a pair of highly conserved Sox21 regulatory elements. Dev. Biol. 365, 310–318. https://doi.org/10.1016/j.ydbio.2012.02.025
Plaisancié, J., Ceroni, F., Holt, R., Zazo Seco, C., Calvas, P., Chassaing, N., Ragge, N.K., 2019. Genetics of anophthalmia and microphthalmia. Part 1: Non-syndromic anophthalmia/microphthalmia. Hum. Genet. 138, 799–830. https://doi.org/10.1007/s00439-019-01977-y
Plaisancié, J., Tarilonte, M., Ramos, P., Jeanton-Scaramouche, C., Gaston, V., Dollfus, H., Aguilera, D., Kaplan, J., Fares-Taie, L., Blanco-Kelly, F., Villaverde, C., Francannet, C., Goldenberg, A., Arroyo, I., Rozet, J.M., Ayuso, C., Chassaing, N., Calvas, P., Corton, M., 2018. Implication of non-coding PAX6 mutations in aniridia. Hum. Genet. 137, 831–846. https://doi.org/10.1007/s00439-018-1940-x
Plank, J.L., Dean, A., 2014. Enhancer function: mechanistic and genome-wide insights come together. Mol. Cell 55, 5–14. https://doi.org/10.1016/j.molcel.2014.06.015
Pozza, E., Verdin, H., Deconinck, H., Dheedene, A., Menten, B., De Baere, E., Balikova, I., 2020. Microcoria due to first duplication of 13q32.1 including the GPR180 gene and maternal mosaicism. Eur. J. Med. Genet. 63, 103918. https://doi.org/10.1016/j.ejmg.2020.103918
Purves, D., Augustine, G.J., Fitzpatrick, D., Katz, L.C., LaMantia, A.-S., McNamara, J.O., Williams, S.M., 2001. Anatomical Distribution of Rods and Cones, in: Neuroscience. 2nd Edition. Sinauer Associates.
Quaranta-Leoni, F.M., 2011. Congenital anophthalmia: current concepts in management. Curr. Opin. Ophthalmol. 22, 380–384. https://doi.org/10.1097/ICU.0b013e328349948a

Ragge, N.K., Subak-Sharpe, I.D., Collin, J.R.O., 2007. A practical guide to the management of anophthalmia and microphthalmia. Eye Lond. Engl. 21, 1290–1300. https://doi.org/10.1038/sj.eye.6702858

Raghunathan, V., Nartey, A., Dhamodaran, K., Baidouri, H., Staverosky, J.A., Keller, K.E., Zientek, K., Reddy, A., Acott, T., Vranka, J.A., 2023. Characterization of extracellular matrix deposited by segmental trabecular meshwork cells. Exp. Eye Res. 234, 109605. https://doi.org/10.1016/j.exer.2023.109605

Ratti, M., Lampis, A., Ghidini, M., Salati, M., Mirchev, M.B., Valeri, N., Hahne, J.C., 2020. MicroRNAs (miRNAs) and Long Non-Coding RNAs (lncRNAs) as New Tools for Cancer Therapy: First Steps from Bench to Bedside. Target. Oncol. 15, 261–278. https://doi.org/10.1007/s11523-020-00717-x

Reddy, V.N., Lin, L.-R., Arita, T., Zigler, J.S., Huang, Q.L., 1988. Crystallins and their synthesis in human lens epithelial cells in tissue culture. Exp. Eye Res. 47, 465–478. https://doi.org/10.1016/0014-4835(88)90057-7

Reis, L.M., Maheshwari, M., Capasso, J., Atilla, H., Dudakova, L., Thompson, S., Zitano, L., Lay-Son, G., Lowry, R.B., Black, J., Lee, J., Shue, A., Kremlikova Pourova, R., Vaneckova, M., Skalicka, P., Jedlickova, J., Trkova, M., Williams, B., Richard, G., Bachman, K., Seeley, A.H., Costakos, D., Glaser, T.M., Levin, A.V., Liskova, P., Murray, J.C., Semina, E.V., 2023. Axenfeld-Rieger syndrome: more than meets the eye. J. Med. Genet. 60, 368–379. https://doi.org/10.1136/jmg-2022-108646

Reis, L.M., Semina, E.V., 2011. GENETICS OF ANTERIOR SEGMENT DYSGENESIS DISORDERS. Curr. Opin. Ophthalmol. 22, 314–324. https://doi.org/10.1097/ICU.0b013e328349412b

Richardson, P., Schulenburg, W.E., 1992. Bilateral congenital mydriasis. Br. J. Ophthalmol. 76, 632–633. https://doi.org/10.1136/bjo.76.10.632

Richardson, R., Tracey-White, D., Webster, A., Moosajee, M., 2017. The zebrafish eye—a paradigm for investigating human ocular genetics. Eye 31, 68–86. https://doi.org/10.1038/eye.2016.198

Rogalska, M.E., Vivori, C., Valcárcel, J., 2023. Regulation of pre-mRNA splicing: roles in physiology and disease, and therapeutic prospects. Nat. Rev. Genet. 24, 251–269. https://doi.org/10.1038/s41576-022-00556-8

Rouillac, C., Roche, O., Marchant, D., Bachner, L., Kobetz, A., Toulemont, P.J., Orssaud, C., Urvoy, M., Odent, S., Le Marec, B., Abitbol, M., Dufier, J.L., 1998. Mapping of a congenital microcoria locus to 13q31-q32. Am. J. Hum. Genet. 62, 1117–1122. https://doi.org/10.1086/301841

Roulez, F.M.J., Faes, F., Delbeke, P., Van Bogaert, P., Rodesch, G., De Zaeytijd, J., Depasse, F., Coucke, P.J., Meire, F.M., 2014. Congenital Fixed Dilated Pupils Due to ACTA2–Multisystemic Smooth Muscle Dysfunction Syndrome. J. Neuroophthalmol. 34, 137. https://doi.org/10.1097/WNO.0000000000000090

Schoenfelder, S., Javierre, B.-M., Furlan-Magaril, M., Wingett, S.W., Fraser, P., 2018. Promoter Capture Hi-C: High-resolution, Genome-wide Profiling of Promoter Interactions. J. Vis. Exp. JoVE 57320. https://doi.org/10.3791/57320

Sergouniotis, P.I., Ellingford, J.M., O'Sullivan, J., Fenerty, C.H., Black, G.C., 2017. Genome sequencing identifies a large deletion at 13q32.1 as the cause of microcoria and childhood-onset glaucoma. Acta Ophthalmol. (Copenh.) 95, e249–e250. https://doi.org/10.1111/aos.13246

Shah, S.P., Taylor, A.E., Sowden, J.C., Ragge, N., Russell-Eggitt, I., Rahi, J.S., Gilbert, C.E., Surveillance of Eye Anomalies Special Interest Group, 2012. Anophthalmos, microphthalmos, and Coloboma in the United kingdom: clinical features, results of investigations, and early management. Ophthalmology 119, 362–368. https://doi.org/10.1016/j.ophtha.2011.07.039

Sharif, R., Khaled, M.L., McKay, T.B., Liu, Y., Karamichos, D., 2019. Transcriptional profiling of corneal stromal cells derived from patients with keratoconus. Sci. Rep. 9, 12567. https://doi.org/10.1038/s41598-019-48983-8

Shimada, H., Lu, Q., Insinna-Kettenhofen, C., Nagashima, K., English, M.A., Semler, E.M., Mahgerefteh, J., Cideciyan, A.V., Li, T., Brooks, B.P., Gunay-Aygun, M., Jacobson, S.G., Cogliati, T., Westlake, C.J., Swaroop, A., 2017. In Vitro Modeling Using Ciliopathy-Patient-Derived Cells Reveals Distinct Cilia Dysfunctions Caused by CEP290 Mutations. Cell Rep. 20, 384–396. https://doi.org/10.1016/j.celrep.2017.06.045

Shirazi Fard, S., Blixt, M., Hallböök, F., 2015. Whole Retinal Explants from Chicken Embryos for Electroporation and Chemical Reagent Treatments. J. Vis. Exp. JoVE 53202. https://doi.org/10.3791/53202

Sjödal, M., Edlund, T., Gunhaga, L., 2007. Time of Exposure to BMP Signals Plays a Key Role in the Specification of the Olfactory and Lens Placodes Ex Vivo. Dev. Cell 13, 141–149. https://doi.org/10.1016/j.devcel.2007.04.020

Skalicky, S.E., 2016. The Ciliary Body and Aqueous Fluid Formation and Drainage, in: Skalicky, S.E. (Ed.), Ocular and Visual Physiology: Clinical Application. Springer, Singapore, pp. 67–83. https://doi.org/10.1007/978-981-287-846-5_5

Skalicky, S.E., White, A.J.R., Grigg, J.R., Martin, F., Smith, J., Jones, M., Donaldson, C., Smith, J.E.H., Flaherty, M., Jamieson, R.V., 2013. Microphthalmia, anophthalmia, and coloboma and associated ocular and systemic features: understanding the spectrum. JAMA Ophthalmol. 131, 1517–1524. https://doi.org/10.1001/jamaophthalmol.2013.5305

Slavotinek, A.M., 2011. Eye development genes and known syndromes. Mol. Genet. Metab. 104, 448–456. https://doi.org/10.1016/j.ymgme.2011.09.029

Strungaru, M.H., Footz, T., Liu, Y., Berry, F.B., Belleau, P., Semina, E.V., Raymond, V., Walter, M.A., 2011. PITX2 Is Involved in Stress Response in Cultured Human Trabecular Meshwork Cells through Regulation of SLC13A3. Invest. Ophthalmol. Vis. Sci. 52, 7625–7633. https://doi.org/10.1167/iovs.10-6967

Taha Najim, R., Topa, A., Jugård, Y., Casslén, B., Odersjö, M., Andersson Grönlund, M., 2020. Children and young adults with anophthalmia and microphthalmia: Diagnosis and Management. Acta Ophthalmol. (Copenh.) 98, 848–858. https://doi.org/10.1111/aos.14427

Tang, J., Li, Q., Cheng, B., Jing, L., 2014. Primary culture of human face skin melanocytes for the study of hyperpigmentation. Cytotechnology 66, 891–898. https://doi.org/10.1007/s10616-013-9643-6

Tanizawa, H., Noma, K., 2012. Unravelling global genome organization by 3C-seq. Semin. Cell Dev. Biol. 23, 213–221. https://doi.org/10.1016/j.semcdb.2011.11.003

Tawara, A., Itou, K., Kubota, T., Harada, Y., Tou, N., Hirose, N., 2005. Congenital microcoria associated with late-onset developmental glaucoma. J. Glaucoma 14, 409–413. https://doi.org/10.1097/01.ijg.0000176931.29477.6e

Tenenbaum, E., Kornblueth, W., 1958. Cultivation of adult human iris in vitro. AMA Arch. Ophthalmol. 60, 312–318. https://doi.org/10.1001/archopht.1958.00940080328020

Thakur, J., Packiaraj, J., Henikoff, S., 2021. Sequence, Chromatin and Evolution of Satellite DNA. Int. J. Mol. Sci. 22, 4309. https://doi.org/10.3390/ijms22094309

Thumann, G., 2001. Development and Cellular Functions of the Iris Pigment Epithelium. Surv. Ophthalmol. 45, 345–354. https://doi.org/10.1016/S0039-6257(00)00195-8

Tiukacheva, E.A., Ulianov, S.V., Karpukhina, A., Razin, S.V., Vassetzky, Y., 2023. 3D genome alterations and editing in pathology. Mol. Ther. 31, 924–933. https://doi.org/10.1016/j.ymthe.2023.02.005

Toris, C.B., 2010. Pharmacology of Aqueous Humor Formation, in: Dartt, D.A. (Ed.), Encyclopedia of the Eye. Academic Press, Oxford, pp. 312–315. https://doi.org/10.1016/B978-0-12-374203-2.00091-9

Toulemont, P.J., Urvoy, M., Coscas, G., Lecallonnec, A., Cuvilliers, A.F., 1995. Association of congenital microcoria with myopia and glaucoma. A study of 23 patients with congenital microcoria. Ophthalmology 102, 193–198. https://doi.org/10.1016/s0161-6420(95)31036-6

Trejo-Reveles, V., McTeir, L., Summers, K., Rainger, J., 2018. An analysis of anterior segment development in the chicken eye. Mech. Dev. 150, 42–49. https://doi.org/10.1016/j.mod.2018.03.001

Tripathy, K., Salini, B., 2023. Aniridia, in: StatPearls. StatPearls Publishing, Treasure Island (FL).

Tseng, A.-S., 2017. Seeing the future: using Xenopus to understand eye regeneration. Genes. N. Y. N 2000 55. https://doi.org/10.1002/dvg.23003

Tümer, Z., Bach-Holm, D., 2009. Axenfeld–Rieger syndrome and spectrum of PITX2 and FOXC1 mutations. Eur. J. Hum. Genet. 17, 1527. https://doi.org/10.1038/ejhg.2009.93

Ugarković, Đ., Sermek, A., Ljubić, S., Feliciello, I., 2022. Satellite DNAs in Health and Disease. Genes 13, 1154. https://doi.org/10.3390/genes13071154

Van de Sompele, S., Small, K.W., Cicekdal, M.B., Soriano, V.L., D'haene, E., Shaya, F.S., Agemy, S., Van der Snickt, T., Rey, A.D., Rosseel, T., Van Heetvelde, M., Vergult, S., Balikova, I., Bergen, A.A., Boon, C.J.F., De Zaeytijd, J., Inglehearn, C.F., Kousal, B., Leroy, B.P., Rivolta, C., Vaclavik, V., van den Ende, J., van Schooneveld, M.J., Gómez-Skarmeta, J.L., Tena, J.J., Martinez-Morales, J.R., Liskova, P., Vleminckx, K., De Baere, E., 2022. Multi-omics approach dissects cis-regulatory mechanisms underlying North Carolina macular dystrophy, a retinal enhanceropathy. Am. J. Hum. Genet. 109, 2029–2048. https://doi.org/10.1016/j.ajhg.2022.09.013

van Zyl, T., Yan, W., McAdams, A., Peng, Y.-R., Shekhar, K., Regev, A., Juric, D., Sanes, J.R., 2020. Cell atlas of aqueous humor outflow pathways in eyes of humans and four model species provides insight into glaucoma pathogenesis. Proc. Natl. Acad. Sci. 117, 10339–10349. https://doi.org/10.1073/pnas.2001250117

Verma, A.S., Fitzpatrick, D.R., 2007. Anophthalmia and microphthalmia. Orphanet J. Rare Dis. 2, 47. https://doi.org/10.1186/1750-1172-2-47

Vielle, A., Park, Y.K., Secora, C., Vergara, M.N., 2021. Organoids for the Study of Retinal Development and Developmental Abnormalities. Front. Cell. Neurosci. 15, 667880. https://doi.org/10.3389/fncel.2021.667880

Vincent, A., Billingsley, G., Priston, M., Glaser, T., Oliver, E., Walter, M., Ritch, R., Levin, A., Heon, E., 2006. Further support of the role of CYP1B1 in patients with Peters anomaly. Mol. Vis. 12, 506–510.

Volkmann, B.A., Zinkevich, N.S., Mustonen, A., Schilter, K.F., Bosenko, D.V., Reis, L.M., Broeckel, U., Link, B.A., Semina, E.V., 2011. Potential novel mechanism for Axenfeld-Rieger syndrome: deletion of a distant region containing regulatory elements of PITX2. Invest. Ophthalmol. Vis. Sci. 52, 1450–1459. https://doi.org/10.1167/iovs.10-6060

Wang, C., Lee, J.-E., Lai, B., Macfarlan, T.S., Xu, S., Zhuang, L., Liu, C., Peng, W., Ge, K., 2016. Enhancer priming by H3K4 methyltransferase MLL4 controls cell fate transition. Proc. Natl. Acad. Sci. 113, 11871–11876. https://doi.org/10.1073/pnas.1606857113

Wang, J., Rattner, A., Nathans, J., 2021. A transcriptome atlas of the mouse iris at single-cell resolution defines cell types and the genomic response to pupil dilation. eLife 10, e73477. https://doi.org/10.7554/eLife.73477

Wang, R., Wang, W.-Q., Li, X.-Q., Zhao, J., Yang, K., Feng, Y., Guo, M.-M., Liu, M., Liu, X., Wang, X., Yuan, Y.-Y., Gao, X., Xu, J.-C., 2021. A novel variant in FOXC1 associated with atypical Axenfeld-Rieger syndrome. BMC Med. Genomics 14, 277. https://doi.org/10.1186/s12920-021-01130-7

Wang, R., Wiggs, J.L., 2014. Common and Rare Genetic Risk Factors for Glaucoma. Cold Spring Harb. Perspect. Med. 4, a017244. https://doi.org/10.1101/cshperspect.a017244

Weasner, B.P., Anderson, J., Kumar, J.P., 2004. The Eye Specification Network in Drosophila. Proc. Indian Natl. Sci. Acad. Part B Biol. Sci. B70, 517–530.

Weh, E., Reis, L.M., Tyler, R.C., Bick, D., Rhead, W.J., Wallace, S., McGregor, T.L., Dills, S.K., Chao, M.-C., Murray, J.C., Semina, E.V., 2014. Novel B3GALTL mutations in classic Peters plus syndrome and lack of mutations in a large cohort of patients with similar phenotypes. Clin. Genet. 86, 142–148. https://doi.org/10.1111/cge.12241

Wheway, G., Nazlamova, L., Turner, D., Cross, S., 2019. 661W Photoreceptor Cell Line as a Cell Model for Studying Retinal Ciliopathies. Front. Genet. 10, 308. https://doi.org/10.3389/fgene.2019.00308

Wilde, W.R. (William R., Wilde, W.R. (William R., University College, L.L.S., 1862. An essay on the malformations and congenital diseases of the organs of sight / by W. R. Wilde. London : John Churchill.

Wisely, C.E., Sayed, J.A., Tamez, H., Zelinka, C., Abdel-Rahman, M.H., Fischer, A.J., Cebulla, C.M., 2017. The chick eye in vision research: an excellent model for the study of ocular disease. Prog. Retin. Eye Res. 61, 72–97. https://doi.org/10.1016/j.preteyeres.2017.06.004

Wong, M.D., van Eede, M.C., Spring, S., Jevtic, S., Boughner, J.C., Lerch, J.P., Henkelman, R.M., 2015. 4D atlas of the mouse embryo for precise morphological staging. Dev. Camb. Engl. 142, 3583–3591. https://doi.org/10.1242/dev.125872

Xu, S., 2015. microRNAs and inherited retinal dystrophies. Proc. Natl. Acad. Sci. U. S. A. 112, 8805–8806. https://doi.org/10.1073/pnas.1511019112

Yemanyi, F., Vranka, J., Raghunathan, V., 2020. Chapter 12 - Generating cell-derived matrices from human trabecular meshwork cell cultures for mechanistic studies, in: Caballero, D., Kundu, S.C., Reis, R.L. (Eds.), Methods in Cell Biology, Cell-Derived Matrices - Part A. Academic Press, pp. 271–307. https://doi.org/10.1016/bs.mcb.2019.10.008

Zagozewski, J.L., Zhang, Q., Eisenstat, D.D., 2014. Genetic regulation of vertebrate eye development: Review of eye development. Clin. Genet. 86, 453–460. https://doi.org/10.1111/cge.12493

Zamora, E.A., Salini, B., 2023. Axenfeld-Rieger Syndrome, in: StatPearls. StatPearls Publishing, Treasure Island (FL).

Zhang, Q., Liang, D., Yue, Y., He, L., Li, N., Jiang, D., Hu, P., Zhao, Q., 2020. Axenfeld-Rieger syndrome-associated mutants of the transcription factor FOXC1 abnormally regulate NKX2-5 in model zebrafish embryos. J. Biol. Chem. 295, 11902–11913. https://doi.org/10.1074/jbc.RA120.013287

Zheng, H., Xie, W., 2019. The role of 3D genome organization in development and cell differentiation. Nat. Rev. Mol. Cell Biol. 20, 535–550. https://doi.org/10.1038/s41580-019-0132-4

Zhou, J., Kherani, F., Bardakjian, T.M., Katowitz, J., Hughes, N., Schimmenti, L.A., Schneider, A., Young, T.L., 2008. Identification of novel mutations and sequence variants in the SOX2 and CHX10 genes in patients with anophthalmia/microphthalmia. Mol. Vis. 14, 583–592.

Résumé substantiel

Les anomalies de développement oculaire (ODDs) englobent un groupe de pathologies malformatives relativement rares, à l'origine de troubles visuels sévères, voire de cécité. Les ODDs résultent de diverses causes, et de multiples gènes sont identifiés comme responsables de ces défauts de développement. Cependant, une grande partie des patients demeure sans diagnostic moléculaire à ce jour. En effet, la morphogénèse de l'œil constitue un processus complexe et minutieusement orchestré, nécessitant l'intervention de nombreux facteurs de transcription (TF). Ces derniers régulent l'expression d'autres gènes en se liant à des séquences spécifiques de l'ADN, appelées éléments cis-régulateurs (CRE). Actuellement, une meilleure compréhension de ces éléments émerge, révélant une fréquence croissante de découvertes de variants dans ces régions non codantes de l'ADN, grâce à l'utilisation du séquençage de génome (WGS). Dans ce contexte, l'étude approfondie de ces éléments encore trop peu explorés apparaît essentielle pour résoudre les cas d'ODDs. La compréhension des fondements moléculaires de ces anomalies revêt une importance capitale pour améliorer le diagnostic et les conseils prodigués aux patients. Cette thèse vise à élucider l'étiologie moléculaire et la physiopathologie des anomalies oculaires qui surviennent à différents stades du développement, s'appuyant sur l'analyse du génome, tant codant que non codant.

La première partie de ce travail s'intéresse à cette maladie très rare qu'est la microcorie congénitale (MCOR), caractérisée par une petite pupille résultant d'un défaut de développement de l'iris. Nous avons rassemblé toutes les données disponibles de la littérature portant sur des cas de miosis congénital isolé afin de réaliser la première revue sur cette maladie depuis sa description originale en 1862. L'objectif de ce projet, en plus de fournir un travail complet sur ce sujet, était de trouver des pistes pour expliquer l'étiologie du glaucome (GLC) et de la myopie, fréquemment associés à ce défaut du muscle dilatateur de l'iris. Nous avons rassemblé toutes les informations provenant d'un total de 122 patients, décrits dans 37 articles publiés entre 1862 et 2020 et nous avons extrait toutes les données accessibles sur les patients, en accordant une grande attention à l'erreur de réfraction, à l'âge de début du GLC, à la pression intraoculaire (PIO) et à l'histologie de l'angle iridocornéen, lorsque les informations étaient disponibles.

Cette revue offre un aperçu complet des anomalies du muscle dilatateur, ainsi que d'autres caractéristiques associées, et explore leurs interconnexions. Cette enquête confirme les constatations suivantes :

- Le muscle dilatateur présente des anomalies diverses chez les patients, allant de zones musculaires bien développées à l'absence totale de myofibrilles.
- Des anomalies de la chambre antérieures, dont l'insertion haute de la racine de l'iris dans l'éperon scléral et les spicules iriens, sont des observations presque constantes.
- La maladie est significativement associée à des erreurs de réfraction, y compris l'astigmatisme et la forte myopie.

- Un glaucome à angle ouvert à pression élevée se développe chez environ la moitié des individus myopes, ceux qui développent un GLC présentant des niveaux de myopie plus élevés par rapport à ceux qui n'en développent pas.
- Les individus sans immaturité de l'angle iridocornéen (seulement quelques cas rapportés) semblent ne présenter aucun risque - ou un risque moindre - de développer un GLC.
- Tous les individus testés présentent des variations structurelles sur le locus 13q32.1, et la taille de ces variations n'impacte pas la présentation de la maladie. Les variations comprennent à la fois des délétions et une duplication réciproque de la région du locus, soutenant un mécanisme de maladie impliquant la dérégulation de l'architecture régulatrice 3D de la région.

Ensemble, ces résultats démontrent une variabilité substantielle de l'expression de la maladie. Cela suggère que les anomalies de l'angle iridocornéen et la myopie axiale peuvent jouer un rôle dans l'apparition du GLC qui lui-même influence la gravité de la myopie, mais ils ne sont pas les seuls facteurs. La variabilité observée tant dans les caractéristiques cliniques que dans les anomalies du muscle dilatateur dans l'iris suggère l'implication de processus stochastiques en plus des facteurs génétiques et malformatifs dans l'étiologie. Dans le but de comprendre comment les variations structurelles impliquant le chromosome 13q32.1 chez les individus atteints de MCOR impactent le développement de l'iris et conduisent à une croissance oculaire anormale et à un glaucome dans un cas sur trois, nous avons utilisé la technologie CRISPR-Cas9 pour reproduire la délétion minimale de 35 kb responsable de la maladie, dans le génome de la souris. Dans ce travail, nous rendons compte de notre analyse de la structure en 3D et de l'organisation de la région génomique contenant le locus MCOR, et nous la comparons avec la région correspondante au chromosome 14qE4 dans le génome de la souris.

À l'aide de données HIC-seq, qui permet d'étudier la structure tridimensionelle de l'ADN, nous démontrons l'existence chez l'homme de deux domaines topologiquement associés (TADs) au sein de la région 13q32.2, dont l'un contient un regroupement de trois sous-TADs. Nous montrons que le locus MCOR, est situé à la frontière de deux sous-TADs. Enfin, en analysant la région synténique chez les souris, nous avons démontré une conservation étonnamment élevée à la fois du contenu génique et de la structure organisationnelle. Cette découverte souligne l'importance de supprimer la région critique causant la MCOR dans le génome de la souris afin de modéliser fidèlement la maladie sur les plans moléculaire et phénotypique.

Nous présentons les phénotypes du modèle murin portant la délétion critique MCOR en homozygotie et en hétérozygotie simple. Nous révélons que l'homozygotie pour la délétion est létale in utero chez les souris. En revanche, les souris hétérozygotes étaient viables et ont présenté un développement normal. Cependant, leurs iris présentaient une réduction modérée et statistiquement significative de la taille de la pupille, corrélée à une diminution de l'abondance de l'ARNm de la desmine (comme rapporté dans l'iris d'un cas de MCOR), déterminée respectivement par la pupillométrie et l'analyse RNAseq. L'analyse du transcriptome a en outre révélé

l'expression significative du facteur de transcription Sox21 dans les iris hétérozygotes, tandis qu'elle est restée indétectable dans les iris sauvages.

L'analyse détaillée du patron d'expression spatiotemporel de l'ARNm de Sox21 pendant le développement normal de l'œil, réalisé par une analyse RNAscope à haute résolution, a démontré que Sox21 n'est exprimé ni dans les yeux adultes ni dans les yeux en développement chez la souris. L'absence d'expression de Sox21 pendant le développement oculaire des souris contraste avec les données d'études chez le poisson-zèbre et le poulet où il est détecté dans le cristallin. Cette absence d'expression de Sox21 dans le développement de l'œil de la souris s'aligne avec l'absence de défauts oculaires observés chez la souris Sox21-/-. Chez les souris MCOR hétérozygotes, Sox21 présentait une expression dans la couche externe de la cupule optique, formant l'épithélium pigmentaire rétinien, l'épithélium antérieur du corps ciliaire et l'épithélium antérieur de l'iris, à partir duquel se développe le muscle dilatateur. Notamment, ce schéma d'expression coïncidait avec celui de Dct, qui code pour la dopachrome tautomérase, un marqueur des tissus pigmentés. Dct est positionné juste en amont du locus MCOR, tandis que Sox21 se trouve en aval du locus dans le sous-TAD suivant, suggérant que l'expression ectopique de Sox21 serait induite par l'adoption des enhancers de Dct par son promoteur.

De façon intéressante, nous rendons compte de la liaison de SOX21 à une séquence consensus située dans le premier intron du gène Tgfb2 dans les iris MCOR hétérozygotes. Cette découverte est particulièrement significative puisque nous avons observé une expression accrue de Tgfb2 dans les iris de souris hétérozygotes et une accumulation de TGFB2 dans l'humeur aqueuse d'un patient MCOR, déterminées respectivement par l'analyse du transcriptome irien et le dosage ELISA. Il est déjà connu qu'une concentration élevée de TGFB2 dans l'humeur aqueuse est corrélée avec l'accumulation de protéines de la matrice extracellulaire (ECM) dans le trabéculum meshwork et le développement du glaucome à angle ouvert, et il a été suggéré que cette augmentation de TGFB2 pourrait induire une croissance anormale de l'œil. Cela suppose un rôle majeur de la signalisation SOX21-TGFB2 dans le glaucome, chez les patients atteints de MCOR. Des preuves d'accumulation de l'ECM dans le trabéculum d'un cas MCOR, dont l'iris a été échantillonné lors d'une chirurgie de trabéculectomie, soutiennent également cette hypothèse.

En résumé, notre recherche suggère que la MCOR résulte d'une perturbation du TAD dans lequel se situent les délétions, entraînant l'expression ectopique de Sox21 dans l'iris. Cette dérégulation de Sox21 contribuerait à un mauvais développement du muscle dilatateur de l'iris et pourrait déclencher le glaucome, probablement par la dérégulation de la cascade de signalisation TGFB2. De plus, une corrélation proposée entre TGFB2 et l'allongement de l'œil soutient davantage ces découvertes. Dans l'ensemble, ces observations suggèrent que la dérégulation de SOX21 pourrait être l'élément liant les symptômes de la MCOR entre eux.

Le deuxième projet présenté dans cet ouvrage révèle un nouveau variant ponctuel dans la région régulatrice de FOXE3. Ce projet a pris naissance suite à l'identification d'un patient unique présentant une microphtalmie complexe unilatérale, accompagnée

d'une anomalie de Peters et d'une cataracte. Le séquençage initial du panel de gènes, se concentrant sur 119 gènes associés aux ODDs, a révélé un seul variant non-sens dans la région codante de FOXE3. Cependant, ce variant seul, normalement rapporté dans des formes récessives, ne semblait pas suffire pour expliquer le phénotype du patient. Des investigations approfondies pour trouver un second événement génétique ont conduit à la découverte d'un variant ponctuel (SNV) non référencé dans la région 5' UTR de FOXE3.

L'analyse in vitro par test de luciférase de ce SNV a indiqué son effet potentiel sur la régulation de l'expression génique. Pour valider cette hypothèse, nous avons créé deux modèles murins porteurs soit d'une mutation causant la perte de fonction du gène (KO), soit le SNV de la région non-codante (KI). Ces variants étaient portés en hétérozygotie simple, homozygotie et, par croisement des lignées, en hétérozygotie composite (imitant le génotype du patient). L'analyse de ces modèles murins a fourni des preuves convaincantes de l'impact significatif du SNV non codant sur l'expression de Foxe3. Les souris hétérozygotes ne présentaient aucun phénotype notable, tandis que les souris homozygotes KO pour Foxe3 présentaient une microphthalmie, comme attendu. Les animaux composites KI/KO présentaient des anomalies sévères du segment antérieur, sans microphtalmie réelle. Au niveau moléculaire, les animaux homozygotes KI présentaient des niveaux réduits à la fois d'ARN messager et de protéines dans le cristallin, avec une diminution encore plus marquée de FOXE3 dans le cristallin des souris en hétérozygotie composée.

De plus, nous avons mené des expériences de capture d'ADN pour identifier les protéines qui se lient préférentiellement aux séquences 5'UTR mutées et sauvages, respectivement. Cette étude a révélé des schémas de liaison différentiels pour trois protéines. L'analyse de ces résultats devrait éclairer la régulation de l'expression de Foxe3 et son importance dans le développement du cristallin. De plus, cela pourrait offrir des perspectives précieuses pour identifier des gènes potentiels dans le diagnostic de la microphthalmie. Dans l'ensemble, nos découvertes confirment fortement l'impact pathogène du SNV identifié dans la région 5'UTR du gène FOXE3. De plus, cette découverte met en lumière un nouvel élément régulateur qui devrait être pris en compte dans le diagnostic moléculaire des défauts de développement oculaire.

Une troisième partie de cette recherche s'est concentrée sur la caractérisation génétique des dystrophies rétiniennes pédiatriques au Chili. Les dystrophies rétiniennes héréditaires (IRDs) englobent toute une gamme de troubles rétiniens traditionnellement considérés comme dégénératifs. Cependant, leur association fréquente avec des gènes impliqués dans le développement soulève la question de possibles défauts développementaux dans les IRDs pédiatriques.

Dans cette étude, nous avons analysé une cohorte de 67 individus atteints d'IRDs pédiatriques provenant de l'Hôpital del Salvador au Chili afin de caractériser le paysage génétique des IRDs pédiatriques dans le pays. Les patients ont subi des examens ophtalmologiques approfondis et des tests génétiques utilisant un panel de

212 gènes liés aux IRDs. La ségrégation des variants candidats avec la maladie a été analysée à l'aide du séquençage de Sanger.

Ce travail a permis de résoudre avec succès 95 % des cas en identifiant un nombre limité de variants génétiques, la majorité étant homozygotes, mettant en évidence un taux élevé de consanguinité. Plusieurs de ces variants étaient uniques au Chili, tandis que d'autres avaient probablement une origine espagnole. Les gènes CRB1, RDH12 et LCA5, à eux trois, permettaient de résoudre 70 % des cas. Bien que certains cas présentaient des mutations dans des gènes liés au développement des photorécepteurs, elles n'étaient pas prédominantes. Alors que la majorité des cas résolus portaient des mutations dans des gènes connus pour causer des IRDs pédiatriques, nous avons également identifié des mutations dans RP1 et ADAM9, dont l'implication n'avait été suggérée que par l'identification de variants candidats dans des cas pédiatriques uniques.

Cette étude, qui représente la première analyse de l’architecture génétique des IRDs pédiatriques au Chili, rapporte un fiable nombre de variants rendant compte du phénotype des patients. Cette observation est d’une importance primordiale et permettra de faciliter l’accès au diagnostic génétique dans ce pays où l’accès aux séquençages à haut débit est très limité.

Dans son ensemble, cette thèse met en exergue l'importance critique de l'étude des variants non codants dans le cadre des ODDs. L’identification de ces nouveaux variants est facilitée de nos jours par l’accessibilité au WGS, néanmoins leur interprétation demeure complexe. Les travaux présentés ici contribuent à la compréhension de l’impact des variants ponctuels et structuraux dans la régulation de gènes à distance dans les pathologies oculaire. Cette thèse souligne la nécessité d'approfondir notre compréhension des mécanismes pathologiques sous-jacents à ces troubles oculaires, ce qui pourrait ouvrir la voie au développement de solutions diagnostiques et thérapeutiques novatrices pour ces conditions souvent délicates à traiter.

Deciphering the molecular mechanisms of ocular developmental defects through the analysis of coding and non-coding genome.

Abstract: Ocular development relies on precise regulation by multiple transcription factors (TFs) that control gene expression through binding DNA in cis-regulatory elements (CREs). Variants, whether punctual (SNV) or structural (SV), in these regions can disrupt proper embryogenesis. Many ocular development defects (ODD) result from mutations in TF, yet more than half of affected patients do not have genetic diagnosis to date. Therefore, focusing on CREs is essential to understand ODD etiology. This thesis reports TF dysregulation in two distinct pathologies using transgenic mice. First, Congenital Microcoria (MCOR) a rare iris defect frequently associated with glaucoma (GL) and linked to deletions of varying size in the 13q32.1 locus. We suggest that these deletions disrupt the TAD in which they lie, inducing ectopic expression of Sox21 in the iris of a MCOR mouse model. In addition, we demonstrate that SOX21 binds to Tgfb2, whose involvement in GL is well known. The second part reveals a new SNV in the regulating region of FOXE3 in a case of complex microphthalmia, significantly impacting in the Foxe3 expression. We showed that Foxe3-/- animals reproduce a severe microphthalmia phenotype through a mechanism of lens degeneration. Furthermore, analysis of SNV binding elements highlighted new candidate genes in ocular development. Finally, a third part is dedicated to determine the genetic architecture of pediatric retinal dystrophies in Chile. This study discloses a high degree of inbreeding resulting in a very limited repertoire of mutations. This enables cost-effective molecular diagnosis despite limited access to next-generation sequencing. Overall, this thesis emphasizes the importance of studying non-coding variants, which are poorly understood despite their major contribution to diseases. The aim of this project is to gain a deeper understanding of the disease mechanisms involved in ODD, which is crucial for developing innovative diagnostic and therapeutic solutions.

Keywords: Congenital microcoria, microphthalmia, gene regulation, TAD, mouse model

Décrypter les mécanismes moléculaires des atteintes du développement oculaire par l'analyse du génome codant et non-codant.

Résumé : Le développement oculaire est un processus finement orchestré par de nombreux facteurs transcription (TFs) qui modulent l'expression de gènes cibles en se liant à l'ADN dans des régions cis-régulatrices (CREs). Des variants, qu'ils soient ponctuels (SNV) ou structuraux (SV), dans ces régions peut entraver le bon déroulement de l'embryogénèse. Les défauts de développement oculaire (ODDs) résultent fréquemment de mutations de TFs, toutefois plus de la moitié des patients n'ont pas de diagnostic génétique à ce jour. Il apparaît donc nécessaire de s'intéresser aux CREs pour comprendre l'étiologie de ces ODDs. Cette thèse rapporte la dérégulation de TFs dans deux pathologies, en utilisant des souris transgéniques. La première, la microcorie congénitale (MCOR), est une maladie rare de l'iris associée à un glaucome (GL) et reliée à des délétions de taille variable dans le locus 13q.32.1. Nous suggérons que ces SVs perturbent le TAD dans lequel ils se situent, induisant l'expression ectopique du TF *Sox21* dans l'iris du modèle murin MCOR. Ce TF se fixe à *Tgfb2*, dont l'implication dans le GL est bien connue. La seconde partie de ce travail révèle un nouveau SNV dans la région régulatrice de *FOXE3* chez un cas de microphtalmie complexe, impactant significativement l'expression de *Foxe3*. Nous avons montré que les animaux *Foxe3*$^{-/-}$ reproduisent un phénotype de microphtalmie sévère par un mécanisme de dégénérescence du cristallin. De plus l'analyse des éléments se fixant à ce CRE a mis en évidence de nouveaux gènes candidat dans le développement oculaire. Enfin, une troisième partie se consacre à la caractérisation génétique des dystrophies rétiniennes pédiatriques au Chili. Cette étude révèle un degré élevé de consanguinité entraînant un répertoire de mutations très limité, facilitant un diagnostic moléculaire rentable malgré l'accès limité au séquençage de nouvelle génération. Dans son ensemble, cette thèse souligne l'importance d'étudier les variants non codants. L'objectif de ce projet est d'acquérir une compréhension plus approfondie des mécanismes pathologiques impliqués dans les ODDs, cruciale pour développer des solutions diagnostiques et thérapeutiques innovantes.

Mots clés : Microcorie congénitale, microphtalmie, régulation de gènes, TAD, modèle murin